

**EXPERIMENT AND NUMERICAL MODELING OF SMALL DISCRETE
OBJECT TRACKING IN SURF AND SWASH ZONES ON SAND BEACHES**

by

JIRAT LAKSANALAMAI AND NOBUHISA KOBAYASHI

RESEARCH REPORT NO. CACR-23-01

February 2023



CENTER FOR APPLIED COASTAL RESEARCH
University of Delaware
Newark, Delaware 19716

ACKNOWLEDGMENTS

The first author was supported by the Office of the Civil Service Commission under the Government of Thailand, during his study at the Center for Applied Coastal Research, University of Delaware, Newark, Delaware. This study was partially supported by the U.S. Army Corps of Engineers under Agreement No. W912HZ18P 0134 and W912HZ20-2-0016.

TABLE OF CONTENTS

LIST OF TABLES	iv
LIST OF FIGURES	vii
ABSTRACT	xiv
1 Introduction	1
2 Experiment	4
2.1 Wave Flume, Sand Beach, and Instruments	4
2.2 Sand, Gravel, and Microplastic Characteristics	7
2.3 Experimental Procedure	9
3 Data Analysis.....	37
3.1 Hydrodynamics.....	37
3.2 Beach Profile Changes	70
3.3 Lagrangian Movement of 20 Individual Particles	78
4 Numerical Model.....	146
4.1 Combined Wave and Current Model in Wet Zone.....	146
4.2 Hydrodynamic Model for Impermeable Wet and Dry Zone	150
4.3 Sediment Transport Model	156
4.4 Time-averaged Model for Tracking Small Discrete Object	160
5 Comparison with Data.....	164
5.1 Cross-shore Wave Transformation.....	164
5.2 Beach Profile Evolution	172
5.3 Temporal Variation of Cross-shore Location of Discrete Object	176
6 Conclusions	184
REFERENCES	186

LIST OF TABLES

Table 2.1	Wave gauge locations (WG1-WG8) and velocimeter locations (ADV; Red Vectrino, RV; and Blue-Vectrino, BV)	6
Table 2.2	Sand, gravel, and microplastic characteristics.....	8
Table 2.3	Sequence of six tests on near Equilibrium (E) beach and Nourished (N) foreshore consisting of 100 runs with each run lasting 400s	10
Table 3.1	Incident wave characteristics, Test EG.	39
Table 3.2	Incident wave characteristics, Test EL.....	40
Table 3.3	Incident wave characteristics, Test ES.	41
Table 3.4	Incident wave characteristics, Test NG.....	42
Table 3.5	Incident wave characteristics, Test NL.	43
Table 3.6	Incident wave characteristics, Test NS.....	44
Table 3.7	Mean free-surface elevation $\bar{\eta}$ (cm) at 8 wave gauge locations, Test EG.....	45
Table 3.8	Mean free-surface elevation $\bar{\eta}$ (cm) at 8 wave gauge locations, Test EL.	46
Table 3.9	Mean free-surface elevation $\bar{\eta}$ (cm) at 8 wave gauge locations, Test ES.	47
Table 3.10	Mean free-surface elevation $\bar{\eta}$ (cm) at 8 wave gauge locations, Test NG.	48
Table 3.11	Mean free-surface elevation $\bar{\eta}$ (cm) at 8 wave gauge locations, Test NL.....	49
Table 3.12	Mean free-surface elevation $\bar{\eta}$ (cm) at 8 wave gauge locations, Test NS.....	50

Table 3.13	Free-surface standard deviation σ_η (cm) at 8 wave gauge locations, Test EG.	51
Table 3.14	Free-surface standard deviation σ_η (cm) at 8 wave gauge locations, Test EL.	52
Table 3.15	Free-surface standard deviation σ_η (cm) at 8 wave gauge locations, Test ES.	53
Table 3.16	Free-surface standard deviation σ_η (cm) at 8 wave gauge locations, Test NG.	54
Table 3.17	Free-surface standard deviation σ_η (cm) at 8 wave gauge locations, Test NL.	55
Table 3.18	Free-surface standard deviation σ_η (cm) at 8 wave gauge locations, Test NS.	56
Table 3.19	Mean \bar{U} and standard deviation σ_U of measured cross-shore velocity U , Test EG.	57
Table 3.20	Mean \bar{U} and standard deviation σ_U of measured cross-shore velocity U , Test EL.	58
Table 3.21	Mean \bar{U} and standard deviation σ_U of measured cross-shore velocity U , Test ES.	59
Table 3.22	Mean \bar{U} and standard deviation σ_U of measured cross-shore velocity U , Test NG.	60
Table 3.23	Mean \bar{U} and standard deviation σ_U of measured cross-shore velocity U , Test NL.	61
Table 3.24	Mean \bar{U} and standard deviation σ_U of measured cross-shore velocity U , Test NS.	62
Table 3.25	Lagrangian movement of DO#1-10 for EG1-EG5 (a)	79
Table 3.25	Lagrangian movement of DO#11-20 for EG1-EG5 (b)	80
Table 3.26	Lagrangian movement of DO#1-10 for EG6-EG10 (a)	81
Table 3.26	Lagrangian movement of DO#11-20 for EG6-EG10 (b)	82

Table 3.27	Lagrangian movement of DO#1-10 (after DO resetting) for EG11-EG20 (a)	83
Table 3.27	Lagrangian movement of DO#11-20 (after DO resetting) for EG11-EG20 (b)	84
Table 3.28	Lagrangian movement of DO#1-10 for EL1-EL10 (a).....	86
Table 3.28	Lagrangian movement of DO#11-20 for EL1-EL10 (b)	87
Table 3.29	Lagrangian movement of DO#1-10 (after DO resetting) for EL11-EL20 (a).....	89
Table 3.29	Lagrangian movement of DO#11-20 (after DO resetting) for EL11-EL20 (b).....	90
Table 3.30	Lagrangian movement of DO#1-10 for ES1-ES5 (a)	92
Table 3.30	Lagrangian movement of DO#11-20 for ES1-ES5 (b).....	93
Table 3.31	Lagrangian movement of DO#1-10 (after DO resetting) for ES6-ES10 (a).....	94
Table 3.31	Lagrangian movement of DO#11-20 (after DO resetting) for ES6-ES10 (b)	95
Table 3.32	Lagrangian movement of DO#1-10 for NG1-NG20 (a).....	96
Table 3.32	Lagrangian movement of DO#11-20 for NG1-NG20 (b).....	98
Table 3.33	Lagrangian movement of DO#1-10 for NL1-NL20 (a).....	100
Table 3.33	Lagrangian movement of DO#11-20 for NL1-NL20 (b)	102
Table 3.34	Lagrangian movement of DO#1-10 for NS1-NS10 (a)	104
Table 3.34	Lagrangian movement of DO#11-20 for NS1-NS10 (b).....	105
Table 3.35	Measured (M) and Computed (C) numbers of DOs found in four different zones for equilibrium profile tests	136
Table 3.36	Measured (M) and Computed (C) numbers of DOs found in four different zones for nourished foreshore profile tests.....	139

LIST OF FIGURES

Figure 2.1	Experimental setup at start of Equilibrium (E) profile tests.....	5
Figure 2.2	Twenty DOs were selected and each DO was colored for its identification.....	8
Figure 2.3	Initial cross-shore locations of 20 gravel DOs (a), alongshore locations in pair at $y = -0.3$ and 0.3 m (b)-(c), on equilibrium sand beach profile in Test EG.....	11
Figure 2.3	Bathymetric contour measured by laser line scanner displaying initial DO locations before Test EG (d).....	12
Figure 2.3	Surface plot displaying initial DO locations (with spikes at the locations of WG7 and WG8) in inner surf zone and foreshore before Test EG (e).	13
Figure 2.3	Surface plot displaying initial DO locations in inner and outer surf zones before Test EG (f).....	14
Figure 2.4	Initial cross-shore locations of 20 large plastic DOs (with dowels placed for laser measurement) and alongshore locations in pair at $y = -0.3$ and 0.3 m (a)-(b), on equilibrium sand beach profile in Test EL. ...	15
Figure 2.4	Bathymetric contour measured by laser line scanner displaying initial DO locations before Test EL (c).	16
Figure 2.4	Surface plot displaying initial DO locations in inner surf zone and foreshore before Test EL (d).	17
Figure 2.4	Surface plot displaying initial DO locations in inner and outer surf zones before Test EL (e).....	18
Figure 2.5	Initial cross-shore locations of 20 small plastic DOs (with dowels placed for laser measurement) and alongshore locations in pair at $y = -0.3$ and 0.3 m (a)-(b), on equilibrium sand beach profile in Test ES.....	19
Figure 2.5	Bathymetric contour measured by laser line scanner displaying initial DO locations before Test ES (c).....	20

Figure 2.5	Surface plot displaying initial DO locations in inner surf zone and foreshore before Test ES (d).	21
Figure 2.5	Surface plot displaying initial DO locations in inner and outer surf zones before Test ES (e).	22
Figure 2.6	Initial cross-shore locations of 20 gravel DOs (a), and alongshore locations in pair at $y = -0.3$ and 0.3 m (b)-(c) on nourished foreshore profile in Test NG.	25
Figure 2.6	Bathymetric contour measured by laser line scanner displaying initial DO locations before Test NG (d).	26
Figure 2.6	Surface plot displaying initial DO locations in inner surf zone and foreshore before Test NG (e).	27
Figure 2.6	Surface plot displaying initial DO locations in inner and outer surf zones before Test NG (f).	28
Figure 2.7	Initial cross-shore locations of 20 large plastic DOs (a), and alongshore locations in pair at $y = -0.3$ and 0.3 m (with dowels placed for laser measurement) (b), on nourished foreshore profile in Test NL.	29
Figure 2.7	Bathymetric contour measured by laser line scanner displaying initial DO locations before Test NL (c).	30
Figure 2.7	Surface plot displaying initial DO locations in inner surf zone and foreshore before Test NL (d).	31
Figure 2.7	Surface plot displaying initial DO locations in inner and outer surf zones before Test NL (e).	32
Figure 2.8	Initial cross-shore locations of 20 small plastic DOs (a), and alongshore locations in pair at $y = -0.3$ and 0.3 m (with dowels placed for laser measurement) (b), on nourished foreshore profile in Test NS.	33
Figure 2.8	Bathymetric contour measured by laser line scanner displaying initial DO locations before Test NS (c).	34
Figure 2.8	Surface plot displaying initial DO locations in inner surf zone and foreshore before Test NS (d).	35
Figure 2.8	Surface plot displaying initial DO locations in inner and outer surf zones before Test NS (e).	36

Figure 3.1	Cross-shore variations of mean and standard deviation of measured free surface elevation η and horizontal velocity U for 20 runs in Test EG.....	64
Figure 3.2	Cross-shore variations of mean and standard deviation of measured free surface elevation η and horizontal velocity U for 20 runs in Test EL.	65
Figure 3.3	Cross-shore variations of mean and standard deviation of measured free surface elevation η and horizontal velocity U for 10 runs in Test ES.	66
Figure 3.4	Cross-shore variations of mean and standard deviation of measured free surface elevation η and horizontal velocity U for 20 runs in Test NG.	67
Figure 3.5	Cross-shore variations of mean and standard deviation of measured free surface elevation η and horizontal velocity U for 20 runs in Test NL (WG8 was not functional in this test).	68
Figure 3.6	Cross-shore variations of mean and standard deviation of measured free surface elevation η and horizontal velocity U for 10 runs in Test NS.....	69
Figure 3.7	Measured initial, middle, and final beach profiles and changes of bottom elevation (Z_b) for Test EG.	71
Figure 3.8	Measured initial, middle, and final beach profiles and changes of bottom elevation (Z_b) for Test EL.	72
Figure 3.9	Measured initial, middle, and final beach profiles and changes of bottom elevation (Z_b) for Test ES.....	73
Figure 3.10	Measured initial, middle, and final beach profiles and changes of bottom elevation (Z_b) for Test NG.	74
Figure 3.11	Measured initial, middle, and final beach profiles and changes of bottom elevation (Z_b) for Test NL.....	75
Figure 3.12	Measured initial and final beach profiles and changes of bottom elevation (Z_b) for Test NS.	76
Figure 3.13	Differences and similarities of near equilibrium profiles of EG, EG20 = EL0, EL20 = ES0, ES10	77

Figure 3.14	Similarities amongst measured beach profiles NG0, NL0, and NS0 depicting careful profile rebuilding.	77
Figure 3.15	Similarities amongst measured beach profiles NG20, NL20, and NS20 depicting repeatable profile evolution.	78
Figure 3.16	Final locations of 20 gravel DOs (a) on equilibrium sand beach profile in Test EG.	107
Figure 3.16	Bathymetric contour measured by laser line scanner displaying final DO locations after Test EG (b).	108
Figure 3.16	Surface plot displaying final DO locations (with spikes at the locations of WG7 and WG8) in inner surf zone and foreshore after Test EG (c).	109
Figure 3.16	Surface plot measured by laser line scanner displaying final DO locations in inner and outer surf zones after Test EG (d).	110
Figure 3.17	Final locations of 20 large plastic DOs (a) on equilibrium sand beach profile in Test EL.	111
Figure 3.17	Bathymetric contour measured by laser line scanner displaying final DO locations after Test EL (b).	112
Figure 3.17	Surface plot displaying final DO locations in inner surf zone and foreshore after Test EL (c).	113
Figure 3.17	Surface plot displaying final DO locations in inner and outer surf zones after Test EL (d).	114
Figure 3.18	Final locations of 20 small plastic DOs (a) on equilibrium sand beach profile in Test ES.	115
Figure 3.18	Bathymetric contour measured by laser line scanner displaying final DO locations after Test ES (b).	116
Figure 3.18	Surface plot displaying final DO locations in inner surf zone and foreshore after Test ES (c).	117
Figure 3.18	Surface plot displaying final DO locations in inner and outer surf zones after Test ES (d).	118
Figure 3.19	Final locations of 20 gravel DOs (a) on nourished foreshore profile in Test NG.	119

Figure 3.19	Bathymetric contour measured by laser line scanner displaying final DO locations after Test NG (b).	120
Figure 3.19	Surface plot displaying final DO locations in inner surf zone and foreshore after Test NG (c)	121
Figure 3.19	Surface plot displaying final DO locations in inner and outer surf zones after Test NG (d)	122
Figure 3.20	Final locations of 20 large plastic DOs (a) on nourished sand beach profile in Test NL.	123
Figure 3.20	Bathymetric contour measured by laser line scanner displaying final DO locations after Test NL (b).	124
Figure 3.20	Surface plot displaying final DO locations in inner surf zone and foreshore after Test NL (c)	125
Figure 3.20	Surface plot displaying final DO locations in inner and outer surf zones after Test NL (d)	126
Figure 3.21	Final locations of 20 small plastic DOs (a) on nourished sand beach profile in Test NS.	127
Figure 3.21	Bathymetric contour measured by laser line scanner displaying final DO locations after Test NS (b).	128
Figure 3.21	Surface plot displaying final DO locations in inner surf zone and foreshore after Test NS (c)	129
Figure 3.21	Surface plot displaying final DO locations in inner and outer surf zones after Test NS (d)	130
Figure 3.22	Initial and final cross-shore and alongshore locations of 20 gravel DOs for equilibrium profile test EG where the DOs were reset after EG10 and the number of DOs in each zone is indicated.	132
Figure 3.23	Initial and final cross-shore and alongshore locations of 20 large plastics DOs for equilibrium profile test EL where the DOs were reset after EL10 and DO No.1 was missing in EL10.	134
Figure 3.24	Initial and final cross-shore and alongshore locations of 20 small plastics DOs for equilibrium profile test ES where the DOs were reset after ES5. DO No.4, 7, and 12 were missing in ES5. DO No.8, 12, and 19 were missing in ES10.	135

Figure 3.25	Final cross-shore and alongshore locations of 20 DOs for nourished foreshore tests NG, NL, and NS, where the number of missing DOs was 2, 5, and 4 in NG20, NL20, and NS10, respectively.....	138
Figure 3.26	Temporal variations of cross-shore locations of 10 gravel DOs initially located at $y = 0.3$ m during 10 runs of EG0-EG10 and EG10-EG20 with DO resetting after EG10.	141
Figure 3.27	Temporal variations of cross-shore locations of 10 large plastics DOs initially located at $y = 0.3$ m during 10 runs of EL0-EL10 and EL10-EL20 with DO resetting after EL10.	142
Figure 3.28	Temporal variations of cross-shore locations of 10 small plastics DOs initially located at $y = 0.3$ m during 5 runs of ES0-ES5 and ES5-ES10 with DO resetting after ES5. Each missing DO identified by the letter M.	143
Figure 3.29	Temporal variations of cross-shore locations of 10 DOs initially located at $y = 0.3$ m during 20 runs of NG0-NG20, NL0-NL20 and 10 runs of NS0-NS10.	145
Figure 4.1	CSHORE definition sketch for cross-shore hydrodynamic variation from wet zone to wet and dry zone on foreshore sand beach.....	147
Figure 5.1	Measured and computed cross-shore variations of mean and standard deviation of free surface elevation η and horizontal velocity U for 20 runs during EG1-EG20.....	166
Figure 5.2	Measured and computed cross-shore variations of mean and standard deviation of free surface elevation η and horizontal velocity U for 20 runs during EL1-EL20.....	167
Figure 5.3	Measured and computed cross-shore variations of mean and standard deviation of free surface elevation η and horizontal velocity U for 10 runs during ES1-ES10.	168
Figure 5.4	Measured and computed cross-shore variations of mean and standard deviation of free surface elevation η and horizontal velocity U for 20 runs during NG1-NG20.....	169
Figure 5.5	Measured and computed cross-shore variations of mean and standard deviation of free surface elevation η and horizontal velocity U for 20 runs during NL1-NL20 (WG8 was not functional in this test).	170

Figure 5.6	Measured and computed cross-shore variations of mean and standard deviation of free surface elevation η and horizontal velocity U for 10 runs during NS1-NS10.	171
Figure 5.7	Measured and computed beach profiles for equilibrium profile test EG10.....	173
Figure 5.8	Measured and computed beach profiles for equilibrium profile test EL10	173
Figure 5.9	Measured and computed beach profiles for equilibrium profile test ES5	174
Figure 5.10	Measured and computed beach profiles for nourished foreshore profile test NG10.....	174
Figure 5.11	Measured and computed beach profiles for nourished foreshore profile test NL10	175
Figure 5.12	Measured and computed beach profiles for nourished foreshore profile test NS10	175
Figure 5.13	Computed temporal variations of cross-shore locations of 10 DOs during EG0-EG10 (gravel), EL0-EL10 (large plastics), and ES0-ES5 (small plastics).....	178
Figure 5.14	Computed cross-shore variations of DO bed load movement probability P_b and DO suspension probability P_s during EG10, EL10, and ES5 as well as for hypothetical ES5 (sand).....	179
Figure 5.15	Computed temporal variations of cross-shore locations of 10 hypothetical sand DOs for the beach and wave conditions of tests ES0-ES5 to show the sensitivity to the bed load parameter $C_b = 0.02$ and 0.04	181
Figure 5.16	Computed temporal variations of cross-shore locations of 10 DOs during nourished foreshore tests NG0-NG20, NL0-NL20, and NS0-NS10.....	183

ABSTRACT

The significant part of this study was to conduct an experiment in a wave flume to measure the trajectories of 20 small objects (gravel and microplastics) in the surf and swash zones on an equilibrium beach and a nourished foreshore beach with erosion and accretion in the swash zone. To develop a tracking model based on a kinematic Lagrangian model, the trajectory of each of the 20 objects was measured in six tests consisting of 100 runs with each run lasting 400 s. From the measurement, gravel particles were mobile only in the swash zone and moved seaward under wave downrush. Large and small microplastics moved onshore from the surf zone and accumulated in the lower swash zone of wave rundown or in the upper swash or berm zone of wave runup. Plastic particles remained on the evolving sand surface despite the erosion and accretion of the nourished foreshore. A simple tracking model is developed to predict the measured trajectories of the 20 particles of gravel and microplastics. The model was calibrated to predict limited net displacements of hypothetical sand particles on the equilibrium profile beach. For future applications, the tracking model may eventually be applied to track and clean up microplastics on beaches as well as to predict the destinations of sand particles placed on eroding beaches in beach nourishment projects.

Chapter 1

Introduction

Despite continual efforts to improve the numerical modeling of beach and dune profile evolution, it is still difficult to predict the profile evolution accurately and consistently. For example, Kalligeris et al. (2020) compared the model for eXtreme BEACH behavior (XBEACH) (Roelvink et al. 2009) and the cross-shore model CSHORE (Kobayashi 2016) with six energetic wave events at two southern California beaches. Cohn et al. (2021) compared the models XBEACH and CSHORE with variable dune profile changes during weeks of sustained, elevated wave and water level conditions at a southeastern Atlantic beach. These comparisons indicated the limitations and capabilities of the two models in predicting beach and dune erosion during storms. Sediment transport models should be able to predict both beach erosion during a storm and subsequent recovery. Kobayashi and Jung (2012) compared CSHORE with beach erosion and recovery data of 272 days at two beaches in Delaware. The onshore bed load parameter in CSHORE was from necessity adjusted by a factor of two to reproduce the morphological changes of both erosion and accretion. To improve the profile evolution prediction, the trajectories of small discrete objects were measured and analyzed in this study.

A number of researchers investigated the sediment particle movements in the nearshore zone by placing the given mass of fluorescent sand tracers at selected

locations of the seabed (e.g., Suzuki et al. 2019). Then, core samples of specified lengths were collected at a number of seabed locations on specified dates. Due to the advection and dispersion of tracer sands placed in the midst of an enormous number of native sands, the number of tracer sands in the core sample inevitably decreased with time. The tracer sand movements need to be inferred from the measured tracer sand concentrations. The advection and diffusion equation of the tracer sand is typically used to estimate sand transport patterns in the nearshore (e.g., Beck et al. 2020). In this laboratory study, each discrete object was tracked directly. An experiment was conducted to measure the displacements of small discrete objects (gravel and microplastics) in the surf and swash zones on sand beaches. A kinematic Lagrangian model is adopted to predict the time-averaged displacement of each discrete object.

Marine litter is an environmental problem of global significance, and plastics form the bulk of the litter (Williams and Rangel-Buitrago 2019). Microplastics with diameters less than 5 mm are difficult to filter out. Numerical models, such as the Delft3D suite (Lesser et al. 2004), were applied to simulate the transport and dispersal of microplastics released from rivers to coastal waters (e.g., Raimundo et al. 2020). The transport and mixing of small particles inside the surf zone are affected by breaking waves, wave-induced onshore water flux near the mean water level, and offshore undertow current below the wave trough level (e.g., Kobayashi et al. 2008). Microplastic particles with a density of 0.975 g/cm^3 were used in the wave flume experiment of Abolfathi et al. (2020). In their regular wave experiment, surface and bed-generated turbulence determined mixing and dispersion. Microplastics that settle in

water are purposely adopted in this study because the proposed kinematic Lagrangian model is intended for both sediment and plastic particles that are heavier than water.

A laboratory experiment consisting of six tests was conducted in a wave flume with irregular waves to measure the displacement of a small discrete object (DO) in the surf and swash zones of an equilibrium sand beach and nourished foreshore beach. In the following, the experimental setup and procedure for the six tests are described in Chapter 2. Twenty DOs were placed on the sand surface in the surf and swash zones. Gravel particles of 2.0 cm diameter and spherical microplastics of 0.33 and 0.20 cm diameters were used in three tests on the equilibrium beach, consisting of 20, 20, and 10 runs, with each run lasting for 400 sec. These three tests on the equilibrium profile were continued with a nourished foreshore profile to examine the effect of erosion and accretion on the DO movement. In Chapter 3, the hydrodynamics, beach profile changes, and the movement of 20 DOs were analyzed for all the six tests. The displacements of the three different DOs on the equilibrium and nourished beach profiles were analyzed to quantify the spatial and temporal variations of the DO movements. In Chapter 4, the cross-shore numerical model CSHORE is presented concisely. The model CSHORE is expanded to predict the DO movement on a sand beach under irregular breaking waves. An empirical formula for the cross-shore DO velocity is proposed based on the formulas of bed load and suspended load in CSHORE. In Chapter 5, the expanded model is compared with the measurements of the wave transformation, beach profile change, and DO displacements in the six tests. Finally, the findings in this study are summarized in Chapter 6.

Chapter 2

Experiment

The laboratory experiment was conducted to measure the displacement of small discrete objects (DO) in the surf and swash zones of the equilibrium and nourished beach profiles. This chapter provides an overview of the experiment in a wave flume located in the basement of the Dupont Hall of the University of Delaware.

2.1 Wave Flume, Sand Beach, and Instruments

The experiment was conducted in a wave flume that is 23 m long, 1.15 m wide, and 1.5 m high. The setup for the first equilibrium (E) profile test before the placement of 20 gravel (G) particles is shown in Figure 2.1. The instrument setup for the experiment was based on the previous equilibrium profile tests performed by Kobayashi et al. (2018). The sand beach on a plywood slope of 1/30 (vertical/ horizontal) consisted of well-sorted fine sand with a median diameter of 0.018 cm. The fall velocity, density, and porosity of the sand were 2.0 cm/s, 2.6 g/cm³, and 0.4, respectively. Fine sand used in this small-scale experiment might be considered as coarse sand at the prototype scale. This small-scale experiment explored the feasibility of tracking small mobile DOs on a live sand beach with active bed load and suspended load. The possibility of DO burial was presumed to be small on the equilibrium beach. A 400-s run of irregular waves corresponding to a Texel, Marsen, and Arsloe (TMA) spectrum was generated by a piston-type wave maker equipped at one end of the wave flume in a water depth of 88 cm. The spectral significant wave height and peak period were approximately 0.2 m and

2.6 s. A vertical wall was located at the landward edge of the sand beach with the wall crest elevation of 0.2 m above the still water level (SWL) in the wave flume. No wave overtopping of the wall occurred in this experiment.

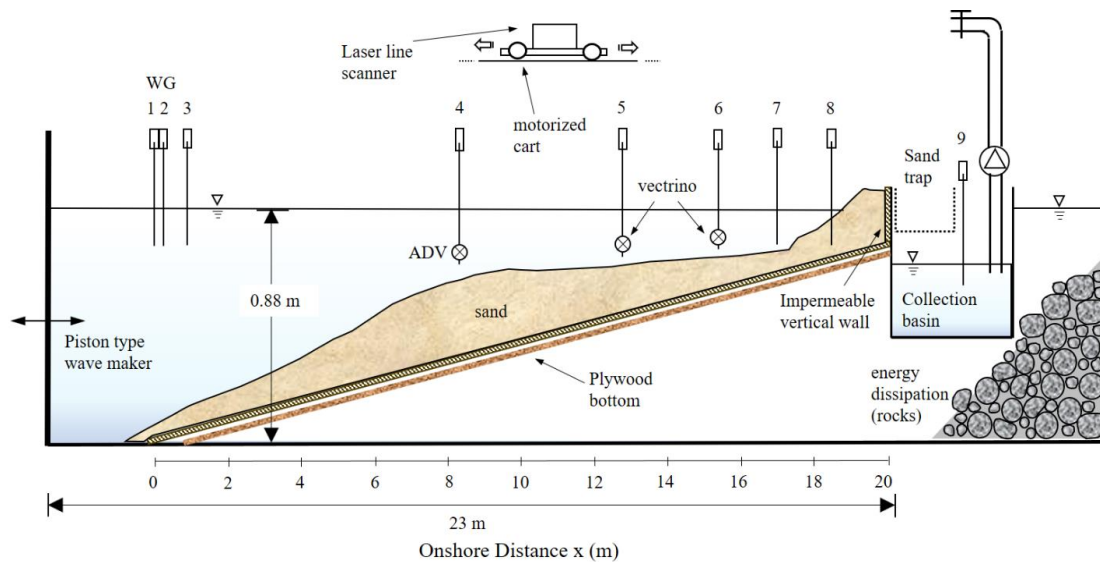


Figure 2.1 Experimental setup at start of Equilibrium (E) profile tests.

Eight capacitance wave gauges (WG1-WG8) were installed across the cross-shore profile to measure the free surface elevation in the shoaling, surf, and swash zones. The WG9 was used to measure the wave level in the collection basin (behind the sand berm) after each run to measure the volume of overtopped water in the previous wave overtopping experiment (Figlus et al. 2011). The locations of each wave gauge are tabulated in Table 2.1. The vertical wall was located at the onshore distance x of 19.9 m with $x = 0$ at WG1. The alongshore coordinate y is positive to the left from the direction

of wave propagation with $y = 0$ along the center line of the wave flume. The vertical coordinate z is positive upward with $z = 0$ at SWL. WG1, WG2, and WG3 were located offshore to separate incident and reflected wave signals and examine the repeatability of each 400-s run. WG4 and WG5 were in the outer surf zone, WG6 and WG7 were in the inner surf zone, and WG8 was in the swash zone. WG7 and WG8 were partially buried in sand to avoid emergence in air and were not removed during the profile measurement in each test.

The fluid velocities were measured by one acoustic Doppler velocimeter (ADV) and two Vectrinos (Nortek, Rud, Norway) which were co-located at WG4, WG5 and WG6 (WG4 with 2D ADV and WG5-WG6 with Red and Blue Vectrinos) at an elevation of one-third of the local water depth as listed in Table 2.1.

Table 2.1 Wave gauge locations (WG1-WG8) and velocimeter locations (ADV; Red Vectrino, RV; and Blue Vectrino, BV)

Wave Gauge	WG1	WG2	WG3	WG4	WG5	WG6	WG7	WG8
x (m)	0.00	0.25	0.95	8.30	12.90	15.50	17.10	18.60
y (m)	0.00	0.00	0.00	0.00	0.00	0.00	0.00	0.00
Velocity Gauge				ADV	RV	BV		
x (m)				8.30	12.90	15.50		
y (m)				0.15	0.15	0.00		
z (m)				-2d/3	-2d/3	-2d/3		

d = local water depth at the start of each run

x = onshore coordinate with $x = 0$ at WG1

y = alongshore coordinate with $y = 0$ at the middle of the wave flume

z = vertical coordinate with $z = 0$ at SWL

After draining water in the tank, the sand beach profile was measured by the combination of a class III acuity AR4000-LIR laser line scanner system mounted on a motorized cart and a fixed class II Acuity AR1000 laser range finder located next to the collection basin as explained by Figlus et al. (2011). The laser scanner system obtained accurate three-dimensional profile data by recording alongshore transect across the flume width at 2 cm cross-shore intervals with a vertical error of about 1 mm. After confirming alongshore uniformity, the three-dimensional bathymetry data were averaged alongshore to obtain the averaged cross-shore beach profile.

2.2 Sand, Gravel, and Microplastic Characteristics

The characteristics of three different discrete objects and the sand used in the experiment are listed in Table 2.2. Twenty gravel DOs of similar size and shape were selected and colored for the identification of each DO (Figure 2.2a). The nominal diameter, density, and fall velocity of the gravel (G) were 2.0 cm, 2.7 g/cm³, and 100 cm/s. The G DOs were expected to move little under the generated irregular waves. A number of spherical plastics DOs that were screened for 20 large plastics DOs (Figure 2.2b) and 20 small plastics DOs (Figure 2.2c). The average diameter and fall velocity were 0.33 cm and 15.6 cm/s for the large plastic DOs and 0.20 cm and 7.9 cm/s for the small plastics DOs. The density was 1.38 g/cm³ for both the large (L) and small (S) plastics. The L DOs were expected to be transported mostly as bed load, whereas the S DOs were presumed to be suspended as well. Each plastic DO was identified with specific colors. The 0.2-cm diameter of the S DOs was the practical limit of the individual color identification. In addition, hypothetical sand DOs on the equilibrium beach were examined numerically in this study.

Table 2.2 Sand, gravel, and microplastic characteristics

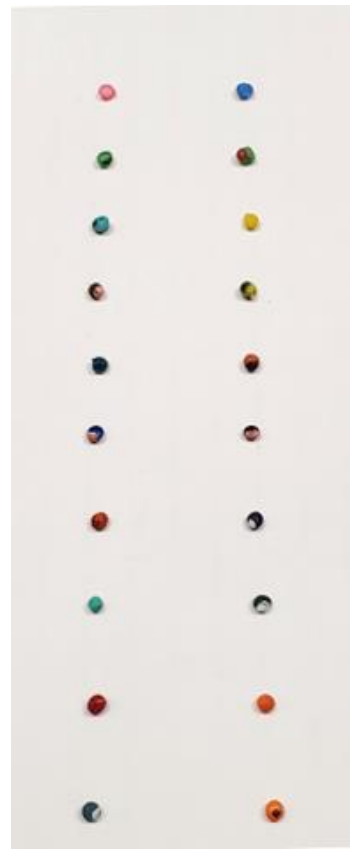
Discrete Object (DO)	Gravel (G)	Large (L) Plastics	Small (S) Plastics	Sand
Diameter (cm)	2.0	0.33	0.20	0.018
Density (g/cm ³)	2.70	1.38	1.38	2.60
Fall Velocity (cm/s)	100	15.6	7.9	2.0



(a) Gravel DOs



(b) Large plastic DOs



(c) Small plastic DOs

Figure 2.2 Twenty DOs were selected and each DO was colored for its identification

2.3 Experimental Procedure

The sequence of six tests is summarized in Table 2.3 and explained in the following. The equilibrium beach profile was built based on the previous equilibrium profile tests performed by Kobayashi et al. (2018). The first equilibrium (E) profile test EG with the G DOs was started from the initial profile EG0, where the numeral after the two letters EG corresponds to the run number starting from the initial profile and DO positions of EG0. Figure 2.3a-c shows the 20 gravel DOs placed on the surface in pairs at the alongshore locations of $y = -0.3$ and 0.3 m along the 10 cross-shore locations. Preliminary tests were performed to decide appropriate DO placement locations. One pair at $x = 12.0$ m represented the DO movement in the outer surf zone of gradual cross-shore variability. Four pairs at $x = 14.2, 14.7, 16.2,$ and 16.7 m were used to resolve the DO movement in the inner surf zone. Five pairs at $x = 17.8, 18.1, 18.4, 18.7,$ and 19.0 m represented the DO movement in the swash zone of rapid cross-shore variability. The approximate boundary locations of the four zones including the berm zone in front of the vertical wall are depicted in Figure 2.3a. The SWL shoreline of $z = 0$ was located at $x = 18$ m in the E test series. DOs were placed in pairs at $y = -0.3$ and 0.3 m (Figures 2.3b and 2.3c) to examine the alongshore variability of DO movement. The locations of each DO were measured by the laser line scanner before the test. The laser measurement was displayed on the bathymetric contour (Figure 2.3d) and the 3-D surface plot (Figure 2.3e-f). Dowels were placed closely next to each DO in order to create an elevation difference for the laser measurement.

For the EG test, the beach profiles of EG5, EG10, and EG20 were measured by the laser line scanner after draining water at the end of 5, 10, and 20 runs. After each 400-s run, the locations of the 20 DOs were searched on the sand surface despite occasional difficulty to locate some DOs under the SWL. The laser line scanner was

used to measure the exact location of each DO after lowering the water level to facilitate the DO search. The beach profile changes were less than 1 cm during the EG test and the beach profile was allowed to evolve slightly. On the other hand, the 20 DOs appeared to have settled at their destinations after EG10. The 20 DOs were reinstalled at their initial locations of EG0 on the slightly evolved profile of EG10. The DO movements during EG0-EG10 and EG10-EG20 with the DO resetting after EG10 were compared to examine the repeatability of the DO movements.

Table 2.3 Sequence of six tests on near Equilibrium (E) beach and Nourished (N) foreshore consisting of 100 runs with each run lasting 400s

Test	Profile	DO	Run Number of Profile Measurement
EG	E	G	EG 0, 5, 10*, and 20
EL	E	L	EL 0, 10*, and 20
ES	E	S	ES 0, 5*, and 10
NG	N	G	NG 0, 10, and 20
NL	N	L	NL 0, 10, and 20
NS	N	S	NS 0, 5, and 10

*20 particles reached their destinations after 10(5) runs for EG and EL tests (ES test) and were placed back at their initial locations after 10(5) runs in order to examine the degree of repeatability of the 20 particle destinations.

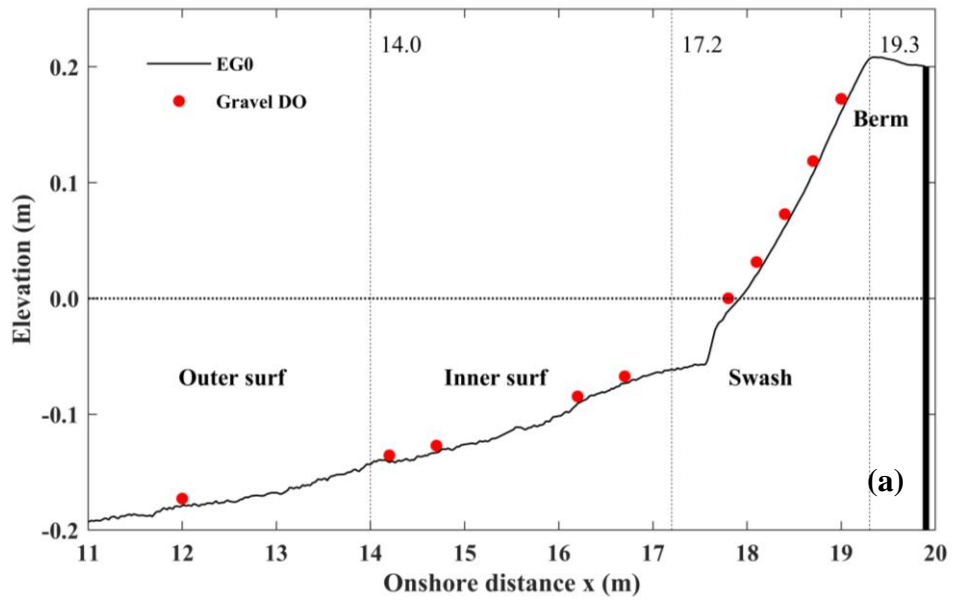


Figure 2.3 Initial cross-shore locations of 20 gravel DOs (a), alongshore locations in pair at $y = -0.3$ and 0.3 m (b)-(c), on equilibrium sand beach profile in Test EG.

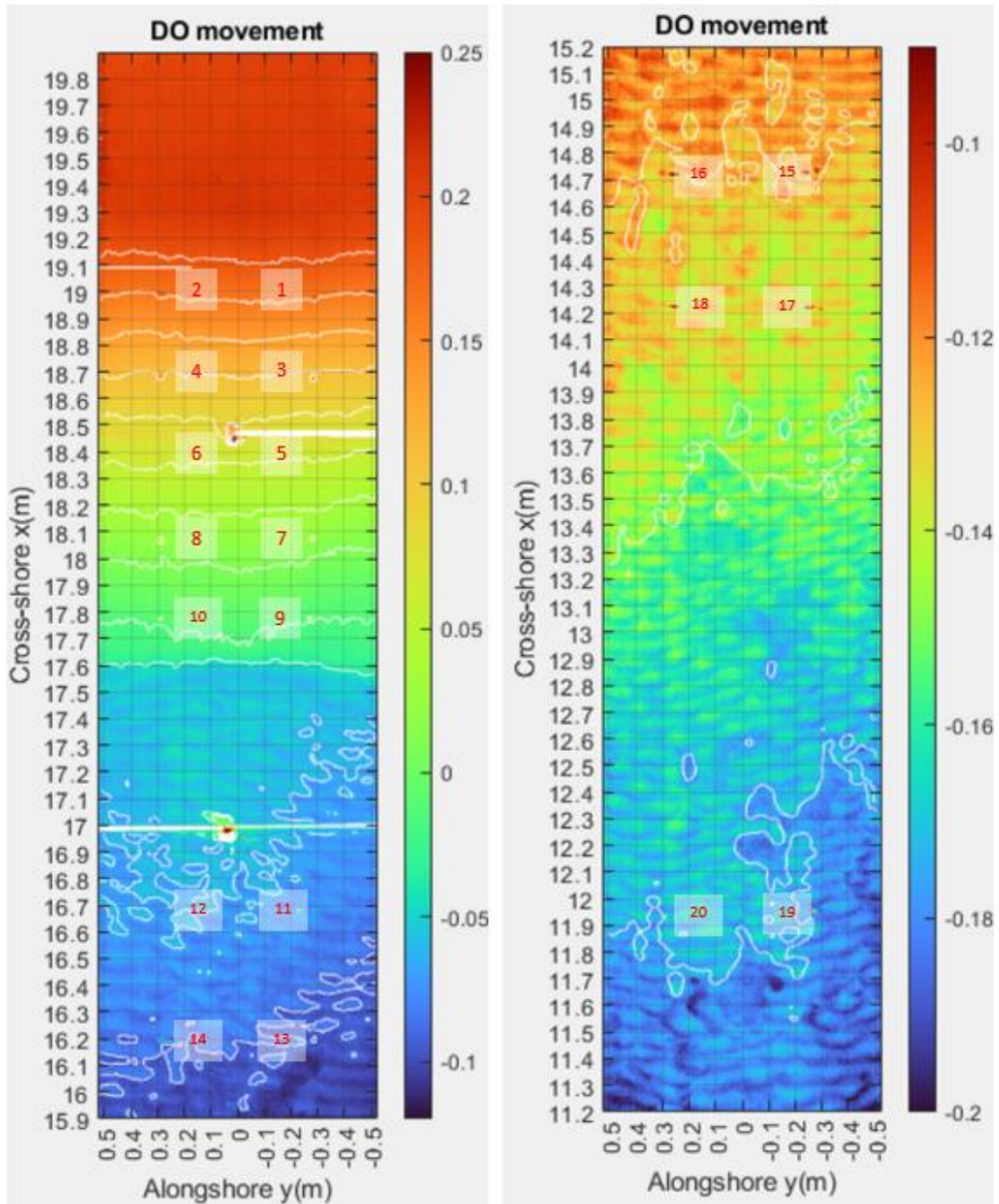


Figure 2.3 Bathymetric contour measured by laser line scanner displaying initial DO locations before Test EG (d).

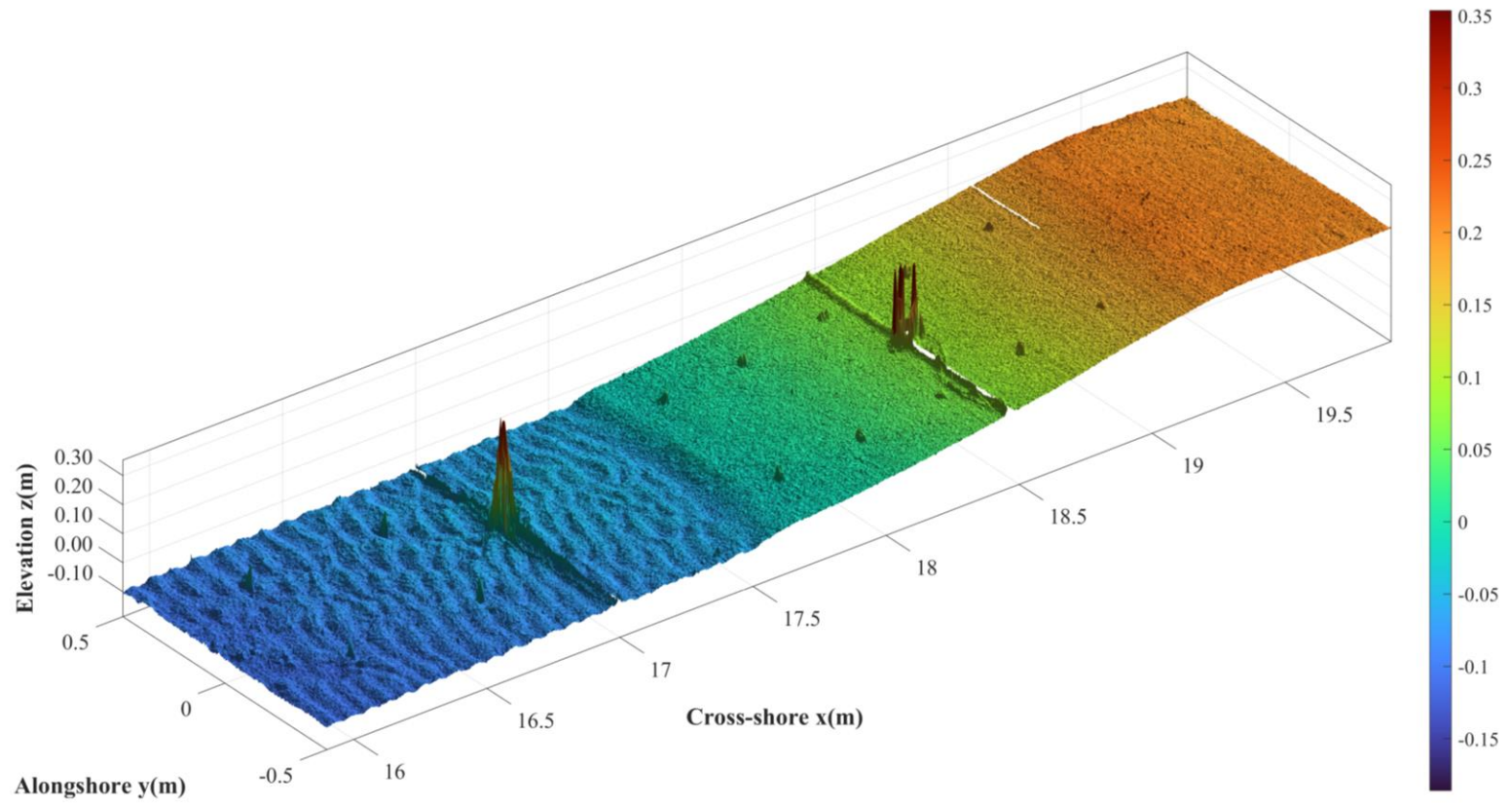


Figure 2.3 Surface plot displaying initial DO locations (with spikes at the locations of WG7 and WG8) in inner surf zone and foreshore before Test EG (e).

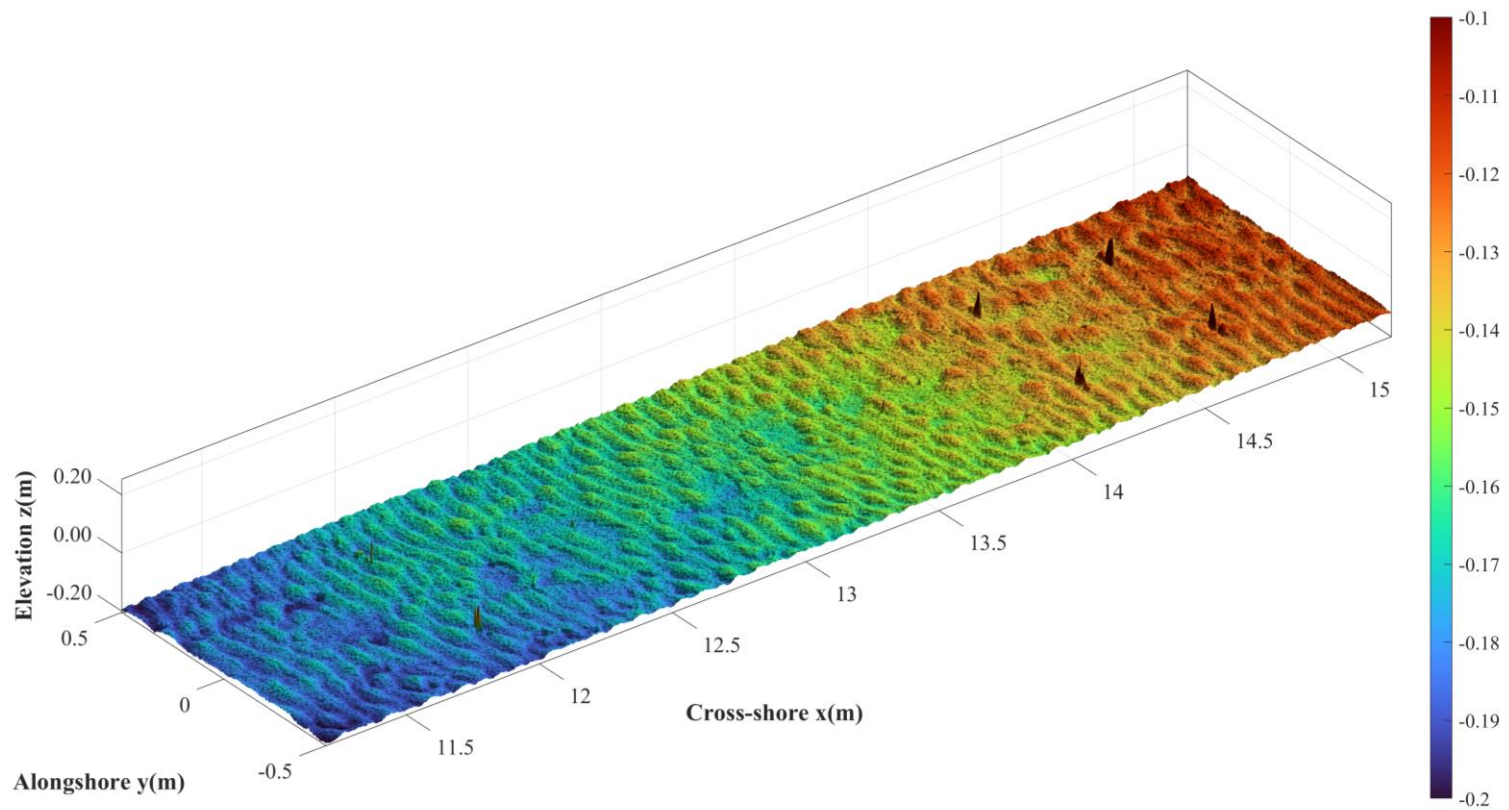


Figure 2.3 Surface plot displaying initial DO locations in inner and outer surf zones before Test EG (f).

The final profile EG20 in the EG test was taken as the initial profile EL0 in the EL test. The gravel DOs were replaced by the large (L) plastics DOs in the EL test. Figure 2.4a-e displays the initial cross-shore and alongshore locations of the 20 L DOs identical to those in Figure 2.3 in order to compare the movement differences between the L and G DOs. The profile EL5 was not measured because of the little change in profile evolution, and hence, only the profiles EL10 and EL20 were measured in the EL test. The L DOs after EL10 were reset to examine the repeatability of the L DO displacements during 10 runs.



Figure 2.4 Initial cross-shore locations of 20 large plastic DOs (with dowels placed for laser measurement) and alongshore locations in pair at $y = -0.3$ and 0.3 m (a)-(b), on equilibrium sand beach profile in Test EL.

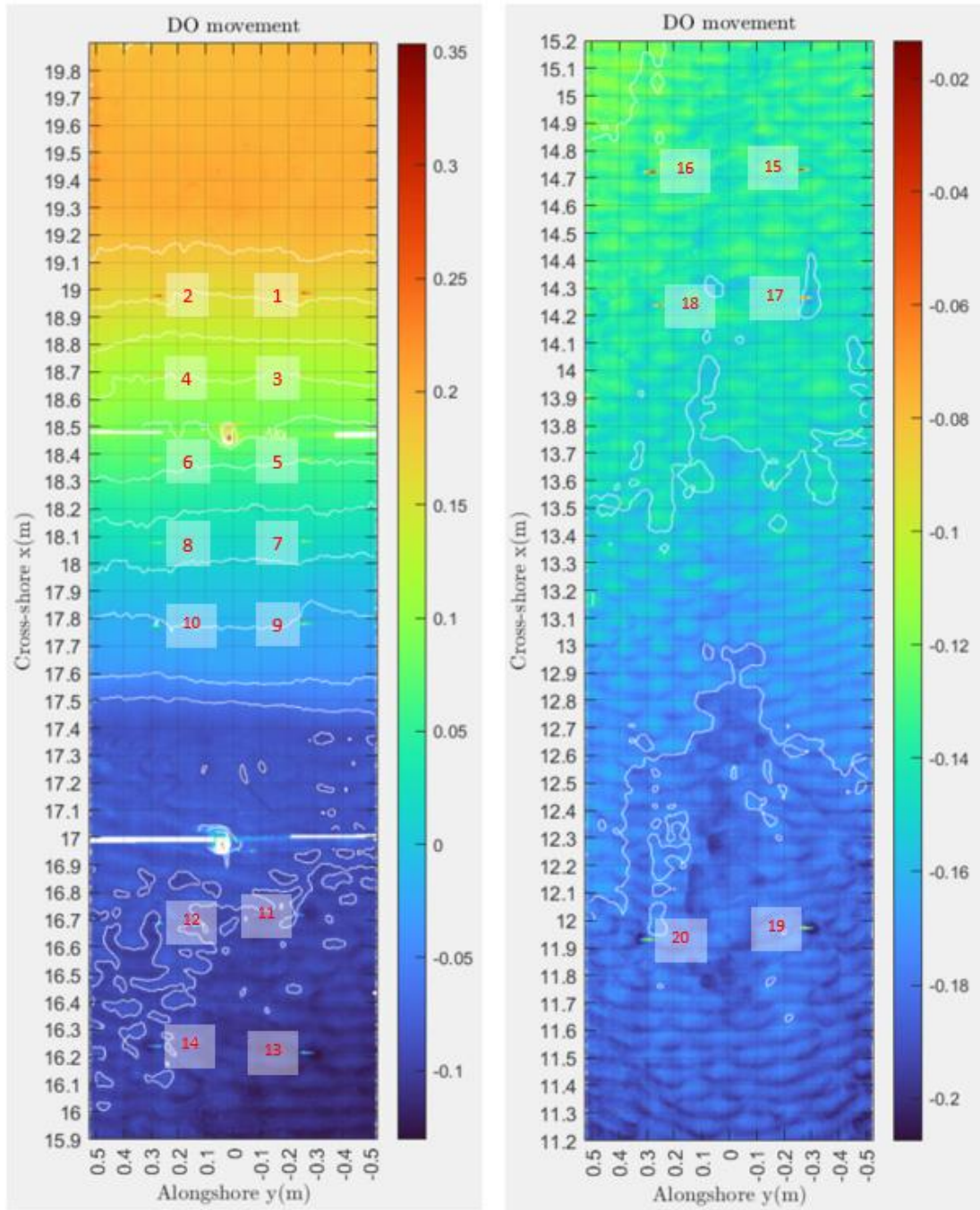


Figure 2.4 Bathymetric contour measured by laser line scanner displaying initial DO locations before Test EL (c).

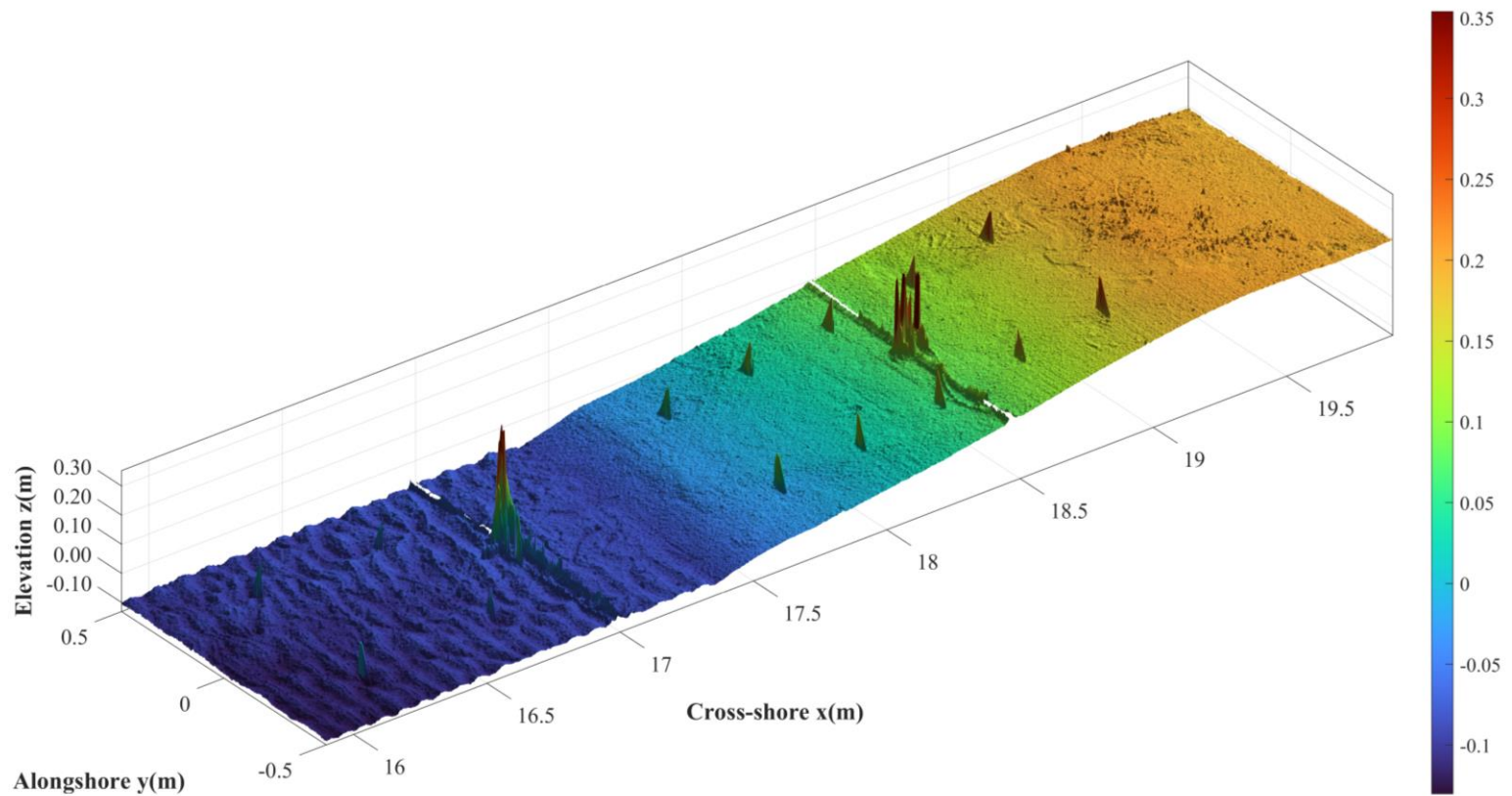


Figure 2.4 Surface plot displaying initial DO locations in inner surf zone and foreshore before Test EL (d).

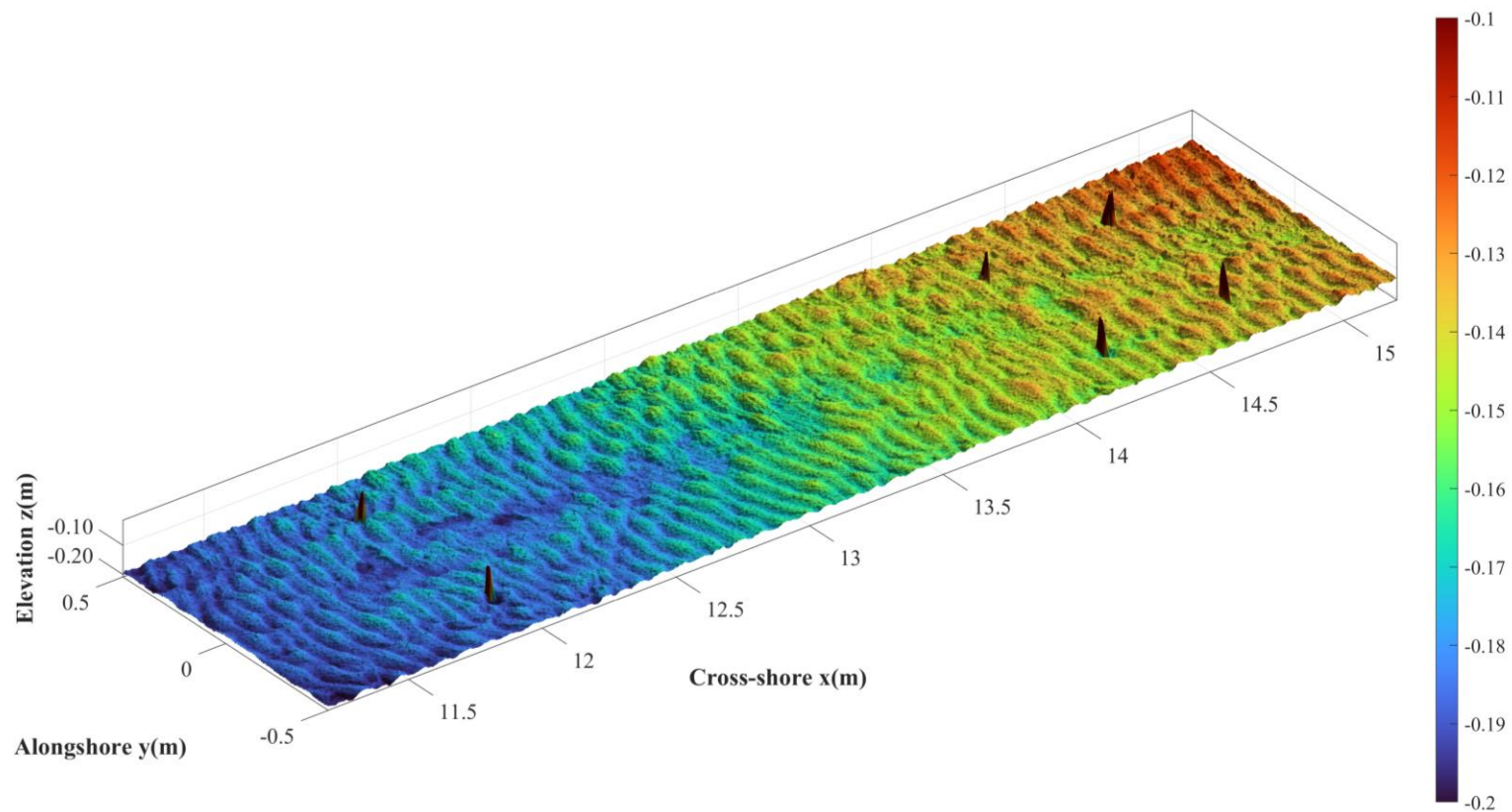


Figure 2.4 Surface plot displaying initial DO locations in inner and outer surf zones before Test EL (e).

The initial profile ES0 in the ES test was the final profile EL20 in the EL test. The L DOs were replaced by the small (S) plastics DOs (Figure 2.5a-e). The beach profiles of ES5 and ES10 were measured because the S DOs were more mobile and appeared to have reached their destinations after 5 runs. The S DOs were reset after ES5 and their locations on the profile of ES10 were measured to examine the repeatability of the ES test.

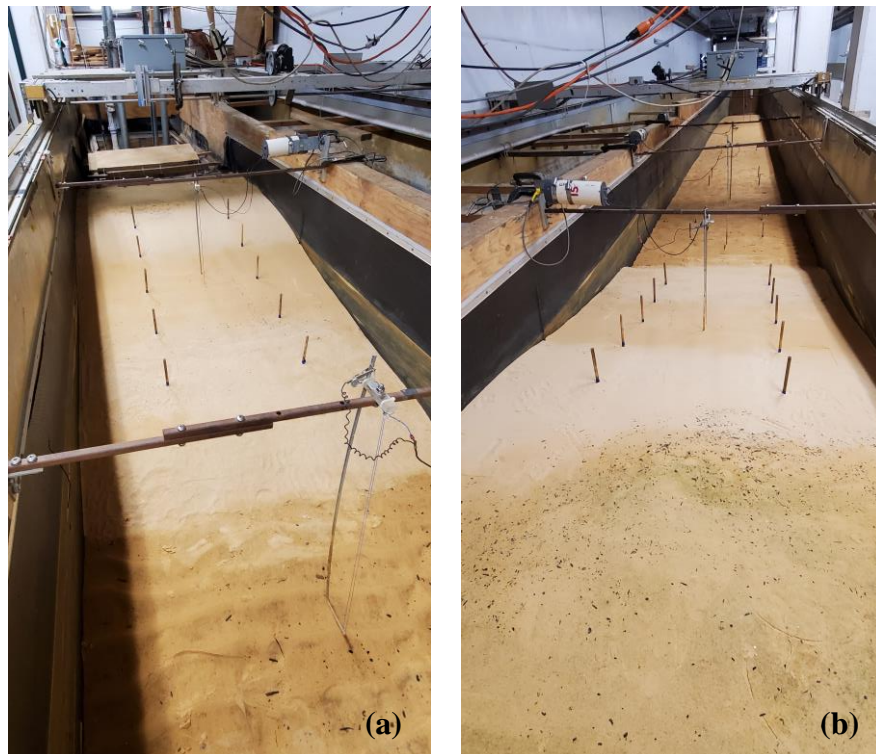


Figure 2.5 Initial cross-shore locations of 20 small plastic DOs (with dowels placed for laser measurement) and alongshore locations in pair at $y = -0.3$ and 0.3 m (a)-(b), on equilibrium sand beach profile in Test ES.

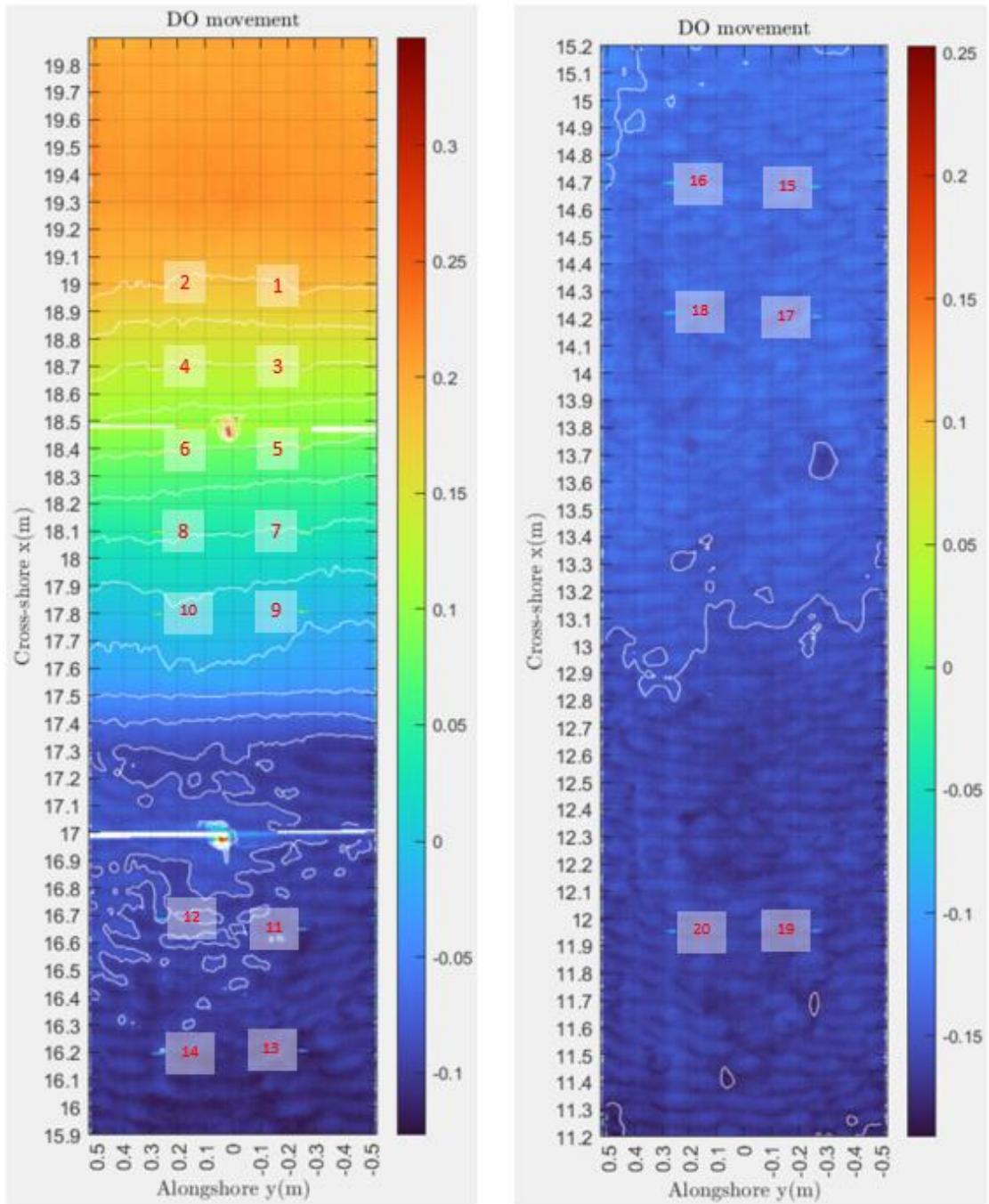


Figure 2.5 Bathymetric contour measured by laser line scanner displaying initial DO locations before Test ES (c).

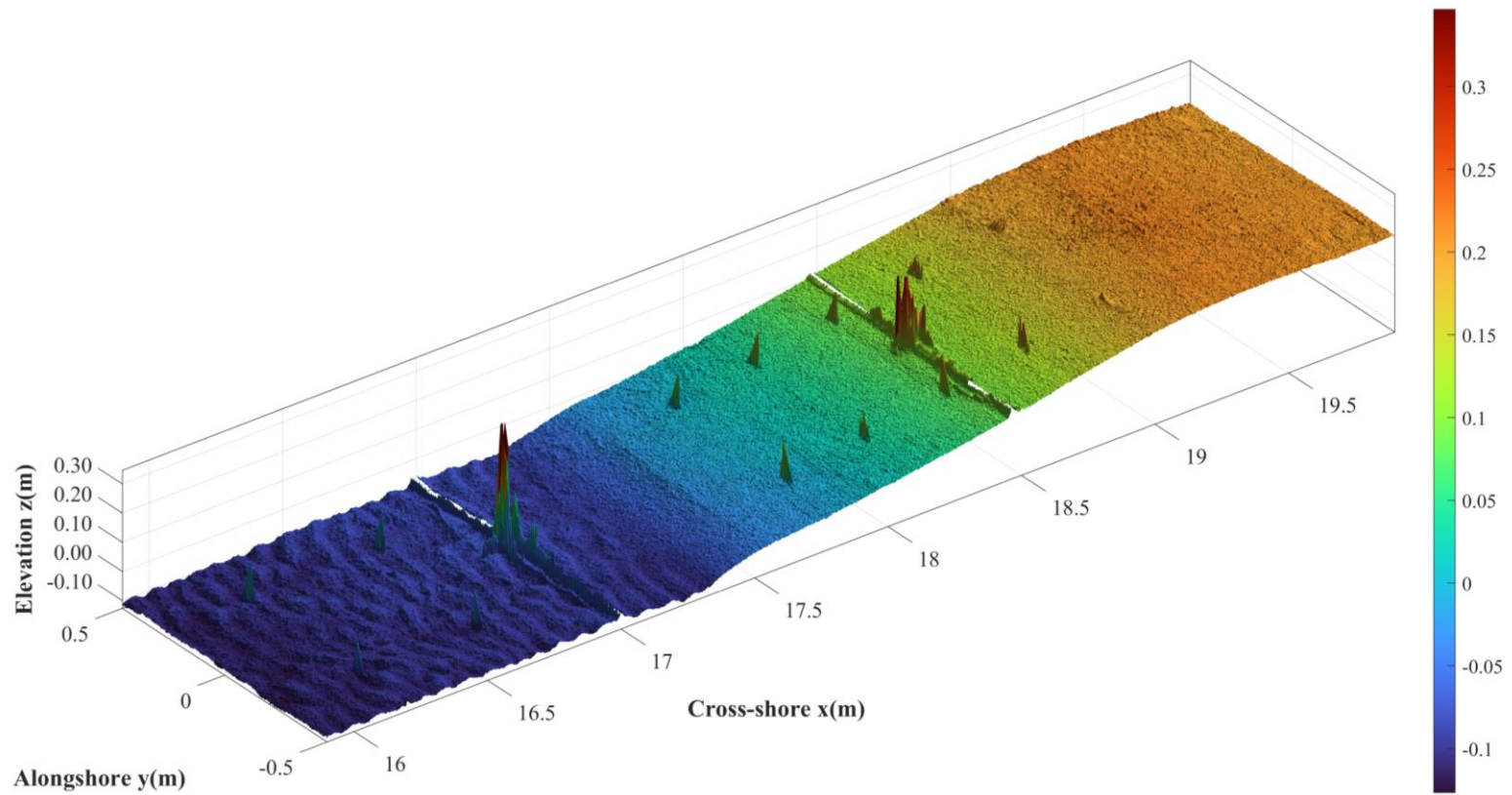


Figure 2.5 Surface plot displaying initial DO locations in inner surf zone and foreshore before Test ES (d).

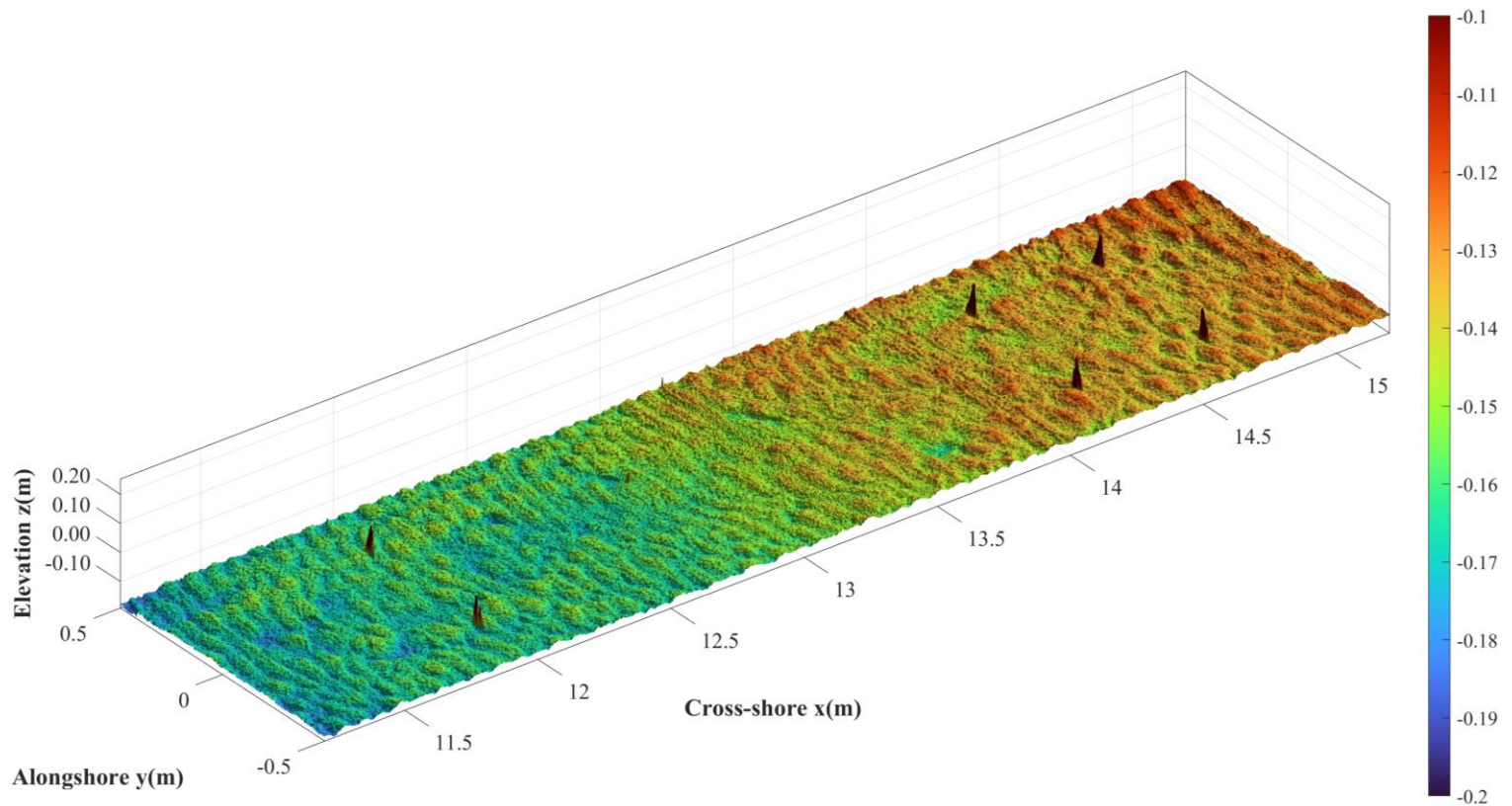


Figure 2.5 Surface plot displaying initial DO locations in inner and outer surf zones before Test ES (e).

Throughout the entire series (50 runs) of the E tests (Table 2.3), none of the DOs were buried under the sand. Wave uprush and downrush in the swash zone created scour holes around some of the 10 gravel DOs in the swash zone on the slope of 1/6. Local scour around a heavy object was studied experimentally to predict the burial depth of sea mines (e.g., Demir and Garcia 2007). The scour hole depth underneath the gravel DO of 2.0-cm diameter was of the order of 1 cm in the swash zone but was almost zero in the other zones. The large and small plastics DOs with the density of 1.38 g/cm^3 (Table 2.2) were more mobile and remained on the sand surface without any presence of local scour. In Chapter 3, beach profile changes, hydrodynamic conditions, and movement of DOs were discussed more in detail.

The N test series were performed on a steeper foreshore above the SWL to examine the effect of erosion and deposition on the DO movement. Figure 2.6 shows the initial profile NG0 in the NG test. The initial profiles NL0 and NS0 were rebuilt nearly the same as that of NG0. The seaward edge of the berm at the elevation of $z = 0.2 \text{ m}$ was located at $x = 18.6 \text{ m}$ at the start of the NG, NL, and NS tests. The SWL shoreline was observed initially at $x = 18 \text{ m}$ as was the case with the EG test (Figure 2.3a). The slope of the nourished foreshore was 1/3 as opposed to the slope 1/6 of the equilibrium tests. The beach profile below the SWL was the same as that of ES10 at the end of the E test series. The initial cross-shore and alongshore locations of the 10 pairs of the DOs were kept the same in the six tests. The number of the DO pairs was one and four in the outer and inner surf zones, respectively. Three pairs were placed on the steep foreshore which was presumed to be eroded. Two pairs on the wider berm (relative to the equilibrium profile berm) were expected to be affected by the foreshore erosion. The beach profiles were measured after 10 and 20 runs in the NG and NL tests and after 5

and 10 runs in the NS test as indicated in Table 2.3. The N test series consisted of 50 runs. The DO locations were measured visually after each run and painstakingly when the water level was lowered for the beach profile measurement by the laser line scanner. The DOs were not reset in the N test series of noticeable profile changes in order to examine the effect of profile changes on the DO movement. Figures 2.6-2.8 show the initial DO locations and the corresponding surface plots from the laser line scanner before the NG, NL, and NS tests, respectively.

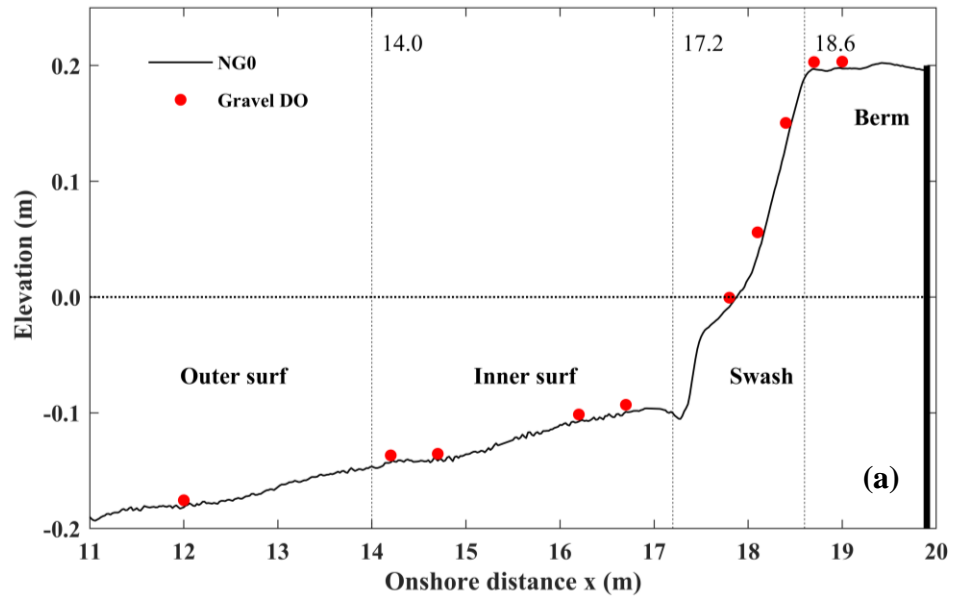


Figure 2.6 Initial cross-shore locations of 20 gravel DOs (a) and alongshore locations in pair at $y = -0.3$ and 0.3 m (b)-(c) on nourished foreshore profile in Test NG.

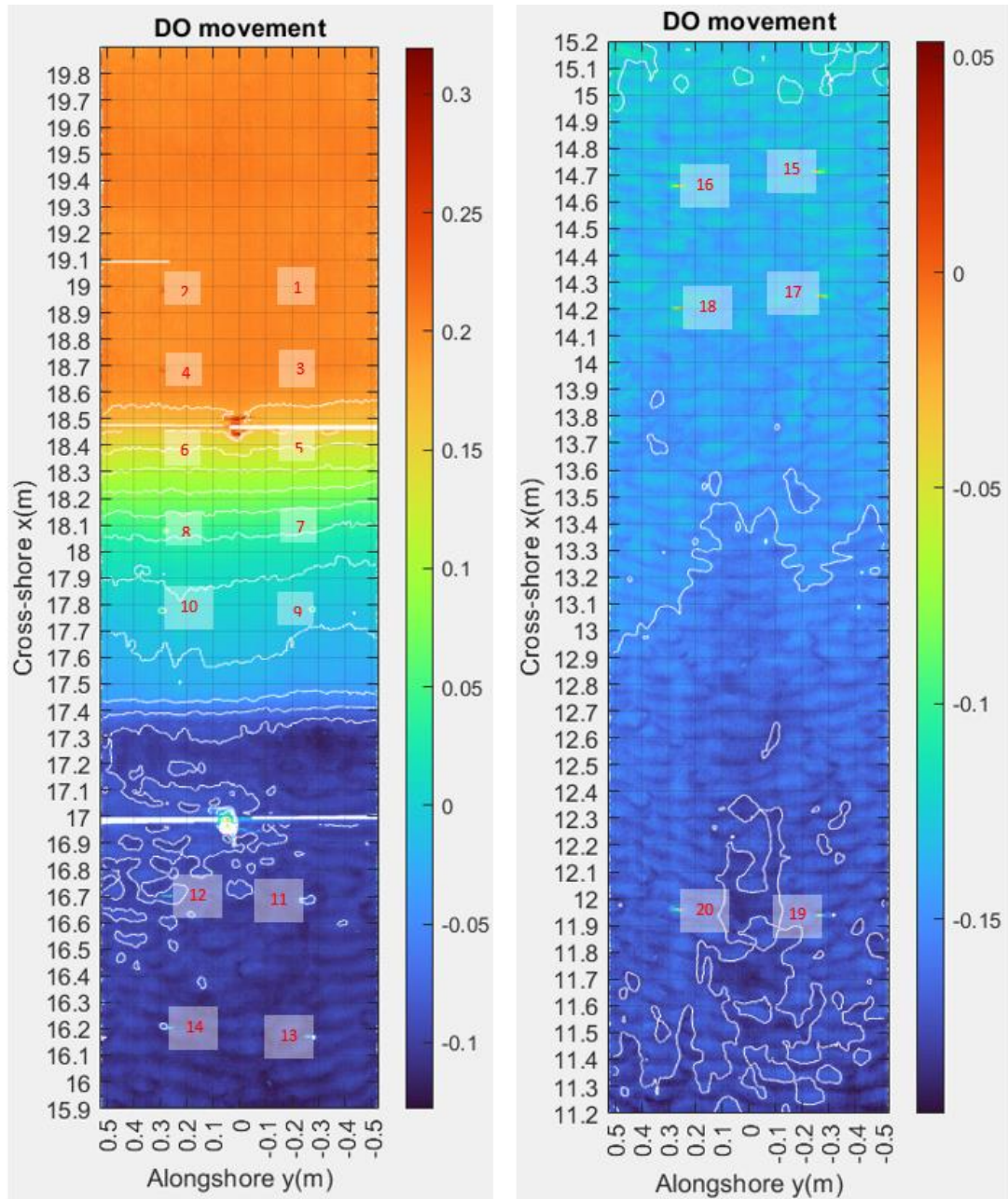


Figure 2.6 Bathymetric contour measured by laser line scanner displaying initial DO locations before Test NG (d).

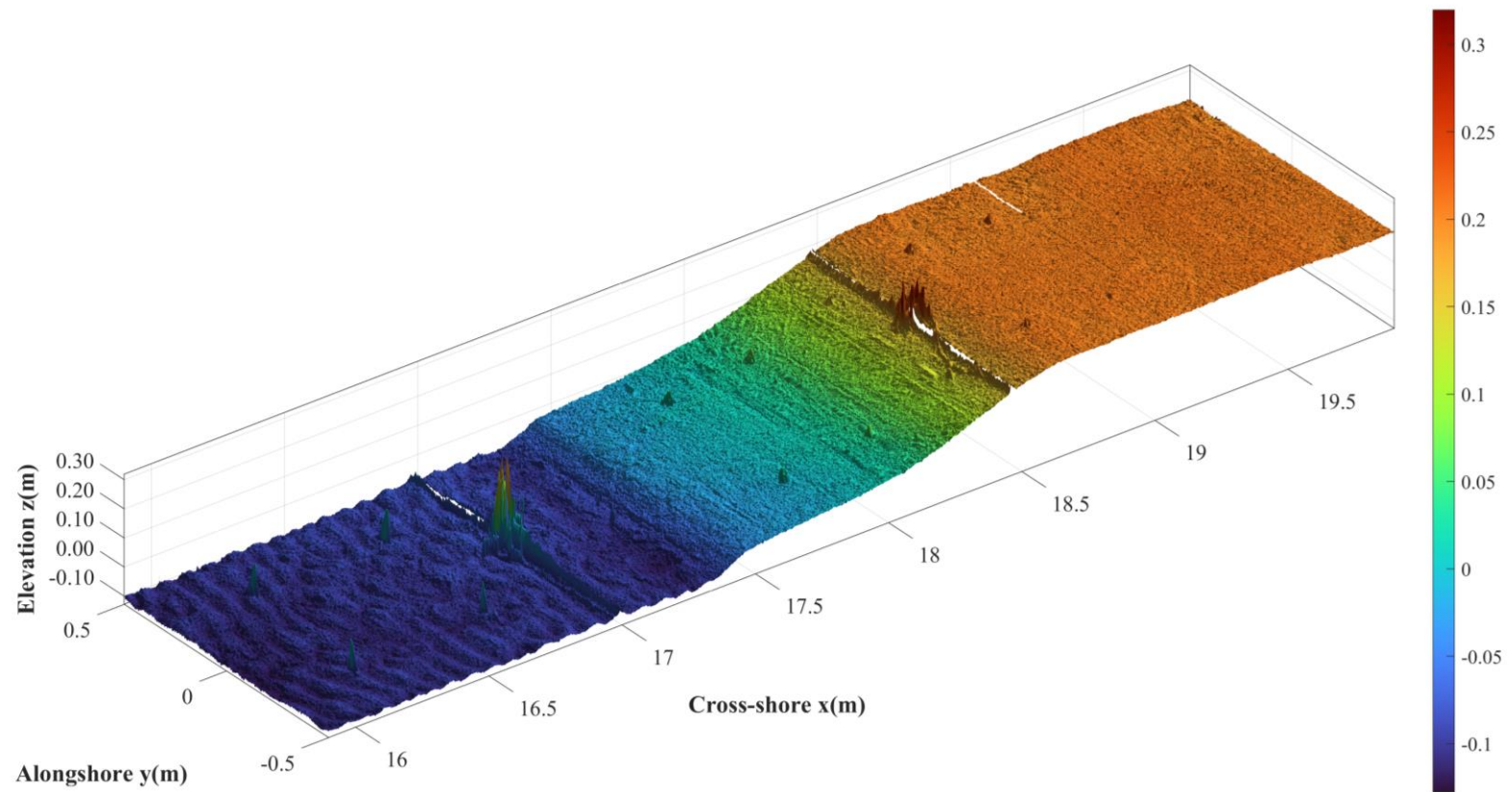


Figure 2.6 Surface plot displaying initial DO locations in inner surf zone and foreshore before Test NG (e).

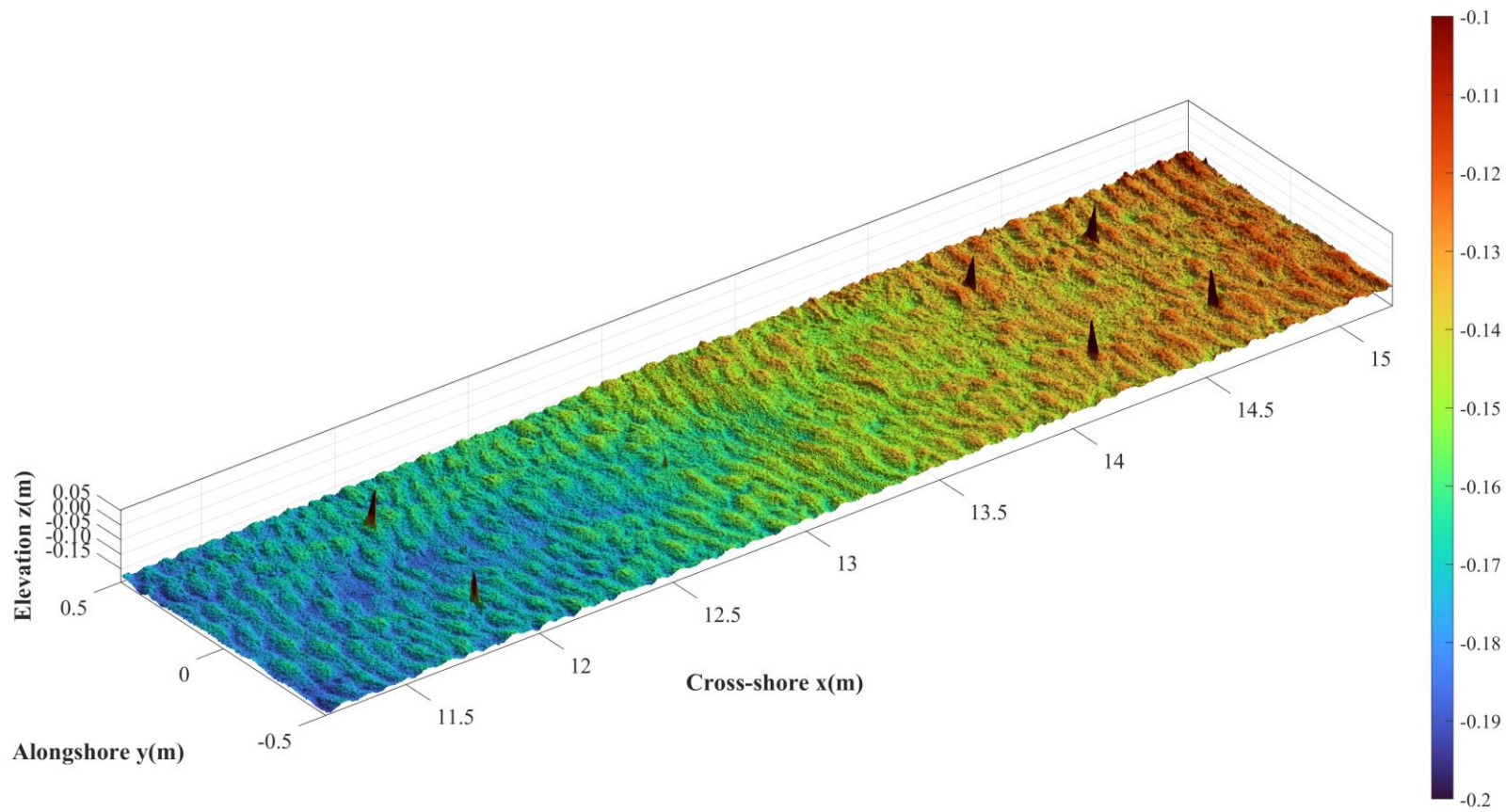


Figure 2.6 Surface plot displaying initial DO locations in inner and outer surf zones before Test NG (f).



Figure 2.7 Initial cross-shore locations of 20 large plastic DOs and alongshore locations in pair at $y = -0.3$ and 0.3 m (with dowels placed for laser measurement) (a)-(b) on nourished foreshore profile in Test NL.

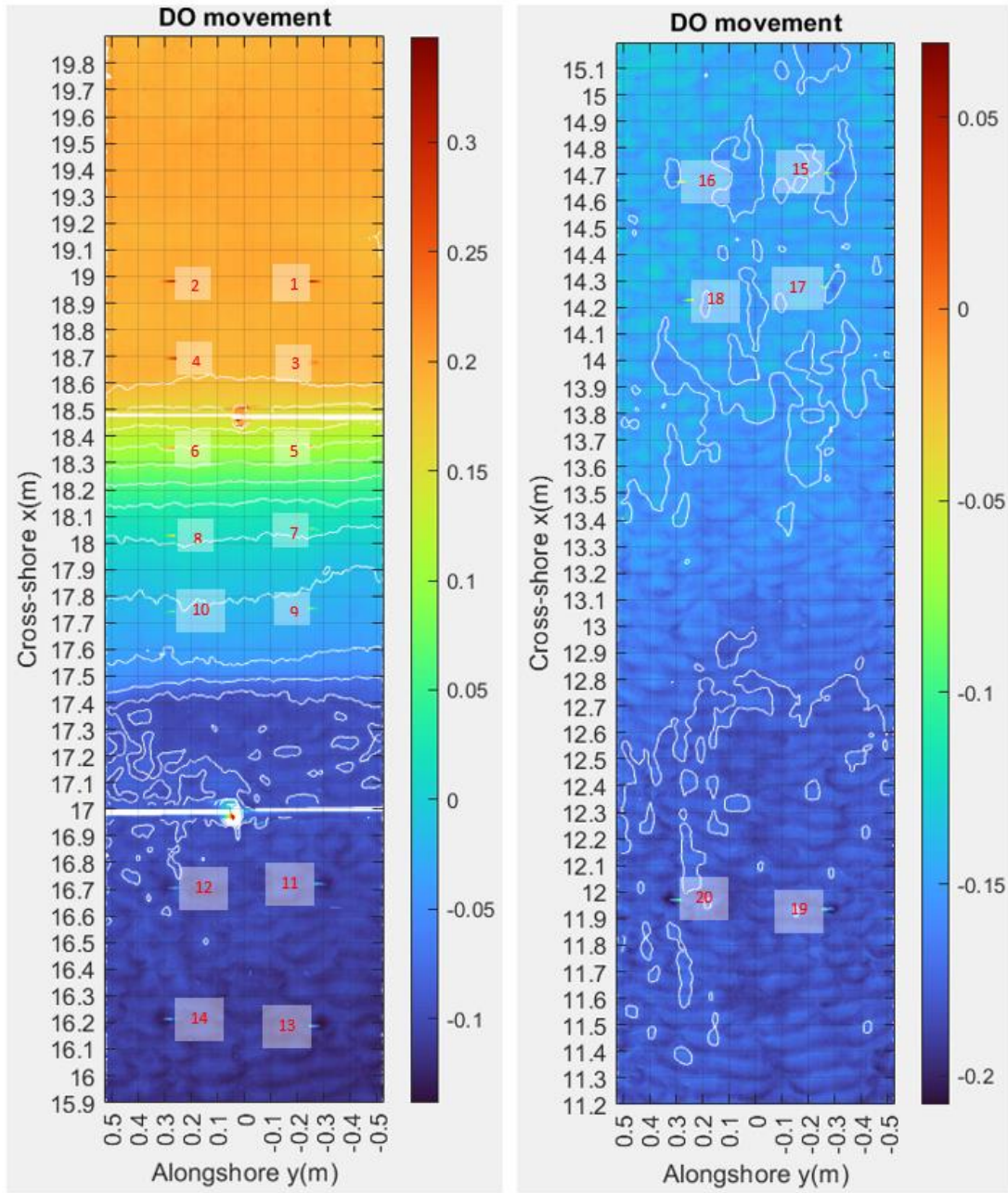


Figure 2.7 Bathymetric contour measured by laser line scanner displaying initial DO locations before Test NL (c).

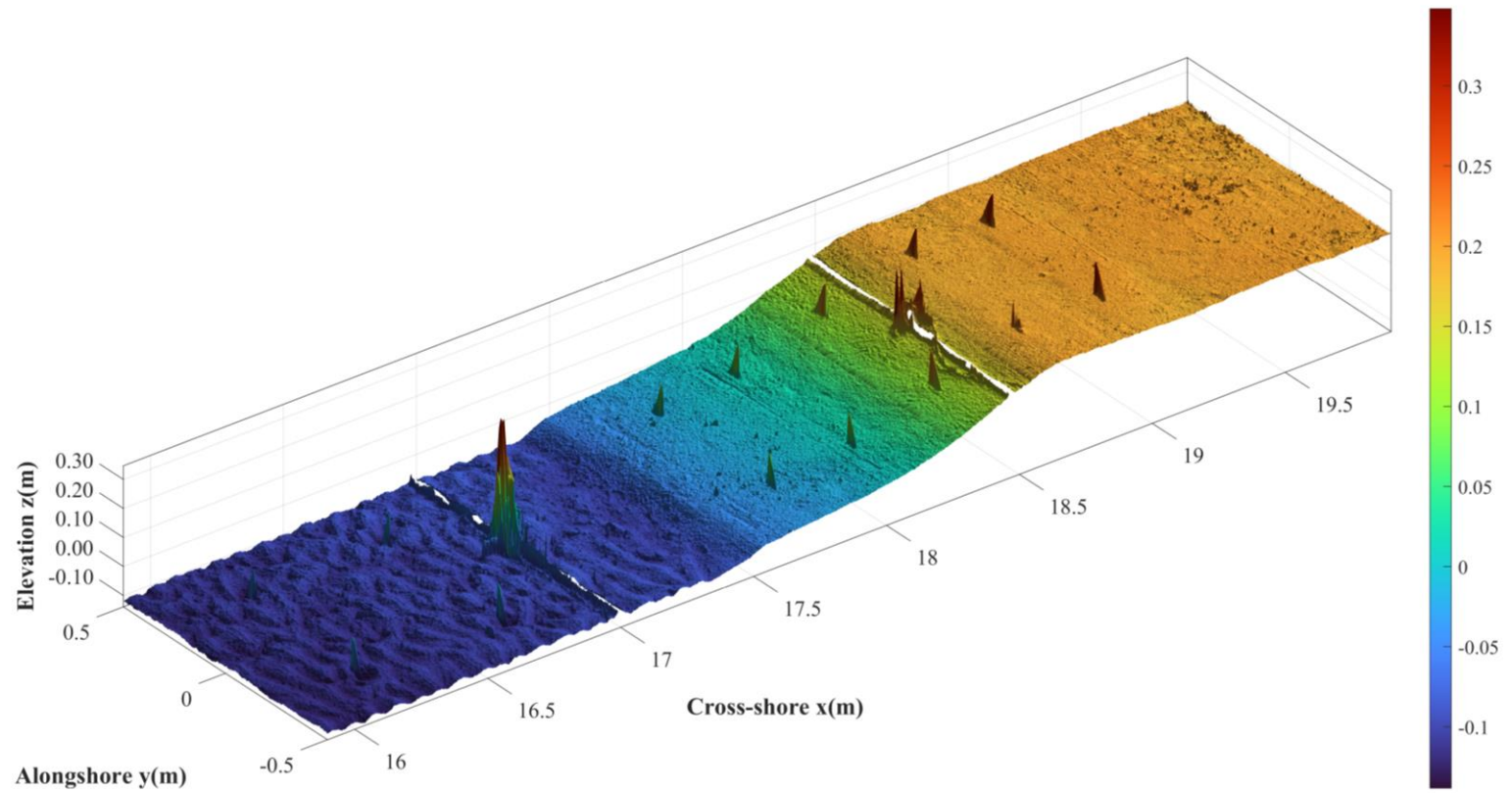


Figure 2.7 Surface plot displaying initial DO locations in inner surf zone and foreshore before Test NL (d).

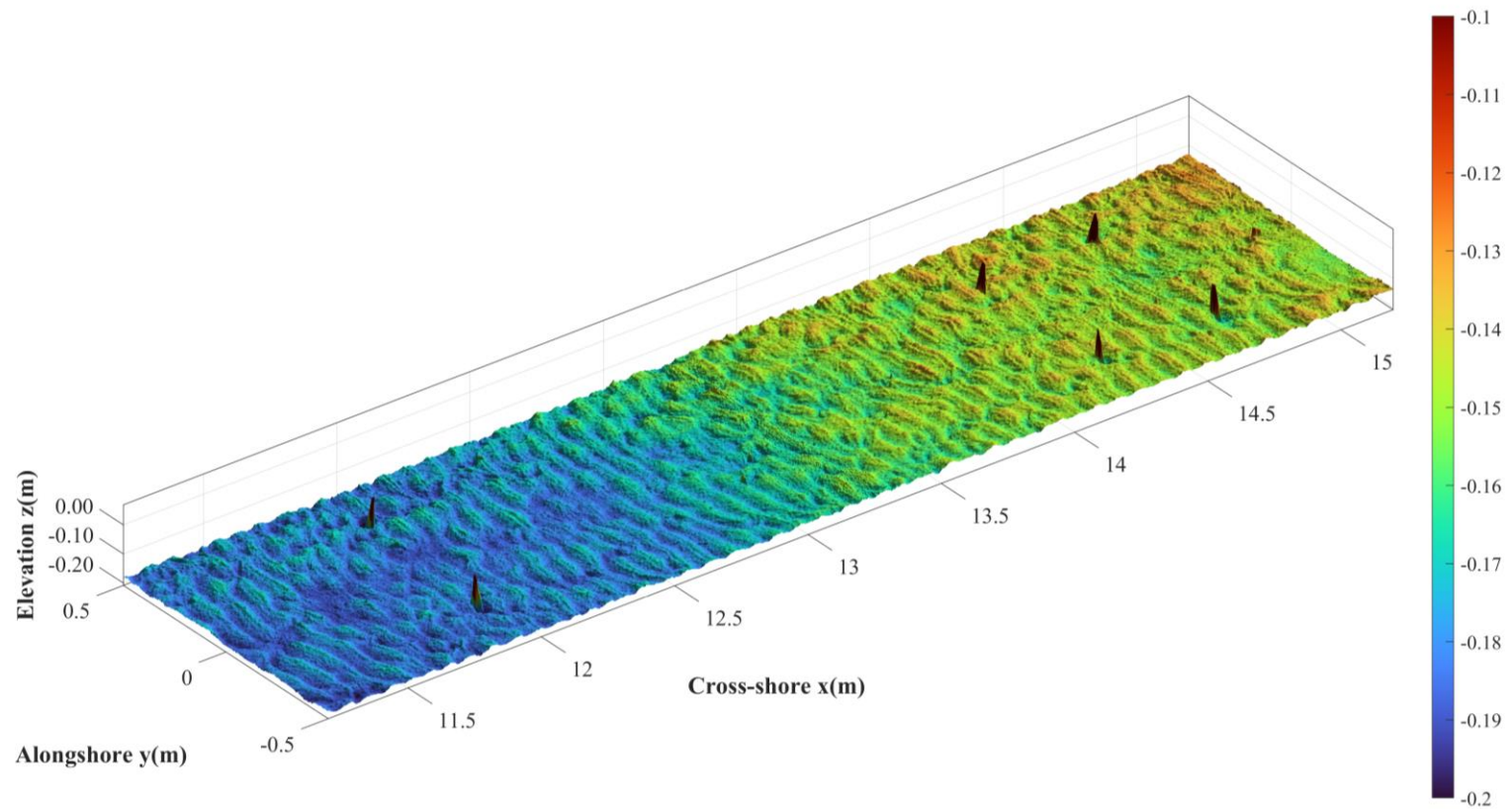


Figure 2.7 Surface plot displaying initial DO locations in inner and outer surf zones before Test NL (e).

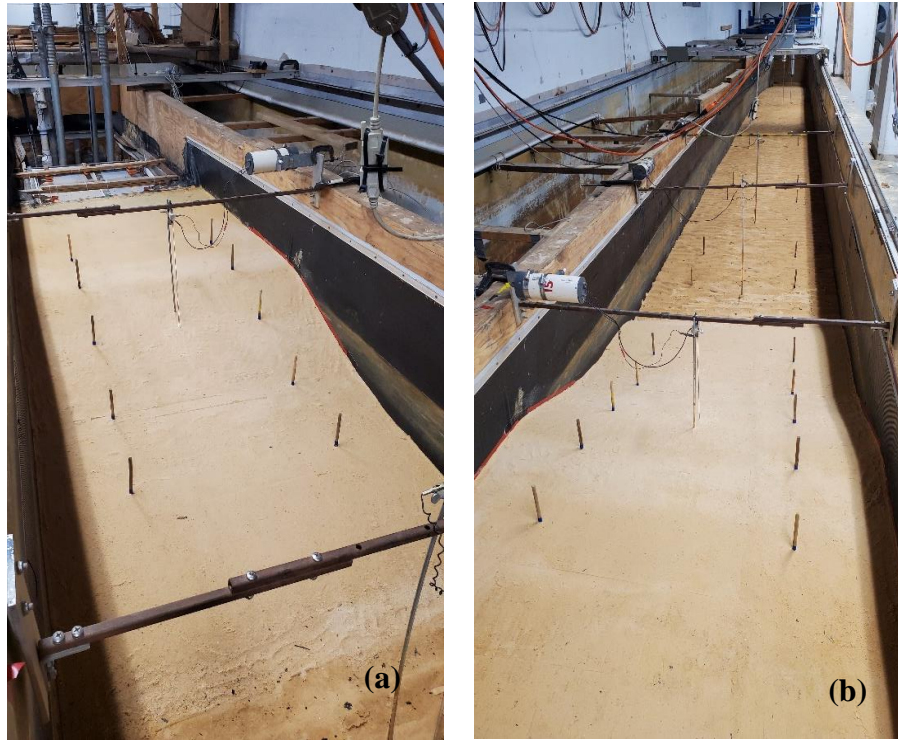


Figure 2.8 Initial cross-shore locations of 20 small plastic DOs and alongshore locations in pair at $y = -0.3$ and 0.3 m (with dowels placed for laser measurement) (a)-(b) on nourished foreshore profile in Test NS.

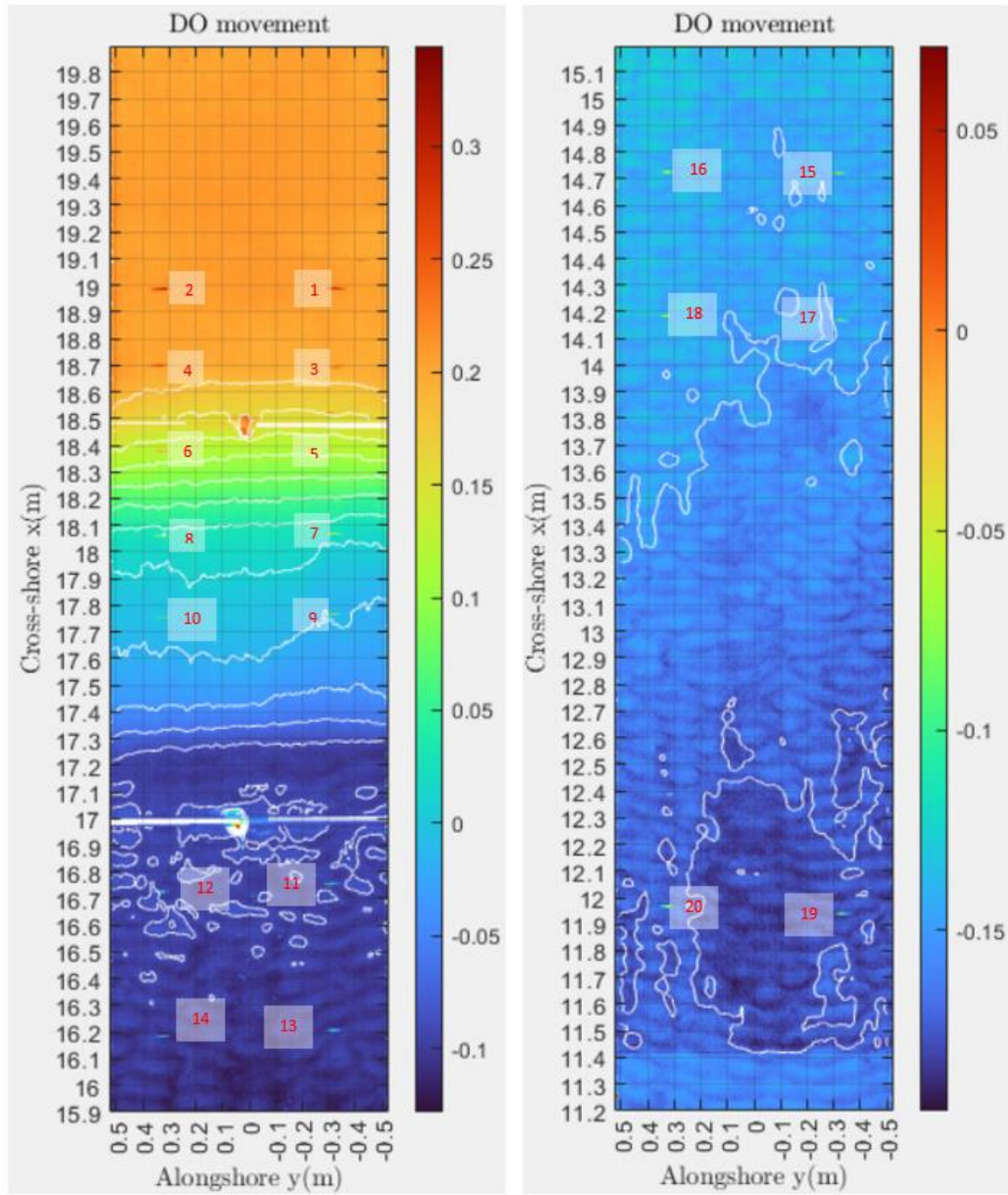


Figure 2.8 Bathymetric contour measured by laser line scanner displaying initial DO locations before Test NS (c).

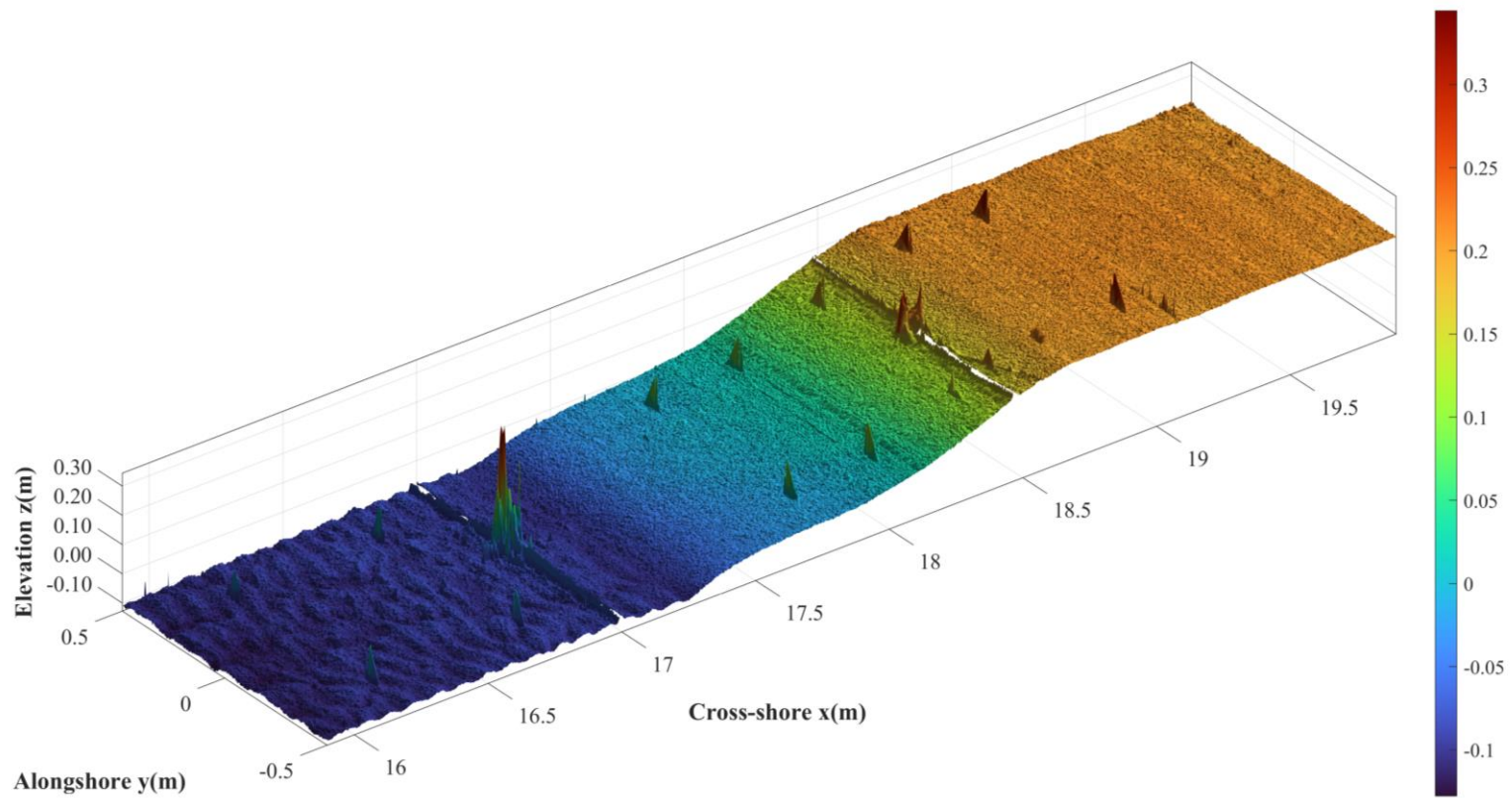


Figure 2.8 Surface plot displaying initial DO locations in inner surf zone and foreshore before Test NS (d).

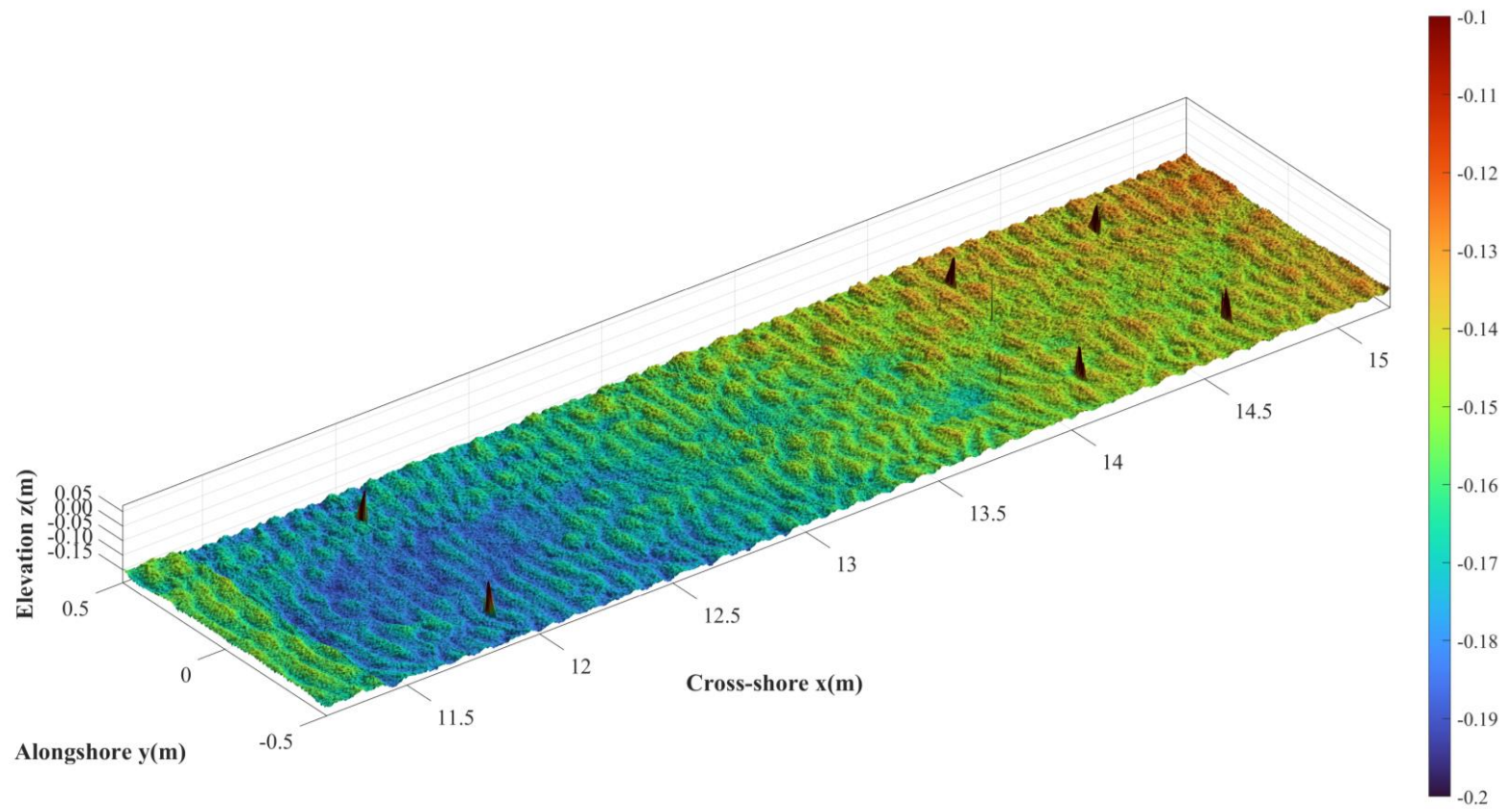


Figure 2.8 Surface plot displaying initial DO locations in inner and outer surf zones before Test NS (e)

Chapter 3

Data Analysis

The experimental data were analyzed and presented in this chapter. The analyzed data for all the six tests were used to quantify the cross-shore wave transformation, beach profile evolution, and DO trajectories.

3.1 Hydrodynamics

The time series obtained by the eight wave gauges and three velocimeters in Figure 2.1 were analyzed for each of the 100 runs from the six tests. The incident wave characteristics and reflection coefficient were estimated using the measured time series at the locations of $x = 0.0, 0.25,$ and 0.95 m of WG1, WG2, and WG3, respectively, as listed in Table 3.1-3.6, where H_{mo} = spectral significant wave height, H_{rms} = root-mean-square wave height, H_s = significant wave height, T_p = spectral wave period, T_s = significant wave period, and R = wave reflection coefficient. The spectral significant wave height H_{mo} and peak period T_p of the incident waves at $x = 0.0$ m were 0.2 m and 2.6 s, respectively. The wave reflection coefficient was defined as the ratio between the values of H_{mo} for the reflected and incident waves. The reflection coefficient was 0.15 for the E test series and 0.16 for the N test series with the steeper foreshore. WG4 ($x = 8.3$ m) and WG5 ($x = 12.9$ m) were located in the outer surf zone of large wave breaking. WG6 ($x = 15.5$ m) and WG7 ($x = 17.1$ m) were situated in the inner surf zone of broken waves. WG8 ($x = 18.6$ m) was in the swash zone in Figure 2.3a and at the seaward edge of the berm in Figure 2.6a.

The mean $\bar{\eta}$ and standard deviation σ_{η} of the free surface elevation η above SWL measured at the eight wave gauges from each run of the six tests (EG1-EG20, EL1-EL20, ES1-ES10, NG1-NG20, NL1-NL20, and NS1-NS10) are presented in Table 3.7-3.18, respectively. The mean \bar{U} and standard deviation σ_U of the cross-shore velocity U measured by ADV, RV, and BV are tabulated in Table 3.19-3.24. The measured alongshore and vertical velocities were relatively small compared to the cross-shore horizontal velocities. The values of $\bar{\eta}$, σ_{η} , \bar{U} and σ_U were analyzed to examine the cross-shore wave transformation from offshore to the seaward edge of the berm.

Table 3.1 Incident wave characteristics, Test EG.

Run	H_{mo} (cm)	H_{rms} (cm)	H_s (cm)	T_p (s)	T_s (s)	R
EG1	18.99	13.43	18.29	2.62	2.14	0.146
EG2	19.21	13.58	18.46	2.62	2.12	0.149
EG3	19.29	13.64	18.82	2.62	2.14	0.162
EG4	19.15	13.54	18.65	2.62	2.16	0.152
EG5	19.11	13.51	18.47	2.62	2.17	0.149
EG6	19.98	14.12	19.38	2.62	2.16	0.152
EG7	20.23	14.31	19.41	2.62	2.12	0.146
EG8	20.21	14.29	19.50	2.62	2.14	0.149
EG9	20.16	14.26	19.54	2.62	2.16	0.150
EG10	20.12	14.23	19.34	2.62	2.11	0.150
EG11	20.18	14.27	19.51	2.62	2.17	0.153
EG12	20.41	14.43	19.68	2.62	2.13	0.150
EG13	20.33	14.37	19.61	2.62	2.14	0.151
EG14	20.33	14.37	19.79	2.62	2.16	0.148
EG15	20.26	14.33	19.60	2.62	2.13	0.151
EG16	20.60	14.56	19.85	2.62	2.13	0.153
EG17	20.42	14.44	19.71	2.62	2.15	0.148
EG18	20.30	14.36	19.62	2.62	2.15	0.149
EG19	20.26	14.33	19.58	2.62	2.14	0.148
EG20	20.32	14.37	19.59	2.62	2.13	0.152
Average	19.99	14.14	19.32	2.62	2.14	0.150

Table 3.2 Incident wave characteristics, Test EL.

Run	H_{mo} (cm)	H_{rms} (cm)	H_s (cm)	T_p (s)	T_s (s)	R
EL1	20.04	14.17	19.44	2.62	2.15	0.151
EL2	20.24	14.31	19.43	2.62	2.12	0.151
EL3	20.10	14.22	19.29	2.62	2.13	0.147
EL4	20.10	14.21	19.39	2.62	2.14	0.151
EL5	20.07	14.19	19.42	2.62	2.13	0.147
EL6	20.23	14.30	19.59	2.62	2.11	0.151
EL7	20.33	14.38	19.77	2.62	2.13	0.149
EL8	20.33	14.37	19.76	2.62	2.15	0.147
EL9	20.21	14.29	19.48	2.62	2.14	0.149
EL10	20.17	14.26	19.52	2.62	2.15	0.148
EL11	20.29	14.34	19.61	2.62	2.17	0.152
EL12	20.74	14.67	20.01	2.62	2.11	0.149
EL13	20.59	14.56	19.87	2.62	2.16	0.156
EL14	20.45	14.46	19.77	2.62	2.14	0.152
EL15	20.42	14.44	19.80	2.62	2.15	0.152
EL16	20.28	14.34	19.65	2.62	2.14	0.150
EL17	20.51	14.50	19.86	2.62	2.14	0.152
EL18	20.45	14.46	19.74	2.62	2.13	0.152
EL19	20.42	14.44	19.69	2.62	2.14	0.149
EL20	20.50	14.49	19.77	2.62	2.14	0.155
Average	20.32	14.37	19.64	2.62	2.14	0.151

Table 3.3 Incident wave characteristics, Test ES.

Run	H_{mo} (cm)	H_{rms} (cm)	H_s (cm)	T_p (s)	T_s (s)	R
ES1	20.19	14.28	19.62	2.62	2.14	0.156
ES2	20.42	14.44	19.80	2.62	2.14	0.156
ES3	20.44	14.46	19.73	2.62	2.12	0.151
ES4	20.43	14.45	19.75	2.62	2.16	0.153
ES5	20.41	14.43	19.68	2.62	2.14	0.151
ES6	20.35	14.39	19.67	2.62	2.14	0.151
ES7	20.51	14.51	19.85	2.62	2.13	0.152
ES8	20.54	14.52	19.89	2.62	2.15	0.151
ES9	20.50	14.50	19.75	2.62	2.13	0.153
ES10	20.37	14.40	19.54	2.62	2.13	0.152
Average	20.42	14.44	19.73	2.62	2.14	0.153

Table 3.4 Incident wave characteristics, Test NG.

Run	H_{mo} (cm)	H_{rms} (cm)	H_s (cm)	T_p (s)	T_s (s)	R
NG1	20.46	14.46	19.97	2.62	2.17	0.175
NG2	20.63	14.58	19.90	2.62	2.13	0.170
NG3	20.42	14.44	19.62	2.62	2.13	0.165
NG4	20.45	14.46	19.84	2.62	2.16	0.167
NG5	20.37	14.40	19.62	2.62	2.15	0.167
NG6	20.69	14.63	20.03	2.62	2.14	0.164
NG7	20.50	14.50	19.76	2.62	2.12	0.164
NG8	20.35	14.39	19.64	2.62	2.14	0.163
NG9	20.12	14.23	19.53	2.62	2.16	0.162
NG10	19.95	14.11	19.14	2.62	2.14	0.160
NG11	19.92	14.08	19.39	2.62	2.19	0.159
NG12	19.91	14.08	19.08	2.62	2.14	0.160
NG13	19.85	14.04	19.07	2.62	2.14	0.163
NG14	19.71	13.94	18.95	2.62	2.15	0.163
NG15	19.66	13.90	19.10	2.62	2.16	0.160
NG16	19.57	13.84	18.83	2.62	2.15	0.164
NG17	19.48	13.77	18.77	2.62	2.13	0.164
NG18	19.33	13.67	18.57	2.62	2.16	0.161
NG19	19.29	13.64	18.63	2.62	2.15	0.161
NG20	19.32	13.66	18.57	2.62	2.15	0.163
Average	20.00	14.14	19.30	2.62	2.15	0.164

Table 3.5 Incident wave characteristics, Test NL.

Run	H_{mo} (cm)	H_{rms} (cm)	H_s (cm)	T_p (s)	T_s (s)	R
NL1	19.52	13.80	18.85	2.62	2.17	0.178
NL2	19.50	13.79	18.75	2.62	2.16	0.172
NL3	19.41	13.72	18.68	2.62	2.19	0.167
NL4	19.82	14.02	19.09	2.62	2.15	0.166
NL5	20.03	14.16	19.34	2.62	2.15	0.165
NL6	19.92	14.08	19.11	2.62	2.17	0.161
NL7	20.20	14.29	19.57	2.62	2.17	0.164
NL8	20.24	14.31	19.61	2.62	2.17	0.166
NL9	20.21	14.29	19.49	2.62	2.18	0.162
NL10	20.11	14.22	19.45	2.62	2.17	0.163
NL11	19.95	14.11	19.47	2.62	2.21	0.169
NL12	20.27	14.33	19.47	2.62	2.15	0.163
NL13	20.40	14.42	19.72	2.62	2.16	0.166
NL14	20.35	14.39	19.63	2.62	2.17	0.164
NL15	20.40	14.43	19.67	2.62	2.13	0.164
NL16	19.92	14.09	19.16	2.62	2.15	0.155
NL17	20.33	14.38	19.64	2.62	2.15	0.158
NL18	20.37	14.41	19.70	2.62	2.15	0.155
NL19	20.39	14.42	19.64	2.62	2.16	0.163
NL20	20.35	14.39	19.70	2.62	2.15	0.161
Average	20.08	14.20	19.39	2.62	2.16	0.164

Table 3.6 Incident wave characteristics, Test NS.

Run	H_{mo} (cm)	H_{rms} (cm)	H_s (cm)	T_p (s)	T_s (s)	R
NS1	20.21	14.29	19.64	2.62	2.16	0.176
NS2	20.42	14.44	19.62	2.62	2.15	0.165
NS3	20.44	14.45	19.82	2.62	2.16	0.162
NS4	20.50	14.49	19.68	2.62	2.14	0.161
NS5	20.41	14.43	19.65	2.62	2.13	0.160
NS6	20.34	14.38	19.59	2.62	2.15	0.160
NS7	20.52	14.51	19.73	2.62	2.14	0.161
NS8	20.58	14.55	19.86	2.62	2.16	0.159
NS9	20.54	14.52	19.77	2.62	2.14	0.160
NS10	20.42	14.44	19.77	2.62	2.15	0.161
Average	20.44	14.45	19.71	2.62	2.15	0.163

Table 3.7 Mean free-surface elevation $\bar{\eta}$ (cm) at 8 wave gauge locations, Test EG.

Run	WG1	WG2	WG3	WG4	WG5	WG6	WG7	WG8
EG1	-0.17	-0.19	-0.21	-0.00	0.30	0.53	0.64	1.63
EG2	-0.21	-0.24	-0.16	-0.01	0.35	0.45	0.54	1.07
EG3	-0.20	-0.19	-0.15	0.01	0.32	0.51	0.54	1.06
EG4	-0.18	-0.17	-0.13	-0.02	0.34	0.51	0.56	1.01
EG5	-0.21	-0.17	-0.09	-0.00	0.31	0.48	0.53	1.06
EG6	-0.23	-0.22	-0.17	-0.01	0.36	0.49	0.74	1.73
EG7	-0.22	-0.19	-0.14	-0.02	0.40	0.48	0.64	1.20
EG8	-0.18	-0.21	-0.10	0.00	0.39	0.50	0.69	1.13
EG9	-0.16	-0.22	-0.15	-0.02	0.39	0.47	0.66	1.10
EG10	-0.15	-0.24	-0.12	-0.01	0.41	0.44	0.65	1.16
EG11	-0.19	-0.20	-0.20	-0.03	0.32	0.51	0.65	1.93
EG12	-0.23	-0.23	-0.17	0.03	0.38	0.50	0.62	1.15
EG13	-0.17	-0.17	-0.11	0.03	0.35	0.51	0.60	0.88
EG14	-0.18	-0.18	-0.09	0.02	0.39	0.49	0.53	0.91
EG15	-0.17	-0.18	-0.15	0.04	0.38	0.49	0.57	0.97
EG16	-0.24	-0.28	-0.18	0.05	0.36	0.54	0.59	0.93
EG17	-0.20	-0.19	-0.11	0.04	0.37	0.50	0.63	1.05
EG18	-0.18	-0.20	-0.14	0.03	0.39	0.52	0.60	0.94
EG19	-0.16	-0.18	-0.17	0.03	0.34	0.48	0.62	1.02
EG20	-0.18	-0.21	-0.16	0.03	0.36	0.51	0.62	0.96
Average	-0.19	-0.20	-0.15	0.01	0.36	0.50	0.61	1.14

Table 3.8 Mean free-surface elevation $\bar{\eta}$ (cm) at 8 wave gauge locations, Test EL.

Run	WG1	WG2	WG3	WG4	WG5	WG6	WG7	WG8
EL1	-0.27	-0.28	-0.22	-0.02	0.29	0.53	0.59	1.66
EL2	-0.24	-0.27	-0.19	0.03	0.37	0.50	0.60	1.12
EL3	-0.24	-0.26	-0.22	0.04	0.36	0.50	0.61	0.88
EL4	-0.19	-0.24	-0.14	0.02	0.37	0.48	0.61	0.98
EL5	-0.17	-0.23	-0.12	0.03	0.34	0.49	0.62	0.92
EL6	-0.27	-0.30	-0.21	0.03	0.34	0.52	0.62	1.03
EL7	-0.20	-0.24	-0.13	0.07	0.38	0.49	0.62	0.93
EL8	-0.19	-0.23	-0.14	0.08	0.36	0.48	0.61	1.21
EL9	-0.19	-0.25	-0.19	0.08	0.38	0.50	0.62	0.92
EL10	-0.19	-0.23	-0.13	0.06	0.37	0.49	0.62	1.00
EL11	-0.19	-0.18	-0.20	0.07	0.33	0.51	0.60	1.73
EL12	-0.27	-0.27	-0.24	0.08	0.39	0.50	0.60	1.13
EL13	-0.21	-0.20	-0.15	0.10	0.38	0.49	0.59	1.10
EL14	-0.22	-0.23	-0.17	0.10	0.39	0.45	0.58	1.04
EL15	-0.20	-0.19	-0.15	0.08	0.35	0.52	0.58	1.00
EL16	-0.27	-0.34	-0.21	0.05	0.35	0.45	0.61	1.12
EL17	-0.23	-0.27	-0.15	0.11	0.37	0.52	0.62	1.05
EL18	-0.22	-0.24	-0.14	0.09	0.40	0.49	0.63	1.05
EL19	-0.20	-0.22	-0.14	0.10	0.36	0.51	0.63	0.99
EL20	-0.19	-0.25	-0.12	0.12	0.35	0.48	0.62	0.98
Average	-0.22	-0.25	-0.17	0.07	0.36	0.50	0.61	1.09

Table 3.9 Mean free-surface elevation $\bar{\eta}$ (cm) at 8 wave gauge locations, Test ES.

Run	WG1	WG2	WG3	WG4	WG5	WG6	WG7	WG8
ES1	-0.20	-0.24	-0.24	0.09	0.32	0.53	0.79	2.15
ES2	-0.20	-0.19	-0.20	0.12	0.37	0.54	0.66	1.08
ES3	-0.18	-0.20	-0.14	0.10	0.37	0.51	0.68	1.12
ES4	-0.19	-0.18	-0.14	0.11	0.39	0.51	0.72	1.19
ES5	-0.20	-0.20	-0.12	0.12	0.38	0.50	0.70	1.15
ES6	-0.20	-0.22	-0.18	0.07	0.34	0.53	0.54	1.82
ES7	-0.21	-0.22	-0.17	0.12	0.37	0.48	0.57	1.21
ES8	-0.21	-0.24	-0.15	0.13	0.37	0.52	0.55	1.16
ES9	-0.19	-0.19	-0.14	0.12	0.39	0.48	0.60	1.24
ES10	-0.19	-0.19	-0.12	0.10	0.39	0.51	0.55	1.22
Average	-0.20	-0.21	-0.16	0.11	0.37	0.51	0.64	1.33

Table 3.10 Mean free-surface elevation $\bar{\eta}$ (cm) at 8 wave gauge locations, Test NG.

Run	WG1	WG2	WG3	WG4	WG5	WG6	WG7	WG8
NG1	-0.26	-0.28	-0.22	0.13	0.32	0.53	0.73	NR
NG2	-0.22	-0.24	-0.16	0.12	0.38	0.50	0.67	NR
NG3	-0.17	-0.19	-0.15	0.13	0.38	0.52	NR	NR
NG4	-0.21	-0.24	-0.15	0.14	0.39	0.56	0.74	NR
NG5	-0.15	-0.20	-0.16	0.11	0.38	0.49	0.67	NR
NG6	-0.24	-0.27	-0.16	0.15	0.39	0.54	0.74	NR
NG7	-0.21	-0.18	-0.13	0.19	0.38	0.55	0.75	NR
NG8	-0.18	-0.23	-0.14	0.13	0.36	0.57	0.70	NR
NG9	-0.17	-0.27	-0.13	0.14	0.36	0.50	0.69	NR
NG10	-0.20	-0.24	-0.13	0.13	0.36	0.49	0.60	NR
NG11	-0.16	-0.18	-0.16	0.12	0.34	0.41	0.56	1.33
NG12	-0.17	-0.16	-0.12	0.10	0.32	0.49	0.51	0.77
NG13	-0.19	-0.18	-0.13	0.13	0.33	0.48	0.56	0.80
NG14	-0.18	-0.19	-0.12	0.15	0.32	0.46	0.51	0.72
NG15	-0.16	-0.14	-0.12	0.15	0.32	0.43	0.56	0.72
NG16	-0.15	-0.19	-0.11	0.13	0.33	0.47	0.50	0.70
NG17	-0.14	-0.13	-0.11	0.13	0.31	0.44	0.54	0.67
NG18	-0.12	-0.15	-0.10	0.12	0.32	0.41	0.51	0.68
NG19	-0.12	-0.14	-0.11	0.11	0.29	0.40	0.51	0.61
NG20	-0.15	-0.19	-0.10	0.13	0.30	0.44	0.51	0.65
Average	-0.18	-0.20	-0.14	0.13	0.34	0.48	0.61	0.77

NR implies 'Not reliable'.

Table 3.11 Mean free-surface elevation $\bar{\eta}$ (cm) at 8 wave gauge locations, Test NL.

Run	WG1	WG2	WG3	WG4	WG5	WG6	WG7	WG8
NL1	-0.26	-0.31	-0.21	0.11	0.25	0.45	0.54	NR
NL2	-0.23	-0.24	-0.16	0.13	0.30	0.44	0.53	NR
NL3	-0.20	-0.22	-0.13	0.16	0.28	0.44	0.53	NR
NL4	-0.23	-0.23	-0.14	0.19	0.29	0.43	0.54	NR
NL5	-0.23	-0.23	-0.14	0.17	0.35	0.44	0.52	NR
NL6	-0.23	-0.28	-0.17	0.19	0.33	0.44	0.53	NR
NL7	-0.26	-0.25	-0.14	0.21	0.35	0.44	0.55	NR
NL8	-0.21	-0.24	-0.13	0.23	0.36	0.50	0.57	NR
NL9	-0.20	-0.23	-0.14	0.22	0.37	0.47	0.55	NR
NL10	-0.22	-0.28	-0.16	0.18	0.36	0.45	0.53	NR
NL11	-0.13	-0.14	-0.23	0.21	0.34	0.46	0.57	NR
NL12	-0.17	-0.18	-0.15	0.19	0.41	0.47	0.50	NR
NL13	-0.17	-0.18	-0.14	0.21	0.42	0.46	0.47	NR
NL14	-0.19	-0.19	-0.15	0.22	0.40	0.49	0.49	NR
NL15	-0.16	-0.18	-0.14	0.21	0.37	0.48	0.54	NR
NL16	-0.21	-0.26	-0.17	0.21	0.30	0.45	0.52	NR
NL17	-0.21	-0.20	-0.14	0.21	0.35	0.49	0.52	NR
NL18	-0.23	-0.21	-0.13	0.23	0.38	0.46	0.53	NR
NL19	-0.22	-0.20	-0.14	0.25	0.38	0.52	0.52	NR
NL20	-0.21	-0.20	-0.14	0.24	0.38	0.47	0.53	NR
Average	-0.21	-0.22	-0.15	0.20	0.35	0.46	0.53	NR

NR implies 'Not reliable'.

Table 3.12 Mean free-surface elevation $\bar{\eta}$ (cm) at 8 wave gauge locations, Test NS.

Run	WG1	WG2	WG3	WG4	WG5	WG6	WG7	WG8
NS1	-0.15	-0.16	-0.22	0.19	0.37	0.40	0.55	1.58
NS2	-0.19	-0.20	-0.16	0.18	0.38	0.47	0.49	1.04
NS3	-0.18	-0.18	-0.15	0.22	0.38	0.43	0.50	0.91
NS4	-0.19	-0.22	-0.15	0.20	0.35	0.44	0.46	0.85
NS5	-0.23	-0.24	-0.18	0.22	0.39	0.46	0.49	0.89
NS6	-0.22	-0.25	-0.16	0.25	0.35	0.45	0.47	0.77
NS7	-0.20	-0.23	-0.14	0.23	0.35	0.47	0.49	0.71
NS8	-0.21	-0.24	-0.15	0.20	0.37	0.47	0.55	0.74
NS9	-0.20	-0.23	-0.14	0.24	0.34	0.49	0.52	0.75
NS10	-0.25	-0.29	-0.15	0.23	0.36	0.46	0.51	0.67
Average	-0.20	-0.22	-0.16	0.22	0.36	0.45	0.50	0.89

Table 3.13 Free-surface standard deviation σ_η (cm) at 8 wave gauge locations, Test EG.

Run	WG1	WG2	WG3	WG4	WG5	WG6	WG7	WG8
EG1	4.64	4.65	4.60	3.77	2.88	2.58	1.74	1.09
EG2	4.71	4.72	4.63	3.77	2.90	2.59	1.75	1.08
EG3	4.73	4.73	4.64	3.77	2.88	2.57	1.76	1.06
EG4	4.69	4.71	4.61	3.75	2.89	2.59	1.76	1.06
EG5	4.69	4.70	4.60	3.76	2.89	2.58	1.76	1.07
EG6	4.89	4.89	4.87	3.94	3.02	2.76	2.28	1.12
EG7	4.98	4.96	4.92	3.96	3.03	2.76	2.30	1.09
EG8	4.98	4.97	4.91	3.96	3.04	2.76	2.29	1.10
EG9	4.96	4.94	4.91	3.97	3.02	2.74	2.30	1.08
EG10	4.94	4.95	4.89	3.93	3.04	2.76	2.30	1.08
EG11	4.94	4.93	4.89	3.92	2.99	2.72	2.04	1.00
EG12	5.02	4.99	4.94	3.93	3.02	2.74	2.03	0.98
EG13	5.00	4.97	4.91	3.93	3.00	2.72	2.04	0.98
EG14	5.00	4.97	4.91	3.93	3.01	2.74	2.05	0.98
EG15	4.98	4.97	4.89	3.92	3.02	2.72	2.06	0.98
EG16	5.08	5.05	4.96	3.94	3.03	2.75	2.06	1.00
EG17	5.04	5.02	4.91	3.94	3.04	2.73	2.06	0.97
EG18	5.01	4.99	4.89	3.92	3.03	2.75	2.07	0.98
EG19	5.01	4.99	4.88	3.89	3.03	2.77	2.06	0.98
EG20	5.02	5.00	4.89	3.90	3.04	2.76	2.07	0.98
Average	4.92	4.91	4.83	3.89	2.99	2.70	2.04	1.03

Table 3.14 Free-surface standard deviation σ_η (cm) at 8 wave gauge locations, Test EL.

Run	WG1	WG2	WG3	WG4	WG5	WG6	WG7	WG8
EL1	4.89	4.96	4.88	3.82	3.00	2.69	2.51	1.03
EL2	4.95	5.01	4.90	3.81	2.98	2.67	2.51	0.98
EL3	4.93	4.98	4.87	3.82	2.98	2.68	2.50	1.04
EL4	4.94	4.97	4.86	3.79	2.99	2.68	2.51	0.96
EL5	4.93	4.97	4.86	3.79	2.98	2.69	2.51	1.01
EL6	4.97	5.01	4.88	3.78	2.98	2.70	2.52	1.00
EL7	5.00	5.05	4.90	3.83	3.02	2.71	2.52	1.06
EL8	5.00	5.05	4.90	3.81	3.00	2.71	2.52	1.02
EL9	4.97	5.01	4.87	3.78	3.01	2.71	2.50	0.94
EL10	4.96	5.01	4.87	3.76	3.01	2.69	2.52	1.01
EL11	4.99	5.00	4.93	3.78	3.02	2.71	2.58	1.01
EL12	5.12	5.11	5.03	3.83	3.06	2.74	2.58	1.08
EL13	5.08	5.08	4.99	3.80	3.07	2.74	2.61	1.16
EL14	5.05	5.05	4.94	3.82	3.05	2.73	2.58	1.15
EL15	5.04	5.04	4.94	3.78	3.06	2.73	2.60	1.06
EL16	5.02	5.01	4.89	3.77	3.04	2.74	2.58	0.97
EL17	5.07	5.08	4.93	3.79	3.07	2.75	2.61	1.05
EL18	5.07	5.07	4.92	3.77	3.05	2.74	2.61	1.11
EL19	5.07	5.06	4.92	3.81	3.06	2.74	2.61	1.09
EL20	5.08	5.08	4.92	3.80	3.05	2.75	2.60	1.11
Average	5.01	5.03	4.91	3.80	3.02	2.72	2.55	1.04

Table 3.15 Free-surface standard deviation σ_η (cm) at 8 wave gauge locations, Test ES.

Run	WG1	WG2	WG3	WG4	WG5	WG6	WG7	WG8
ES1	4.99	5.01	4.89	3.76	3.03	2.75	2.32	1.02
ES2	5.06	5.06	4.92	3.79	3.03	2.77	2.32	0.99
ES3	5.07	5.07	4.92	3.75	3.02	2.76	2.32	0.98
ES4	5.07	5.06	4.92	3.78	3.03	2.76	2.31	1.05
ES5	5.06	5.07	4.91	3.76	3.04	2.77	2.33	1.09
ES6	5.04	5.06	4.91	3.77	3.03	2.78	2.62	1.16
ES7	5.09	5.11	4.93	3.77	3.03	2.77	2.64	1.04
ES8	5.11	5.11	4.95	3.77	3.04	2.79	2.65	1.10
ES9	5.10	5.10	4.94	3.76	3.04	2.79	2.63	1.17
ES10	5.07	5.07	4.90	3.75	3.03	2.78	2.63	1.17
Average	5.07	5.07	4.92	3.77	3.03	2.77	2.48	1.08

Table 3.16 Free-surface standard deviation σ_η (cm) at 8 wave gauge locations, Test NG.

Run	WG1	WG2	WG3	WG4	WG5	WG6	WG7	WG8
NG1	5.12	5.11	4.97	3.80	3.04	2.81	2.51	NR
NG2	5.16	5.14	4.98	3.78	3.04	2.79	2.47	NR
NG3	5.11	5.09	4.94	3.75	3.04	2.80	NR	NR
NG4	5.13	5.10	4.93	3.77	3.02	2.80	3.18	NR
NG5	5.10	5.08	4.92	3.75	3.03	2.80	3.17	NR
NG6	5.18	5.17	4.98	3.80	3.04	2.80	3.20	NR
NG7	5.13	5.13	4.94	3.77	3.02	2.80	3.17	NR
NG8	5.09	5.07	4.91	3.76	3.04	2.81	3.15	NR
NG9	5.03	5.03	4.85	3.72	3.02	2.79	3.18	NR
NG10	5.00	4.98	4.82	3.74	3.03	2.79	2.41	NR
NG11	4.97	4.98	4.80	3.73	3.01	2.79	2.66	0.76
NG12	4.98	4.99	4.78	3.67	3.00	2.77	2.68	0.75
NG13	4.96	4.97	4.77	3.71	3.00	2.78	2.67	0.75
NG14	4.93	4.94	4.72	3.68	2.99	2.76	2.68	0.76
NG15	4.91	4.92	4.72	3.69	2.99	2.76	2.67	0.76
NG16	4.90	4.90	4.70	3.67	3.00	2.76	2.66	0.83
NG17	4.87	4.89	4.67	3.66	3.00	2.76	2.66	0.85
NG18	4.83	4.85	4.65	3.67	3.00	2.75	2.65	0.85
NG19	4.82	4.85	4.63	3.67	2.99	2.77	2.64	1.00
NG20	4.83	4.85	4.64	3.66	3.00	2.76	2.65	1.15
Average	5.00	5.00	4.82	3.72	3.02	2.78	2.79	0.85

NR implies 'Not reliable'.

Table 3.17 Free-surface standard deviation σ_η (cm) at 8 wave gauge locations, Test NL.

Run	WG1	WG2	WG3	WG4	WG5	WG6	WG7	WG8
NL1	4.86	4.89	4.72	3.61	2.98	2.76	2.75	NR
NL2	4.86	4.86	4.71	3.59	2.97	2.74	2.74	NR
NL3	4.84	4.85	4.70	3.57	2.96	2.74	2.69	NR
NL4	4.94	4.94	4.80	3.62	2.97	2.76	2.71	NR
NL5	5.07	5.07	4.90	3.75	3.03	2.78	2.63	NR
NL6	4.97	4.97	4.80	3.60	2.95	2.73	2.68	NR
NL7	5.03	5.05	4.88	3.62	2.97	2.75	2.70	NR
NL8	5.04	5.05	4.88	3.60	2.99	2.76	2.70	NR
NL9	5.05	5.05	4.88	3.62	2.97	2.75	2.69	NR
NL10	5.01	5.02	4.84	3.59	2.96	2.74	2.69	NR
NL11	4.93	4.98	4.84	3.61	2.97	2.74	2.14	NR
NL12	5.02	5.07	4.90	3.60	2.98	2.75	2.15	NR
NL13	5.05	5.09	4.93	3.65	2.99	2.76	2.13	NR
NL14	5.04	5.09	4.92	3.63	2.99	2.77	2.14	NR
NL15	5.06	5.11	4.93	3.63	3.00	2.79	2.14	NR
NL16	4.96	5.00	4.81	3.58	2.96	2.76	2.11	NR
NL17	5.06	5.11	4.91	3.61	2.99	2.78	2.14	NR
NL18	5.08	5.12	4.93	3.63	2.99	2.77	2.13	NR
NL19	5.08	5.13	4.91	3.60	2.99	2.78	2.13	NR
NL20	5.06	5.12	4.91	3.62	2.99	2.78	2.15	NR
Average	5.00	5.03	4.86	3.62	2.98	2.76	2.42	NR

NR implies 'Not reliable'.

Table 3.18 Free-surface standard deviation σ_η (cm) at 8 wave gauge locations, Test NS.

Run	WG1	WG2	WG3	WG4	WG5	WG6	WG7	WG8
NS1	5.04	5.08	4.89	3.65	3.01	2.81	2.16	1.11
NS2	5.09	5.14	4.93	3.61	3.00	2.79	2.14	0.94
NS3	5.08	5.14	4.94	3.63	3.00	2.81	2.15	0.90
NS4	5.11	5.16	4.93	3.60	3.00	2.82	2.15	0.90
NS5	5.09	5.14	4.92	3.62	3.00	2.80	2.14	0.88
NS6	5.07	5.13	4.90	3.61	2.99	2.80	2.13	0.83
NS7	5.10	5.17	4.94	3.60	2.98	2.79	2.12	0.85
NS8	5.12	5.18	4.95	3.58	3.00	2.80	2.17	0.85
NS9	5.11	5.18	4.95	3.62	2.99	2.80	2.16	0.85
NS10	5.08	5.15	4.91	3.58	3.00	2.79	2.14	0.85
Average	5.09	5.15	4.93	3.61	3.00	2.80	2.15	0.90

Table 3.19 Mean \bar{U} and standard deviation σ_U of measured cross-shore velocity U ,
Test EG.

Run	2D ADV at WG4		Red Vectrino at WG5		Blue Vectrino at WG6	
	\bar{U} (cm/s)	σ_U (cm/s)	\bar{U} (cm/s)	σ_U (cm/s)	\bar{U} (cm/s)	σ_U (cm/s)
EG1	-7.30	23.22	-4.30	15.92	-3.38	16.70
EG2	-6.88	21.31	-4.15	16.03	-3.82	16.77
EG3	-6.98	22.69	-3.60	15.94	-4.18	16.88
EG4	-7.25	22.35	-4.04	15.79	-3.41	16.79
EG5	-7.43	22.63	-4.46	15.68	-3.64	16.65
EG6	-6.22	22.57	NR	NR	-3.43	16.47
EG7	-7.19	22.54	-2.90	15.63	-3.61	16.70
EG8	-8.38	22.61	-2.73	15.86	-3.75	16.69
EG9	-7.91	22.68	-3.45	15.78	-3.31	16.81
EG10	-6.38	22.33	-3.39	15.91	-3.93	16.88
EG11	-7.74	22.48	-2.80	15.46	-3.77	16.62
EG12	-7.31	22.27	-3.40	15.51	NR	NR
EG13	-7.25	22.30	-2.74	15.57	-3.20	16.52
EG14	-7.45	21.86	-3.02	15.69	-3.77	16.45
EG15	-6.31	21.88	-3.32	15.78	NR	NR
EG16	-7.43	22.02	-3.08	15.93	-3.35	16.55
EG17	-8.16	22.16	-2.93	15.72	-3.68	16.52
EG18	-7.55	21.98	NR	NR	-3.32	16.57
EG19	-7.42	21.61	-2.57	15.72	-3.16	16.52
EG20	-6.80	21.55	NR	NR	NR	NR
Average	-7.27	22.25	-3.35	15.76	-3.57	16.65

NR implies 'Not reliable'.

Table 3.20 Mean \bar{U} and standard deviation σ_U of measured cross-shore velocity U ,
Test EL.

Run	2D ADV at WG4		Red Vectrino at WG5		Blue Vectrino at WG6	
	\bar{U} (cm/s)	σ_U (cm/s)	\bar{U} (cm/s)	σ_U (cm/s)	\bar{U} (cm/s)	σ_U (cm/s)
EL1	-6.63	20.37	-2.59	15.35	-4.04	16.74
EL2	-7.45	21.71	-2.99	15.35	-3.51	16.70
EL3	-6.90	21.73	-2.68	15.28	-3.74	16.71
EL4	-7.47	21.40	-3.27	15.41	-3.60	16.68
EL5	-7.28	21.59	-2.90	15.41	-3.55	16.52
EL6	-7.67	21.28	-2.92	15.34	-3.69	16.39
EL7	-7.29	21.27	-3.10	15.45	-3.84	16.54
EL8	-7.48	21.08	NR	NR	-3.64	16.53
EL9	-8.11	21.20	-2.73	15.41	-4.02	16.52
EL10	-7.67	21.31	-3.16	15.46	-3.55	16.52
EL11	-7.11	21.01	-2.71	16.06	-3.87	16.87
EL12	-7.41	21.02	-3.20	15.96	-3.46	16.95
EL13	-6.31	21.11	-2.87	15.86	-3.53	16.91
EL14	-7.13	20.65	-2.72	15.72	-3.64	16.83
EL15	-7.02	20.98	-3.49	15.71	-3.39	16.71
EL16	-8.26	20.42	-2.38	14.66	-3.66	16.55
EL17	-7.11	20.47	-2.28	14.74	-3.63	16.72
EL18	-7.29	20.36	-3.13	15.03	-3.28	16.65
EL19	-7.00	20.24	-2.48	14.68	-3.20	16.71
EL20	-7.25	20.35	-2.82	14.79	-3.23	16.66
Average	-7.29	20.98	-2.86	15.35	-3.60	16.67

NR implies 'Not reliable'.

Table 3.21 Mean \bar{U} and standard deviation σ_U of measured cross-shore velocity U ,
Test ES.

Run	2D ADV at WG4		Red Vectrino at WG5		Blue Vectrino at WG6	
	\bar{U} (cm/s)	σ_U (cm/s)	\bar{U} (cm/s)	σ_U (cm/s)	\bar{U} (cm/s)	σ_U (cm/s)
ES1	-8.20	20.49	-2.87	15.84	-3.17	16.76
ES2	-7.54	20.58	-2.92	15.81	-3.73	16.77
ES3	-6.42	20.64	-2.44	15.69	NR	NR
ES4	-6.99	20.49	-2.88	15.78	-3.21	16.69
ES5	-8.04	20.34	NR	NR	-3.63	16.64
ES6	-7.46	20.31	-2.95	15.96	-3.52	16.96
ES7	-7.29	20.15	NR	NR	NR	NR
ES8	-7.10	20.49	-2.92	15.79	-3.23	17.00
ES9	-7.34	20.36	NR	NR	-3.58	16.92
ES10	-7.65	20.24	-2.33	15.98	-3.17	16.93
Average	-7.40	20.41	-2.76	15.84	-3.41	16.83

NR implies 'Not reliable'.

Table 3.22 Mean \bar{U} and standard deviation σ_U of measured cross-shore velocity U ,
Test NG.

Run	2D ADV at WG4		Red Vectrino at WG5		Blue Vectrino at WG6	
	\bar{U} (cm/s)	σ_U (cm/s)	\bar{U} (cm/s)	σ_U (cm/s)	\bar{U} (cm/s)	σ_U (cm/s)
NG1	-7.85	20.54	-2.39	15.85	-3.15	17.54
NG2	-7.52	20.12	-2.72	15.71	-3.43	17.12
NG3	-7.33	20.43	-2.58	15.86	NR	NR
NG4	-7.18	20.38	-2.09	15.60	-3.19	17.14
NG5	-8.34	20.29	-2.23	15.47	-3.49	17.39
NG6	-8.69	20.18	-2.66	15.38	-3.21	17.31
NG7	-7.89	20.09	NR	NR	-3.02	17.16
NG8	-8.64	19.86	NR	NR	-3.56	16.95
NG9	-7.43	19.96	-2.29	15.23	NR	NR
NG10	-7.33	19.86	-2.65	15.15	-3.01	17.03
NG11	-7.20	20.01	-1.99	15.51	-2.72	17.16
NG12	-6.99	19.92	-1.81	15.31	-3.51	17.20
NG13	-7.61	19.57	-2.43	15.43	-3.15	17.23
NG14	-6.95	19.74	-2.21	14.53	NR	NR
NG15	-7.36	19.60	-1.78	13.57	-2.93	17.21
NG16	-6.74	19.57	-1.94	13.30	-3.45	17.38
NG17	-7.72	19.45	-2.16	13.30	-3.14	17.31
NG18	-7.30	19.35	-1.98	13.20	-3.37	17.22
NG19	-6.94	19.34	NR	NR	-3.24	17.18
NG20	-6.73	19.66	-1.87	13.22	NR	NR
Average	-7.49	19.90	-2.22	14.80	-3.22	17.22

NR implies 'Not reliable'.

Table 3.23 Mean \bar{U} and standard deviation σ_U of measured cross-shore velocity U ,
Test NL.

Run	2D ADV at WG4		Red Vectrino at WG5		Blue Vectrino at WG6	
	\bar{U} (cm/s)	σ_U (cm/s)	\bar{U} (cm/s)	σ_U (cm/s)	\bar{U} (cm/s)	σ_U (cm/s)
NL1	-6.68	19.03	-1.23	11.98	-3.13	17.03
NL2	-7.12	18.65	-1.02	11.83	-3.10	16.86
NL3	-7.77	18.66	-1.54	11.79	-3.69	16.75
NL4	-6.75	18.70	-1.08	11.69	-3.60	16.60
NL5	-7.04	18.58	-1.27	11.97	-3.69	16.65
NL6	-7.13	18.52	-0.89	11.34	-3.01	16.76
NL7	-6.22	18.77	-1.80	11.89	-3.11	16.74
NL8	-7.49	18.51	NR	NR	-2.98	16.78
NL9	-7.76	18.45	-1.48	11.61	-3.16	16.58
NL10	-7.94	18.45	-0.72	10.53	-3.07	16.69
NL11	-6.79	19.23	-0.74	11.67	-3.02	17.15
NL12	-7.67	19.09	-1.28	11.28	-3.22	17.13
NL13	-7.65	18.93	-1.39	11.33	-3.04	17.15
NL14	-7.37	18.76	NR	NR	NR	NR
NL15	-8.37	19.07	-1.48	11.25	NR	NR
NL16	-6.68	18.50	NR	NR	NR	NR
NL17	-6.99	18.77	-1.24	11.55	NR	NR
NL18	-7.01	18.63	-1.44	11.74	-3.13	17.00
NL19	-7.20	18.78	-1.35	11.63	-3.14	17.05
NL20	-7.29	18.62	-1.36	12.16	-3.25	17.03
Average	-7.25	18.74	-1.25	10.92	-3.21	16.87

NR implies 'Not reliable'.

Table 3.24 Mean \bar{U} and standard deviation σ_U of measured cross-shore velocity U ,
 Test NS.

Run	2D ADV at WG4		Red Vectrino at WG5		Blue Vectrino at WG6	
	\bar{U} (cm/s)	σ_U (cm/s)	\bar{U} (cm/s)	σ_U (cm/s)	\bar{U} (cm/s)	σ_U (cm/s)
NS1	-7.83	18.99	-1.71	14.08	-3.37	17.38
NS2	-7.92	19.05	-1.95	13.50	-3.27	17.23
NS3	-6.76	19.21	-1.65	13.21	-3.48	17.11
NS4	-7.69	19.18	-2.20	13.32	-3.36	17.02
NS5	-8.34	19.01	-1.37	12.69	-3.07	17.05
NS6	-7.05	18.44	-1.22	12.85	-3.25	16.91
NS7	-7.71	18.51	-1.19	12.51	-3.18	17.04
NS8	-7.25	18.58	-1.15	12.15	NR	NR
NS9	-8.07	18.60	NR	NR	-3.30	16.73
NS10	-6.57	18.85	-1.60	12.65	-3.24	16.77
Average	-7.52	18.84	-1.56	13.00	-3.28	17.03

NR implies 'Not reliable'.

Tables 3.1 to 3.24 are condensed to examine the cross-shore variations of the mean and standard deviation of the measured free surface elevation η and horizontal velocity U for each test in Figures 3.1 to 3.6. These six figures for the six tests are similar and explained using Figure 3.3 for the ES tests. The mean water levels $\bar{\eta}$ were slightly negative (-0.2 cm) due to wave setdown at WG1-WG3 outside the surf zone. The positive $\bar{\eta}$ (wave setup) was 0.1 cm at WG4 ($x = 8.3$ m) in the outer surf zone and increased to 0.7 cm at WG7 ($x = 17.1$ m) in the inner surf zone. The value of $\bar{\eta}$ at WG8 in the swash zone above SWL is the sum of the mean depth and the sand surface elevation at WG8.

The cross-shore variation of the free surface standard deviation σ_{η} is related to the local significant wave height $H_{mo} = 4\sigma_{\eta}$. The values of σ_{η} were approximately 5 cm at WG1-WG3 and decreased from WG4 to WG8 in the surf and swash zones, indicating the wave height decay due to wave breaking. Waves breaking near the toe of the foreshore slope reduced the values of σ_{η} at WG8 ($x = 18.6$ m).

The mean cross-shore velocities were measured at $x = 8.3, 12.9,$ and 15.5 m inside the surf zone. The measured alongshore and vertical velocities were small in comparison to the cross-shore velocity U . The mean horizontal velocity \bar{U} was negative due to the wave-induced offshore return current. The positive value of σ_U corresponds to the intensity of the wave-induced oscillatory velocity. The offshore current decreased from the outer surf zone ($x = 8.3$ m) to the inner surf zone ($x = 12.9-15.5$ m). The standard deviation σ_U also decreased landward. It is noted that Figures 3.1-3.6 together with the computed variations will be presented in Chapter 5.

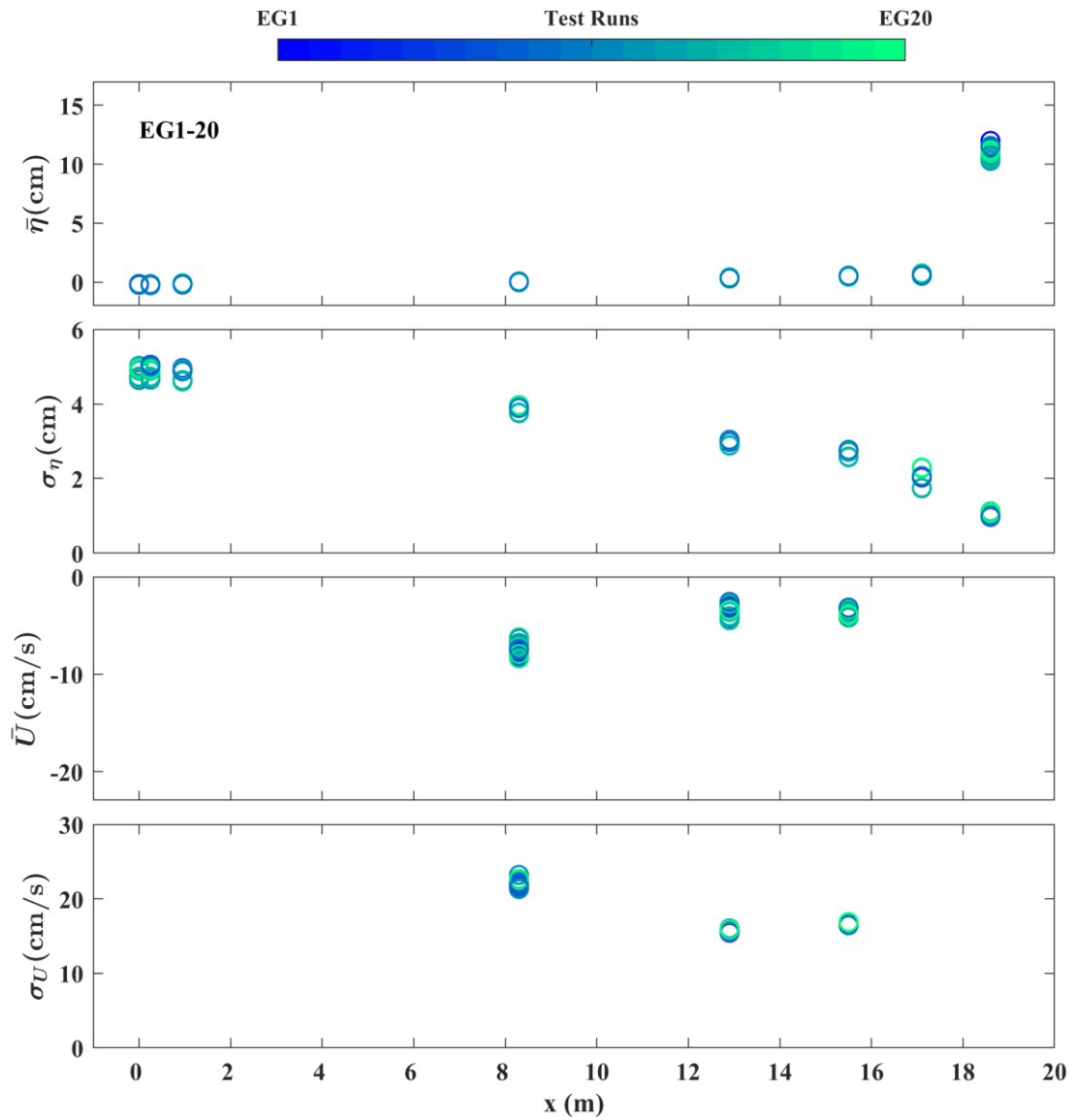


Figure 3.1 Cross-shore variations of mean and standard deviation of measured free surface elevation η and horizontal velocity U for 20 runs in Test EG.

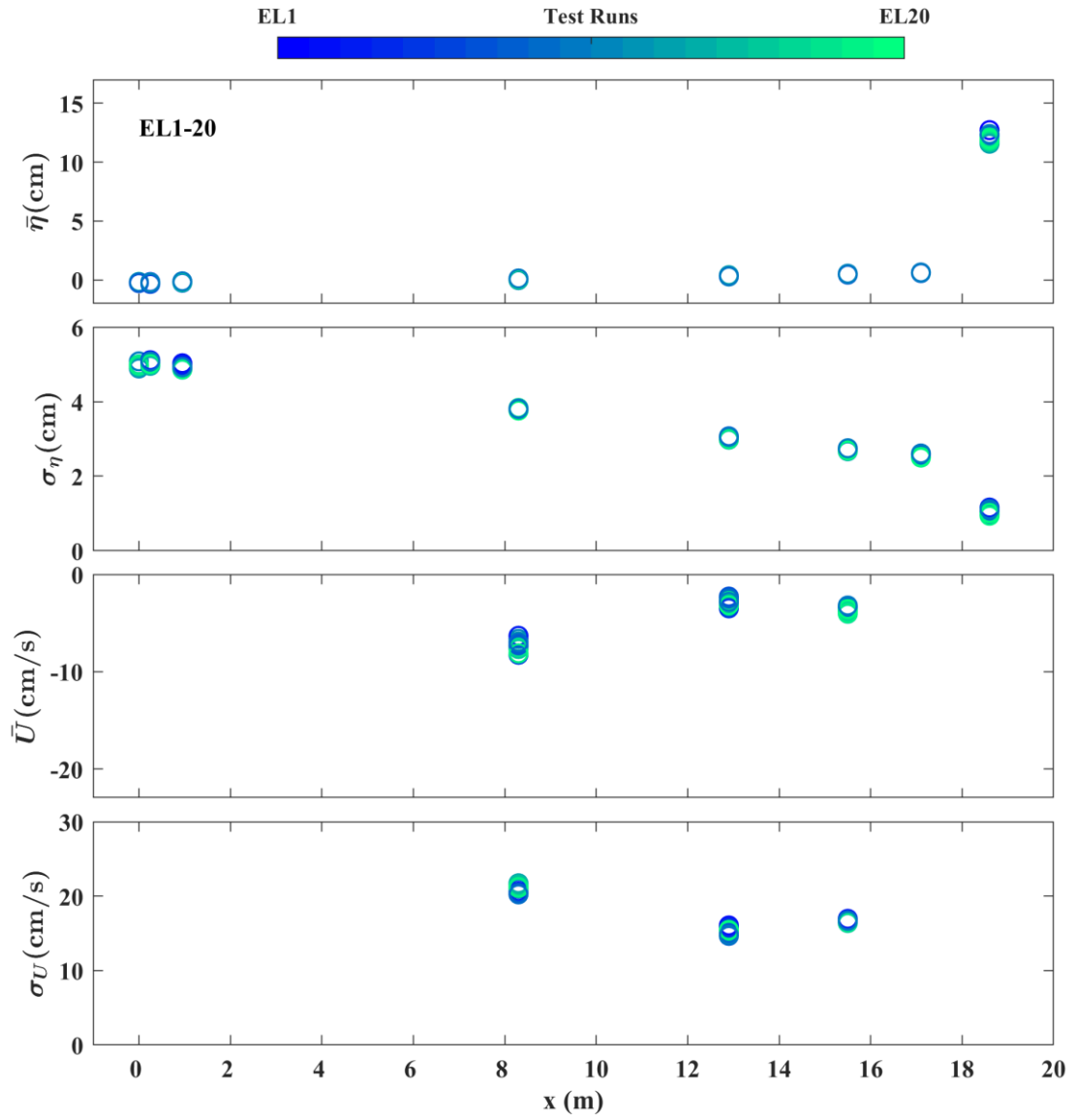


Figure 3.2 Cross-shore variations of mean and standard deviation of measured free surface elevation η and horizontal velocity U for 20 runs in Test EL.

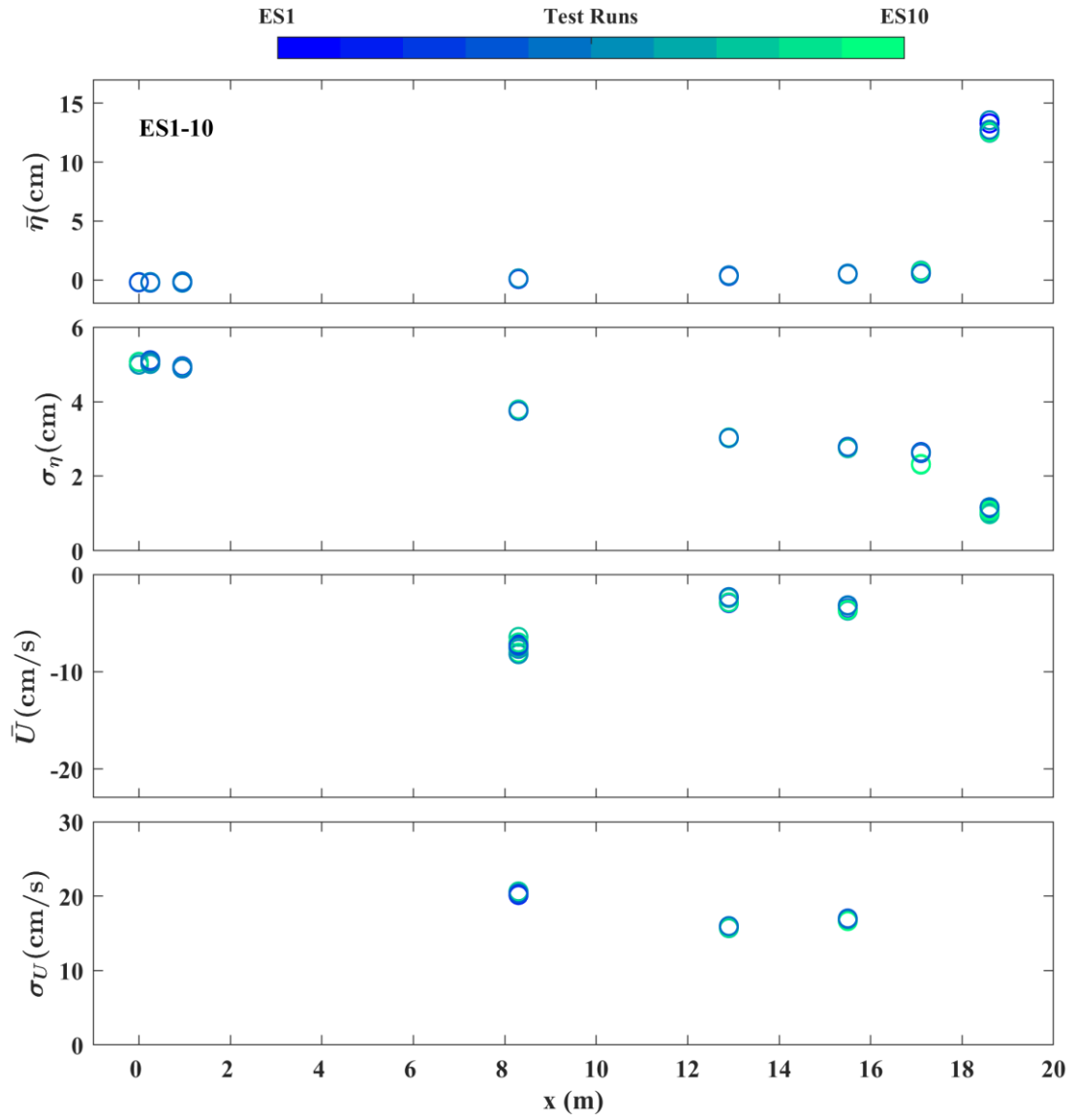


Figure 3.3 Cross-shore variations of mean and standard deviation of measured free surface elevation η and horizontal velocity U for 10 runs in Test ES.

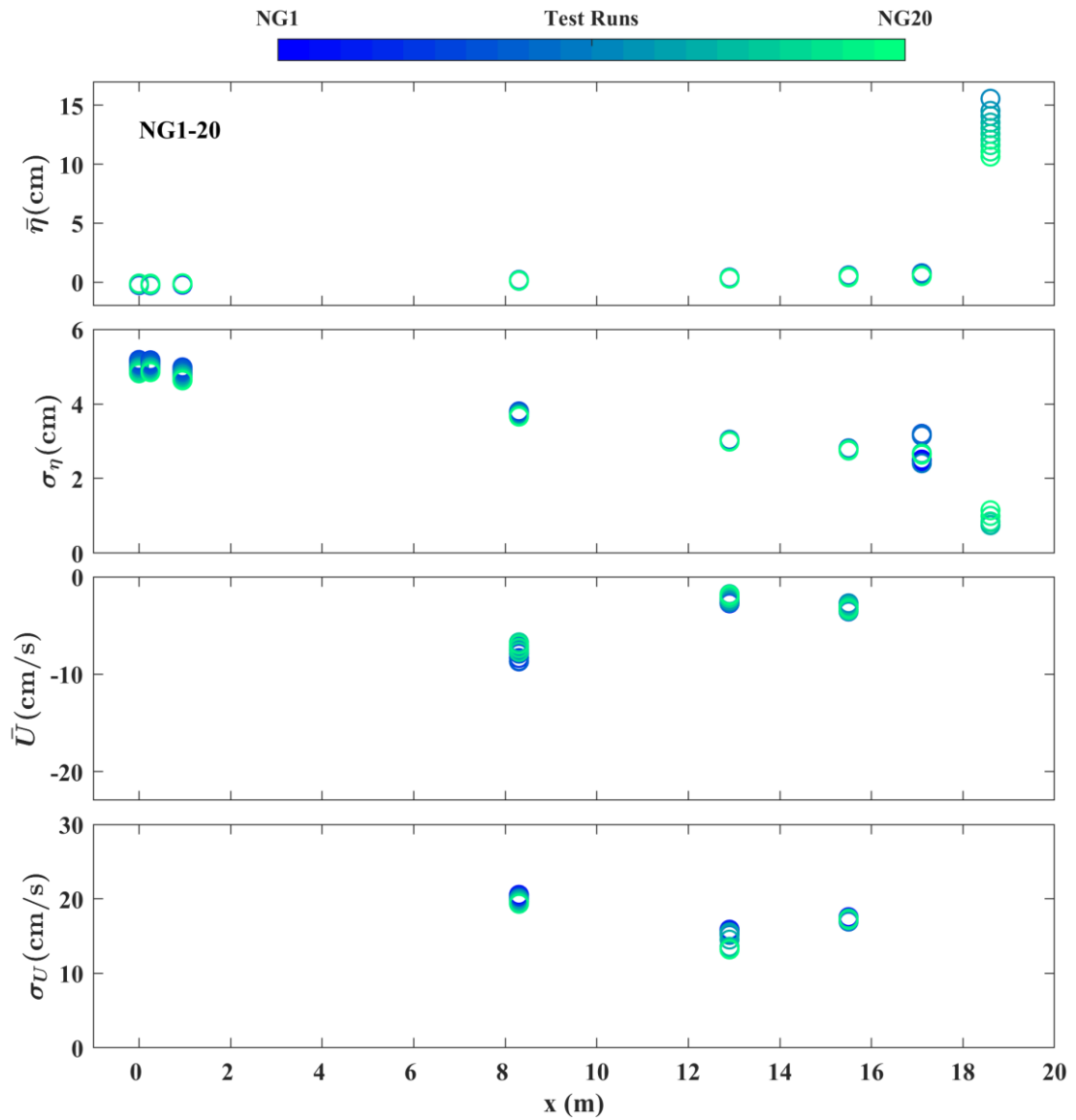


Figure 3.4 Cross-shore variations of mean and standard deviation of measured free surface elevation η and horizontal velocity U for 20 runs in Test NG.

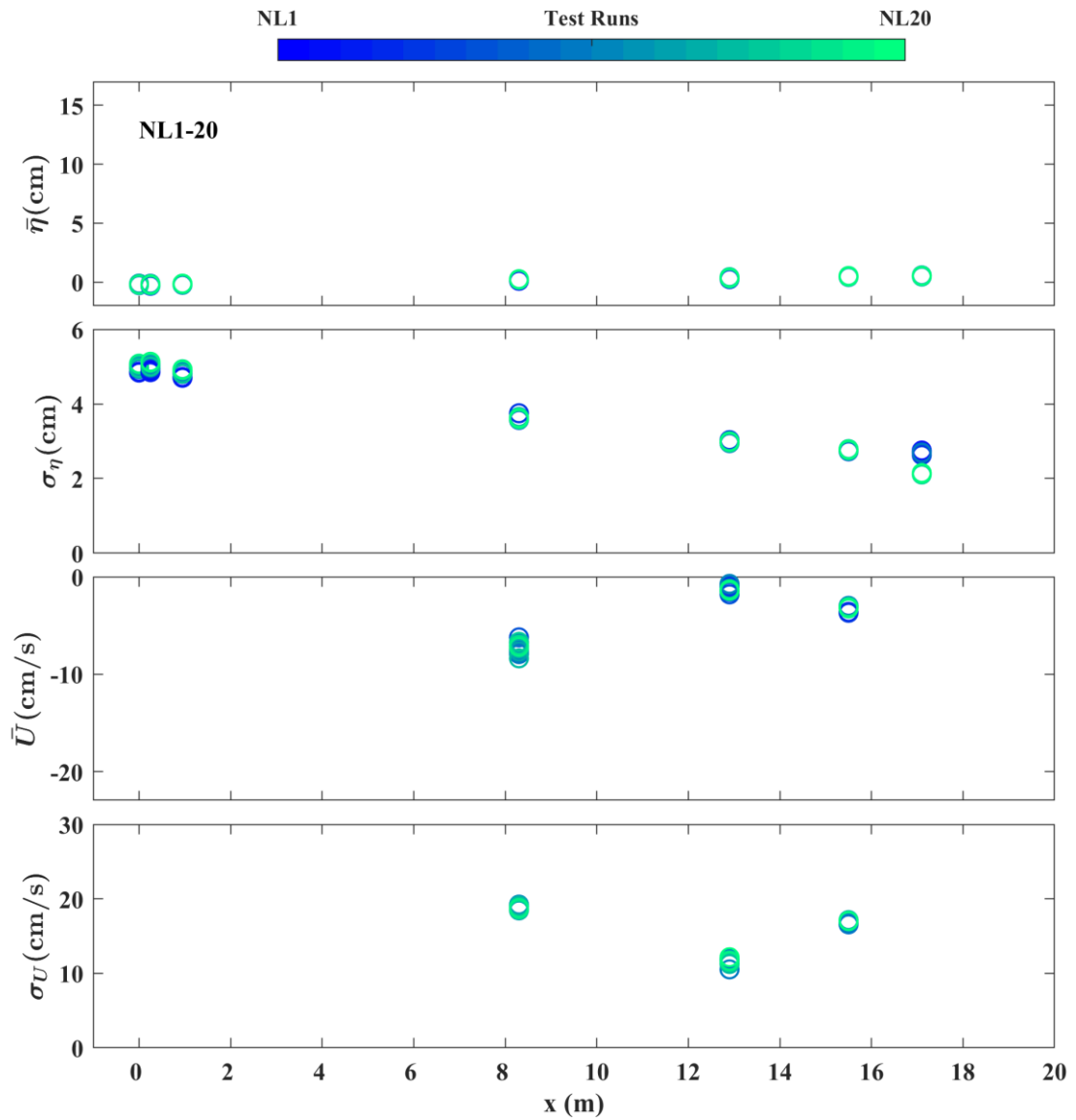


Figure 3.5 Cross-shore variations of mean and standard deviation of measured free surface elevation η and horizontal velocity U for 20 runs in Test NL (WG8 was not functional in this test).

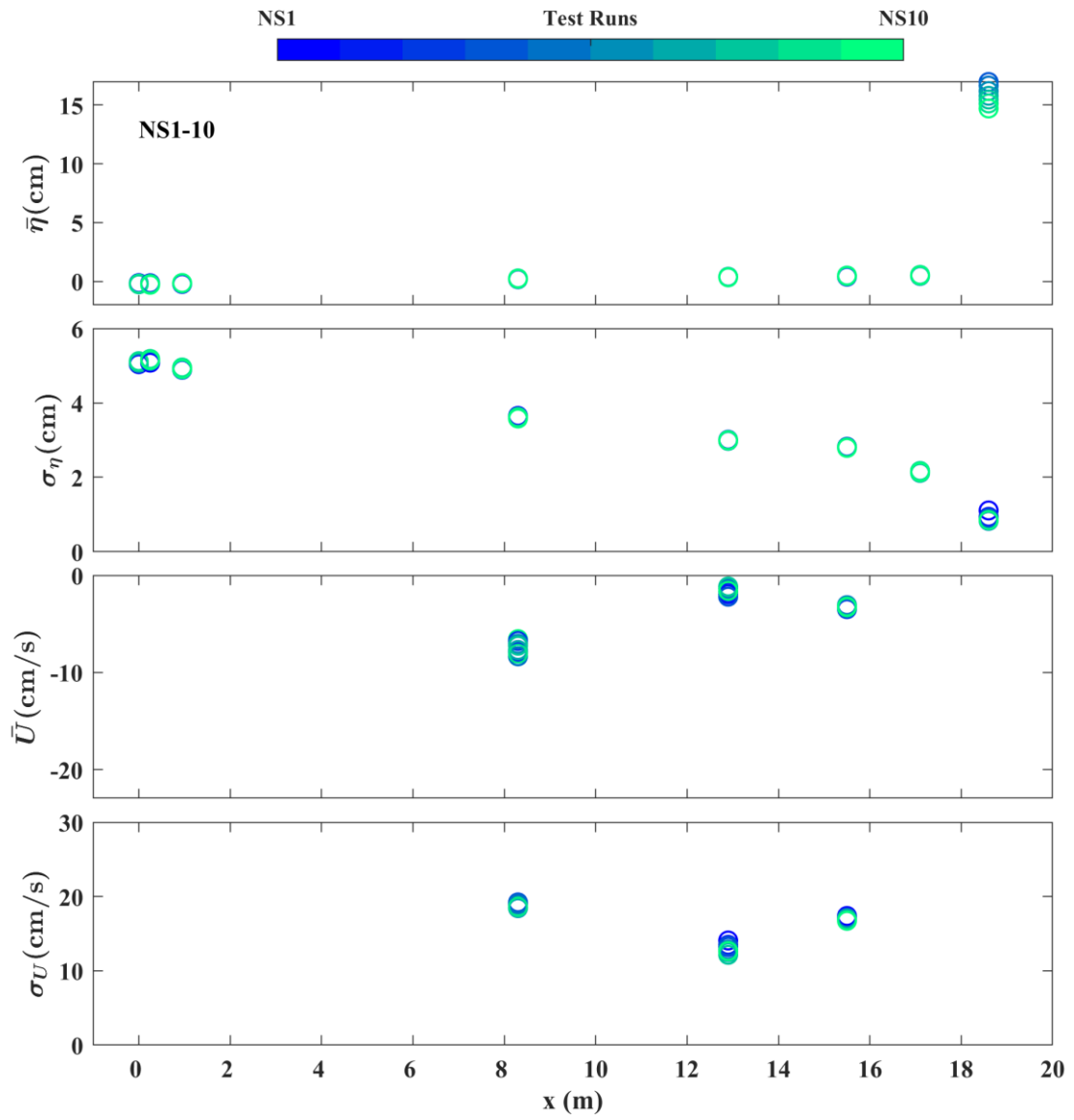


Figure 3.6 Cross-shore variations of mean and standard deviation of measured free surface elevation η and horizontal velocity U for 10 runs in Test NS.

3.2 Beach Profile Changes

The beach profiles measured by the laser line scanner evolved slightly in the equilibrium profile E test series but more noticeably in the nourished profile N test series. The measured initial, middle, and final beach profiles during 20 runs for EG, EL, NG, NL, and 10 runs for ES and NS are depicted in Figure 3.7-3.12 to examine the degree of the profile changes. In these figures, the bottom elevation Z_b varies with time t and with the cross-shore distance x . The vertical elevation change is defined as

$$\Delta Z_b = [Z_b(t, x) - Z_b(t = 0, x)] \quad (3.1)$$

where, ΔZ_b = bottom elevation change from the initial profile at time $t = 0$. To depict the differences and similarities of the near-equilibrium profiles, the measured beach profiles of EG0, EG20 = EL0, EL20 = ES0, and ES10, which were conducted sequentially without rebuilding the beach profile, were plotted together in Figure 3.13.

For the equilibrium beach profile tests EG, EL, and ES, the elevation changes from the initial profile to the middle and the final profile were less than 1 cm except for the vicinity of the lower swash zone where wave uprush and downrush collided (Figures 3.7-3.9). The elevation change increased approximately to 2 cm near $x = 17.4$ m.

For the nourished foreshore tests, the foreshore erosion and deposition pattern during the N test series were very similar. The elevation changes from the initial profile to the middle and the final profile were less than 1 cm except for the foreshore zone of $x = 17-19$ m (Figures 3.10-3.12). The upper foreshore was eroded up to 5 cm, resulting in the deposition of the lower foreshore up to 5 cm. Figure 3.14 compares the initial profiles of NG0, NL0, and NS0 to indicate the degree of the careful profile rebuilding at the start of the NG, NL, and NS tests. Figure 3.15 compares the profile evolutions

starting from the initial profiles (Figure 3.14) to the final profiles of NG20, NL20, and NS10 in this figure. The profile evolution was repeatable in the three tests with the three different DOs.

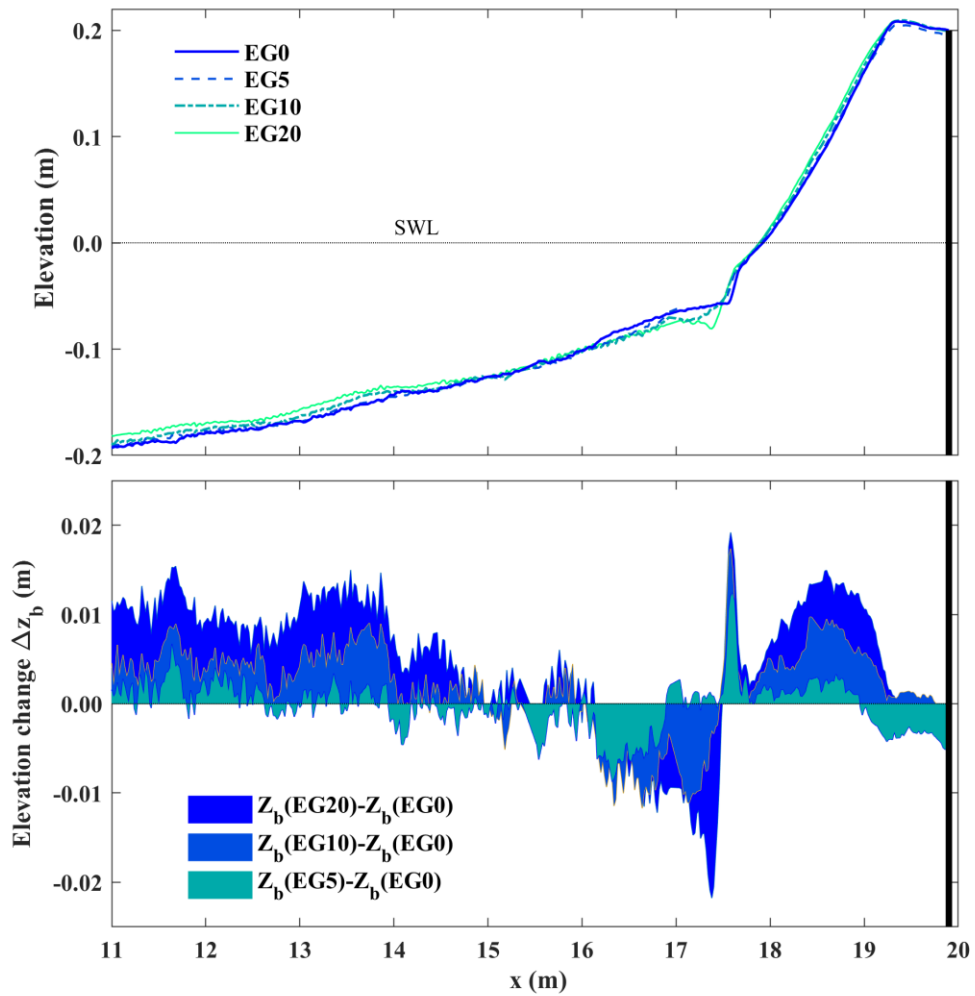


Figure 3.7 Measured initial, middle, and final beach profiles and changes of bottom elevation (ΔZ_b) for Test EG.

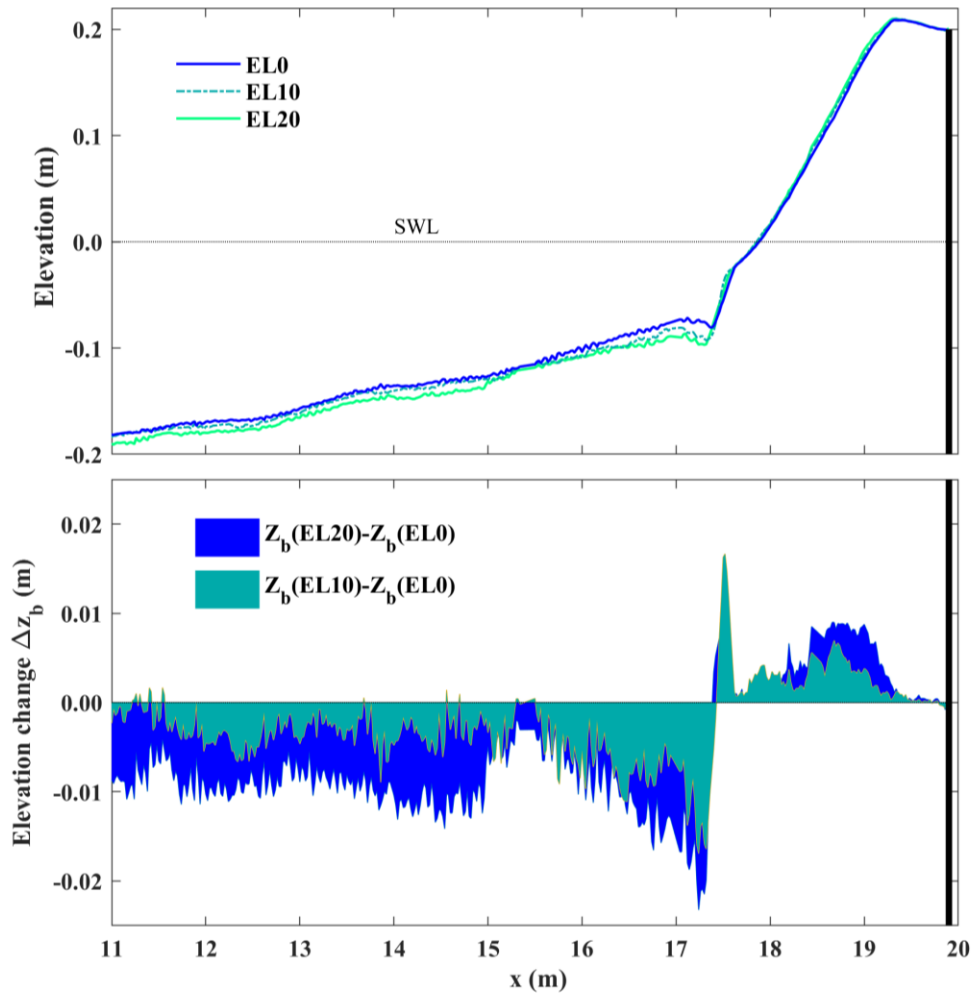


Figure 3.8 Measured initial, middle, and final beach profiles and changes of bottom elevation (ΔZ_b) for Test EL.

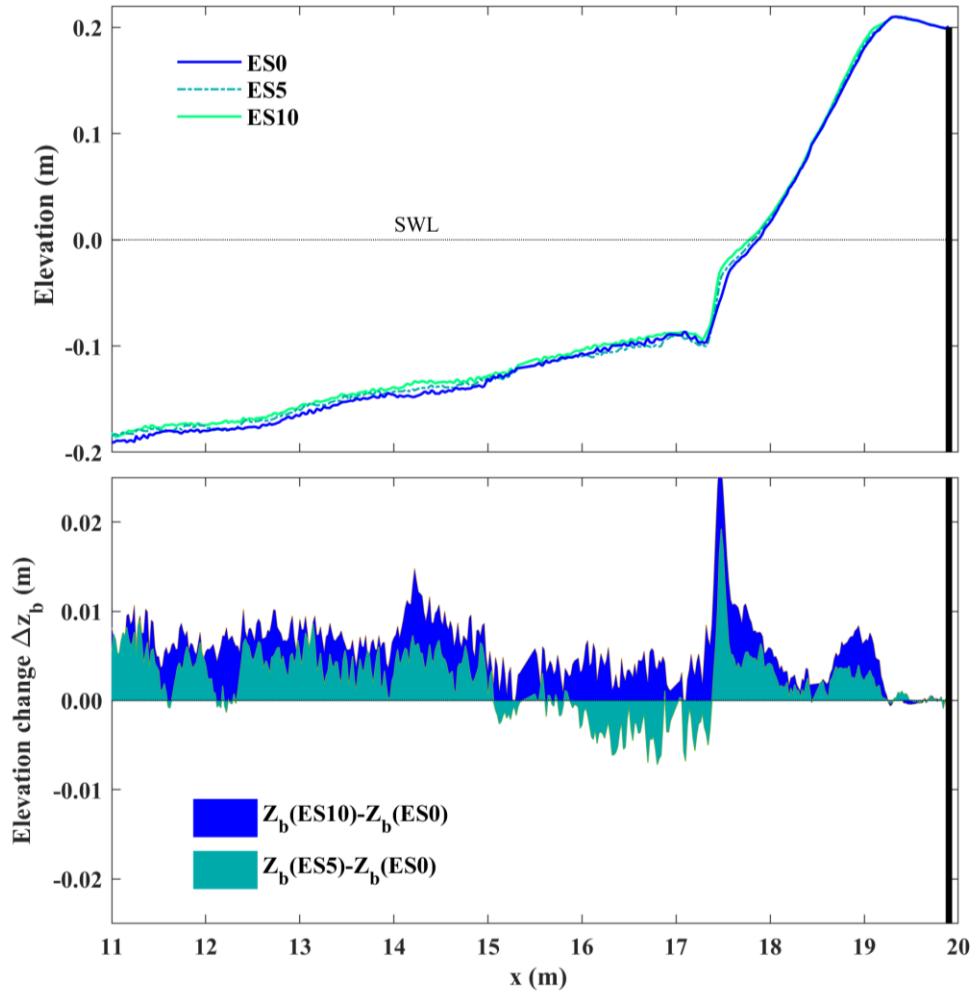


Figure 3.9 Measured initial, middle, and final beach profiles and changes of bottom elevation (ΔZ_b) for Test ES.

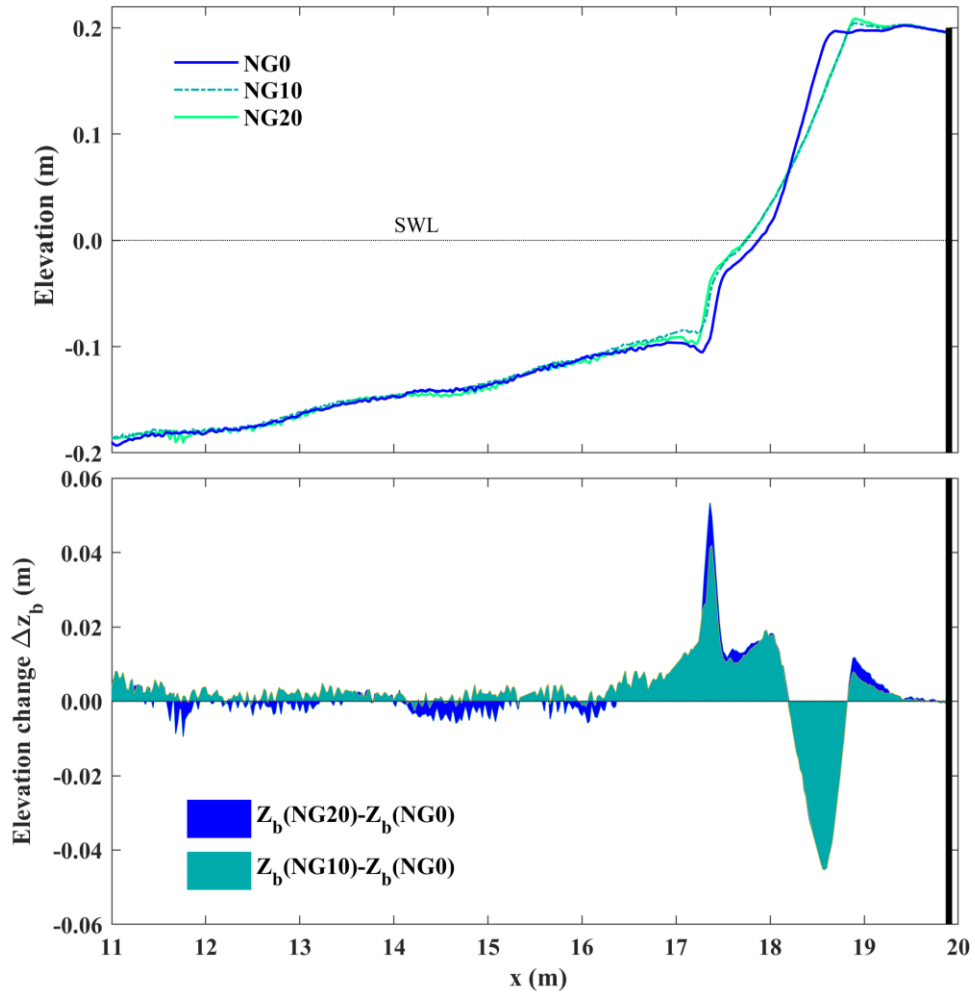


Figure 3.10 Measured initial, middle, and final beach profiles and changes of bottom elevation (ΔZ_b) for Test NG.

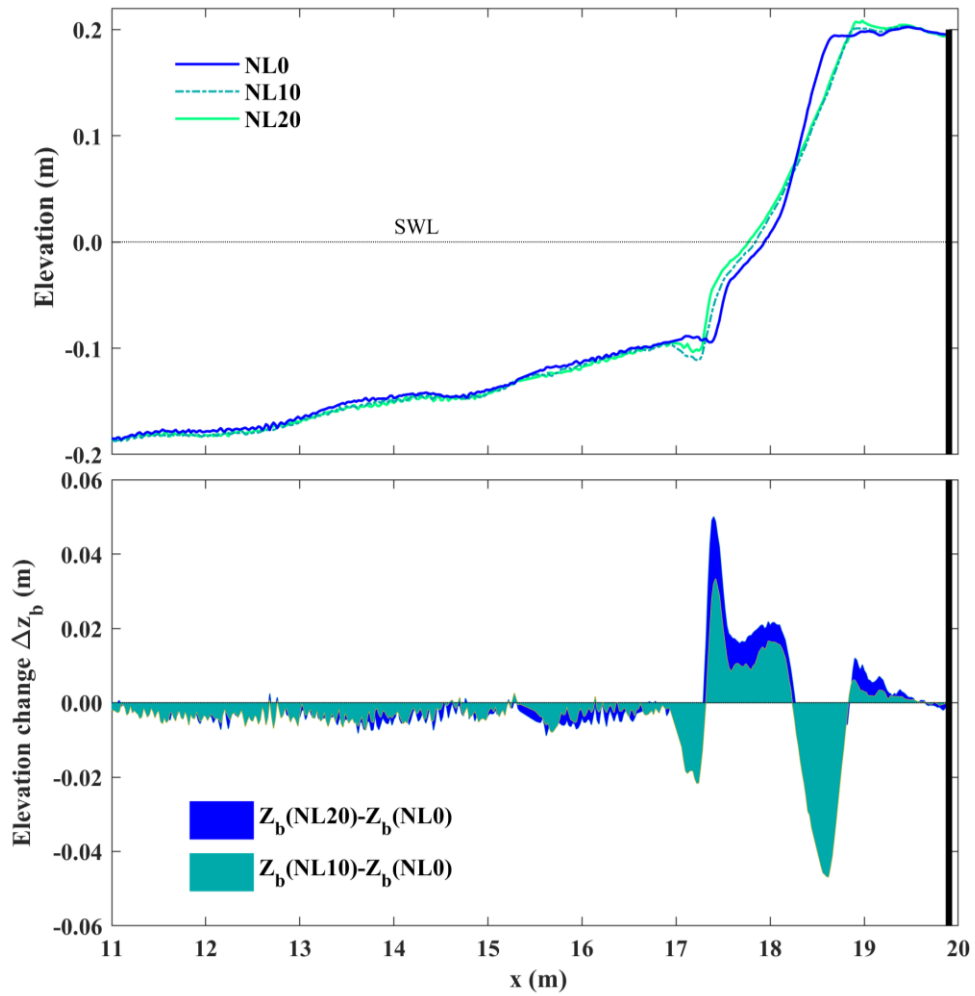


Figure 3.11 Measured initial, middle, and final beach profiles and changes of bottom elevation (ΔZ_b) for Test NL.

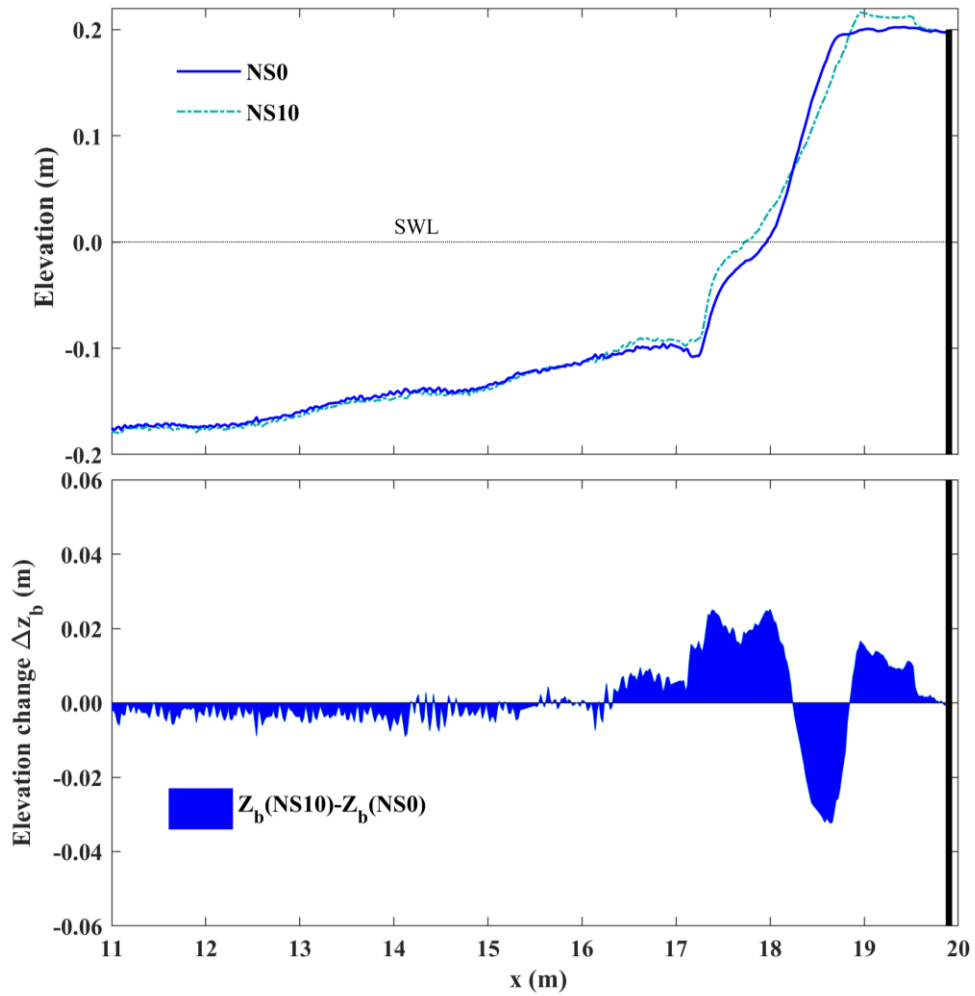


Figure 3.12 Measured initial and final beach profiles and changes of bottom elevation (ΔZ_b) for Test NS.

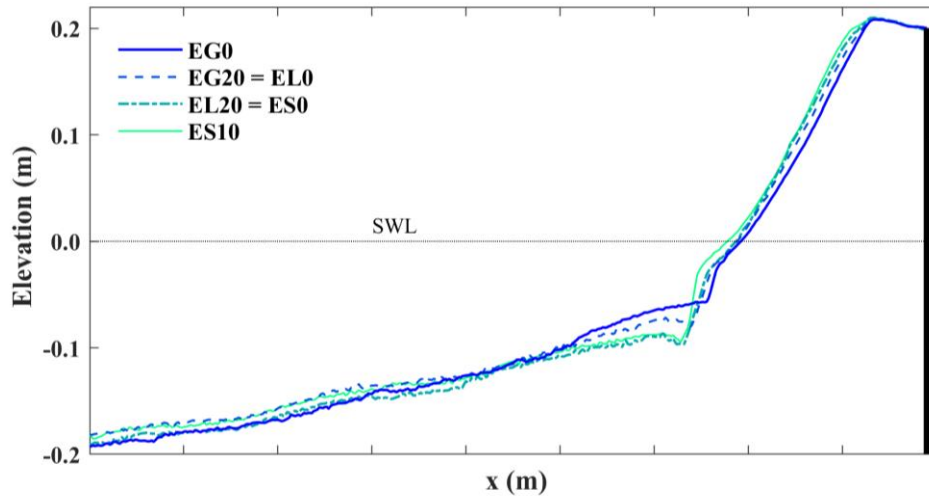


Figure 3.13 Differences and similarities of near equilibrium profiles of EG, EG20 = EL0, EL20 = ES0, ES10

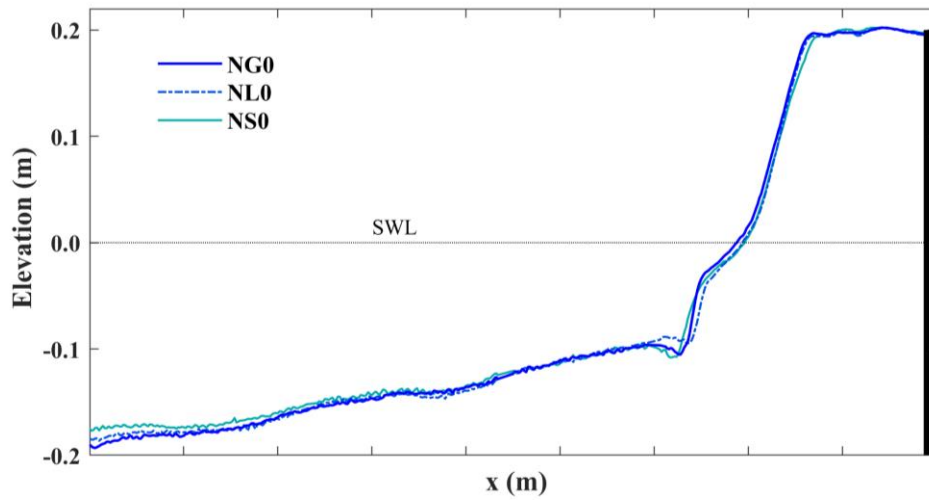


Figure 3.14 Similarities amongst measured beach profiles NG0, NL0, and NS0 depicting careful profile rebuilding.

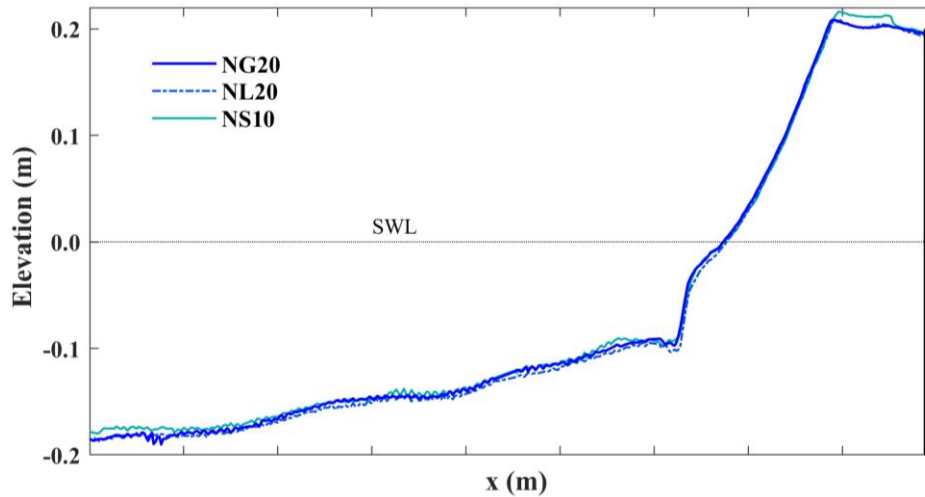


Figure 3.15 Similarities amongst measured beach profiles NG20, NL20, and NS20 depicting repeatable profile evolution.

3.3 Lagrangian Movement of 20 Individual Particles

The DO trajectory measurements during each of the six tests are documented because of the potential use by other researchers. For equilibrium profile tests, the 20 particles reached their destinations after 10 runs for the EG and EL tests and 5 runs for the ES test. The 20 particles were placed back at their initial locations for another 10(5) runs in order to examine the degree of repeatability of the 20 particle trajectories. For the nourished profile tests, the 20 particle destinations were recorded over 20(10) runs for NG and NL tests (NS test) without resetting DO locations. The Lagrangian movement of each DO for the six tests are tabulated in Tables 3.25-3.30 where XDO, YDO, and ZDO are the x , y and z coordinates of each DO and BDO is the DO bottom elevation relative to the local sand surface (negative for local scour). The 20 DOs were colored and numbered from 1 to 20. The final beach profiles and the final DO locations measured by the laser line scanner are depicted in Figures 3.16-3.21. It should be noted

that some data were not available because DOs were missing or undetectable below SWL.

Table 3.25 Lagrangian movement of DO#1-10 for EG1-EG5 (a)

DO#	1	2	3	4	5	6	7	8	9	10
	W	R	B	G	W/R	W/B	W/G	R/B	R/G	B/G
Initial location*										
XDO (m)	18.97	18.98	18.67	18.68	18.37	18.37	18.07	18.06	17.77	17.77
YDO (m)	-0.286	+0.285	-0.287	+0.280	-0.286	+0.291	-0.288	+0.279	-0.282	+0.293
ZDO (m)	+0.159	+0.157	+0.103	+0.107	+0.060	+0.065	+0.020	+0.021	-0.013	-0.016
BDO (m)	+0.000	+0.000	+0.000	+0.000	+0.000	+0.000	+0.000	+0.000	+0.000	+0.000
Location after EG1										
XDO (m)	18.97	18.97	18.57	17.57	17.60	18.06	18.06	18.11	18.08	17.70
YDO (m)	-0.286	+0.271	-0.279	+0.314	-0.307	+0.331	-0.313	+0.249	-0.285	+0.296
Location after EG2										
XDO (m)	18.97	18.97	18.57	17.57	17.60	18.06	18.06	18.11	17.74	17.70
YDO (m)	-0.286	+0.271	-0.279	+0.314	-0.307	+0.331	-0.313	+0.249	-0.292	+0.296
Location after EG3										
XDO (m)	18.97	18.97	18.57	17.57	17.60	18.06	18.06	18.11	17.74	17.70
YDO (m)	-0.286	+0.271	-0.279	+0.314	-0.307	+0.331	-0.313	+0.249	-0.292	+0.296
Location after EG4										
XDO (m)	18.97	18.97	18.57	17.57	17.60	18.06	18.06	18.11	17.74	17.70
YDO (m)	-0.286	+0.271	-0.279	+0.314	-0.307	+0.331	-0.313	+0.249	-0.292	+0.296
Final location after EG5*										
XDO (m)	18.97	18.97	18.57	17.57	17.60	18.06	18.06	18.11	17.65	17.70
YDO (m)	-0.286	+0.271	-0.279	+0.314	-0.307	+0.331	-0.313	+0.249	-0.292	+0.296
ZDO (m)	+0.155	+0.162	+0.092	-0.039	-0.030	+0.026	+0.018	+0.035	-0.024	-0.012
BDO (m)	-	-	-0.015	-0.018	-0.015	-0.020	-0.012	-0.022	-0.008	-

*Runs with DO locations measured by the laser line scanner but manual measurement for the other runs.

W-white, R-red, B-blue, G-green, W/R-white/red, W/B-white/blue, W/G-white/green, R/B-red/blue, R/G-red/green, B/G-blue/green.

Negative BDO implies the DO bottom below the local sand surface (local scour).

Table 3.25 Lagrangian movement of DO#11-20 for EG1-EG5 (b)

DO#	11	12	13	14	15	16	17	18	19	20
	O	W/O	O/R	O/B	O/G	[-]	[-]	[-]	[-]	[-]
Initial location*										
XDO (m)	16.67	16.75	16.18	16.19	14.72	14.71	14.21	14.21	11.95	11.95
YDO (m)	-0.266	+0.278	-0.269	+0.288	-0.278	+0.285	-0.294	+0.285	-0.289	+0.300
ZDO (m)	-0.064	-0.067	-0.100	-0.090	-0.131	-0.131	-0.137	-0.130	-0.183	-0.172
BDO (m)	+0.000	+0.000	+0.000	+0.000	+0.000	+0.000	+0.000	+0.000	+0.000	+0.000
Location after EG1										
XDO (m)	16.67	16.75	16.18	16.19	14.72	14.71	14.21	14.21	11.95	11.95
YDO (m)	-0.266	+0.278	-0.269	+0.288	-0.278	+0.285	-0.294	+0.285	-0.289	+0.300
Location after EG2										
XDO (m)	16.67	16.75	16.18	16.19	14.72	14.71	14.21	14.21	11.95	11.95
YDO (m)	-0.266	+0.278	-0.269	+0.288	-0.278	+0.285	-0.294	+0.285	-0.289	+0.300
Location after EG3										
XDO (m)	16.67	16.75	16.18	16.19	14.72	14.71	14.21	14.21	11.95	11.95
YDO (m)	-0.266	+0.278	-0.269	+0.288	-0.278	+0.285	-0.294	+0.285	-0.289	+0.300
Location after EG4										
XDO (m)	16.67	16.75	16.18	16.19	14.72	14.71	14.21	14.21	11.95	11.95
YDO (m)	-0.266	+0.278	-0.269	+0.288	-0.278	+0.285	-0.294	+0.285	-0.289	+0.300
Final location after EG5*										
XDO (m)	16.67	16.75	16.18	16.19	14.72	14.71	14.21	14.21	11.95	11.95
YDO (m)	-0.266	+0.278	-0.269	+0.288	-0.278	+0.285	-0.294	+0.285	-0.289	+0.300
ZDO (m)	-0.080	-0.071	-0.105	-0.081	-0.150	-0.131	-0.145	-0.147	-0.190	-0.183
BDO (m)	+0.000	+0.000	+0.000	+0.000	+0.000	+0.000	+0.000	+0.000	+0.000	+0.000

*Runs with DO locations measured by the laser line scanner but manual measurement for the other runs.

O-orange, W/O-white/orange, O/R-orange/red, O/B-orange/blue, O/G-orange/green, [-] numbered in Figure 2.2(a).

Table 3.26 Lagrangian movement of DO#1-10 for EG6-EG10 (a)

DO#	1	2	3	4	5	6	7	8	9	10
	W	R	B	G	W/R	W/B	W/G	R/B	R/G	B/G
Initial location*										
XDO (m)	18.93	18.97	18.57	17.57	17.60	18.06	18.06	18.11	17.65	17.70
YDO (m)	-0.286	+0.271	-0.279	+0.294	-0.307	+0.331	-0.274	+0.257	-0.292	+0.296
ZDO (m)	+0.155	+0.162	+0.092	-0.039	-0.030	+0.026	+0.018	+0.035	-0.024	-0.012
BDO (m)	+0.000	+0.000	-0.015	-0.018	-0.015	-0.020	-0.012	-0.022	-0.008	+0.000
Location after EG6										
XDO (m)	18.97	18.97	18.57	17.57	17.60	18.06	18.06	18.11	17.65	17.70
YDO (m)	-0.286	+0.271	-0.279	+0.294	-0.307	+0.331	-0.274	+0.257	-0.292	+0.296
Location after EG7										
XDO (m)	18.97	18.97	18.57	17.57	17.60	18.06	18.06	18.11	17.65	17.70
YDO (m)	-0.286	+0.271	-0.279	+0.294	-0.307	+0.331	-0.274	+0.257	-0.292	+0.296
Location after EG8										
XDO (m)	18.97	18.97	18.57	17.57	17.60	18.06	18.06	18.11	17.65	17.70
YDO (m)	-0.286	+0.271	-0.279	+0.294	-0.307	+0.331	-0.274	+0.257	-0.292	+0.296
Location after EG9										
XDO (m)	18.97	18.97	18.57	17.57	17.60	18.06	18.06	18.11	17.65	17.70
YDO (m)	-0.286	+0.271	-0.279	+0.294	-0.307	+0.331	-0.274	+0.257	-0.292	+0.296
Final location after EG10*										
XDO (m)	18.93	18.97	18.57	17.57	17.60	18.06	18.06	18.11	17.65	17.70
YDO (m)	-0.286	+0.271	-0.279	+0.294	-0.307	+0.331	-0.274	+0.257	-0.292	+0.296
ZDO (m)	+0.151	+0.158	+0.090	-0.041	-0.033	+0.026	+0.016	+0.035	-0.022	-0.014
BDO (m)	-0.009	-0.008	-0.013	-0.023	-0.018	-0.013	-0.011	-0.015	-0.014	-0.011

*DO locations measured by the laser line scanner in this table and subsequent tables

W-white, R-red, B-blue, G-green, W/R-white/red, W/B-white/blue, W/G-white/green, R/B-red/blue, R/G-red/green, B/G-blue/green

Table 3.26 Lagrangian movement of DO#11-20 for EG6-EG10 (b)

DO#	11	12	13	14	15	16	17	18	19	20
	O	W/O	O/R	O/B	O/G	[-]	[-]	[-]	[-]	[-]
Initial location*										
XDO (m)	16.72	16.75	16.18	16.19	14.72	14.71	14.21	14.21	11.95	11.95
YDO (m)	-0.266	+0.278	-0.269	+0.288	-0.278	+0.285	-0.294	+0.285	-0.289	+0.300
ZDO (m)	-0.080	-0.071	-0.105	-0.081	-0.150	-0.131	-0.145	-0.147	-0.190	-0.183
BDO (m)	+0.000	+0.000	+0.000	+0.000	+0.000	+0.000	+0.000	+0.000	+0.000	+0.000
Location after EG6										
XDO (m)	16.72	16.75	16.18	16.19	14.72	14.71	14.21	14.21	11.95	11.95
YDO (m)	-0.266	+0.278	-0.269	+0.288	-0.278	+0.285	-0.294	+0.285	-0.289	+0.300
Location after EG7										
XDO (m)	16.72	16.75	16.18	16.19	14.72	14.71	14.21	14.21	11.95	11.95
YDO (m)	-0.266	+0.278	-0.269	+0.288	-0.278	+0.285	-0.294	+0.285	-0.289	+0.300
Location after EG8										
XDO (m)	16.72	16.75	16.18	16.19	14.72	14.71	14.21	14.21	11.95	11.95
YDO (m)	-0.266	+0.278	-0.269	+0.288	-0.278	+0.285	-0.294	+0.285	-0.289	+0.300
Location after EG9										
XDO (m)	16.72	16.75	16.18	16.19	14.72	14.71	14.21	14.21	11.95	11.95
YDO (m)	-0.266	+0.278	-0.269	+0.288	-0.278	+0.285	-0.294	+0.285	-0.289	+0.300
Final location after EG10*										
XDO (m)	16.72	16.75	16.18	16.19	14.72	14.71	14.21	14.21	11.95	11.95
YDO (m)	-0.266	+0.278	-0.269	+0.288	-0.278	+0.285	-0.294	+0.285	-0.289	+0.300
ZDO (m)	-0.086	-0.072	-0.101	-0.091	-0.149	-0.130	-0.153	-0.141	-0.190	-0.180
BDO (m)	+0.000	+0.000	+0.000	+0.000	+0.000	+0.000	+0.000	+0.000	+0.000	+0.000

O-orange, W/O-white/orange, O/R-orange/red, O/B-orange/blue, O/G-orange/green, [-] numbered

Table 3.27 Lagrangian movement of DO#1-10 (after DO resetting) for EG11-EG20 (a)

DO#	1	2	3	4	5	6	7	8	9	10
	W	R	B	G	W/R	W/B	W/G	R/B	R/G	B/G
Initial location*										
XDO (m)	18.96	18.99	18.67	18.68	18.35	18.38	18.06	18.06	17.75	17.76
YDO (m)	-0.286	+0.313	-0.275	+0.274	-0.288	+0.294	-0.286	+0.296	-0.287	+0.301
ZDO (m)	+0.156	+0.165	+0.108	+0.116	+0.059	+0.065	+0.017	+0.028	-0.022	-0.016
BDO (m)	+0.000	+0.000	+0.000	+0.000	+0.000	+0.000	+0.000	+0.000	+0.000	+0.000
Location after EG11										
XDO (m)	18.96	18.99	18.23	18.52	17.47	17.62	17.86	18.13	17.78	17.56
YDO (m)	-0.286	+0.313	-0.293	+0.331	-0.130	+0.314	-0.465	+0.303	-0.300	+0.267
Location after EG12										
XDO (m)	18.96	18.99	18.23	18.52	17.47	17.62	17.87	18.13	17.78	17.56
YDO (m)	-0.286	+0.313	-0.293	+0.331	-0.130	+0.314	-0.345	+0.303	-0.300	+0.267
Location after EG13										
XDO (m)	18.96	18.99	18.23	18.52	17.47	17.62	17.48	18.13	17.78	17.56
YDO (m)	-0.286	+0.313	-0.293	+0.331	-0.130	+0.314	-0.323	+0.303	-0.300	+0.267
Location after EG14										
XDO (m)	18.96	18.99	18.23	18.52	17.47	17.62	17.48	18.13	17.78	17.56
YDO (m)	-0.286	+0.313	-0.293	+0.331	-0.130	+0.314	-0.323	+0.303	-0.300	+0.267
Location after EG15										
XDO (m)	18.96	18.99	18.23	18.52	17.47	17.62	17.48	18.13	17.78	17.56
YDO (m)	-0.286	+0.313	-0.293	+0.331	-0.130	+0.314	-0.323	+0.303	-0.300	+0.267
Location after EG16										
XDO (m)	18.96	18.99	18.23	18.52	17.47	17.62	17.48	18.13	17.78	17.56
YDO (m)	-0.286	+0.313	-0.293	+0.331	-0.130	+0.314	-0.323	+0.303	-0.300	+0.267
Location after EG17										
XDO (m)	18.96	18.99	18.23	18.52	17.47	17.62	17.48	18.13	17.78	17.56
YDO (m)	-0.286	+0.313	-0.293	+0.331	-0.130	+0.314	-0.323	+0.303	-0.300	+0.267
Location after EG18										
XDO (m)	18.96	18.99	18.23	18.52	17.47	17.62	17.48	18.13	17.78	17.56
YDO (m)	-0.286	+0.313	-0.293	+0.331	-0.130	+0.314	-0.323	+0.303	-0.300	+0.267
Location after EG19										

XDO (m)	18.96	18.99	18.23	18.52	17.47	17.62	17.48	18.13	17.78	17.56
YDO (m)	-0.286	+0.313	-0.293	+0.331	-0.130	+0.314	-0.323	+0.303	-0.300	+0.267
Final location after EG20*										
XDO (m)	18.96	18.99	18.23	18.52	17.47	17.62	17.48	18.13	17.78	17.56
YDO (m)	-0.286	+0.313	-0.293	+0.331	-0.130	+0.314	-0.323	+0.303	-0.300	+0.267
ZDO (m)	+0.156	+0.165	+0.047	+0.093	-0.062	-0.018	-0.041	+0.038	-0.011	-0.031
BDO (m)	+0.005	+0.007	+0.013	+0.015	+0.016	+0.010	+0.016	+0.010	+0.012	+0.013

W-white, R-red, B-blue, G-green, W/R-white/red, W/B-white/blue, W/G-white/green, R/B-red/blue,
R/G-red/green, B/G-blue/green

Table 3.27 Lagrangian movement of DO#11-20 (after DO resetting) for EG11-EG20 (b)

DO#	11	12	13	14	15	16	17	18	19	20
	O	W/O	O/R	O/B	O/G	[-]	[-]	[-]	[-]	[-]
Initial location*										
XDO (m)	16.74	16.71	16.23	16.26	14.74	14.74	14.26	14.25	11.99	11.95
YDO (m)	-0.268	+0.284	-0.282	+0.308	-0.288	+0.317	-0.286	+0.286	-0.292	+0.322
ZDO (m)	-0.092	-0.091	-0.111	-0.102	-0.122	-0.141	-0.142	-0.150	-0.199	-0.195

BDO (m)	+0.000	+0.000	+0.000	+0.000	+0.000	+0.000	+0.000	+0.000	+0.000	+0.000
Location after EG11										
XDO (m)	16.74	16.71	16.23	16.26	14.74	14.74	14.26	14.25	11.99	11.95
YDO (m)	-0.268	+0.284	-0.282	+0.308	-0.288	+0.317	-0.286	+0.286	-0.292	+0.322
Location after EG12										
XDO (m)	16.74	16.71	16.23	16.26	14.74	14.74	14.26	14.25	11.99	11.95
YDO (m)	-0.268	+0.284	-0.282	+0.308	-0.288	+0.317	-0.286	+0.286	-0.292	+0.322
Location after EG13										
XDO (m)	16.74	16.71	16.23	16.26	14.74	14.74	14.26	14.25	11.99	11.95
YDO (m)	-0.268	+0.284	-0.282	+0.308	-0.288	+0.317	-0.286	+0.286	-0.292	+0.322
Location after EG14										
XDO (m)	16.74	16.71	16.23	16.26	14.74	14.74	14.26	14.25	11.99	11.95
YDO (m)	-0.268	+0.284	-0.282	+0.308	-0.288	+0.317	-0.286	+0.286	-0.292	+0.322
Location after EG15										
XDO (m)	16.74	16.71	16.23	16.26	14.74	14.74	14.26	14.25	11.99	11.95
YDO (m)	-0.268	+0.284	-0.282	+0.308	-0.288	+0.317	-0.286	+0.286	-0.292	+0.322
Location after EG16										
XDO (m)	16.74	16.71	16.23	16.26	14.74	14.74	14.26	14.25	11.99	11.95
YDO (m)	-0.268	+0.284	-0.282	+0.308	-0.288	+0.317	-0.286	+0.286	-0.292	+0.322
Location after EG17										
XDO (m)	16.74	16.71	16.23	16.26	14.74	14.74	14.26	14.25	11.99	11.95
YDO (m)	-0.268	+0.284	-0.282	+0.308	-0.288	+0.317	-0.286	+0.286	-0.292	+0.322
Location after EG18										
XDO (m)	16.74	16.71	16.23	16.26	14.74	14.74	14.26	14.25	11.99	11.95
YDO (m)	-0.268	+0.284	-0.282	+0.308	-0.288	+0.317	-0.286	+0.286	-0.292	+0.322
Location after EG19										
XDO (m)	16.74	16.71	16.23	16.26	14.74	14.74	14.26	14.25	11.99	11.95
YDO (m)	-0.268	+0.284	-0.282	+0.308	-0.288	+0.317	-0.286	+0.286	-0.292	+0.322
Final location after EG20*										
XDO (m)	16.74	16.71	16.23	16.26	14.74	14.74	14.26	14.25	11.99	11.95
YDO (m)	-0.268	+0.284	-0.282	+0.308	-0.288	+0.317	-0.286	+0.286	-0.292	+0.322
ZDO (m)	-0.092	-0.091	-0.111	-0.102	-0.128	-0.135	-0.144	-0.150	-0.192	-0.191
BDO (m)	+0.000	+0.000	+0.000	+0.000	+0.000	+0.000	+0.000	+0.000	+0.000	+0.000

O=orange, W/O=white/orange, O/R=orange/red, O/B=orange/blue, O/G=orange/green, [-] numbered

Table 3.28 Lagrangian movement of DO#1-10 for EL1-EL10 (a)

DO#	1	2	3	4	5	6	7	8	9	10
	O	R	B	M/O	G	O/G	R/B	B/O	M/G	G/R
Initial location*										
XDO (m)	18.98	18.98	18.68	18.68	18.38	18.37	18.08	18.07	17.77	17.77
YDO (m)	-0.274	+0.292	-0.277	+0.285	-0.272	+0.293	-0.275	+0.288	-0.275	+0.295
ZDO (m)	+0.163	+0.166	+0.112	+0.109	+0.062	+0.070	+0.017	+0.025	-0.021	-0.020
BDO (m)	+0.000	+0.000	+0.000	+0.000	+0.000	+0.000	+0.000	+0.000	+0.000	+0.000
Location after EL1										
XDO (m)	-	19.14	19.21	19.23	19.44	17.9	17.40	19.15	17.97	17.9
YDO (m)	-	+0.115	-0.055	+0.175	-0.285	-0.285	-0.355	-0.515	-0.350	-0.315
Location after EL2										
XDO (m)	-	19.27	19.24	19.27	19.44	17.83	17.86	-	-	17.86
YDO (m)	-	+0.160	-0.015	+0.167	-0.305	+0.245	-0.085	-	-	-0.035
Location after EL3										
XDO (m)	-	19.27	19.10	19.27	19.44	17.88	17.96	-	17.95	17.96
YDO (m)	-	+0.165	+0.080	+0.167	-0.305	-0.290	-0.435	-	-0.095	-0.395
Location after EL4										
XDO (m)	-	19.27	19.21	19.27	19.53	17.95	17.66	19.32	-	-
YDO (m)	-	+0.165	+0.105	+0.167	-0.254	-0.445	-0.360	-0.523	-	-
Location after EL5										
XDO (m)	-	19.27	19.21	19.27	19.53	-	17.94	19.32	17.85	-
YDO (m)	-	+0.165	+0.105	+0.167	-0.254	-	-0.295	-0.523	-0.135	-
Location after EL6										
XDO (m)	-	19.27	19.21	19.27	19.53	-	17.88	19.32	17.88	-
YDO (m)	-	+0.165	+0.105	+0.167	-0.254	-	-0.355	-0.523	-0.575	-
Location after EL7										
XDO (m)	-	19.27	19.21	19.27	19.53	17.91	-	19.32	17.90	18.02
YDO (m)	-	+0.165	+0.105	+0.167	-0.254	-0.240	-	-0.523	-0.515	-0.425
Location after EL8										
XDO (m)	-	19.27	19.23	19.27	19.53	18.14	-	19.32	19.15	17.90
YDO (m)	-	+0.165	+0.095	+0.167	-0.254	+0.025	-	-0.523	-0.085	-0.015
Location after EL9										

XDO (m)	-	19.27	19.22	19.27	19.53	-	-	19.32	19.19	17.90
YDO (m)		+0.165	+0.107	+0.167	-0.265	-	-	-0.523	-0.033	-0.075
Final location after EL10*										
XDO (m)	-	19.27	19.22	19.27	19.53	19.16	17.85	19.32	19.19	17.86
YDO (m)	-	+0.165	+0.107	+0.167	-0.254	+0.137	+0.060	-0.523	-0.033	-0.455
ZDO (m)		+0.202	+0.200	+0.202	+0.202	+0.188	-0.001	+0.203	+0.195	-0.008
BDO (m)		+0.000	+0.000	+0.000	+0.000	+0.000	+0.000	+0.000	+0.000	+0.000

O-orange, R-red, B-blue, M/O-magenta/orange, G-green, O/G-orange/green, R/B-red/blue, B/O-blue/orange, M/G-magenta/green, G/R-green/red

' - ' not detected

Table 3.28 Lagrangian movement of DO#11-20 for EL1-EL10 (b)

DO#	11	12	13	14	15	16	17	18	19	20
	O/B	R/O	B/G	M/B	G/O	O/R	R/G	B/R	M/R	G/B
Initial location *										
XDO (m)	16.72	16.68	16.22	16.24	14.73	14.71	14.26	14.23	11.97	11.93
YDO (m)	-0.277	+0.299	-0.306	+0.320	-0.301	+0.328	-0.307	+0.294	-0.317	+0.336
ZDO (m)	-0.111	-0.091	-0.129	-0.113	-0.150	-0.140	-0.157	-0.155	-0.204	-0.200
BDO (m)	+0.000	+0.000	+0.000	+0.000	+0.000	+0.000	+0.000	+0.000	+0.000	+0.000
Location after EL1										
XDO (m)	-	17.44	-	17.95	-	15.50	-	-	12.43	-

YDO (m)	-	-0.315	-	-0.200	-	+0.315	-	-	+0.155	-
Location after EL2										
XDO (m)	17.96	-	17.90	17.88	-	-	15.11	-	-	-
YDO (m)	-0.005	-	+0.175	+0.005	-	-	+0.065	-	-	-
Location after EL3										
XDO (m)	18.99	17.84	17.94	17.95	-	-	-	-	-	-
YDO (m)	-0.575	-0.145	-0.425	-0.195	-	-	-	-	-	-
Location after EL4										
XDO (m)	17.95	17.86	17.88	17.88	-	-	17.81	-	-	-
YDO (m)	-0.375	-0.485	-0.495	-0.490	-	-	-0.205	-	-	-
Location after EL5										
XDO (m)	17.92	17.48	17.81	17.71	17.81	17.91	17.84	17.27	13.70	12.38
YDO (m)	-0.435	-0.105	-0.180	-0.230	-0.185	+0.235	-0.190	+0.125	+0.325	+0.365
Location after EL6										
XDO (m)	17.71	-	-	17.71	-	17.84	-	17.86	-	-
YDO (m)	+0.085	-	-	+0.065	-	-0.135	-	+0.285	-	-
Location after EL7										
XDO (m)	-	17.80	-	17.98	17.85	17.95	19.20	17.98	-	-
YDO (m)	-	-0.300	-	-0.405	-0.300	-0.495	+0.483	-0.545	-	-
Location after EL8										
XDO (m)	17.93	17.89	17.87	17.75	17.80	18.12	19.20	17.83	-	-
YDO (m)	+0.010	-0.445	+0.115	-0.175	-0.195	+0.045	+0.483	-0.495	-	-
Location after EL9										
XDO (m)	17.90	-	17.94	17.81	-	19.10	19.20	17.90	-	-
YDO (m)	-0.165	-	-0.005	+0.210	-	+0.190	+0.483	-0.275	-	-
Final location after EL10										
XDO (m)	17.85	17.85	17.32	17.87	17.80	19.14	19.20	17.40	11.90	12.52
YDO (m)	+0.023	-0.297	-0.232	-0.389	-0.441	+0.243	+0.483	+0.396	-0.043	-0.508
ZDO (m)	-0.002	-0.003	-0.089	-0.003	-0.016	+0.185	+0.194	-0.086	-0.171	-0.168
BDO (m)	+0.000	+0.000	+0.000	+0.000	+0.000	+0.000	+0.000	+0.000	+0.000	+0.000

O/B-orange/blue, R/O-red/orange, B/G-blue/green, M/B-magenta/blue, G/O-green/orange, O/R-orange/red, R/G-red/green, B/R-blue/red, M/R-magenta/red, G/B-green/blue

' - ' not detected

Table 3.29 Lagrangian movement of DO#1-10 (after DO resetting) for EL11-EL20 (a)

DO#	1	2	3	4	5	6	7	8	9	10
	O	R	B	M/O	G	O/G	R/B	B/O	M/G	G/R
Initial location*										
XDO (m)	19.03	19.00	18.73	18.70	18.43	18.40	18.11	18.10	17.82	17.81
YDO (m)	-0.254	0.286	-0.290	0.274	-0.275	0.282	-0.271	0.284	-0.265	0.284
ZDO (m)	+0.173	+0.167	+0.123	+0.118	+0.075	+0.074	+0.027	+0.031	-0.015	-0.009
BDO (m)	+0.000	+0.000	+0.000	+0.000	+0.000	+0.000	+0.000	+0.000	+0.000	+0.000
Location after EL11										
XDO (m)	19.01	19.21	19.14	19.21	19.15	19.23	19.21	-	17.39	-
YDO (m)	-0.295	0.145	-0.115	0.085	-0.125	0.155	-0.155	-	0.065	-
Location after EL12										
XDO (m)	19.01	19.28	19.21	19.24	19.21	19.28	19.20	17.80	17.92	17.92
YDO (m)	-0.295	0.125	-0.105	0.065	-0.125	0.185	-0.155	0.065	-0.425	-0.435
Location after EL13										
XDO (m)	19.01	19.29	19.39	19.26	19.34	19.30	19.34	17.97	18.02	17.88
YDO (m)	-0.295	0.125	-0.075	0.065	-0.065	0.185	-0.045	-0.155	-0.185	-0.045
Location after EL14										
XDO (m)	19.01	19.29	19.39	19.26	19.34	19.30	19.34	17.96	-	-
YDO (m)	-0.295	0.125	-0.075	0.065	-0.065	0.185	-0.045	0.315	-	-
Location after EL15										
XDO (m)	19.01	19.29	19.39	19.26	19.34	19.30	19.34	17.88	17.40	17.93
YDO (m)	-0.295	0.125	-0.075	0.065	-0.065	0.185	-0.045	0.325	0.355	0.205
Location after EL16										
XDO (m)	19.01	19.29	19.39	19.26	19.34	19.30	19.34	17.86	-	17.70
YDO (m)	-0.295	0.125	-0.075	0.065	-0.065	0.185	-0.045	-0.185	-	0.225
Location after EL17										
XDO (m)	19.05	19.29	19.39	19.26	19.34	19.30	19.34	17.85	17.86	-
YDO (m)	-0.295	0.125	-0.075	0.065	-0.065	0.185	-0.045	-0.045	-0.225	-
Location after EL18										
XDO (m)	19.05	19.29	19.39	19.24	19.34	19.30	19.34	17.93	17.93	17.95
YDO (m)	-0.295	0.125	-0.075	0.105	-0.065	0.185	-0.045	0.125	0.375	-0.195
Location after EL19										

XDO (m)	19.05	19.29	19.39	19.22	19.34	19.30	19.34	17.93	17.60	17.86
YDO (m)	-0.295	0.125	-0.075	0.105	-0.065	0.185	-0.045	0.235	-0.475	0.025
Final Location after EL20*										
XDO (m)	19.05	19.28	19.37	19.24	19.33	19.29	19.33	17.94	17.59	17.88
YDO (m)	-0.295	0.135	-0.067	0.110	-0.062	0.206	-0.043	0.411	-0.014	0.023
ZDO (m)	+0.191	+0.208	+0.224	+0.207	+0.212	+0.215	+0.213	+0.016	-0.013	+0.012
BDO (m)	-0.005	+0.000	+0.000	+0.000	+0.000	+0.000	+0.000	+0.000	+0.000	+0.000

O-orange, R-red, B-blue, M/O-magenta/orange, G-green, O/G-orange/green, R/B-red/blue, B/O-blue/orange, M/G-magenta/green, G/R-green/red, O/B-orange/blue, R/O-red/orange, B/G-blue/green, M/B-magenta/blue, G/O-green/orange, O/R-orange/red, R/G-red/green, B/R-blue/red, M/R-magenta/red, G/B-green/blue

' - ' not detected

Table 3.29 Lagrangian movement of DO#11-20 (after DO resetting) for EL11-EL20 (b)

DO#	11	12	13	14	15	16	17	18	19	20
	O/B	R/O	B/G	M/B	G/O	O/R	R/G	B/R	M/R	G/B
Initial location*										
XDO (m)	16.71	16.68	16.24	16.21	14.74	14.73	14.17	14.15	12.04	12.01
YDO (m)	-0.250	0.272	-0.276	0.286	-0.264	0.275	-0.278	0.247	-0.295	0.278
ZDO (m)	-0.109	-0.093	-0.120	-0.097	-0.143	-0.139	-0.141	-0.132	-0.181	-0.173
BDO (m)	+0.000	+0.000	+0.000	+0.000	+0.000	+0.000	+0.000	+0.000	+0.000	+0.000
Location after EL11										

XDO (m)	16.70	17.37	16.53	17.40	-	-	14.80	15.09	11.83	-
YDO (m)	-0.180	-0.195	0.025	0.075	-	-	-0.045	0.045	-0.579	-
Location after EL12										
XDO (m)	17.77	17.70	-	-	-	-	-	-	-	-
YDO (m)	-0.075	-0.315	-	-	-	-	-	-	-	-
Location after EL13										
XDO (m)	-	-	17.88	17.86	-	-	-	-	-	-
YDO (m)	-	-	-0.405	-0.115	-	-	-	-	-	-
Location after EL14										
XDO (m)	17.87	-	17.96	17.94	17.91	-	-	-	-	-
YDO (m)	0.245	-	0.295	0.020	-0.205	-	-	-	-	-
Location after EL15										
XDO (m)	17.26	17.38	17.90	17.93	17.90	15.28	17.85	17.90	12.55	12.85
YDO (m)	0.185	0.185	0.115	0.305	0.255	-0.175	-0.255	0.185	0.045	0.525
Location after EL16										
XDO (m)	-	17.10	-	17.90	17.75	-	17.93	17.75	-	-
YDO (m)	-	0.065	-	0.315	-0.135	-	-0.275	-0.105	-	-
Location after EL17										
XDO (m)	-	-	17.84	-	17.86	-	17.89	17.97	-	-
YDO (m)	-	-	-0.535	-	-0.555	-	-0.225	-0.405	-	-
Location after EL18										
XDO (m)	-	19.13	17.87	19.19	17.93	17.93	17.90	17.83	-	-
YDO (m)	-	0.380	-0.075	0.425	0.025	-0.225	-0.205	0.110	-	-
Location after EL19										
XDO (m)	17.89	19.19	17.90	19.19	17.95	17.83	17.80	-	-	-
YDO (m)	0.295	0.350	0.245	0.425	-0.275	-0.205	0.395	-	-	-
Final location after EL20										
XDO (m)	17.95	19.21	17.80	19.21	17.78	17.33	17.87	17.66	13.95	17.25
YDO (m)	+0.056	+0.324	-0.060	+0.409	+0.206	-0.367	-0.081	+0.073	-0.50	-0.452
ZDO (m)	+0.017	+0.201	+0.001	+0.201	+0.006	-0.103	+0.006	-0.004	-0.149	-0.105
BDO (m)	+0.000	+0.000	+0.000	+0.000	+0.000	+0.000	+0.000	+0.000	+0.000	+0.000

O/B-orange/blue, R/O-red/orange, B/G-blue/green, M/B-magenta/blue, G/O-green/orange, O/R-orange/red, R/G-red/green, B/R-blue/red, M/R-magenta/red, G/B-green/blue

' - ' not detected

Table 3.30 Lagrangian movement of DO#1-10 for ES1-ES5 (a)

DO#	1	2	3	4	5	6	7	8	9	10
	DB	M	B	W	Y	CB	HG	BS	B	PB
Initial location*										
XDO (m)	18.99	18.99	18.69	18.70	18.40	18.39	18.09	18.09	17.80	17.79
YDO (m)	-0.256	0.267	-0.260	0.273	-0.275	0.280	-0.274	0.286	-0.271	0.290
ZDO (m)	+0.186	+0.186	+0.130	+0.136	+0.081	+0.084	+0.032	+0.046	-0.004	+0.001
BDO (m)	+0.000	+0.000	+0.000	+0.000	+0.000	+0.000	+0.000	+0.000	+0.000	+0.000
Location after ES1										
XDO (m)	19.19	-	-	-	19.19	19.24	-	19.24	17.94	-
YDO (m)	-0.135	-	-	-	-0.055	0.225	-	0.215	-0.215	-
Location after ES2										
XDO (m)	19.19	-	-	-	19.17	19.27	-	19.27	-	18.15
YDO (m)	0.015	-	-	-	0.055	0.225	-	0.215	-	0.405
Location after ES3										
XDO (m)	19.26	-	19.26	19.28	19.23	19.30	19.30	19.28	19.16	19.25
YDO (m)	0.015	-	-0.015	0.205	0.110	0.235	0.185	0.195	-0.135	0.295
Location after ES4										
XDO (m)	19.28	-	-	-	19.28	19.28	19.28	19.26	19.29	19.28
YDO (m)	-0.025	-	-	-	0.095	0.215	0.300	0.215	-0.025	0.285
Final location after ES5*										
XDO (m)	19.25	17.19	19.41	-	19.28	19.27	-	19.25	13.00	19.26
YDO (m)	0.024	0.519	-0.003	-	0.093	0.208	-	0.208	-0.223	0.286
ZDO (m)	+0.209	-0.087	+0.209	-	+0.209	+0.202	-	+0.205	-0.167	+0.202
BDO (m)	+0.000	+0.000	+0.000	-	+0.000	+0.000	-	+0.000	+0.000	+0.000

DB-Dark Blue, M-Magenta, B-Black, W-White, Y-Yellow, CB-Cerulean Blue, HG-Hooker's Green,
BS-Burnt Sienna, B-Beige, PB-Prussian Blue

' - ' not detected

Table 3.30 Lagrangian movement of DO#11-20 for ES1-ES5 (b)

DO#	11	12	13	14	15	16	17	18	19	20
	S	B	P	G	SG	EG	O	CR	GY	CB
Initial location*										
XDO (m)	16.64	16.68	16.20	16.19	14.68	14.69	14.20	14.21	11.94	11.95
YDO (m)	-0.268	0.275	-0.267	0.279	-0.275	0.275	-0.275	0.277	-0.279	0.278
ZDO (m)	-0.104	-0.089	-0.112	-0.096	-0.133	-0.125	-0.136	-0.136	-0.165	-0.162
BDO (m)	+0.000	+0.000	+0.000	+0.000	+0.000	+0.000	+0.000	+0.000	+0.000	+0.000
Location after ES1										
XDO (m)	18.20	-	17.96	-	-	-	-	-	-	-
YDO (m)	-0.225	-	0.155	-	-	-	-	-	-	-
Location after ES2										
XDO (m)	18.12	18.13	18.15	-	18.15	18.15	18.12	18.21	-	-
YDO (m)	0.365	0.375	0.085	-	0.455	-0.285	0.395	0.035	-	-
Location after ES3										
XDO (m)	19.27	-	19.25	-	19.29	-	19.29	19.21	-	-
YDO (m)	0.305	-	0.110	-	0.395	-	0.325	0.115	-	-
Location after ES4										
XDO (m)	19.30	-	19.26	-	19.37	18.15	19.32	19.27	-	18.15
YDO (m)	0.285	-	0.105	-	0.385	0.005	0.315	0.115	-	0.165
Final location after ES5*										
XDO (m)	19.29	-	19.26	19.26	19.35	19.30	19.31	19.27	17.71	19.24
YDO (m)	0.277	-	0.108	-0.038	0.362	0.004	0.298	0.110	-0.296	0.122
ZDO (m)	+0.208	-	+0.205	+0.209	+0.206	+0.211	+0.203	+0.203	-0.019	+0.204
BDO (m)	+0.000	-	+0.000	+0.000	+0.000	+0.000	+0.000	+0.000	+0.000	+0.000

S-Silver, B-Brown, P-Purple, G-Gold, SG-Sap Green, EG-Emerald Green, O-Orange, CR-Crimson
Red, GY-Grow Yellow, CB-Cobalt Blue

' - ' not detected

Table 3.31 Lagrangian movement of DO#1-10 (after DO resetting) for ES6-ES10 (a)

DO#	1	2	3	4	5	6	7	8	9	10
	DB	M	G/R	G/B1	Y	CB	Y/B	BS	O/B	G/B2
Initial location*										
XDO (m)	18.96	18.96	18.65	18.66	18.37	18.36	18.07	18.06	17.76	17.76
YDO (m)	-0.258	0.282	-0.276	0.285	-0.254	0.285	-0.260	0.283	-0.265	0.291
ZDO (m)	+0.186	+0.186	+0.132	+0.135	+0.078	+0.082	+0.034	+0.041	-0.004	+0.003
BDO (m)	+0.000	+0.000	+0.000	+0.000	+0.000	+0.000	+0.000	+0.000	+0.000	+0.000
Locations after ES6										
XDO (m)	19.46	19.33	19.46	19.33	19.34	19.33	18.11	17.86	-	17.90
YDO (m)	-0.145	0.295	-0.120	0.305	-0.065	0.280	0.395	0.395	-	-0.375
Locations after ES7										
XDO (m)	19.46	19.47	19.46	19.51	19.34	19.33	19.46	18.14	18.14	-
YDO (m)	-0.145	0.280	-0.120	0.285	-0.065	0.280	0.280	0.265	0.190	-
Locations after ES8										
XDO (m)	19.46	19.47	19.46	19.51	19.34	19.33	19.46	-	19.44	-
YDO (m)	-0.145	0.280	-0.120	0.285	-0.065	0.280	0.280	-	0.265	-
Locations after ES9										
XDO (m)	19.50	19.47	19.50	19.51	19.41	19.33	19.46	-	19.46	17.99
YDO (m)	-0.145	0.280	-0.115	0.285	-0.055	0.215	0.280	-	0.175	0.285
Final location after ES10*										
XDO (m)	19.46	19.44	19.47	19.49	19.42	19.31	19.43	-	19.42	17.32
YDO (m)	-0.146	0.265	-0.122	0.264	-0.037	0.261	0.284	-	0.161	-0.176
ZDO (m)	+0.207	+0.205	+0.207	+0.203	+0.208	+0.207	+0.205	-	+0.209	-0.098
BDO (m)	+0.000	+0.000	+0.000	+0.000	+0.000	+0.000	+0.000	-	+0.000	+0.000

DB-Dark Blue, M-Magenta, G/R-Green/Red, G/B1-Green/Blue1, Y-Yellow, CB-Cerulean Blue, Y/B-Yellow/Blue, BS-Burnt Sienna, O/B-Orange/Blue, G/B2-Green/Blue2

‘ - ’ not detected

Table 3.31 Lagrangian movement of DO#11-20 (after DO resetting) for ES6-ES10 (b)

DO#	11	12	13	14	15	16	17	18	19	20
	Y/R	B/R	P	O/R	SG	EG	O	CR	O/G	CB
Initial location*										
XDO (m)	16.66	16.71	16.17	16.20	14.71	14.70	14.25	14.22	11.98	11.95
YDO (m)	-0.268	0.275	-0.272	0.279	-0.268	0.278	-0.283	0.290	-0.280	0.275
ZDO (m)	-0.092	-0.094	-0.103	-0.100	-0.134	-0.117	-0.130	-0.133	-0.162	-0.154
BDO (m)	+0.000	+0.000	+0.000	+0.000	+0.000	+0.000	+0.000	+0.000	+0.000	+0.000
Location after ES6										
XDO (m)	17.93	18.14	-	-	17.97	-	-	-	-	-
YDO (m)	0.225	0.425	-	-	0.210	-	-	-	-	-
Location after ES7										
XDO (m)	-	-	-	18.14	-	18.14	-	-	18.14	-
YDO (m)	-	-	-	0.260	-	0.355	-	-	0.365	-
Location after ES8										
XDO (m)	-	-	-	19.42	18.14	17.64	18.18	19.40	-	17.96
YDO (m)	-	-	-	0.185	-0.465	-0.415	-0.295	0.230	-	0.365
Location after ES9										
XDO (m)	17.95	-	-	19.44	-	18.13	19.45	19.40	18.13	18.01
YDO (m)	0.240	-	-	0.185	-	0.345	-0.065	0.230	0.535	0.260
Final location after ES10*										
XDO (m)	18.20	-	19.24	19.41	19.30	18.09	19.42	19.38	-	18.13
YDO (m)	0.145	-	0.083	0.185	-0.352	-0.335	-0.059	0.218	-	0.145
ZDO (m)	+0.052	-	+0.203	+0.210	+0.210	+0.033	+0.207	+0.210	-	+0.039
BDO (m)	+0.000	-	+0.000	+0.000	+0.000	+0.000	+0.000	+0.000	-	+0.000

Y/R-Yellow/Red, B/R-Blue/Red, P-Purple, Orange/Red, SG- Sap Green, EG-Emerald Green, O-Orange, CR-Crimson Red, O/G-Orange/Green, CB-Cobalt Blue

' - ' not detected

Table 3.32 Lagrangian movement of DO#1-10 for NG1-NG20 (a)

DO#	1	2	3	4	5	6	7	8	9	10
	W	R	B	G	W/R	W/B	W/G	R/B	R/G	B/G
Initial location*										
XDO (m)	18.99	18.98	18.68	18.68	18.40	18.38	18.09	18.07	17.77	17.77
YDO (m)	-0.286	0.286	-0.275	0.283	-0.263	0.284	-0.280	0.274	-0.282	0.275
ZDO (m)	+0.207	+0.208	+0.201	+0.201	+0.132	+0.135	+0.038	+0.042	-0.008	+0.005
BDO (m)	+0.000	+0.000	+0.000	+0.000	+0.000	+0.000	+0.000	+0.000	+0.000	+0.000
Location after NG1										
XDO (m)	19.00	18.98	18.66	17.30	-	-	-	-	-	-
YDO (m)	-0.281	0.290	-0.268	0.335	-	-	-	-	-	-
Location after NG2										
XDO (m)	19.00	18.98	17.33	17.36	-	-	-	-	-	-
YDO (m)	-0.281	0.290	-0.198	0.346	-	-	-	-	-	-
Location after NG3										
XDO (m)	19.00	18.98	17.33	17.36	-	-	-	-	-	-
YDO (m)	-0.281	0.290	-0.198	0.346	-	-	-	-	-	-
Location after NG4										
XDO (m)	19.00	18.98	17.33	17.36	-	-	-	-	-	-
YDO (m)	-0.281	0.290	-0.198	0.346	-	-	-	-	-	-
Location after NG5										
XDO (m)	19.00	18.98	17.33	17.36	-	-	-	-	-	-
YDO (m)	-0.281	0.290	-0.198	0.346	-	-	-	-	-	-
Location after NG6										
XDO (m)	19.00	18.98	17.33	17.36	-	-	-	-	-	-
YDO (m)	-0.281	0.290	-0.198	0.346	-	-	-	-	-	-
Location after NG7										
XDO (m)	19.00	18.98	17.33	17.36	-	-	-	-	-	-
YDO (m)	-0.281	0.290	-0.198	0.346	-	-	-	-	-	-
Location after NG8										
XDO (m)	19.00	18.98	17.33	17.36	-	-	-	-	-	-
YDO (m)	-0.281	0.290	-0.198	0.346	-	-	-	-	-	-
Location after NG9										
XDO (m)	19.00	18.98	17.33	17.36	-	-	-	-	-	-
YDO (m)	-0.281	0.290	-0.198	0.346	-	-	-	-	-	-
Location after NG10										
XDO (m)	19.00	18.98	17.33	17.36	-	-	-	-	-	-

YDO (m)	-0.281	0.290	-0.198	0.346	-	-	-	-	-	-
Location after NG11										
XDO (m)	19.00	18.98	17.33	17.36	-	-	-	-	-	-
YDO (m)	-0.281	0.290	-0.198	0.346	-	-	-	-	-	-
Location after NG12										
XDO (m)	19.00	18.98	17.33	17.36	-	-	-	-	-	-
YDO (m)	-0.281	0.290	-0.198	0.346	-	-	-	-	-	-
Location after NG13										
XDO (m)	19.00	18.98	17.33	17.36	-	-	-	-	-	-
YDO (m)	-0.281	0.290	-0.198	0.346	-	-	-	-	-	-
Location after NG14										
XDO (m)	19.00	18.98	17.33	17.36	-	-	-	-	-	-
YDO (m)	-0.281	0.290	-0.198	0.346	-	-	-	-	-	-
Location after NG15										
XDO (m)	19.00	18.98	17.33	17.36	-	-	-	-	-	-
YDO (m)	-0.281	0.290	-0.198	0.346	-	-	-	-	-	-
Location after NG16										
XDO (m)	19.00	18.98	17.33	17.36	-	-	-	-	-	-
YDO (m)	-0.281	0.290	-0.198	0.346	-	-	-	-	-	-
Location after NG17										
XDO (m)	19.00	18.98	17.33	17.36	-	-	-	-	-	-
YDO (m)	-0.281	0.290	-0.198	0.346	-	-	-	-	-	-
Location after NG18										
XDO (m)	19.00	18.98	17.33	17.36	-	-	-	-	-	-
YDO (m)	-0.281	0.290	-0.198	0.346	-	-	-	-	-	-
Location after NG19										
XDO (m)	19.00	18.98	17.33	17.36	-	-	-	-	-	-
YDO (m)	-0.281	0.290	-0.198	0.346	-	-	-	-	-	-
Final location after NG20*										
XDO (m)	19.00	18.98	17.33	17.36	17.40	17.40	17.36	17.32	-	-
YDO (m)	-0.281	0.290	-0.198	0.346	-0.289	0.335	-0.288	0.196	-	-
ZDO (m)	+0.208	+0.213	-0.080	-0.067	-0.064	-0.064	-0.067	-0.080	-	-
BDO (m)	+0.000	+0.000	-0.024	-0.025	-0.030	-0.030	-0.025	-0.024	-	-

W-white, R-red, B-blue, G-green, W/R-white/red, W/B-white/blue, W/G-white/green, R/B-red/blue, R/G-red/green, B/G-blue/green

‘ - ’ not detected

Table 3.32 Lagrangian movement of DO#11-20 for NG1-NG20 (b)

DO#	11	12	13	14	15	16	17	18	19	20
	O	W/O	O/R	O/B	O/G	[-]	[-]	[-]	[-]	[-]
Initial location*										
XDO (m)	16.68	16.69	16.16	16.20	14.71	14.65	14.24	14.20	11.93	11.95
YDO (m)	-0.267	0.300	-0.297	0.306	-0.277	0.283	-0.289	0.279	-0.276	0.280
ZDO (m)	-0.091	-0.084	-0.097	-0.096	-0.126	-0.132	-0.135	-0.137	-0.172	-0.164
BDO (m)	+0.000	+0.000	+0.000	+0.000	+0.000	+0.000	+0.000	+0.000	+0.000	+0.000
Location after NG1										
XDO (m)	16.70	16.70	16.17	16.21	14.71	14.67	14.28	14.22	11.93	11.96
YDO (m)	-0.281	0.306	-0.281	0.283	-0.286	0.268	-0.286	0.263	-0.282	0.295
Location after NG2										
XDO (m)	16.70	16.70	16.17	16.21	14.71	14.67	14.28	14.22	11.93	11.96
YDO (m)	-0.281	0.306	-0.281	0.283	-0.286	0.268	-0.286	0.263	-0.282	0.295
Location after NG3										
XDO (m)	16.70	16.70	16.17	16.21	14.71	14.67	14.28	14.22	11.93	11.96
YDO (m)	-0.281	0.306	-0.281	0.283	-0.286	0.268	-0.286	0.263	-0.282	0.295
Location after NG4										
XDO (m)	16.70	16.70	16.17	16.21	14.71	14.67	14.28	14.22	11.93	11.96
YDO (m)	-0.281	0.306	-0.281	0.283	-0.286	0.268	-0.286	0.263	-0.282	0.295
Location after NG5										
XDO (m)	16.70	16.70	16.17	16.21	14.71	14.67	14.28	14.22	11.93	11.96
YDO (m)	-0.281	0.306	-0.281	0.283	-0.286	0.268	-0.286	0.263	-0.282	0.295
Location after NG6										
XDO (m)	16.70	16.70	16.17	16.21	14.71	14.67	14.28	14.22	11.93	11.96
YDO (m)	-0.281	0.306	-0.281	0.283	-0.286	0.268	-0.286	0.263	-0.282	0.295
Location after NG7										
XDO (m)	16.70	16.70	16.17	16.21	14.71	14.67	14.28	14.22	11.93	11.96
YDO (m)	-0.281	0.306	-0.281	0.283	-0.286	0.268	-0.286	0.263	-0.282	0.295
Location after NG8										
XDO (m)	16.70	16.70	16.17	16.21	14.71	14.67	14.28	14.22	11.93	11.96
YDO (m)	-0.281	0.306	-0.281	0.283	-0.286	0.268	-0.286	0.263	-0.282	0.295
Location after NG9										
XDO (m)	16.70	16.70	16.17	16.21	14.71	14.67	14.28	14.22	11.93	11.96
YDO (m)	-0.281	0.306	-0.281	0.283	-0.286	0.268	-0.286	0.263	-0.282	0.295
Location after NG10										
XDO (m)	16.70	16.70	16.17	16.21	14.71	14.67	14.28	14.22	11.93	11.96

YDO (m)	-0.281	0.306	-0.281	0.283	-0.286	0.268	-0.286	0.263	-0.282	0.295
Location after NG11										
XDO (m)	16.70	16.70	16.17	16.21	14.71	14.67	14.28	14.22	11.93	11.96
YDO (m)	-0.281	0.306	-0.281	0.283	-0.286	0.268	-0.286	0.263	-0.282	0.295
Location after NG12										
XDO (m)	16.70	16.70	16.17	16.21	14.71	14.67	14.28	14.22	11.93	11.96
YDO (m)	-0.281	0.306	-0.281	0.283	-0.286	0.268	-0.286	0.263	-0.282	0.295
Location after NG13										
XDO (m)	16.70	16.70	16.17	16.21	14.71	14.67	14.28	14.22	11.93	11.96
YDO (m)	-0.281	0.306	-0.281	0.283	-0.286	0.268	-0.286	0.263	-0.282	0.295
Location after NG14										
XDO (m)	16.70	16.70	16.17	16.21	14.71	14.67	14.28	14.22	11.93	11.96
YDO (m)	-0.281	0.306	-0.281	0.283	-0.286	0.268	-0.286	0.263	-0.282	0.295
Location after NG15										
XDO (m)	16.70	16.70	16.17	16.21	14.71	14.67	14.28	14.22	11.93	11.96
YDO (m)	-0.281	0.306	-0.281	0.283	-0.286	0.268	-0.286	0.263	-0.282	0.295
Location after NG16										
XDO (m)	16.70	16.70	16.17	16.21	14.71	14.67	14.28	14.22	11.93	11.96
YDO (m)	-0.281	0.306	-0.281	0.283	-0.286	0.268	-0.286	0.263	-0.282	0.295
Location after NG17										
XDO (m)	16.70	16.70	16.17	16.21	14.71	14.67	14.28	14.22	11.93	11.96
YDO (m)	-0.281	0.306	-0.281	0.283	-0.286	0.268	-0.286	0.263	-0.282	0.295
Location after NG18										
XDO (m)	16.70	16.70	16.17	16.21	14.71	14.67	14.28	14.22	11.93	11.96
YDO (m)	-0.281	0.306	-0.281	0.283	-0.286	0.268	-0.286	0.263	-0.282	0.295
Location after NG19										
XDO (m)	16.70	16.70	16.17	16.21	14.71	14.67	14.28	14.22	11.93	11.96
YDO (m)	-0.281	0.306	-0.281	0.283	-0.286	0.268	-0.286	0.263	-0.282	0.295
Final location after NG20*										
XDO (m)	16.70	16.70	16.17	16.21	14.71	14.67	14.28	14.22	11.93	11.96
YDO (m)	-0.281	0.306	-0.281	0.283	-0.286	0.268	-0.286	0.263	-0.282	0.295
ZDO (m)	-0.102	-0.085	-0.108	-0.096	-0.141	-0.135	-0.150	-0.135	-0.188	-0.166
BDO (m)	+0.000	+0.000	+0.000	+0.000	+0.000	+0.000	+0.000	+0.000	+0.000	+0.000

O=orange, W/O=white/orange, O/R=orange/red, O/B=orange/blue, O/G=orange/green, [-] numbered

' - ' not detected

Table 3.33 Lagrangian movement of DO#1-10 for NL1-NL20 (a)

DO#	1	2	3	4	5	6	7	8	9	10
	O	R	B	M/O	G	O/G	R/B	B/O	M/G	G/R
Initial location*										
XDO (m)	18.99	18.98	18.68	18.68	18.36	18.35	18.04	18.02	17.74	17.74
YDO (m)	-0.252	0.284	-0.256	0.287	-0.260	0.289	-0.277	0.289	-0.276	0.289
ZDO (m)	+0.197	+0.194	+0.195	+0.192	+0.104	+0.105	+0.013	+0.012	-0.027	-0.022
BDO (m)	+0.000	+0.000	+0.000	+0.000	+0.000	+0.000	+0.000	+0.000	+0.000	+0.000
Location after NL1										
XDO (m)	18.99	-	19.06	19.20	19.07	19.16	17.37	-	17.71	17.72
YDO (m)	-0.295	-	-0.195	0.345	-0.175	0.355	0.145	-	0.075	-0.435
Location after NL2										
XDO (m)	19.28	-	19.18	19.20	19.25	19.16	-	-	17.73	-
YDO (m)	-0.275	-	-0.175	0.345	-0.185	0.355	-	-	0.395	-
Location after NL3										
XDO (m)	19.28	-	19.25	19.20	19.26	19.16	-	-	-	17.78
YDO (m)	-0.275	-	-0.175	0.345	-0.195	0.355	-	-	-	-0.495
Location after NL4										
XDO (m)	19.28	-	19.25	19.24	19.26	19.24	-	18.15	17.74	17.84
YDO (m)	-0.275	-	-0.185	0.355	-0.175	0.350	-	-0.085	-0.025	-0.375
Location after NL5										
XDO (m)	19.28	19.29	19.28	19.35	19.24	19.30	-	19.66	-	17.71
YDO (m)	-0.285	0.375	-0.205	0.345	-0.175	0.345	-	-0.005	-	0.005
Location after NL6										
XDO (m)	19.30	19.29	19.26	19.35	19.26	19.30	-	19.59	-	-
YDO (m)	-0.280	0.375	-0.195	0.345	-0.175	0.345	-	-0.005	-	-
Location after NL7										
XDO (m)	19.37	19.32	19.25	19.33	19.25	19.32	17.72	19.59	-	-
YDO (m)	-0.265	0.354	-0.195	0.340	-0.175	0.332	0.335	-0.005	-	-
Location after NL8										
XDO (m)	19.37	19.32	19.25	19.33	19.25	19.32	17.63	19.59	-	17.79
YDO (m)	-0.265	0.354	-0.195	0.340	-0.175	0.332	-0.305	-0.005	-	-0.015
Location after NL9										
XDO (m)	19.33	19.32	19.25	19.33	19.25	19.32	19.13	19.59	17.18	17.28
YDO (m)	-0.255	0.354	-0.195	0.340	-0.175	0.332	0.475	-0.005	0.445	-0.405
Location after NL10										
XDO (m)	19.34	19.32	19.29	19.33	19.31	19.32	19.13	19.59	17.64	17.53

YDO (m)	-0.230	0.354	-0.185	0.340	-0.199	0.332	0.475	-0.005	-0.111	-0.232
Location after NL11										
XDO (m)	19.38	19.38	19.33	19.38	19.35	19.38	19.04	19.61	-	17.52
YDO (m)	-0.255	0.355	-0.205	0.345	-0.215	0.335	0.495	-0.005	-	0.015
Location after NL12										
XDO (m)	19.38	19.37	19.33	19.37	19.34	19.39	19.26	19.63	17.72	-
YDO (m)	-0.255	0.355	-0.215	0.345	-0.215	0.345	0.485	-0.015	0.345	-
Location after NL13										
XDO (m)	19.39	19.37	19.33	19.37	19.33	19.39	19.26	19.63	17.77	-
YDO (m)	-0.245	0.355	-0.205	0.345	-0.205	0.345	0.485	-0.015	-0.125	-
Location after NL14										
XDO (m)	19.41	19.34	19.41	19.36	19.40	19.37	19.31	19.60	17.74	17.77
YDO (m)	-0.245	0.385	-0.020	0.385	-0.190	0.345	0.475	-0.015	-0.355	-0.485
Location after NL15										
XDO (m)	19.40	19.34	19.39	19.36	19.44	19.37	19.31	19.60	17.78	-
YDO (m)	-0.245	0.385	-0.026	0.385	-0.161	0.345	0.475	-0.015	0.345	-
Location after NL16										
XDO (m)	19.40	19.34	19.39	19.37	19.44	19.37	19.37	19.60	-	-
YDO (m)	-0.245	0.395	-0.026	0.390	-0.161	0.355	0.485	-0.015	-	-
Location after NL17										
XDO (m)	19.40	19.34	19.39	19.37	19.44	19.37	19.37	19.60	17.66	-
YDO (m)	-0.245	0.395	-0.026	0.390	-0.161	0.355	0.485	-0.015	-0.235	-
Location after NL18										
XDO (m)	19.40	19.40	19.39	19.42	19.44	19.43	19.48	19.60	17.66	17.68
YDO (m)	-0.245	0.410	-0.026	0.395	-0.161	0.322	0.445	-0.015	-0.325	-0.325
Location after NL19										
XDO (m)	19.40	19.40	19.39	19.42	19.44	19.43	19.48	19.60	17.70	-
YDO (m)	-0.245	0.410	-0.026	0.395	-0.161	0.322	0.445	-0.015	-0.245	-
Final location after NL20*										
XDO (m)	19.42	19.41	19.39	19.41	19.44	19.45	19.48	19.60	17.67	17.67
YDO (m)	-0.223	0.398	-0.026	0.383	-0.161	0.322	0.445	-0.015	-0.319	-0.094
ZDO (m)	+0.202	+0.200	+0.202	+0.200	+0.202	+0.204	+0.197	+0.199	-0.024	-0.015
BDO (m)	+0.000	+0.000	+0.000	+0.000	+0.000	+0.000	+0.000	+0.000	+0.000	+0.000

O=orange, R=red, B=blue, M/O=magenta/orange, G=green, O/G=orange/green, R/B=red/blue, B/O=blue/orange, M/G=magenta/green, G/R=green/red

' - ' not detected

Table 3.33 Lagrangian movement of DO#11-20 for NL1-NL20 (b)

DO#	11	12	13	14	15	16	17	18	19	20
	O/B	R/O	B/G	M/B	G/O	O/R	R/G	B/R	M/R	G/B
Initial location*										
XDO (m)	16.71	16.71	16.19	16.20	14.70	14.67	14.27	14.22	11.93	11.97
YDO (m)	-0.300	0.275	-0.258	0.293	-0.284	0.294	-0.281	0.266	-0.275	0.310
ZDO (m)	-0.102	-0.097	-0.132	-0.109	-0.159	-0.147	-0.149	-0.149	-0.183	-0.182
BDO (m)	+0.000	+0.000	+0.000	+0.000	+0.000	+0.000	+0.000	+0.000	+0.000	+0.000
Location after NL1										
XDO (m)	-	17.73	-	-	-	-	-	-	-	-
YDO (m)	-	-0.025	-	-	-	-	-	-	-	-
Location after NL2										
XDO (m)	-	-	-	17.73	-	-	-	-	-	-
YDO (m)	-	-	-	0.355	-	-	-	-	-	-
Location after NL3										
XDO (m)	-	-	-	-	-	-	-	-	-	-
YDO (m)	-	-	-	-	-	-	-	-	-	-
Location after NL4										
XDO (m)	-	17.73	-	-	-	-	-	-	-	-
YDO (m)	-	0.245	-	-	-	-	-	-	-	-
Location after NL5										
XDO (m)	-	17.33	-	19.38	17.58	-	-	17.46	-	-
YDO (m)	-	-0.395	-	-0.085	-0.285	-	-	-0.345	-	-
Location after NL6										
XDO (m)	-	17.74	-	19.36	18.97	-	-	-	-	-
YDO (m)	-	0.105	-	-0.100	-0.280	-	-	-	-	-
Location after NL7										
XDO (m)	-	17.58	-	19.36	19.37	-	-	-	-	-
YDO (m)	-	-0.155	-	-0.100	-0.255	-	-	-	-	-
Location after NL8										
XDO (m)	-	-	-	19.36	19.37	-	-	-	-	-
YDO (m)	-	-	-	-0.100	-0.255	-	-	-	-	-
Location after NL9										
XDO (m)	-	17.52	-	19.36	19.36	-	-	17.77	-	-
YDO (m)	-	0.085	-	-0.100	-0.245	-	-	-0.125	-	-
Location after NL10										
XDO (m)	-	17.63	-	19.36	19.33	-	-	16.95	-	12.32

YDO (m)	-	0.017	-	-0.100	-0.237	-	-	-0.423	-	0.005
Location after NL11										
XDO (m)	-	18.07	-	19.37	19.37	-	-	-	-	-
YDO (m)	-	0.490	-	-0.105	-0.245	-	-	-	-	-
Location after NL12										
XDO (m)	-	19.21	-	19.49	19.37	-	-	-	-	-
YDO (m)	-	0.460	-	-0.125	-0.245	-	-	-	-	-
Location after NL13										
XDO (m)	-	19.21	-	19.49	19.38	-	-	-	-	-
YDO (m)	-	0.465	-	-0.125	-0.235	-	-	-	-	-
Location after NL14										
XDO (m)	-	19.36	-	19.49	19.43	-	-	17.72	-	-
YDO (m)	-	0.470	-	-0.133	-0.225	-	-	-0.425	-	-
Location after NL15										
XDO (m)	-	19.36	-	19.49	19.43	-	-	17.78	-	-
YDO (m)	-	0.470	-	-0.133	-0.220	-	-	-0.235	-	-
Location after NL16										
XDO (m)	-	19.37	-	19.49	19.43	-	-	17.82	-	-
YDO (m)	-	0.475	-	-0.133	-0.220	-	-	0.295	-	-
Location after NL17										
XDO (m)	-	19.37	-	19.49	19.43	-	-	-	-	-
YDO (m)	-	-0.475	-	-0.133	-0.220	-	-	-	-	-
Location after NL18										
XDO (m)	-	19.45	-	19.49	19.43	-	-	-	-	-
YDO (m)	-	0.412	-	-0.133	-0.220	-	-	-	-	-
Location after NL19										
XDO (m)	-	19.45	-	19.49	19.43	-	-	-	-	-
YDO (m)	-	0.412	-	-0.133	-0.220	-	-	-	-	-
Final location after NL20*										
XDO (m)	-	19.45	-	19.49	19.43	-	-	17.66	-	12.53
YDO (m)	-	0.412	-	-0.133	-0.220	-	-	-0.312	-	-0.366
ZDO (m)	-	+0.205		+0.200	+0.202	-	-	-0.019	-	-0.177
BDO (m)	-	+0.000	-	+0.000	+0.000	-	-	+0.000	-	+0.000

O/B-orange/blue, R/O-red/orange, B/G-blue/green, M/B-magenta/blue, G/O-green/orange, O/R-orange/red, R/G-red/green, B/R-blue/red, M/R-magenta/red, G/B-green/blue

‘ - ’ not detected

Table 3.34 Lagrangian movement of DO#1-10 for NS1-NS10 (a)

DO#	1	2	3	4	5	6	7	8	9	10
	DB	M	G/R	G/B1.	Y	CB.	Y/B	G/O	O/B	G/B2
Initial location*										
XDO (m)	18.98	18.98	18.68	18.70	18.38	18.37	18.07	18.06	17.76	17.75
YDO (m)	-0.259	0.273	-0.266	0.285	-0.282	0.276	-0.260	0.265	-0.275	0.276
ZDO (m)	+0.194	+0.194	+0.183	+0.188	+0.104	+0.108	+0.013	+0.013	-0.024	-0.022
BDO (m)	+0.000	+0.000	+0.000	+0.000	+0.000	+0.000	+0.000	+0.000	+0.000	+0.000
Location after NS1										
XDO (m)	-	19.44	19.14	19.47	19.20	19.48	-	18.09	17.58	17.90
YDO (m)	-	0.355	-0.140	0.340	-0.155	0.315	-	-0.455	-0.025	-0.025
Location after NS2										
XDO (m)	19.55	19.46	19.54	19.48	-	19.49	-	19.57	17.89	-
YDO (m)	-0.175	0.360	-0.095	0.295	-	0.345	-	-0.265	-0.525	-
Location after NS3										
XDO (m)	19.56	19.51	19.57	19.54	-	19.53	17.99	19.65	-	18.06
YDO (m)	-0.165	0.385	-0.100	0.325	-	0.365	-0.335	-0.210	-	0.545
Location after NL4										
XDO (m)	19.60	19.70	19.54	19.68	19.77	19.67	-	19.67	18.13	18.15
YDO (m)	-0.150	0.360	-0.111	0.325	-0.050	0.360	-	-0.180	-0.555	0.280
Location after NS5										
XDO (m)	19.57	19.71	19.54	19.70	19.77	19.67	-	19.67	19.43	17.28
YDO (m)	-0.145	0.360	-0.111	0.325	-0.050	0.355	-	-0.180	-0.425	0.025
Location after NS6										
XDO (m)	19.57	19.71	19.54	19.70	19.77	19.67	-	19.67	19.43	17.81
YDO (m)	-0.145	0.360	-0.111	0.325	-0.050	0.355	-	-0.180	-0.425	-0.500
Location after NS7										
XDO (m)	19.57	19.71	19.54	19.70	19.77	19.67	-	19.67	19.46	17.74
YDO (m)	-0.145	0.360	-0.111	0.325	-0.050	0.355	-	-0.180	-0.420	-0.325
Location after NS8										
XDO (m)	19.57	19.71	19.54	19.70	19.77	19.67	17.94	19.67	19.46	-
YDO (m)	-0.145	0.360	-0.111	0.325	-0.050	0.355	0.500	-0.180	-0.420	-
Location after NS9										
XDO (m)	19.57	19.71	19.54	19.70	19.77	19.67	18.05	19.67	19.46	17.76
YDO (m)	-0.145	0.360	-0.111	0.325	-0.050	0.355	-0.050	-0.180	-0.420	-0.275
Final location after NS10*										
XDO (m)	19.57	19.69	19.54	19.70	19.77	19.67	-	19.67	19.56	-

YDO (m)	-0.145	0.332	-0.111	0.301	-0.050	0.339	-	-0.180	-0.448	-
ZDO (m)	0.191	0.196	0.195	0.190	0.196	0.189	-	0.191	0.187	-
BDO (m)	+0.000	+0.000	+0.000	+0.000	+0.000	+0.000	-	+0.000	+0.000	-

DB-Dark Blue, M-Magenta, G/R-Green/Red, G/B1.-Green/Blue1, Y-Yellow, CB.-Cerulean Blue, Y/B-Yellow/Blue, G/O-Green/Orange, O/B-Orange/Blue, G/B2-Green/Blue2

‘ - ’ not detected

Table 3.34 Lagrangian movement of DO#11-20 for NS1-NS10 (b)

DO#	11	12	13	14	15	16	17	18	19	20
	P/O	B/O	PW	O/R	SG/W	EG	O	CR	O.	CB/W.
Initial location*										
XDO (m)	16.75	16.72	16.20	16.18	14.71	14.72	14.16	14.18	11.93	11.96
YDO (m)	-0.262	0.274	-0.272	0.273	-0.272	0.279	-0.276	0.285	-0.288	0.271
ZDO (m)	-0.107	-0.109	-0.110	-0.118	-0.155	-0.142	-0.148	-0.146	-0.183	-0.173
BDO (m)	+0.000	+0.000	+0.000	+0.000	+0.000	+0.000	+0.000	+0.000	+0.000	+0.000

Location after NS1										
XDO (m)	18.09	17.88	-	-	-	17.88	-	-	-	-
YDO (m)	-0.425	0.075	-	-	-	-0.425	-	-	-	-
Location after NS2										
XDO (m)	17.73	-	-	-	-	19.38	19.34	-	-	-
YDO (m)	-0.295	-	-	-	-	-0.325	-0.145	-	-	-
Location after NS3										
XDO (m)	19.51	17.90	18.10	17.90	19.67	19.64	19.54	18.08	-	-
YDO (m)	-0.390	0.430	-0.010	-0.300	-0.215	-0.285	-0.115	-0.340	-	-
Location after NS4										
XDO (m)	19.60	18.14	18.11	-	19.68	19.74	19.58	19.65	-	-
YDO (m)	-0.415	0.465	0.455	-	-0.182	-0.236	-0.090	-0.135	-	-
Location after NS5										
XDO (m)	19.60	-	-	18.05	19.68	19.74	19.55	19.63	-	-
YDO (m)	-0.415	-	-	-0.480	-0.182	-0.236	-0.077	-0.131	-	-
Location after NS6										
XDO (m)	19.60	19.35	-	17.91	19.68	19.74	19.55	19.63	17.66	-
YDO (m)	-0.415	0.510	-	-0.445	-0.182	-0.236	-0.077	-0.131	0.215	-
Location after NS7										
XDO (m)	19.60	19.54	-	-	19.68	19.74	19.55	19.63	-	-
YDO (m)	-0.415	0.480	-	-	-0.182	-0.236	-0.077	-0.131	-	-
Location after NS8										
XDO (m)	19.60	19.54	-	17.89	19.68	19.74	19.55	19.63	-	-
YDO (m)	-0.415	0.480	-	-0.350	-0.182	-0.236	-0.077	-0.131	-	-
Location after NS9										
XDO (m)	19.60	19.54	-	18.05	19.68	19.74	19.55	19.63	17.79	-
YDO (m)	-0.415	0.480	-	0.445	-0.182	-0.236	-0.077	-0.131	0.245	-
Final location after NS10*										
XDO (m)	19.60	19.53	-	19.45	19.68	19.74	19.55	19.63	18.03	-
YDO (m)	-0.420	0.455	-	0.430	-0.182	-0.236	-0.077	-0.131	0.056	-
ZDO (m)	0.189	0.189	-	0.192	0.191	0.194	0.196	0.191	0.030	-
BDO (m)	+0.000	+0.000	-	+0.000	+0.000	+0.000	+0.000	+0.000	+0.000	-

P/O-Purple/Orange, B/O-Blue/Orange, P/W-Purple/White, Orange/Red, SG/W-Sap Green/White, EG-Emerald Green, O-Orange, CR-Crimson Red, O.-Orange, CB/W.-Cobalt blue/white.

' - ' not detected

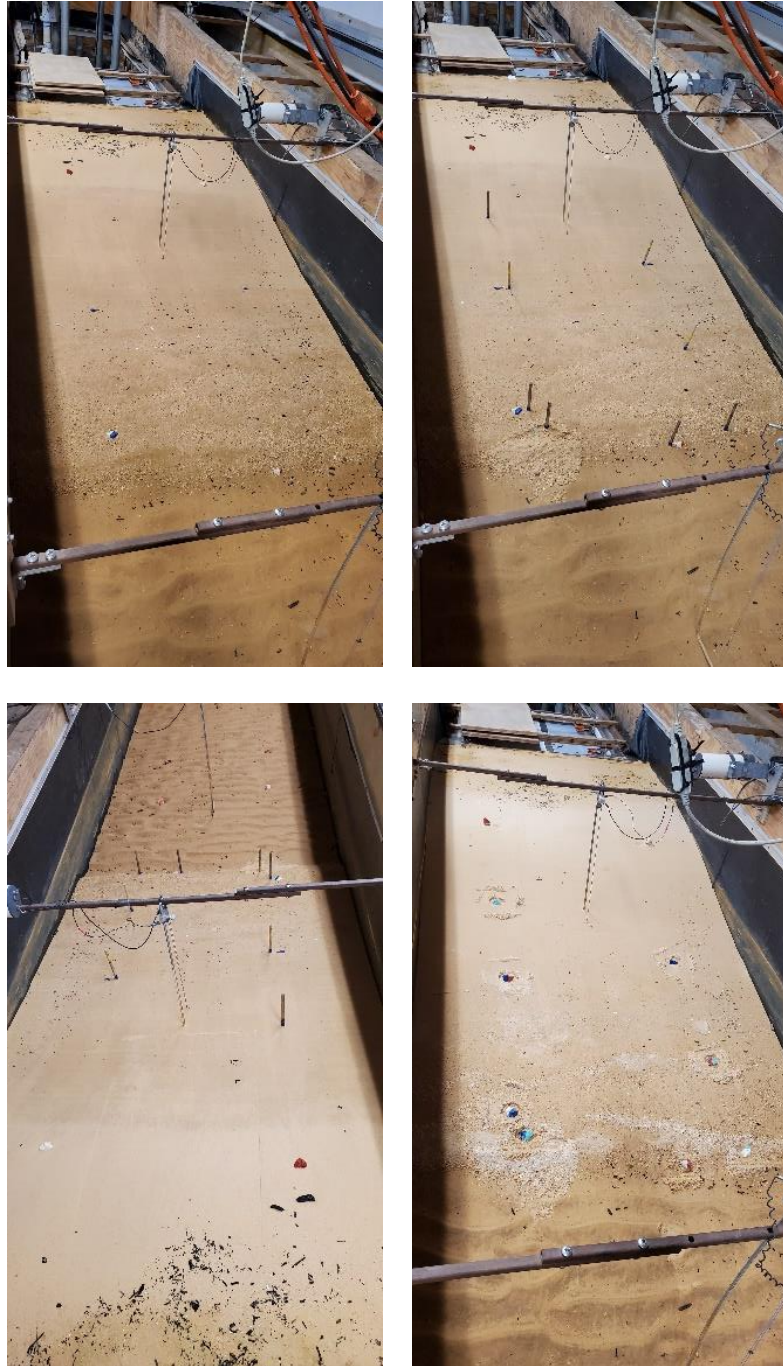


Figure 3.16 Final locations of 20 gravel DOs (a) on equilibrium sand beach profile in Test EG.

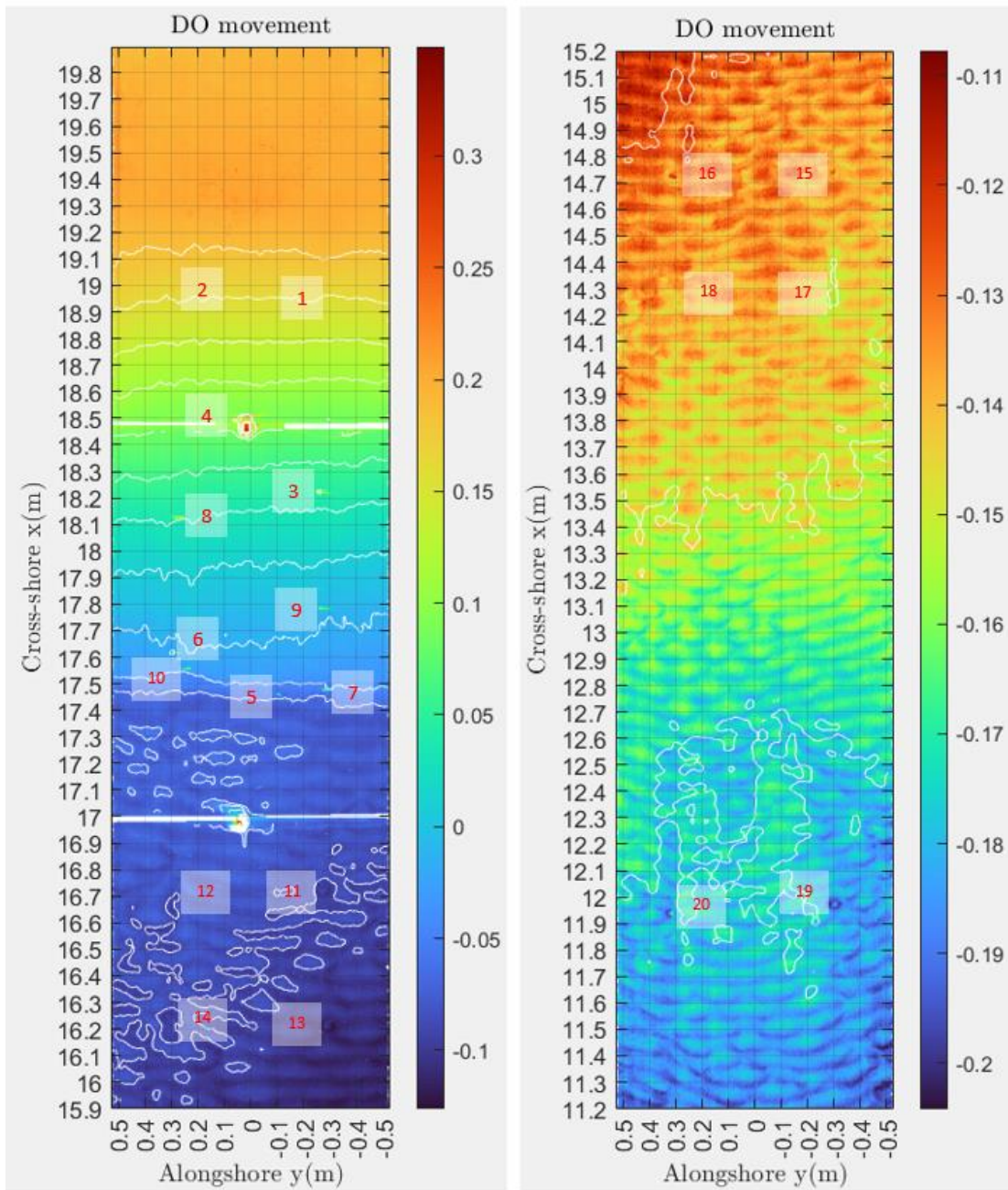


Figure 3.16 Bathymetric contour measured by laser line scanner displaying final DO locations after Test EG (b).

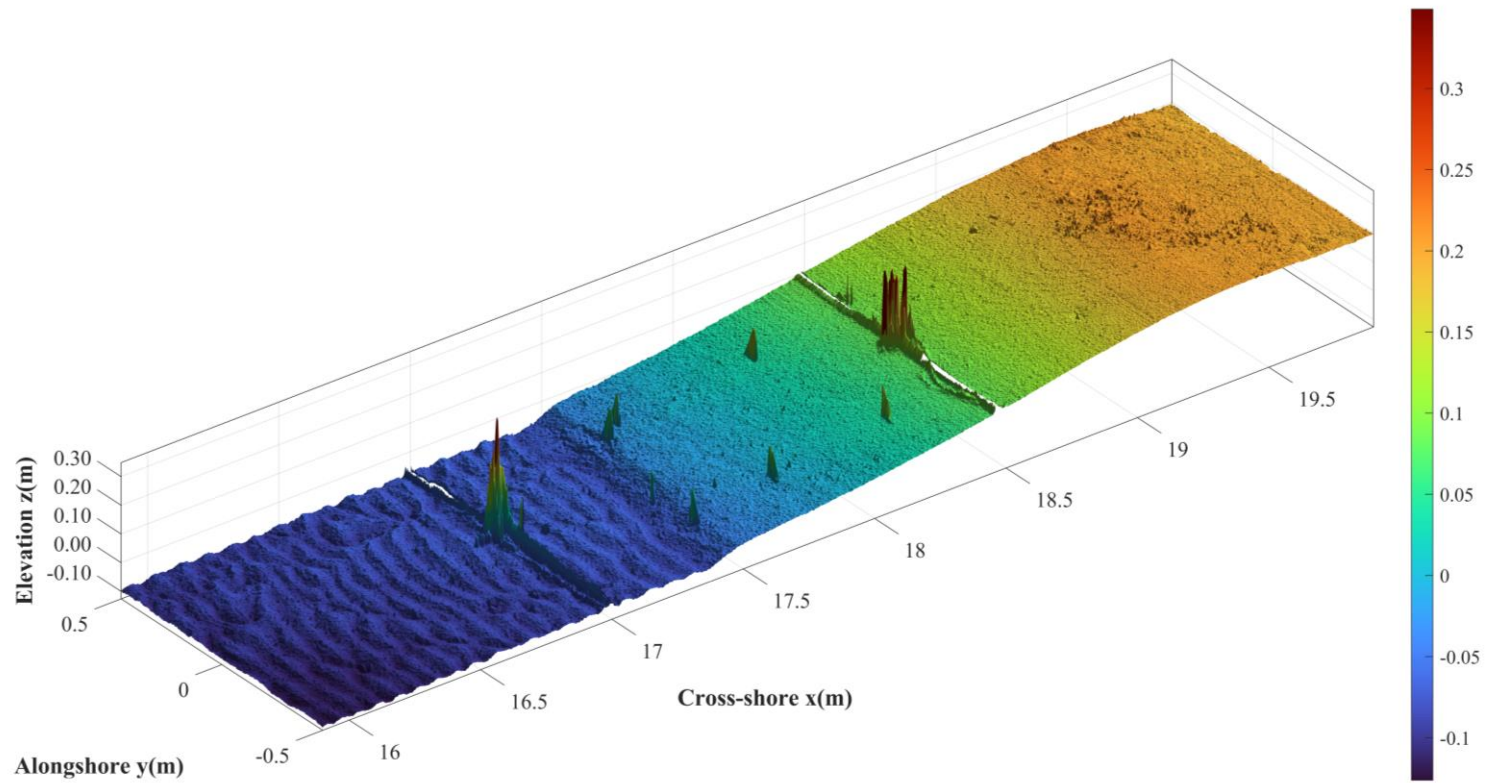


Figure 3.16 Surface plot displaying final DO locations (with spikes at the locations of WG7 and WG8) in inner surf zone and foreshore after Test EG (c).

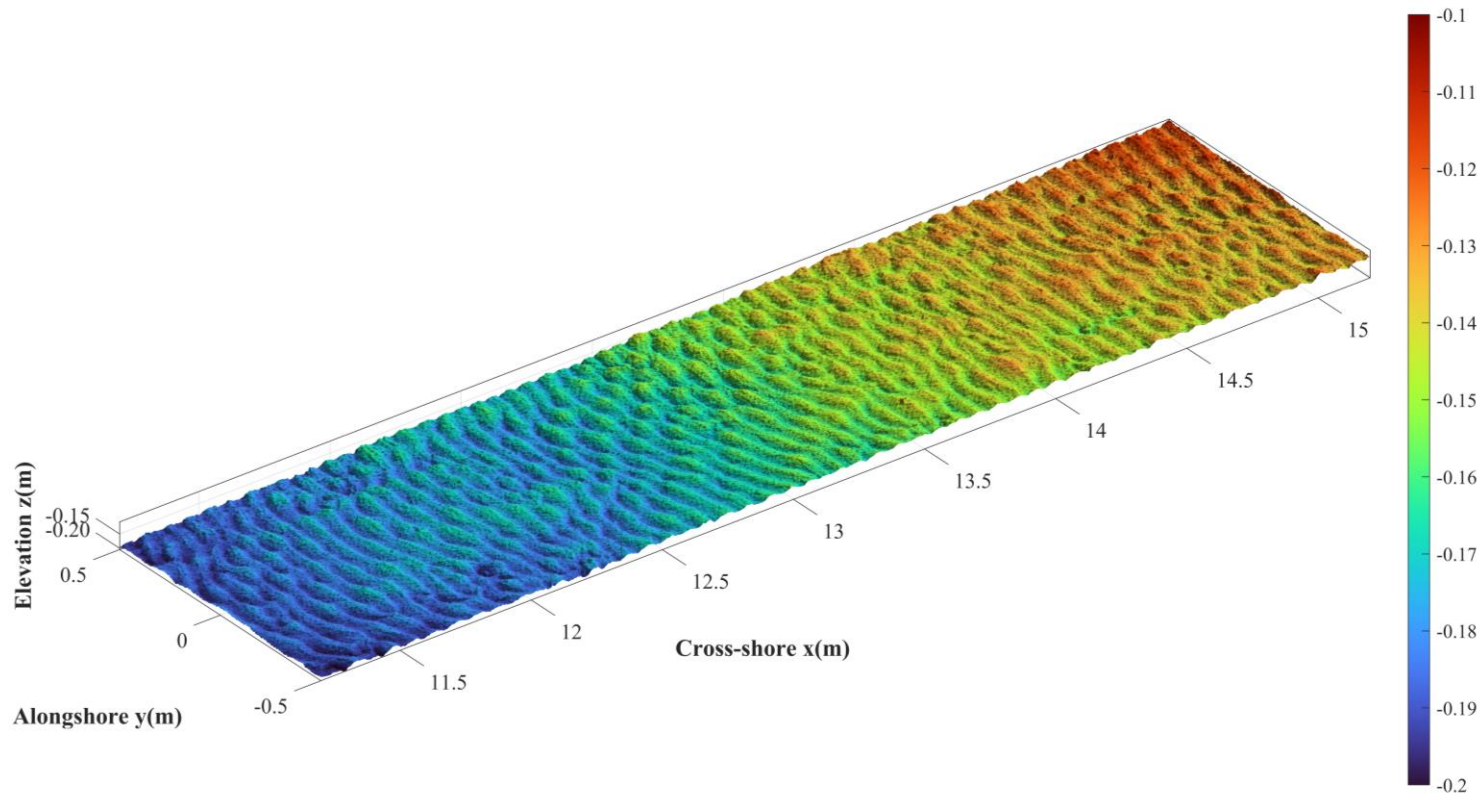


Figure 3.16 Surface plot measured by laser line scanner displaying final DO locations in inner and outer surf zones after Test EG (d).



Figure 3.17 Final locations of 20 large plastic DOs (a) on equilibrium sand beach profile in Test EL.

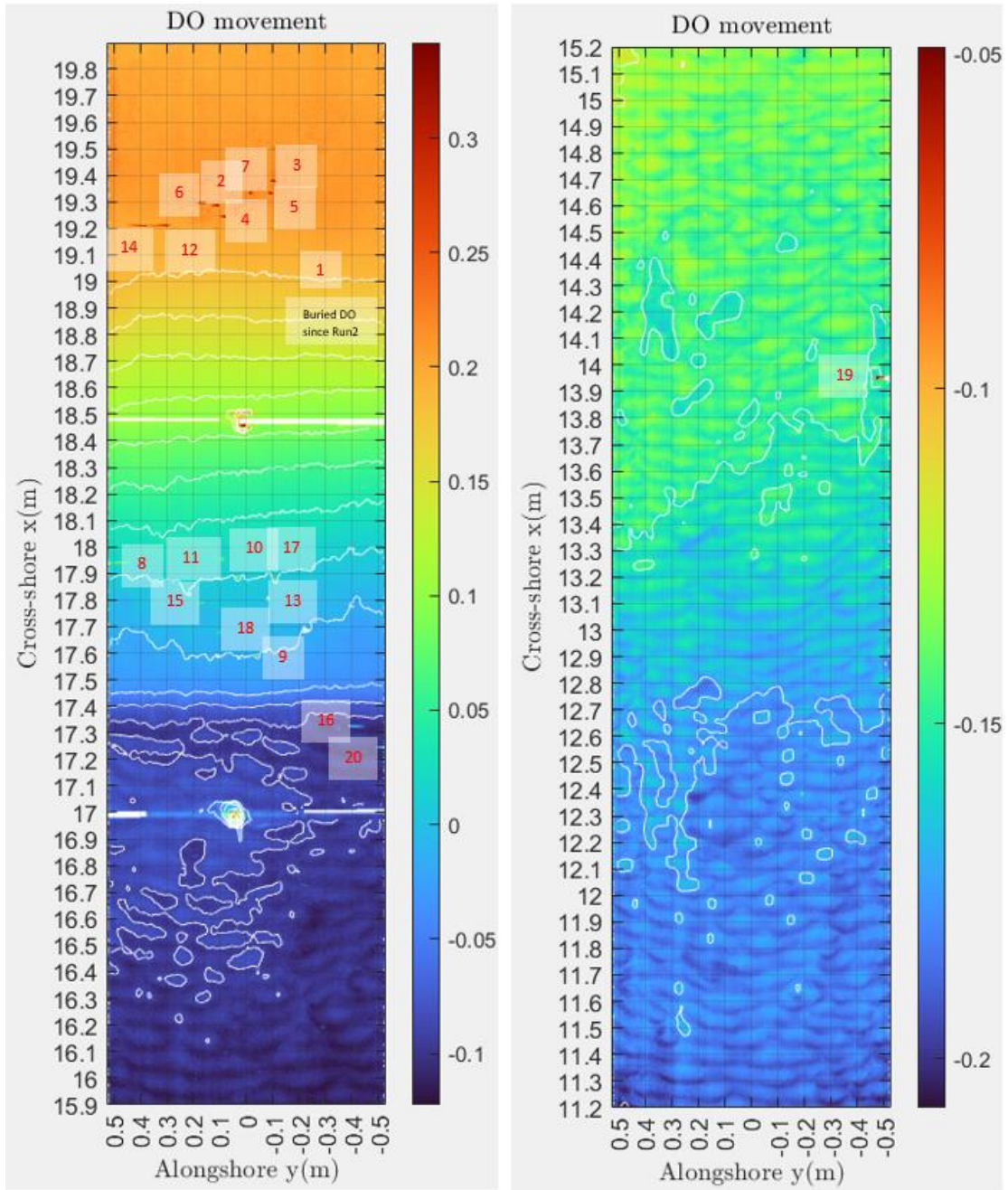


Figure 3.17 Bathymetric contour measured by laser line scanner displaying final DO locations after Test EL (b).

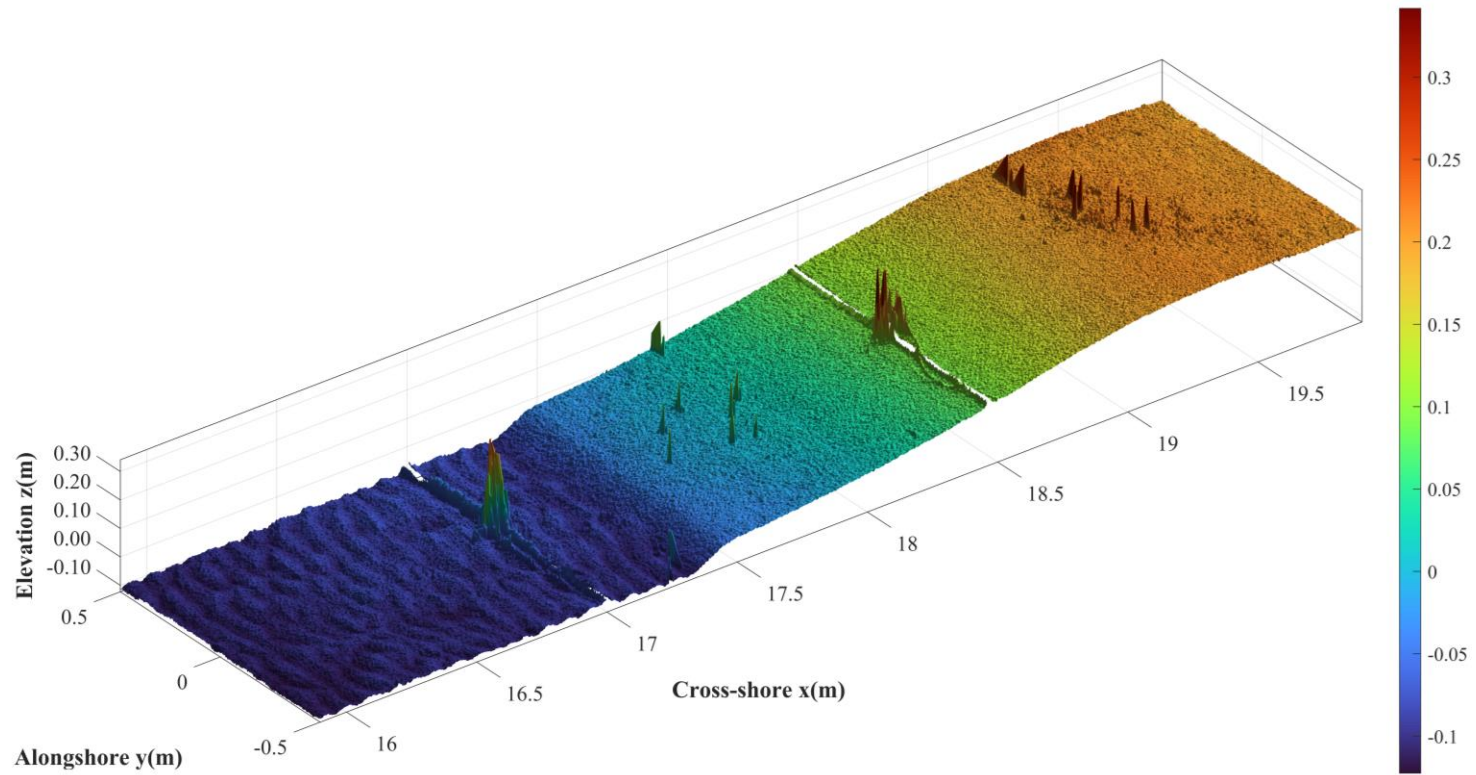


Figure 3.17 Surface plot displaying final DO locations in inner surf zone and foreshore after Test EL (c)

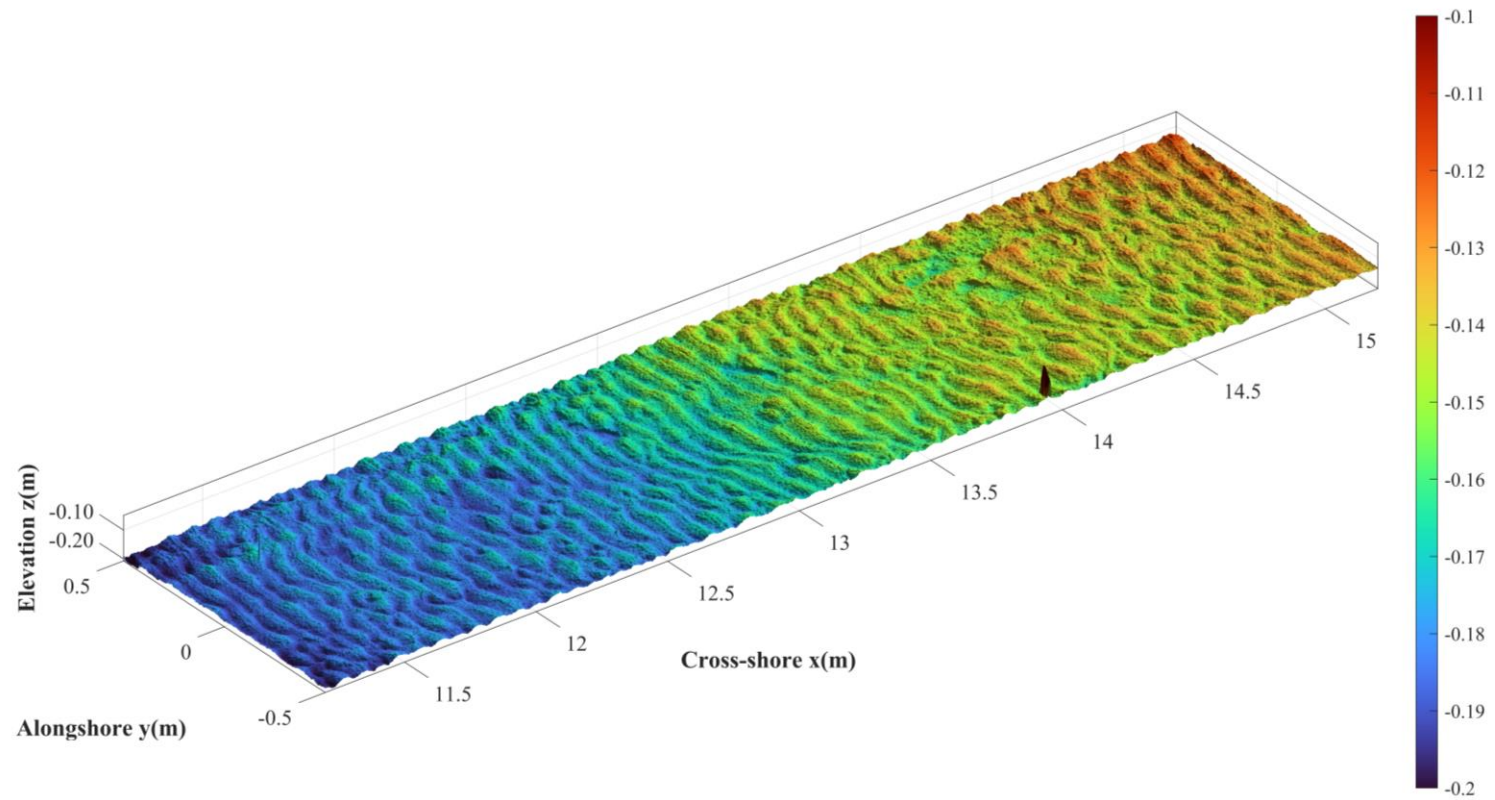


Figure 3.17 Surface plot displaying final DO locations in inner and outer surf zones after Test EL (d)



Figure 3.18 Final locations of 20 small plastic DOs (a) on equilibrium sand beach profile in Test ES.

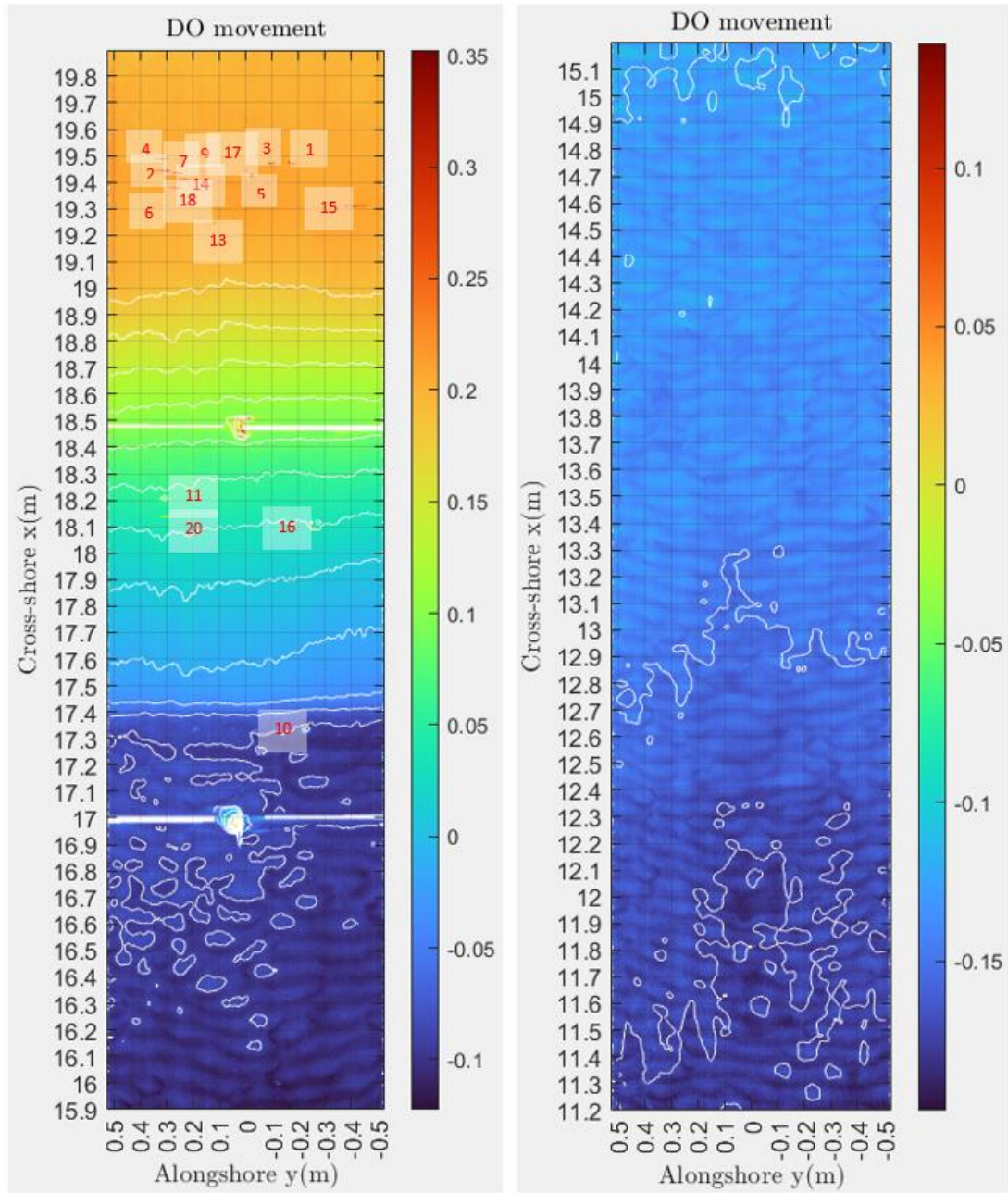


Figure 3.18 Bathymetric contour measured by laser line scanner displaying final DO locations after Test ES (b).

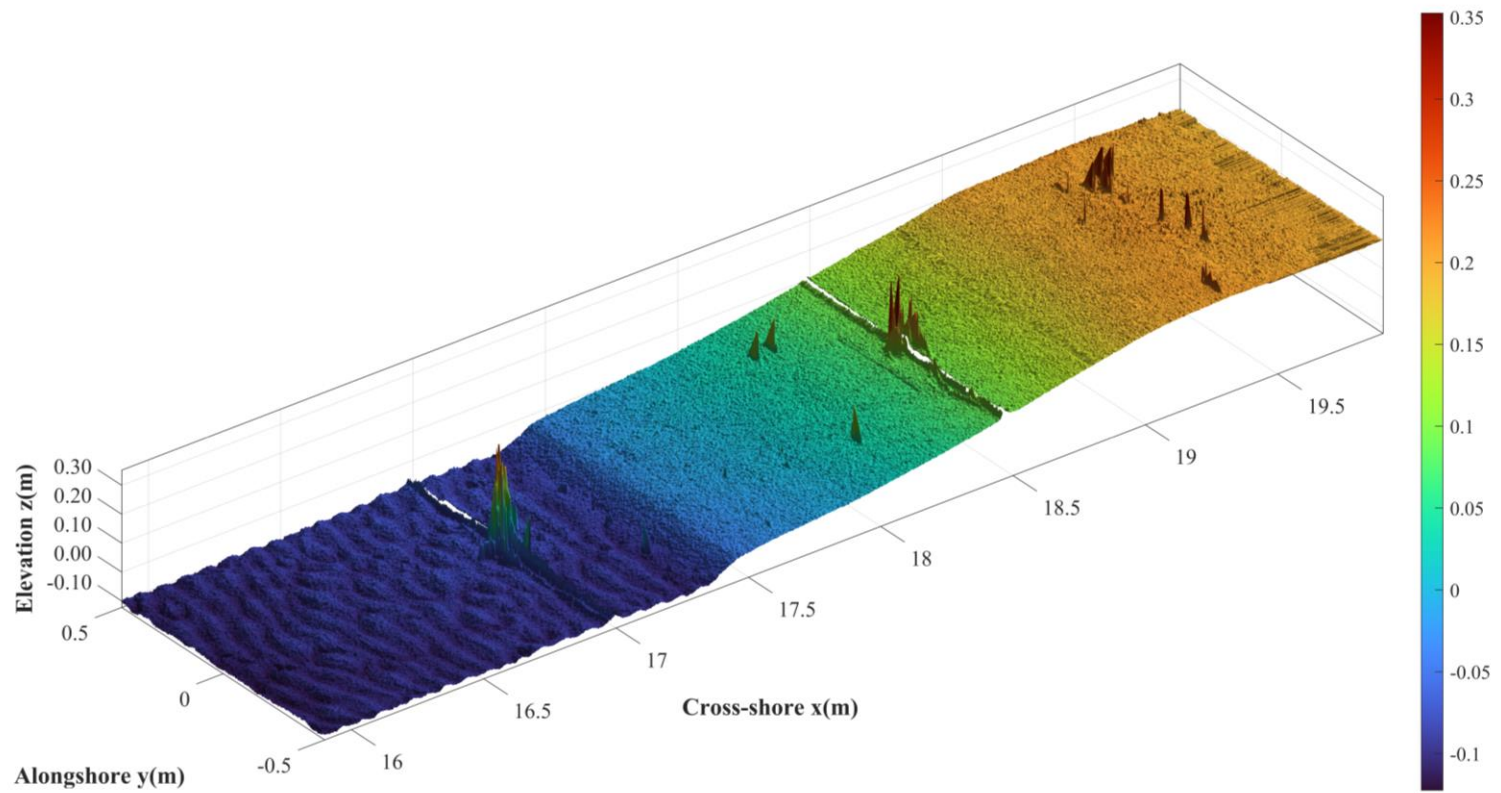


Figure 3.18 Surface plot displaying final DO locations in inner surf zone and foreshore after Test ES (c)

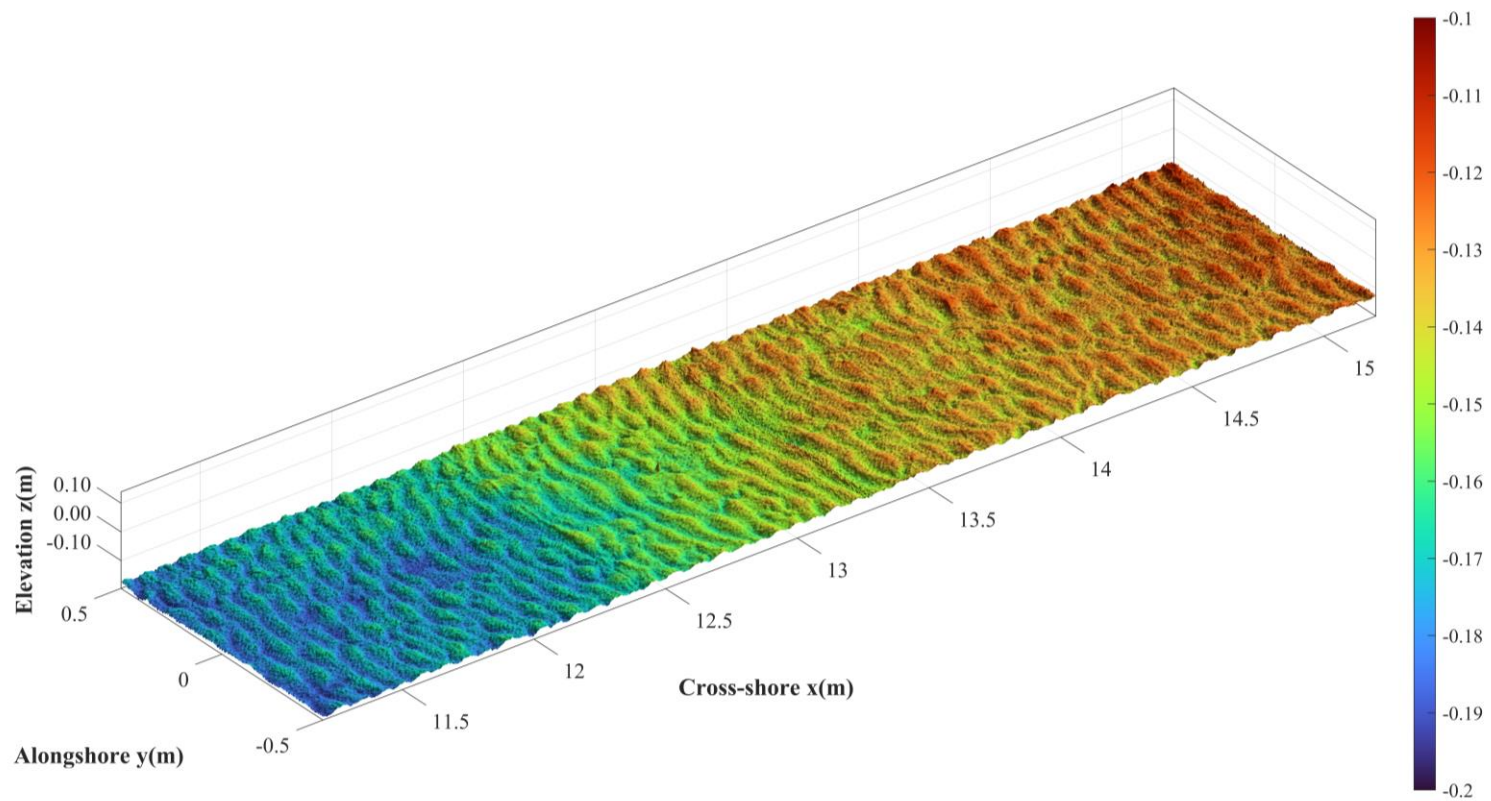


Figure 3.18 Surface plot displaying final DO locations in inner and outer surf zones after Test ES (d)



Figure 3.19 Final locations of 20 gravel DOs (a) on nourished foreshore profile in Test NG.

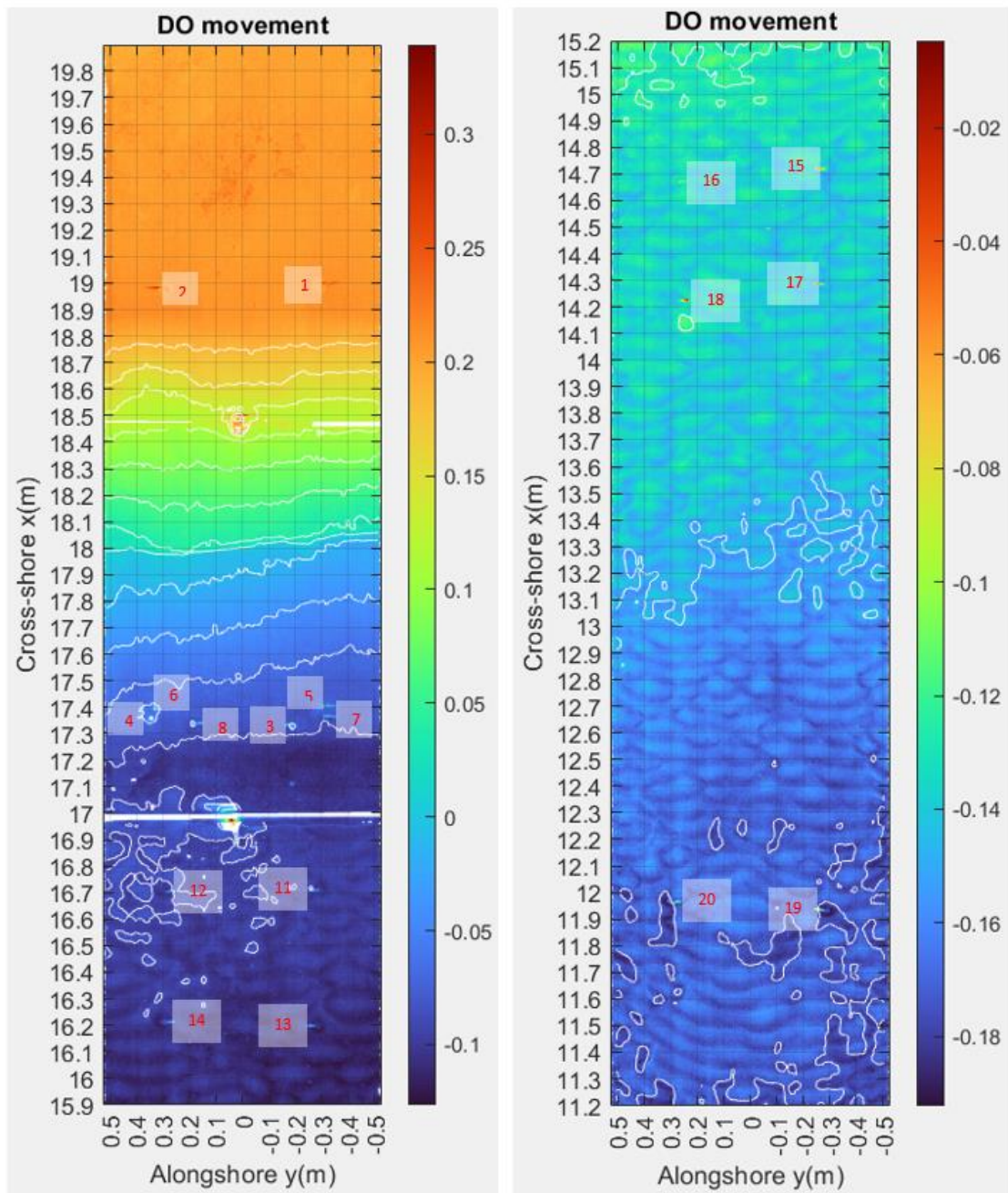


Figure 3.19 Bathymetric contour measured by laser line scanner displaying final DO locations after Test NG (b).

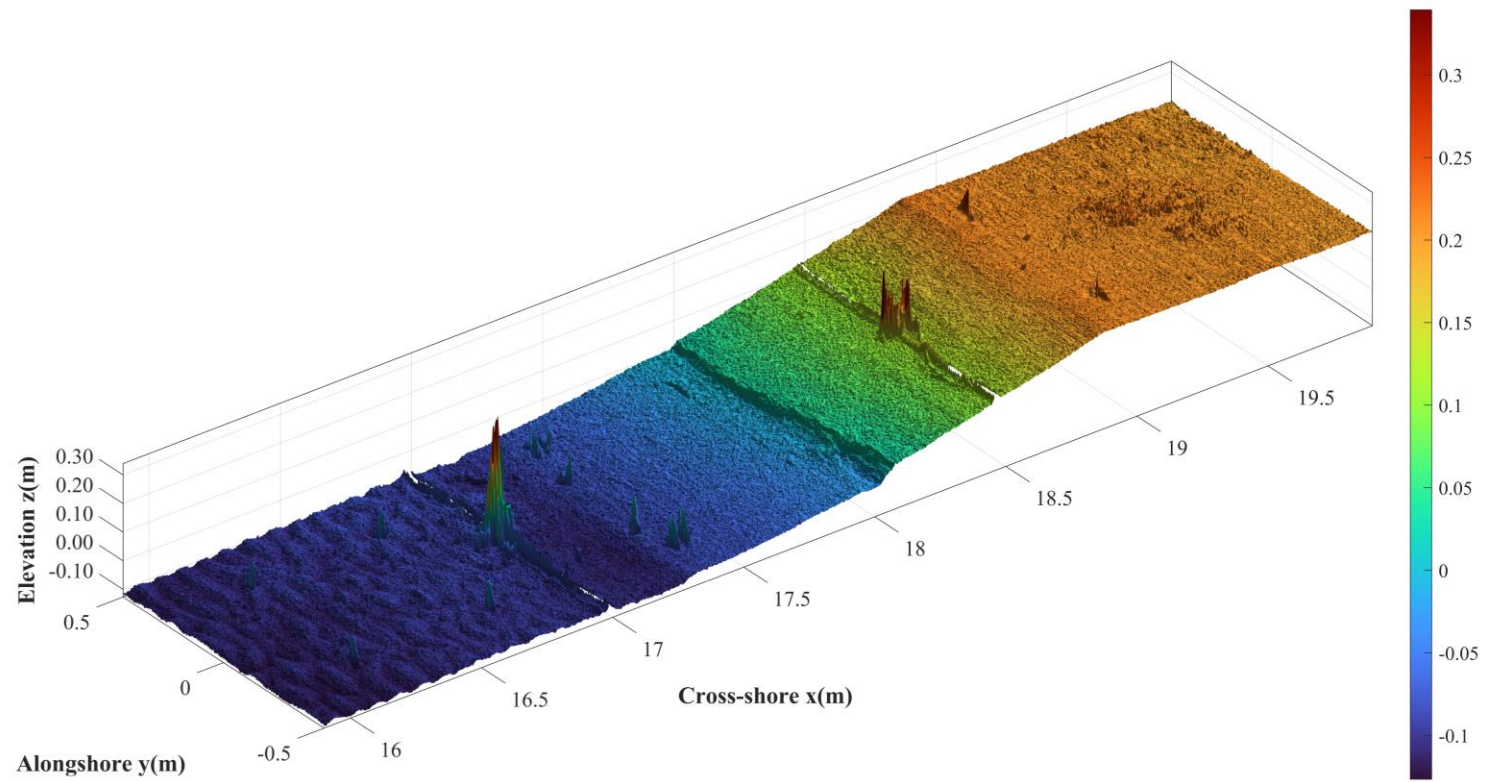


Figure 3.19 Surface plot displaying final DO locations in inner surf zone and foreshore after Test NG (c)

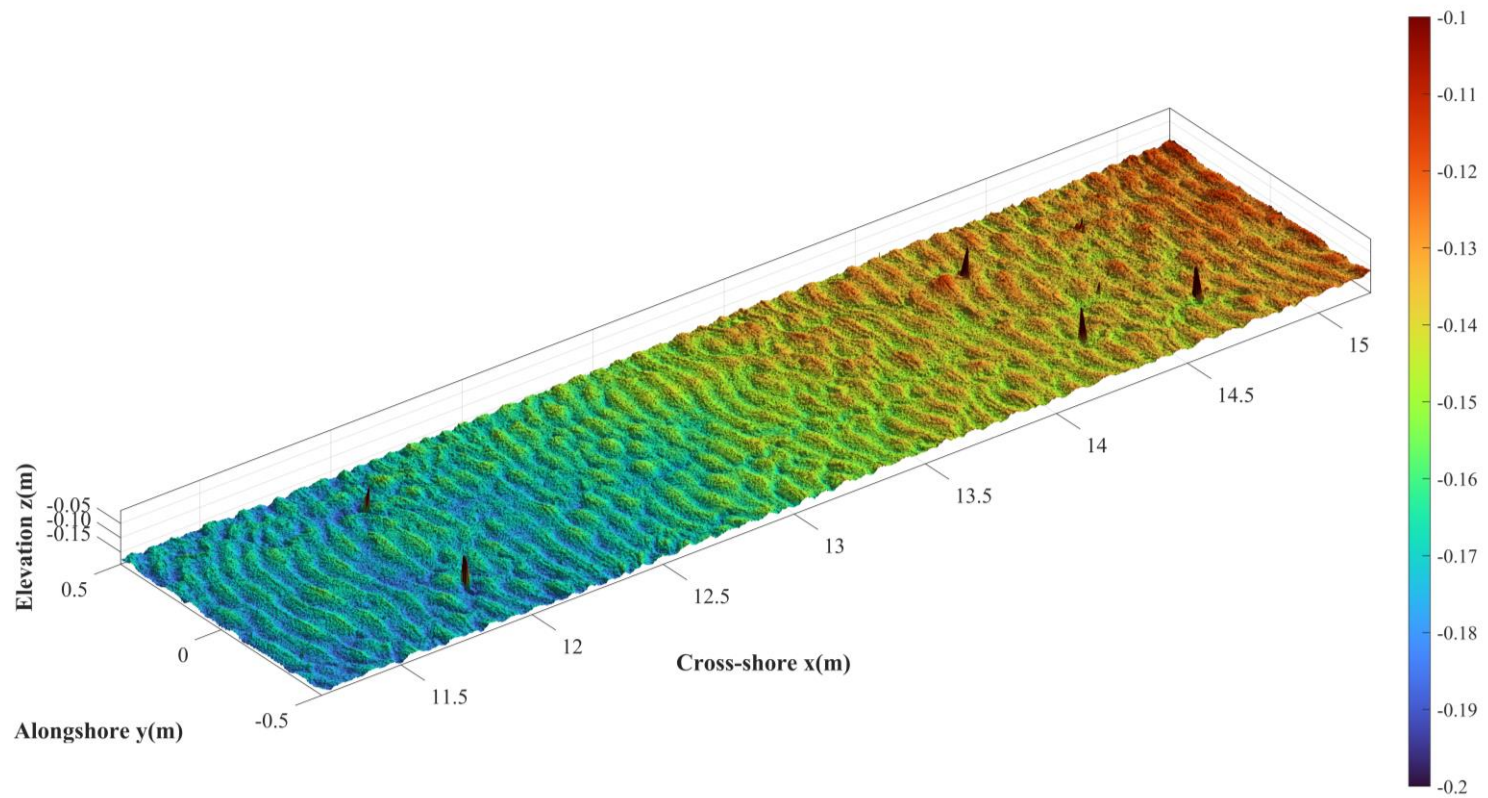


Figure 3.19 Surface plot displaying final DO locations in inner and outer surf zones after Test NG (d)



Figure 3.20 Final locations of 20 large plastic DOs (a) on nourished foreshore profile in Test NL.

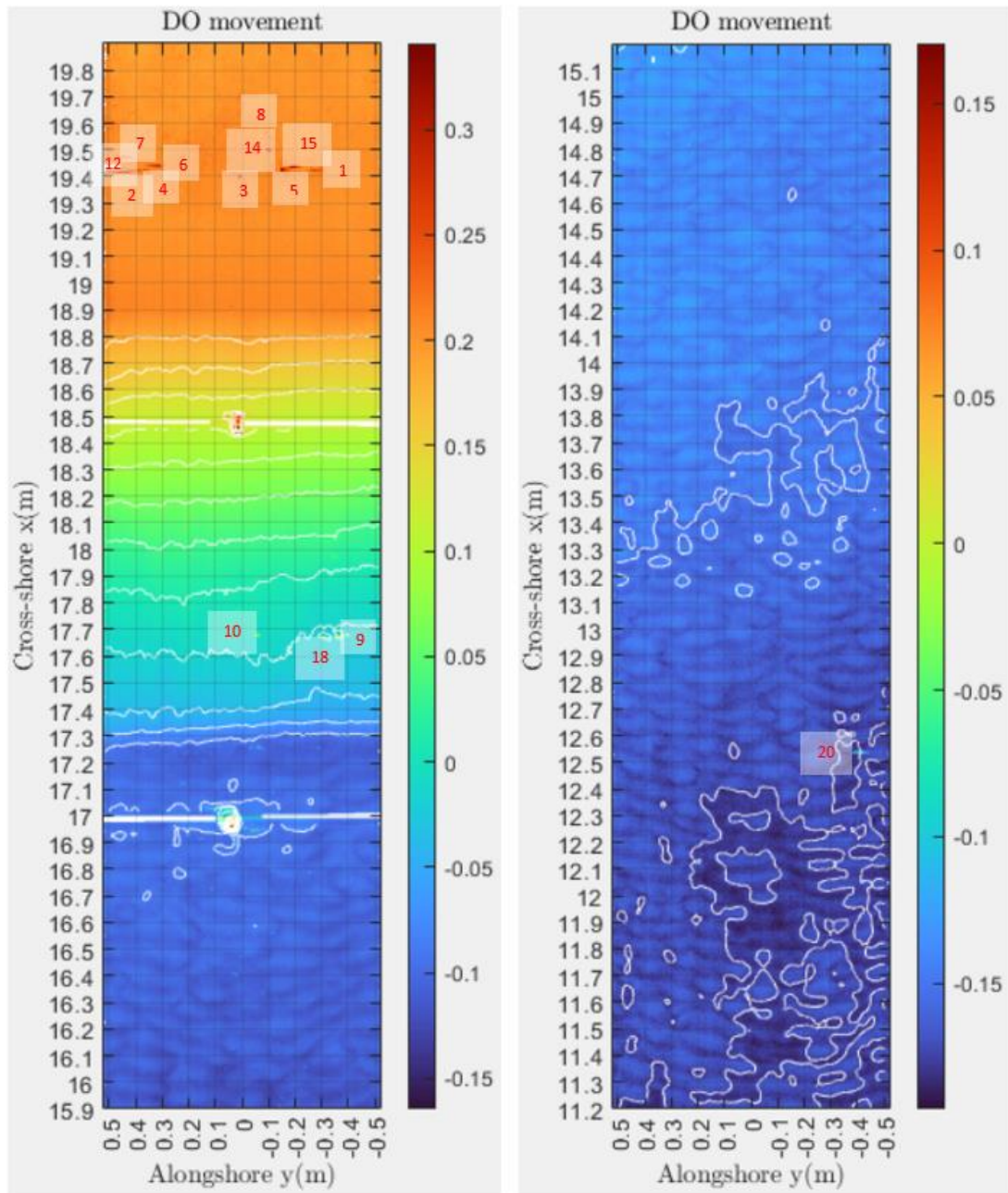


Figure 3.20 Bathymetric contour measured by laser line scanner displaying final DO locations after Test NL (b).

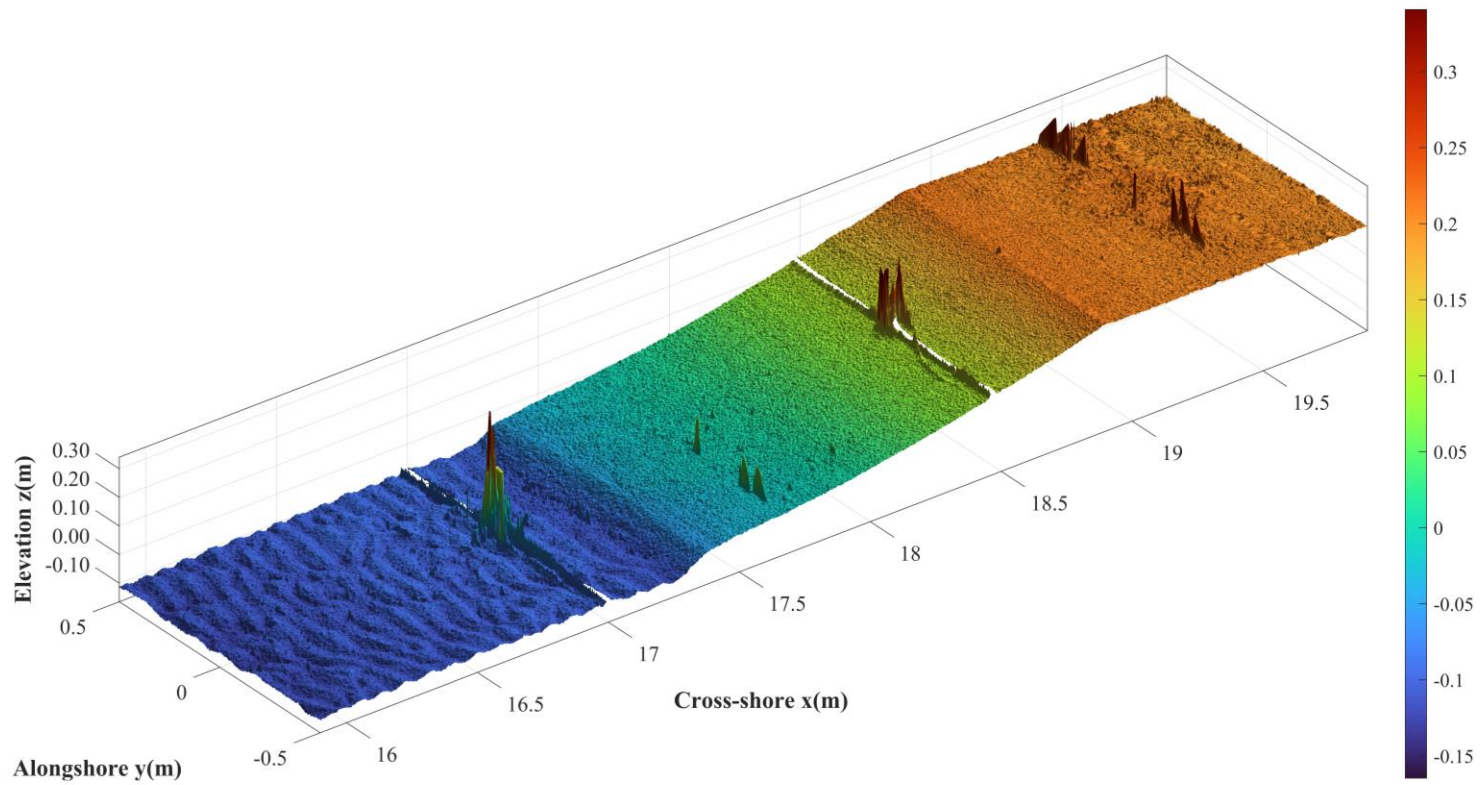


Figure 3.20 Surface plot displaying final DO locations in inner surf zone and foreshore after Test NL (c)

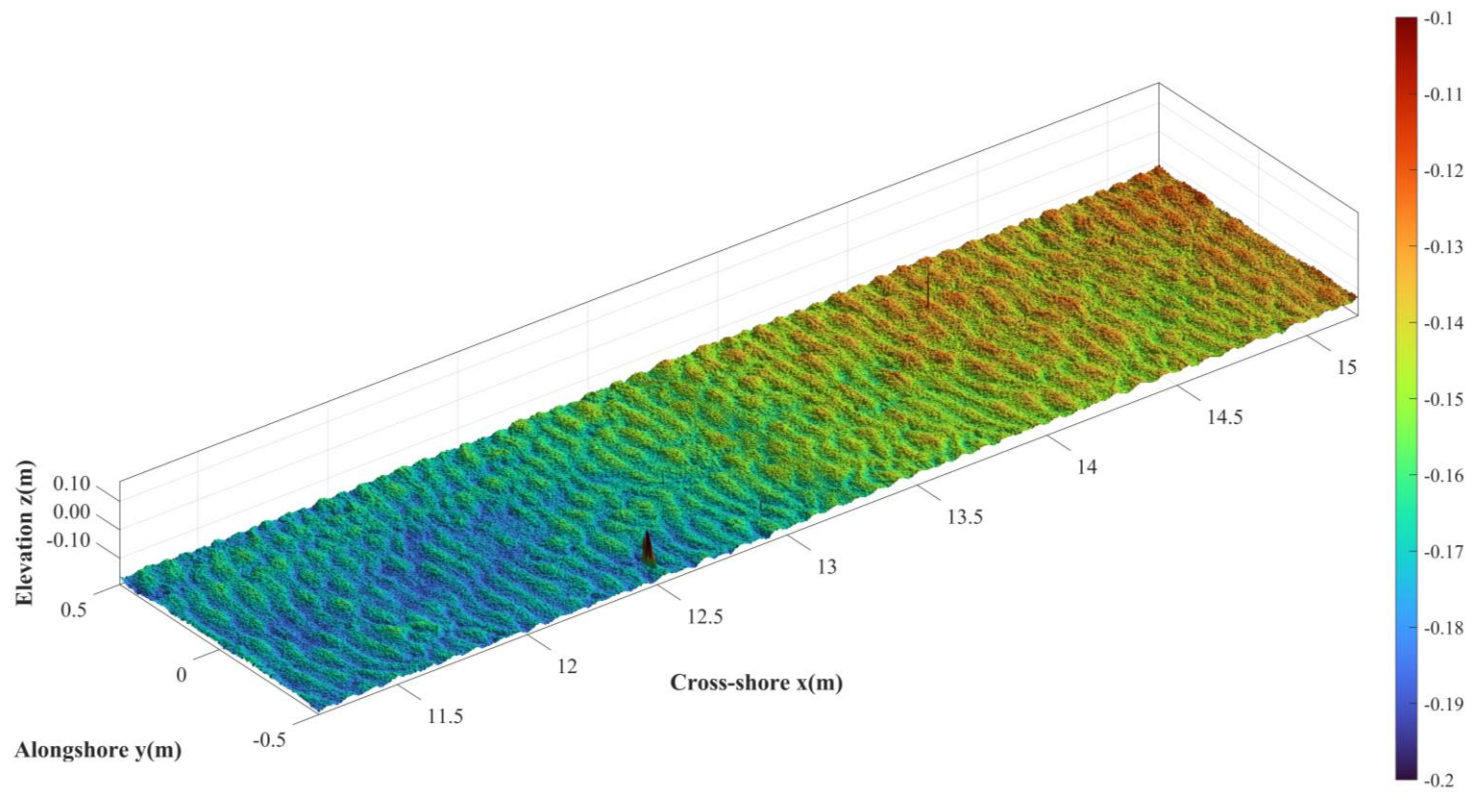


Figure 3.20 Surface plot displaying final DO locations in inner and outer surf zones after Test NL (d)



Figure 3.21 Final locations of 20 small plastic DOs (a) on nourished foreshore profile in Test NS.

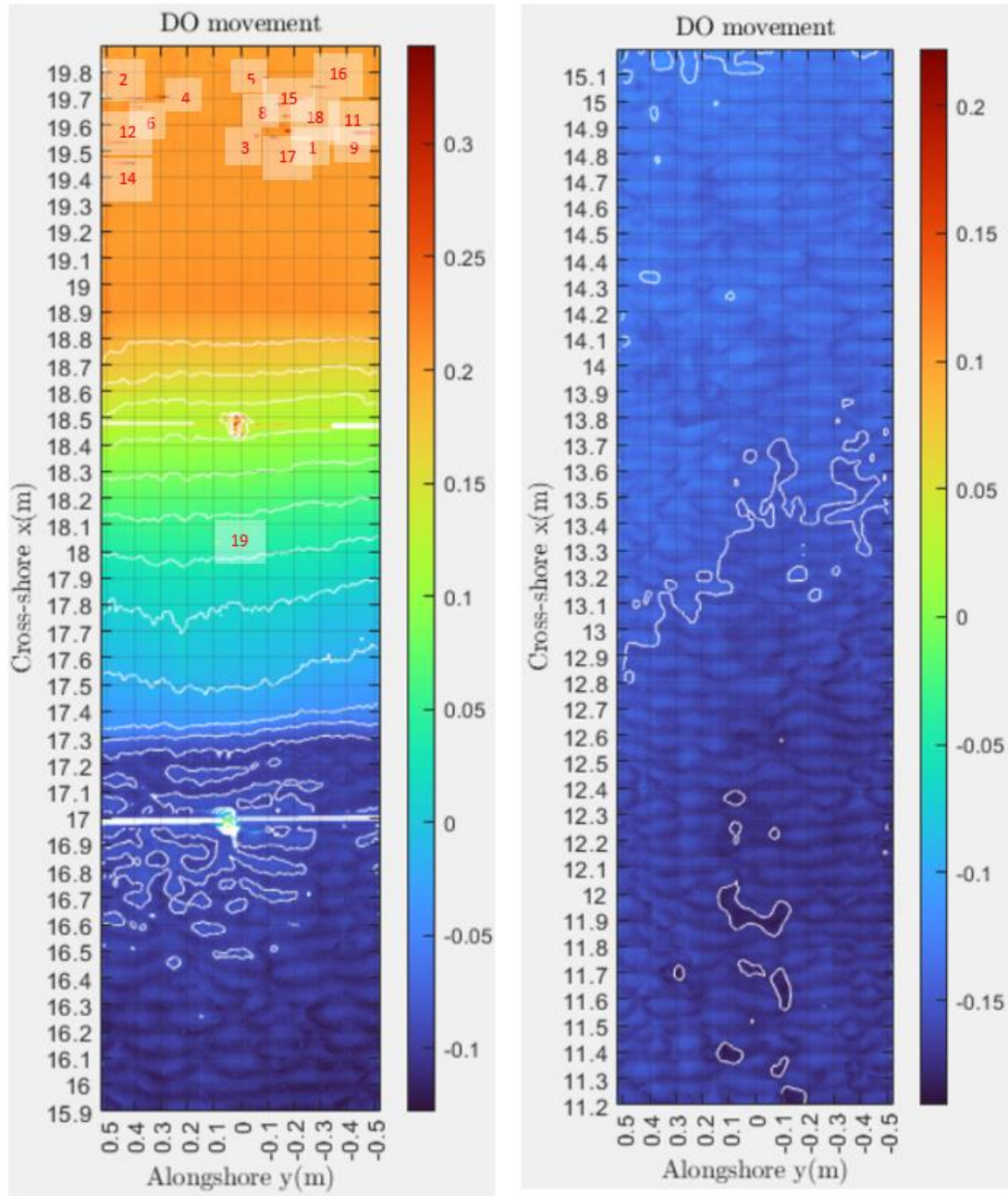


Figure 3.21 Bathymetric contour measured by laser line scanner displaying final DO locations after Test NS (b).

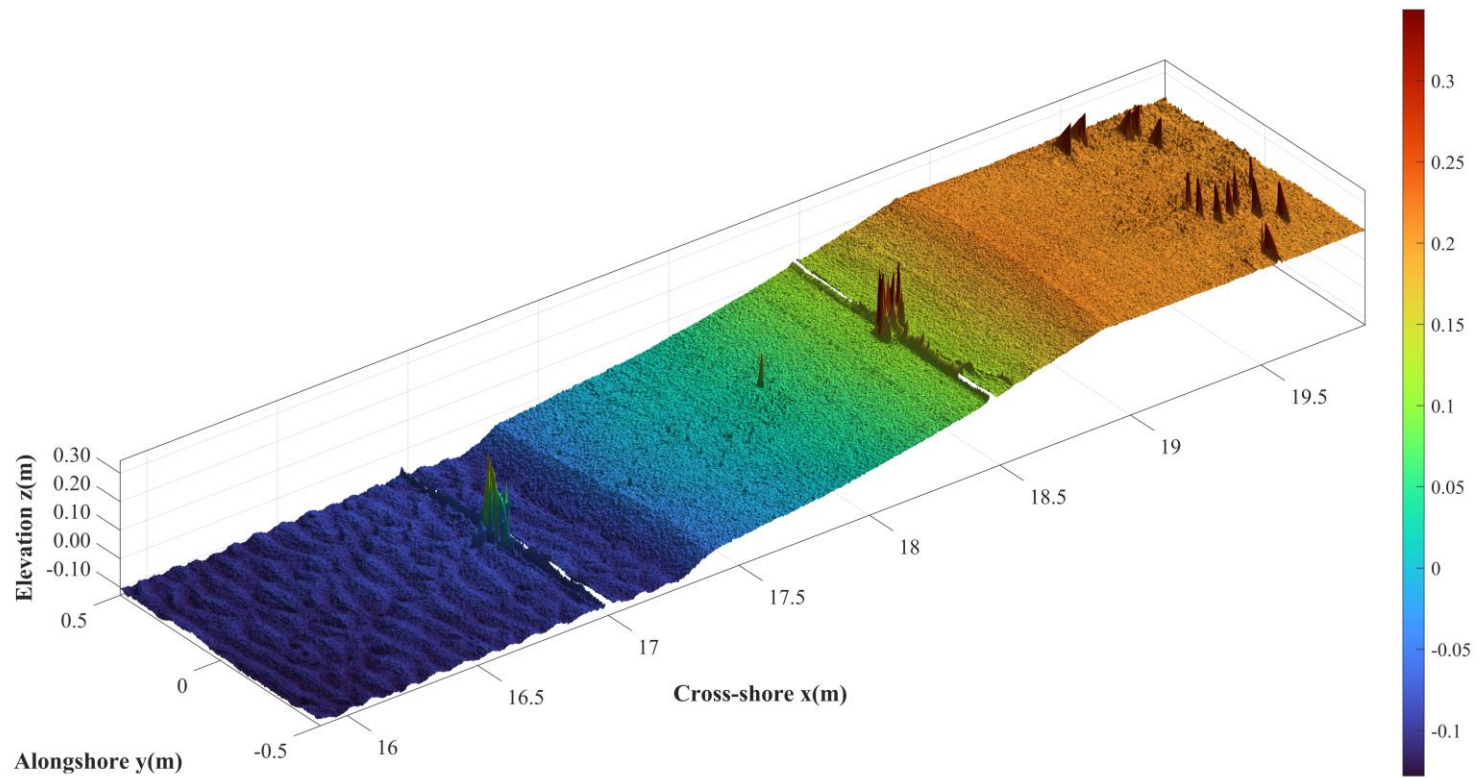


Figure 3.21 Surface plot displaying final DO locations in inner surf zone and foreshore after Test NS (c)

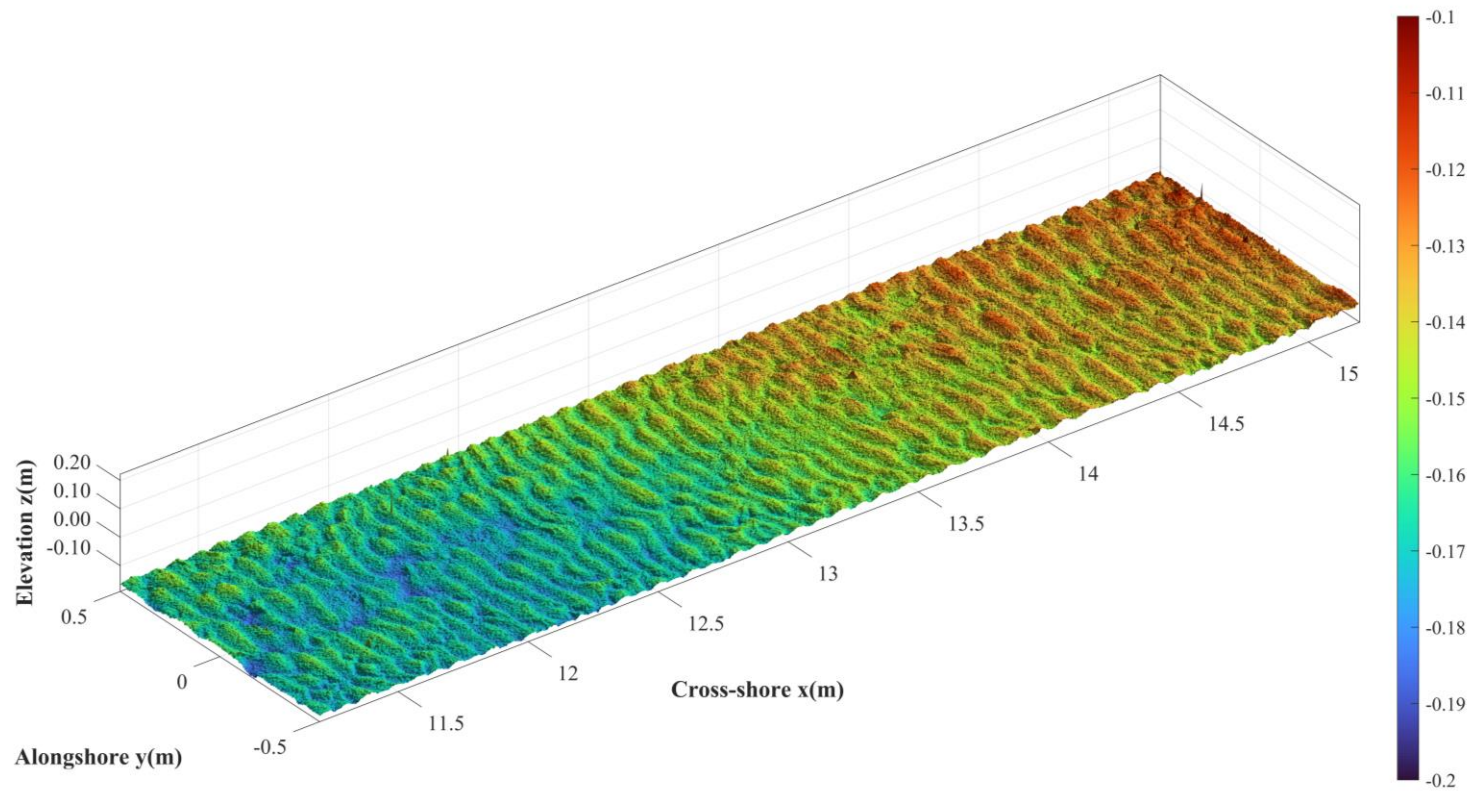


Figure 3.21 Surface plot displaying final DO locations in inner and outer surf zones after Test NS (d)

The initial and final locations of 20 particles measured during each test are depicted in Figures 3.22-3.25 where the measured 20 DO locations are shown from above in the direction of wave propagation. The corresponding side view is shown in Figure 2.3a. The left column in Figure 3.22 shows the initial cross-shore and alongshore locations of 20 gravel DOs on the initial equilibrium profile of EG0. The middle column of EG10 indicates the spatial locations of the 20 gravel DOs after 10 runs. The 20 DOs were placed back to their initial locations of EG0 before the second 10 runs of EG11-EG20. The comparison between EG10 and EG20 may reveal the degree of repeatability or variability in the DO trajectories. The number of the gravel DOs in each of the outer surf, inner surf, swash, and berm zones is denoted for EG0, EG10, and EG20 in Figure 3.22. Some of the gravel DOs in the swash zone moved offshore in wave downrush, but the moved DOs remained in the swash zone. The gravel DOs in the outer and inner surf zones moved little. The DO movement in the swash zone was different for EG10 and EG20, but the degree and pattern of the DO movement were similar for EG10 and EG20. The differences between the paired DOs at $y = -0.3$ and 0.3 m were similar to the differences between EG10 and EG20. The alongshore variability and the test repeatability are considered for the interpretation of the measured DO displacements.

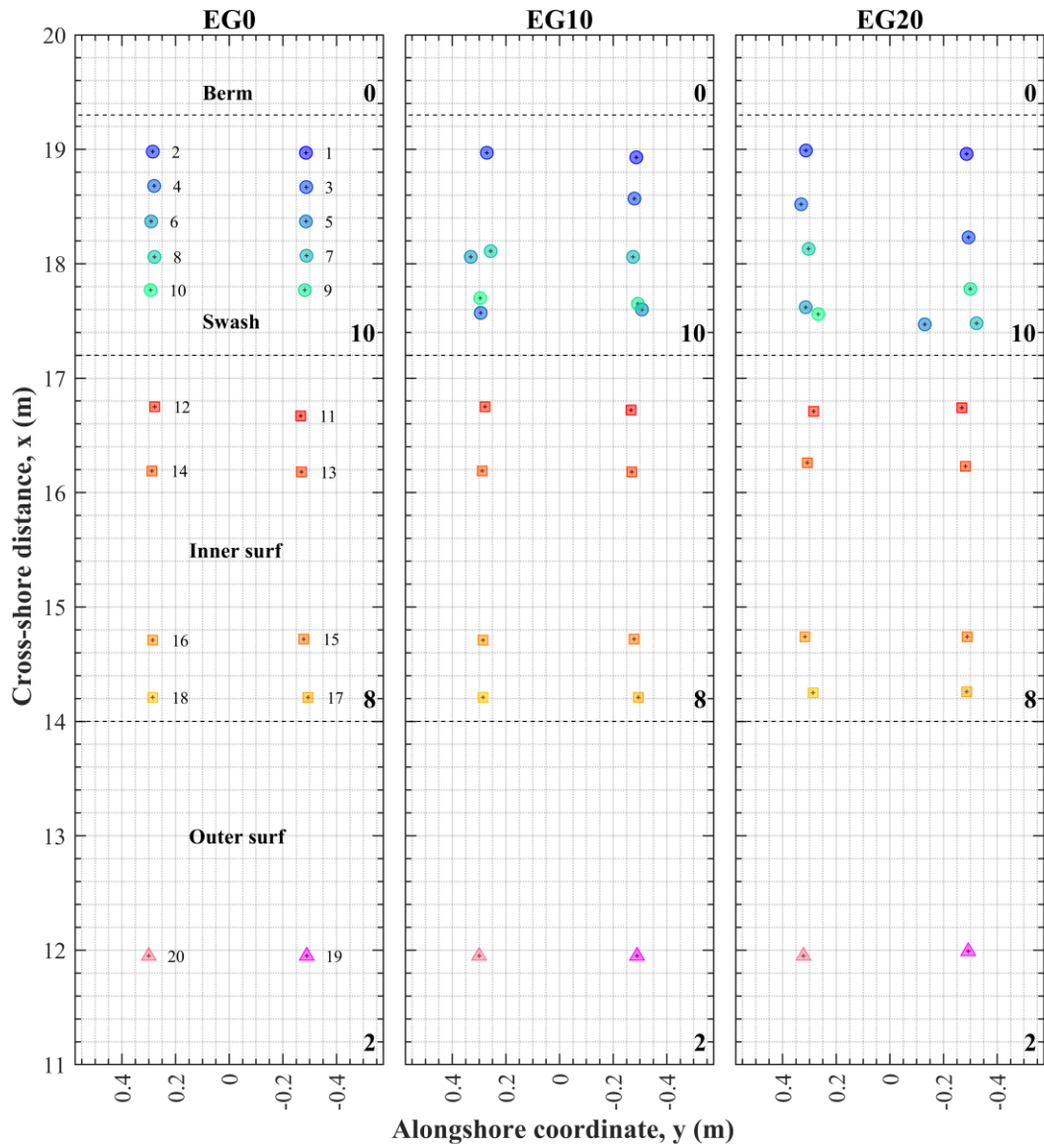


Figure 3.22 Initial and final cross-shore and alongshore locations of 20 gravel DOs for equilibrium profile test EG where the DOs were reset after EG10 and the number of DOs in each zone is indicated.

Figure 3.23 compares the initial and final cross-shore and alongshore locations of 20 large (L) plastics DOs for EL0, EL10, and EL20. The eight DOs in the inner surf zone of EL0 moved onshore into the swash zone of EL10 and EL20. The two L DOs in the outer surf zone of EL0 remained in the same zone of EL10, but one of the two DOs moved to the swash zone of EL20. The final locations of the 20 L DOs in EL10 and EL20 appear to be uncorrelated with their initial alongshore locations ($y = -0.3$ or 0.3 m) in EL0 possibly because of the mobility of the L DOs. The L DOs transported onshore accumulated in the lower swash zone and near the seaward edge of the berm. The DO accumulation pattern was similar for EL10 and EL20 but the destinations of the accumulated DOs were not correlated clearly with their origins. One DO was missing in EL10 but no DO was missing in EL20. The large plastics DOs of 0.33-cm diameter were difficult to detect right after each run where the turbidity caused by suspended sand hindered the visual detection of the DOs on the sand surface.

Figure 3.24 compares the initial and final cross-shore and alongshore locations of 20 small (S) plastics DOs for ES0, ES5, and ES10. The landward displacements of the S DOs during 5 runs were more pronounced than those of the L DOs during 10 runs in Figure 3.23. More DOs were transported to the vicinity of the berm edge. The difference between ES5 and ES10 was more apparent than between EL10 and EL20. The increased variability or randomness may be related to the increased mobility of the smaller S DOs of 0.20-cm diameter. Three DOs were missing in ES5 and ES10.

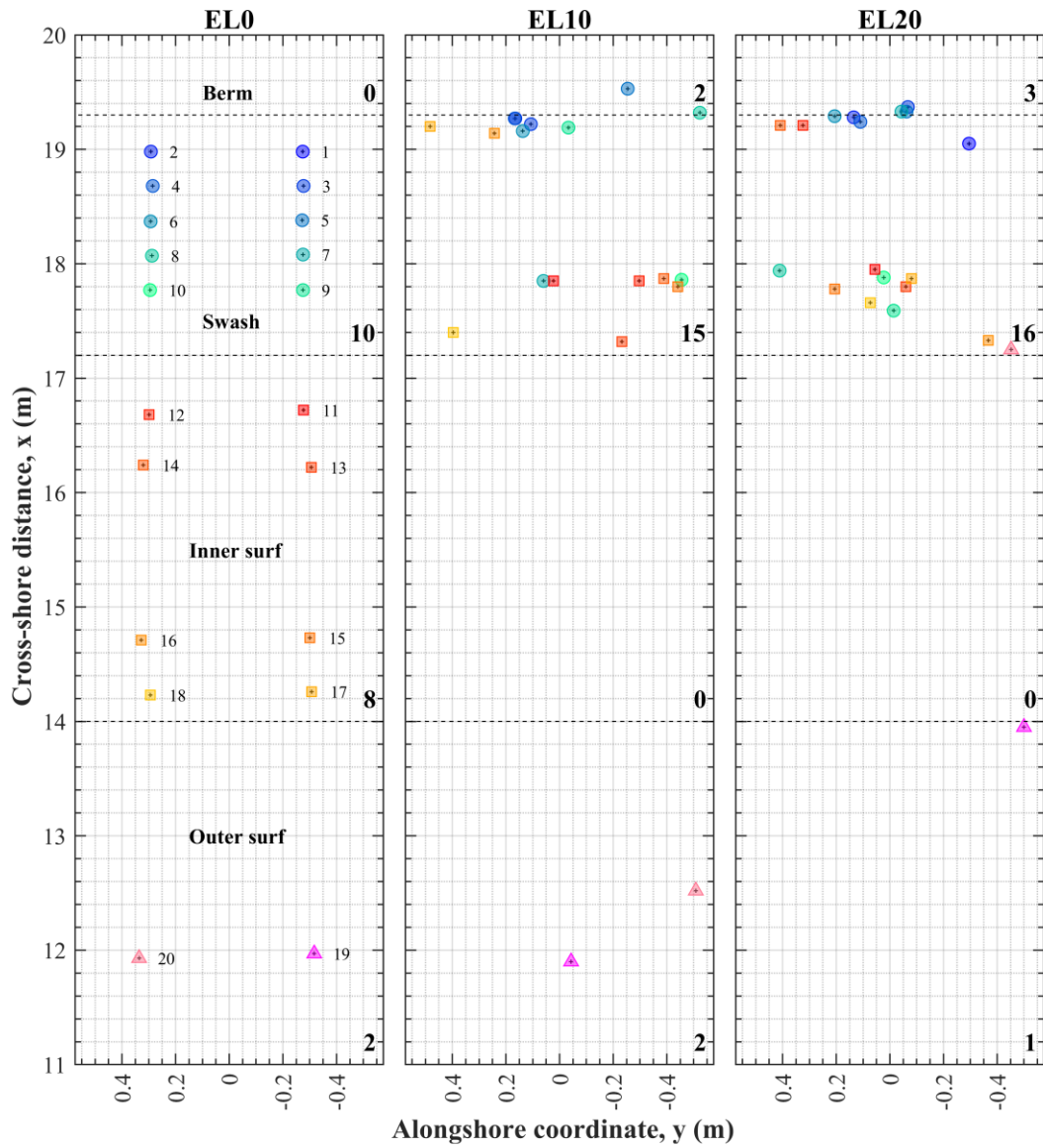


Figure 3.23 Initial and final cross-shore and alongshore locations of 20 large plastics DOs for equilibrium profile test EL where the DOs were reset after EL10 and DO No.1 was missing in EL10.

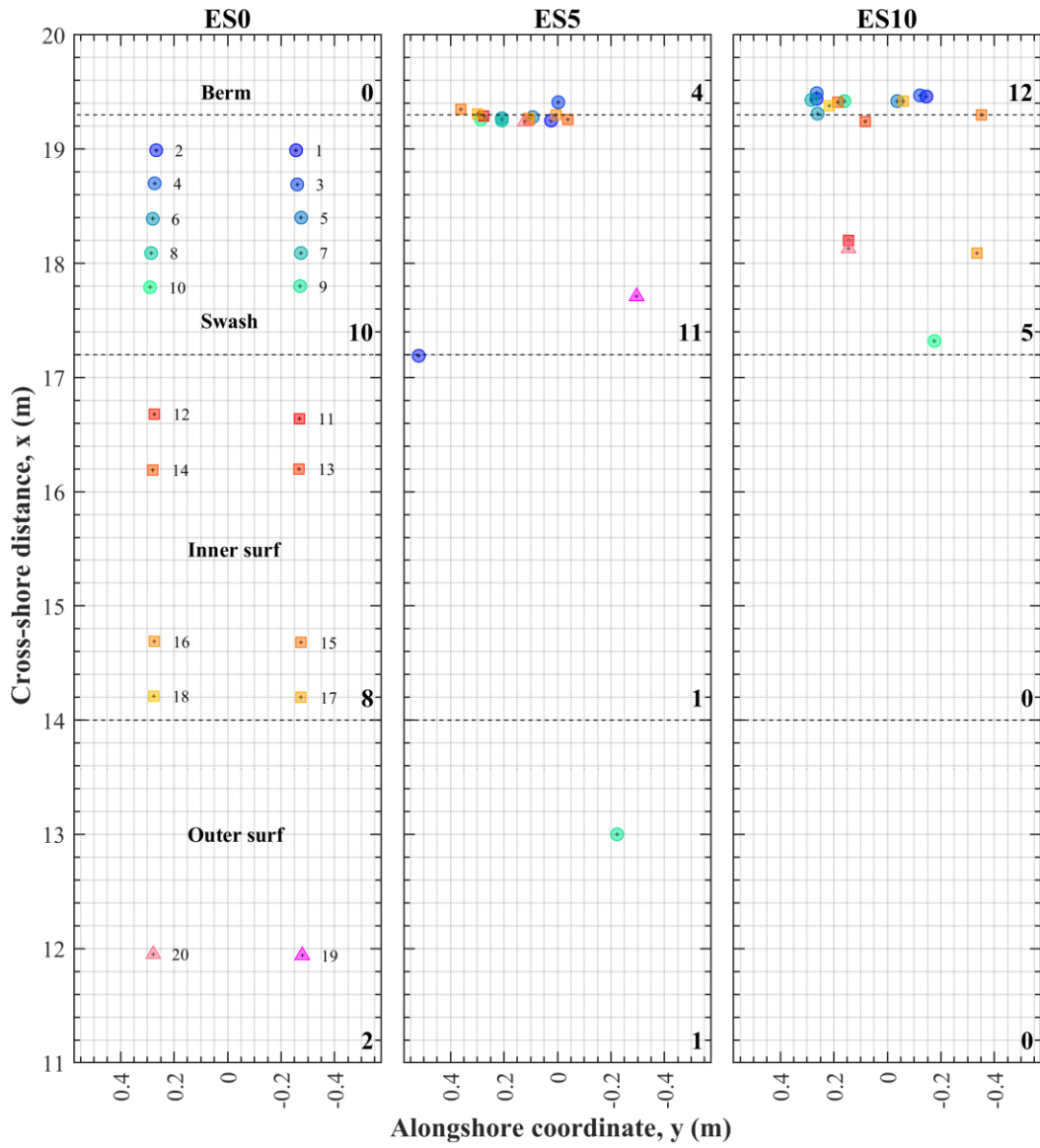


Figure 3.24 Initial and final cross-shore and alongshore locations of 20 small plastics DOs for equilibrium profile test ES where the DOs were reset after ES5. DO No.4, 7, and 12 were missing in ES5. DO No.8, 12, and 19 were missing in ES10.

Table 3.35 summarizes the measured number of DOs found in the four different zones in Figure 2.3a for the equilibrium (E) profile test series for the gravel (G), large (L) plastics, and small (S) plastics DOs. The mobility differences among the G, L, and S DOs were obvious in the table. The computed results are explained in Chapter 5.

Table 3.35 Measured (M) and Computed (C) numbers of DOs found in four different zones for equilibrium profile tests

Zone	EG10		EG20		EL10		EL20		ES5		ES10	
	M	C	M	C	M	C	M	C	M	C	M	C
Berm*	0	0	0	0	2	0	3	0	4	0	12	0
Swash	10	10	10	10	15	20	16	20	11	18	5	18
Inner Surf	8	8	8	8	0	0	0	0	1	2	0	2
Outer Surf	2	2	2	2	2	0	1	0	1	0	0	0
Missing	0	0	0	0	1	0	0	0	3	0	3	0

*The measured DOs located at $x > 19.3$ m are considered to be on the berm.

Figures 3.22-3.24 indicate the movement and accumulation of the plastics DOs in the swash zone on the near equilibrium beach profile. The nourished (N) foreshore tests were performed to examine the DO movement and accumulation on the foreshore of noticeable profile changes. The initial cross-shore distance x of each of the 10 DO pairs was the same in the E and N test series as shown in Figures 2.3a and 2.6a. The

foreshore nourishment shifted the seaward edge of the berm from $x = 19.3$ m in Figure 2.3a to $x = 18.6$ m in Figure 2.6a. The 2 DO pairs were placed on the widened berm and 3 DO pairs were in the narrower swash zone. The initial DO locations in the inner and outer surf zones were the same in the E and N test series.

Figure 3.25 shows the final cross-shore and alongshore locations of 20 DOs after 20 or 10 runs for the NG, NL, and NS tests. The gravel DO locations for NG20 (left column) may be compared with those of the EG test in Figure 3.22. Erosion of the nourished steep foreshore caused the seaward (downslope) movement of the gravel DOs in the swash zone. This downward displacement was expected for the gravel DOs with limited mobility in the inner and outer surf zones in Figures 3.22 and 3.25. On the other hand, the large (L) plastics DO locations of NL20 (middle column) in Figure 3.25 shifted farther landward in comparison with those of EL10 and EL20 in Figure 3.23 probably because of increased wave runup on the steeper nourished foreshore. The small (S) plastics DOs of NS10 (right column) in Figure 3.25 also moved farther landward in comparison with those of ES5 and ES10 in Figure 3.24.

Table 3.36 lists the number of DOs in the four different zones for NG20, NL20, and NS10. The number of missing DOs was 2 for NG20, 5 for NL20, and 4 for NS10. The foreshore erosion and deposition made it more difficult to find the mobile plastics DOs on the evolving sand surface. Some of the missing DOs may have been buried below the surface of 0.18-mm sand where the diameters of L and S plastics particles were 3.3 and 2.0 mm, respectively. The scour hole depth underneath each of the 6 gravel DOs of NG20 in the lower swash zone was about 3 cm below the accreted sand surface.

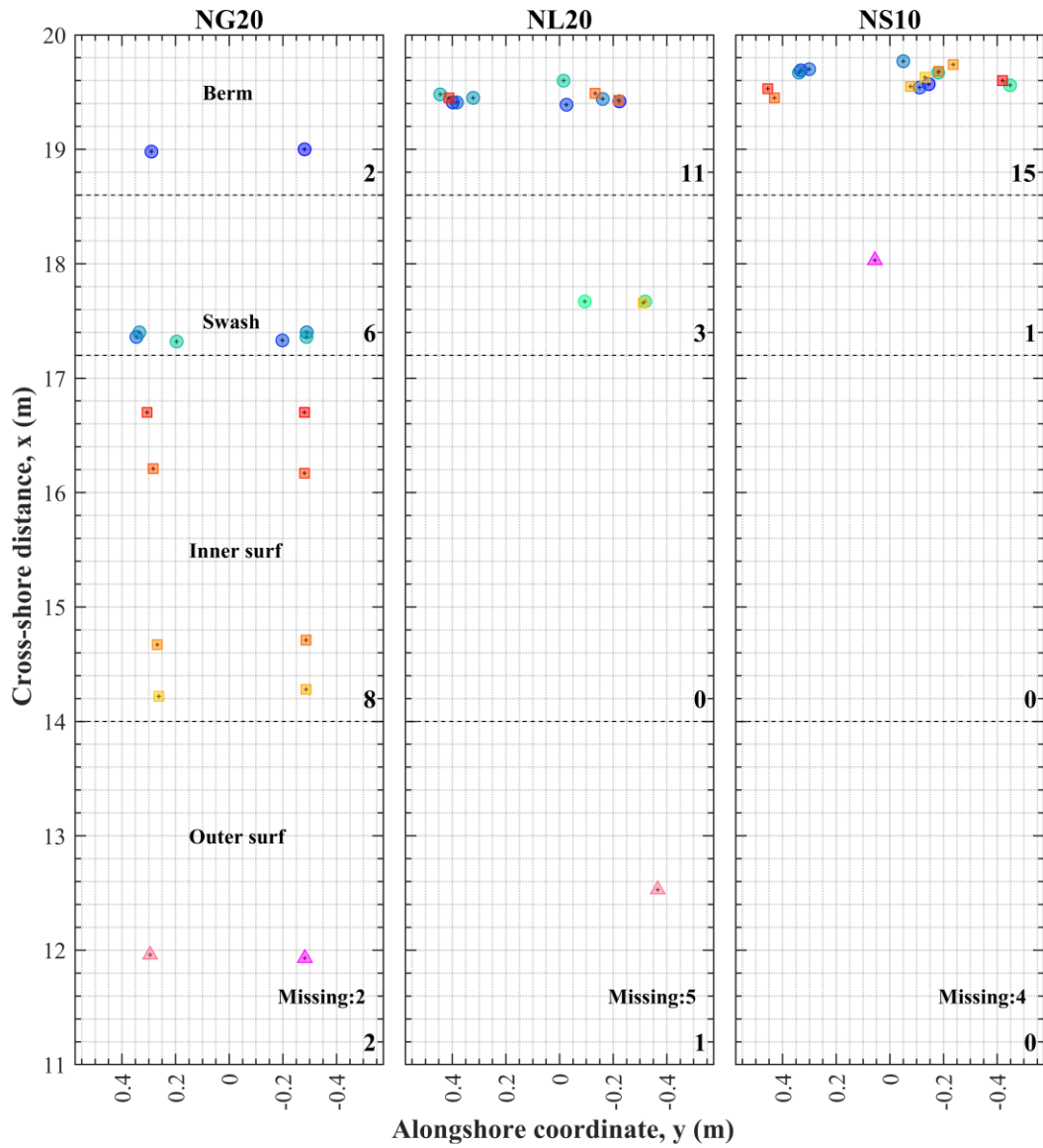


Figure 3.25 Final cross-shore and alongshore locations of 20 DOs for nourished foreshore tests NG, NL, and NS, where the number of missing DOs was 2, 5, and 4 in NG20, NL20, and NS10, respectively.

Table 3.36 Measured (M) and Computed (C) numbers of DOs found in four different zones for nourished foreshore profile tests

Zone	NG20		NL20		NS10	
	M	C	M	C	M	C
Berm*	2	4	11	4	15	4
Swash	6	6	3	16	1	16
Inner Surf	8	8	0	0	0	0
Outer Surf	2	2	1	0	0	0
Missing	2	0	5	0	4	0

*The measured DOs located at $x > 18.6$ m are considered to be on the berm.

The temporal variation of each DO was examined by tracking its cross-shore and alongshore locations after each of 400-s run. The DO tracking was continued until the end of each test or when this DO became missing. The unidentified DO locations, which could not be found for some runs, were interpolated linearly to follow the trajectory of the tracked DO. The trajectories of the paired DOs located initially at $y = -0.3$ m and 0.3 m were compared to examine the alongshore variability of the DO trajectories. This alongshore variability was similar to the alongshore variability of the final DO locations for each test in Figures 3.22-3.25. The gravel DOs were almost immobile and remembered their initial alongshore locations. The L and S plastics DOs

were mobile and lost their alongshore location memories during their migrations. In the following, each pair is represented by the DO at $y = 0.3$ m initially.

Figure 3.26 shows the temporal variations of the cross-shore locations of the 10 gravel DOs at $y = 0.3$ m initially during 10 runs (4000 s) of the equilibrium profile EG test. The repeated tests of EG0-EG10 and EG10-EG20 are presented side by side. Four gravel DOs in the swash zone moved during the first run and became immobile during the subsequent 9 runs. The 4 mobile DOs remained in the swash zone but their displacements were not repeatable. The 6 immobile DOs were stationary in the repeated tests. Likewise, Figure 3.27 shows the temporal variations of the cross-shore locations of the 10 large plastics DOs for EL0-EL10 and EL10-EL20. The 10 L DOs were mobile and transported onshore except for the 2 DOs near SWL at $x = 18$ m. The 3 DOs above the SWL were transported onshore during the first run and became stationary at the seaward edge of the berm. The 4 DOs in the inner surf zone were transported onshore to the lower swash zone and encountered wave downrush near the SWL. One or two of the 4 DOs managed to climb to the berm edge after several runs. One DO in the outer surf zone moved slowly onshore and faster in the inner surf zone. Next, the trajectories of the 10 small plastics DOs for ES0-ES5 and ES5-ES10 are depicted in Figure 3.28. The trajectories of the L and S DOs were similar but the smaller DOs moved landward somewhat faster and farther on the berm.

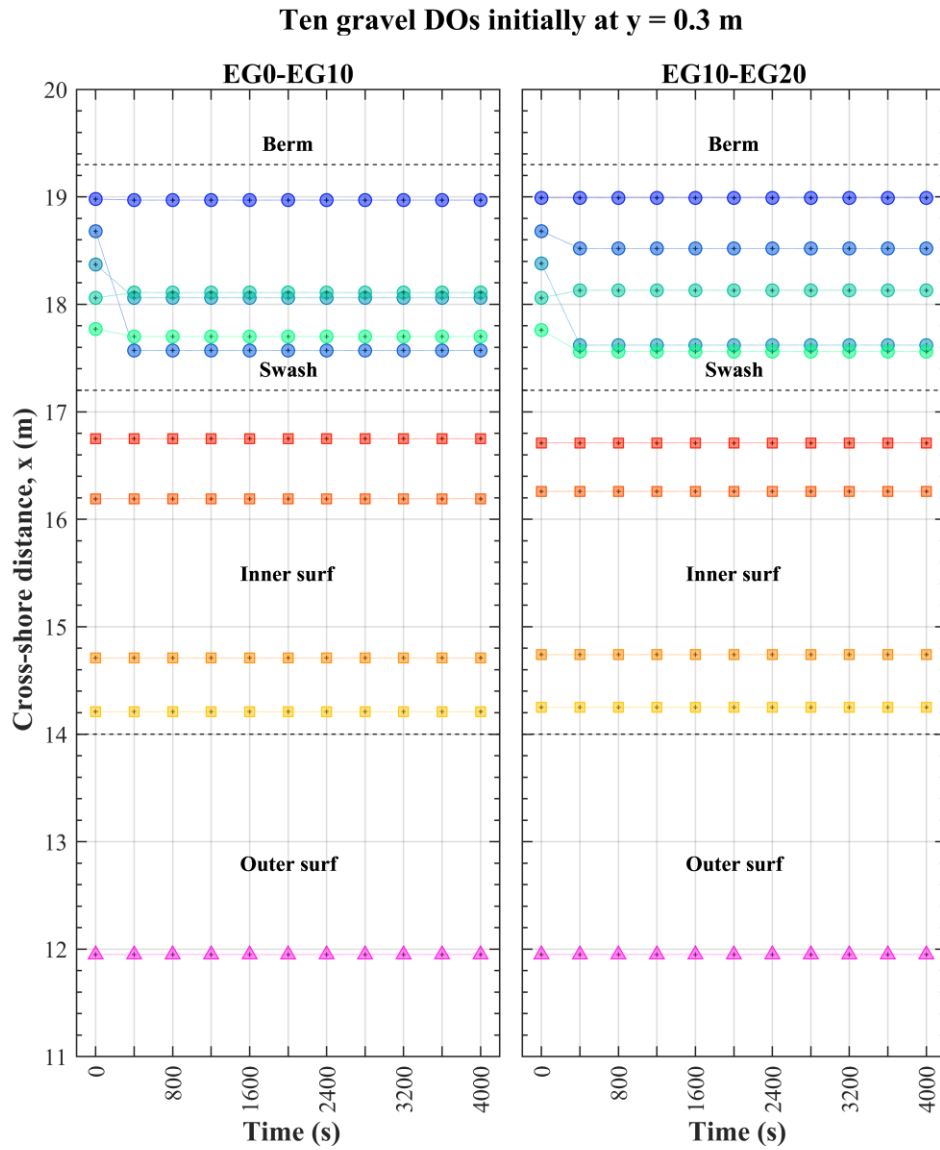


Figure 3.26 Temporal variations of cross-shore locations of 10 gravel DOs initially located at $y = 0.3$ m during 10 runs of EG0-EG10 and EG10-EG20 with DO resetting after EG10.

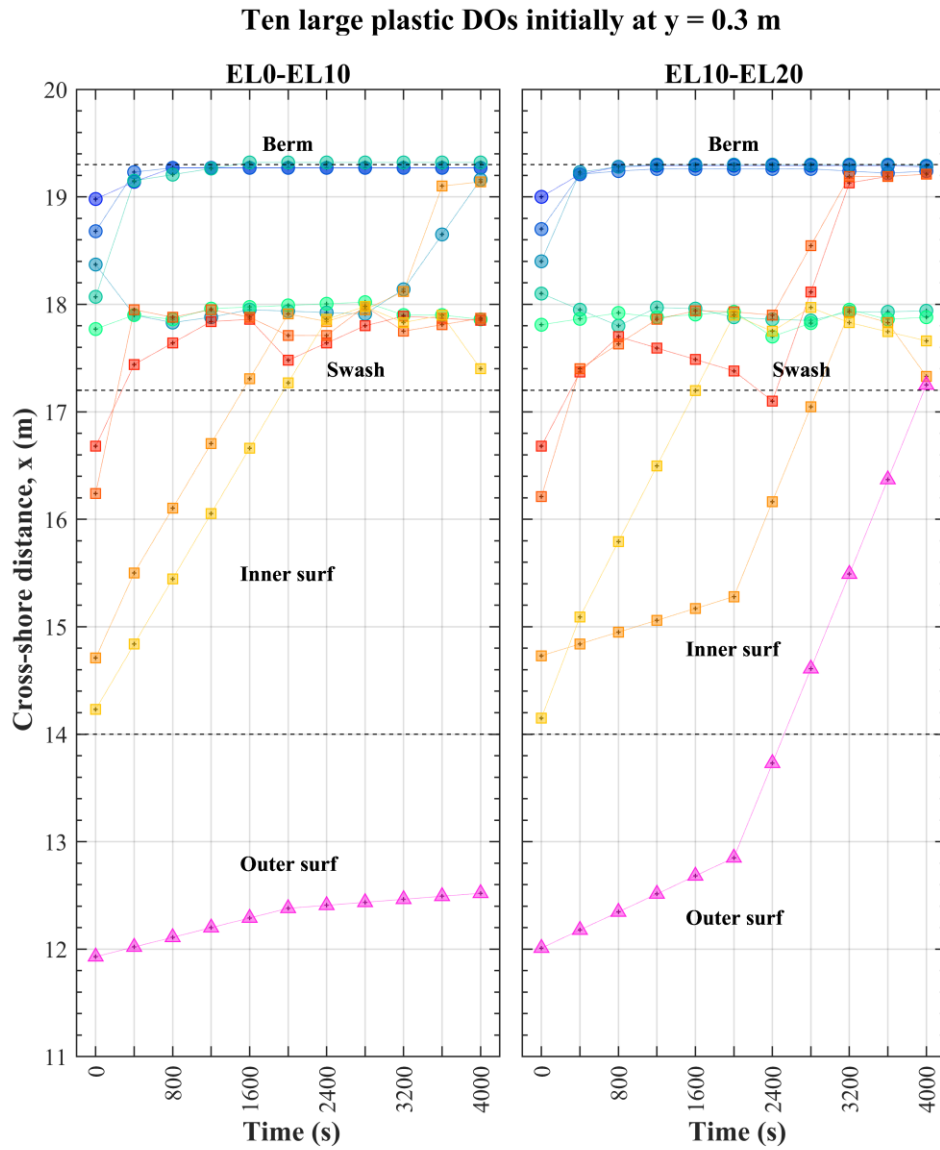


Figure 3.27 Temporal variations of cross-shore locations of 10 large plastics DOs initially located at $y = 0.3$ m during 10 runs of EL0-EL10 and EL10-EL20 with DO resetting after EL10.

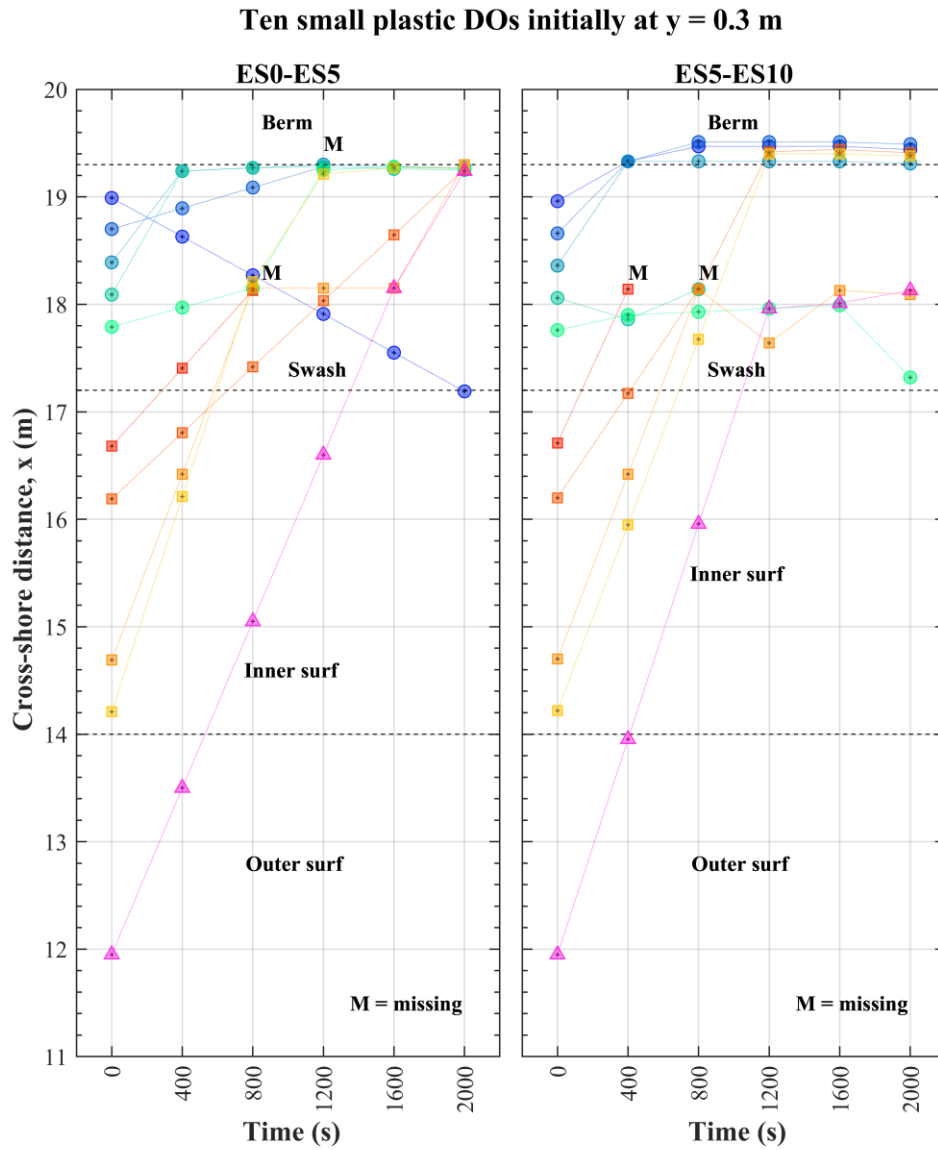


Figure 3.28 Temporal variations of cross-shore locations of 10 small plastics DOs initially located at $y = 0.3$ m during 5 runs of ES0-ES5 and ES5-ES10 with DO resetting after ES5. Each missing DO identified by the letter M.

Finally, Figure 3.29 shows the measured trajectories of the 10 G, L, and S DOs initially located at $y = 0.3$ m in the nourished foreshore tests. For the gravel DOs of NG0-NG20 (left column in Figure 3.29), 4 gravel DOs moved downward on the eroding foreshore and accumulated in the lower swash zone. The gravel DOs were more mobile on the eroding foreshore with the steeper initial slope than on the equilibrium profile in Figure 3.26. For the large plastics DOs of NL0-NL20 (middle column in Figure 3.29), the downward movement of the eroded sand on the foreshore may not have affected the onshore L DO movement. On the contrary, the steeper foreshore increased wave runup, resulting in the farther landward movement of the L DOs on the berm as depicted in Figure 3.29. For the small plastics DOs of NS0-NS10 (right column in Figure 3.29), the effect of the eroding steeper foreshore on the S DO movement was similar to that for the L DOs. It is noted that missing DOs were indicated in Figures 3.28 and 3.29.

Ten DOs initially at $y = 0.3$ m

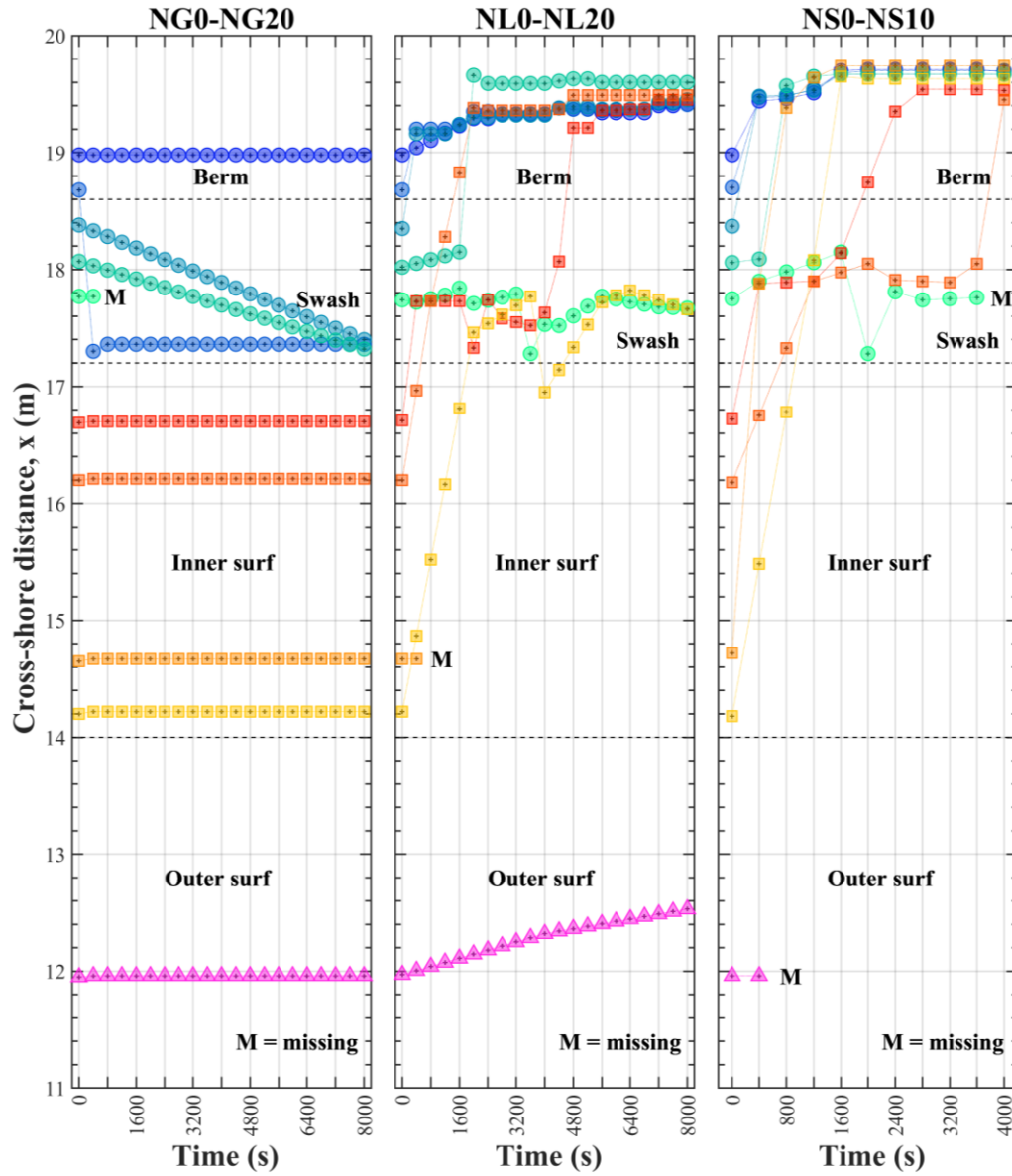


Figure 3.29 Temporal variations of cross-shore locations of 10 DOs initially located at $y = 0.3$ m during 20 runs of NG0-NG20, NL0-NL20 and 10 runs of NS0-NS10.

Chapter 4

Numerical Model

This chapter presents the main components of the time-averaged cross-shore model CSHORE (Kobayashi, 2016). The combined wave and current model based on time-averaged continuity, momentum, and wave energy equations are presented concisely along with the CSHORE probabilistic swash model on impermeable (fine sand) bottom. The sediment transport model for bed and suspended load coupled with the continuity equation of bottom sediment is summarized to explain basic sediment dynamics. Finally, tracking small discrete objects on a sand beach added in CSHORE is introduced.

4.1 Combined Wave and Current Model in Wet Zone

To develop a simple and robust model suitable for coastal engineering applications including coastal hydrodynamics and sediments, Kobayashi et al. (2008) proposed a time-averaged model to predict the cross-shore and longshore transport rates of bedload and suspended load under combined wave and current action. This study is limited to the case of alongshore uniformity and normally incident waves which essentially corresponds to the condition of the wave flume experiment. The time-dependent sediment transport model of Kobayashi and Johnson (2001) is physically appealing as it predicts intense but intermittent sand suspension under irregular breaking

waves (Kobayashi and Tega, 2002). The time-dependent model, however, requires considerable computation time and is not necessarily more accurate than the time-averaged model for the simulation of morphological changes. Figure 4.1 shows the cross-shore variation of hydrodynamics on the foreshore of a sand beach. The bottom is assumed impermeable and its elevation z_b is positive above the still water level S where the vertical coordinate z is positive upward and $z = 0$ at datum. The measured values of T_p , $\bar{\eta}$, and σ_η for each run are specified as input at the seaward boundary $x = 0$ outside the surf zone. The still water level was constant in this experiment and $S = 0$. The computation marches landward to predict the cross-shore variations of $\bar{\eta}$, and σ_η . The landward limit of the wet zone is the upper limit of the mean water level (MWL) at the cross-shore location x_r in Figure 4.1.

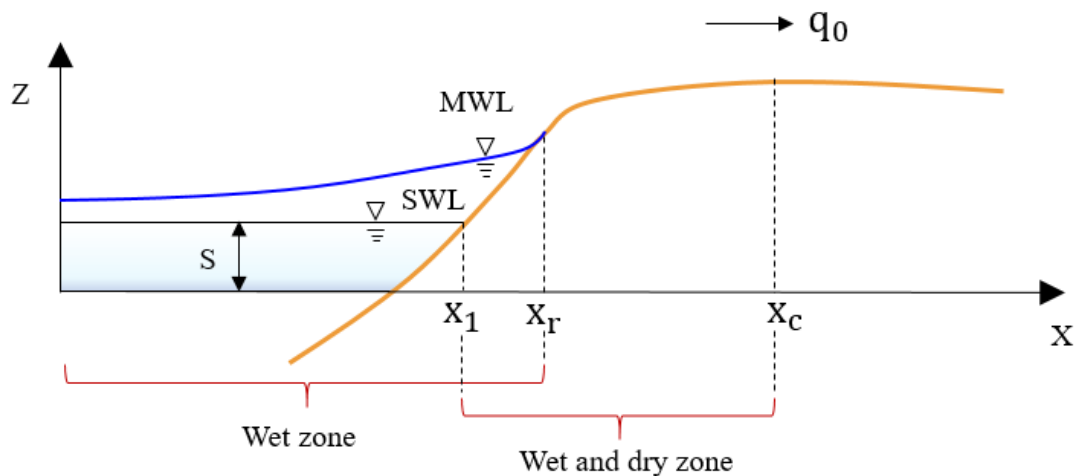


Figure 4.1 CSHORE definition sketch for cross-shore hydrodynamic variation from wet zone to wet and dry zone on a sand beach.

The hydrodynamic equations used in the wet zone of $x = 0$ to $x = x_r$ are presented concisely. For an impermeable bottom, the time-averaged continuity equation requires the time-averaged cross-shore volume flux q to be constant and equal to the wave overtopping rate q_0 on the berm in Figure 4.1. In this experiment of no wave overtopping, $q_0 = 0$. In the wet zone, the current velocity felt by waves is expressed as q/\bar{h} where $\bar{h} = (\bar{\eta} + S - z_b)$ with the overbar indicating time averaging. The representative wave period for irregular waves is assumed to be the spectral peak period T_p . The dispersion relation for linear waves for $q = 0$ is expressed as

$$\omega^2 = kg \tanh(k\bar{h}) \quad (4.1)$$

where ω = angular frequency; k = wave number; g = gravitational acceleration; and \bar{h} = mean water depth including wave setup $\bar{\eta}$. The angular frequency is given by $\omega = 2\pi/T_p$. The phase velocity C and the group velocity C_g are given by

$$C = \frac{\omega}{k} ; C_g = nC ; n = \frac{1}{2} \left[1 + \frac{2k\bar{h}}{\sinh(2k\bar{h})} \right] \quad (4.2)$$

The probability distribution of the depth-averaged cross-shore velocity U is assumed to be Gaussian. The mean and standard deviation of U denoted by \bar{U} and σ_U based on the linear progressive wave theory are expressed as

$$\sigma_U = C \frac{\sigma_\eta}{\bar{h}} ; \frac{g\sigma_\eta^2}{C} + \bar{h}\bar{U} = 0 \quad (4.3)$$

where $(g\sigma_\eta^2)/C$ is the onshore volume flux of linear waves propagating onshore. The negative time-averaged cross-shore velocity \bar{U} represents an offshore return flow.

The time-averaged cross-shore momentum equation is used to compute the cross-shore variation of the mean depth \bar{h}

$$\frac{d}{dx}(S_{xx}) = -\rho g \bar{h} \frac{d\bar{\eta}}{dx} - \tau_b \quad (4.4)$$

with

$$S_{xx} = E \left(2n - \frac{1}{2} \right); E = \rho g \sigma_\eta^2; n = \frac{C_g}{C}; \tau_b = \frac{1}{2} \rho f_b \sigma_U^2 G_2 \quad (4.5)$$

where S_{xx} = cross-shore radiation stress; E = specific wave energy with the root-mean-square wave height defined as $H_{rms} = \sqrt{8} \sigma_\eta$; ρ = water density; τ_b = time-averaged bottom stress; f_b = bottom friction factor; G_2 = analytical function of \bar{U}/σ_U given by Kobayashi et al. (2007). The computed results are not sensitive for f_b of the order of 0.01 and use is made of $f_b = 0.015$ based on Kobayashi et al. (2008) who compared the values of f_b for the time-dependent and time-averaged models.

To predict the cross-shore variation of σ_η , the wave energy equation is used

$$\frac{dF_x}{dx} = -D_B - D_f \quad (4.6)$$

with

$$F_x = \rho g \sigma_\eta^2 C_g ; D_B = \frac{\rho g a_B Q H_B^2}{4T} ; D_f = \frac{1}{2} \rho f_b \sigma_U^3 G_3 \quad (4.7)$$

where F_x = cross-shore energy flux based on linear progressive wave theory; D_B and D_f = energy dissipation rates due to wave breaking and bottom friction, respectively; a_B = empirical parameter accounting for the bottom slope (Kobayashi et al., 2007); Q = fraction of irregular breaking waves based on the formula by Battjes and Stive (1985); H_B = breaker height; and G_3 = analytical function of \bar{U}/σ_U based on the Gaussian distribution of U (Kobayashi et al., 2007).

The landward marching computation using Equations (4.1)-(4.7) is continued as long as \bar{h} and σ_η are positive. The computation domain is terminated at the landward end of the wet zone denoted as x_r . These equations based on linear Gaussian wave theory remain valid in the wet zone. For the wet and dry zone, a probabilistic model is developed accordingly.

4.2 Hydrodynamic Model for Impermeable Wet and Dry Zone

A time-averaged probabilistic model was developed by Kobayashi et al. (2010b) to predict the cross-shore variations of the wet probability, the mean and standard deviation of the water depth, and cross-shore velocity in the swash zone. Such an approach is very efficient computationally and can be calibrated using a large number of data sets. For normally incident waves on an impermeable sand beach of alongshore uniformity, the time-averaged cross-shore continuity and momentum equations derived

from the nonlinear shallow-water wave equations (Kobayashi et al. 1989) are expressed as

$$\overline{hU} = q_0 \quad (4.8)$$

$$\frac{d}{dx} \left(\overline{hU^2} + \frac{g}{2} \overline{h^2} \right) = -gS_b \overline{h} - \frac{1}{2} f_b \overline{|U|U} \quad (4.9)$$

where h = instantaneous water depth; U = cross-shore velocity. q_0 = wave overtopping rate; g = gravitational acceleration; S_b = cross-shore bottom slope given by $S_b = \frac{\partial z_b}{\partial x}$; and f_b = bottom friction factor. The overbar indicates time averaging. The instantaneous water depth h at any given x is described probabilistically rather than in the time domain. Kobayashi et al. (1998) examined the probability distributions of the free surface elevations measured in the shoaling, surf and swash zones. The measured probability distributions were fitted to the exponential gamma distribution which becomes the Gaussian distribution and the exponential distribution when the wave skewness reaches zero offshore and two in the swash zone, respectively. The cross-shore model CSHORE in the wet zone has been simplified significantly using the Gaussian distribution. In the wet and dry (swash) zone, the assumption for the exponential distribution was made by Kobayashi et al. (2010b) to simplify the model.

The probability density function $f(h)$ of the exponential distribution is expressed as

$$f(h) = \frac{P_w^2}{h} \exp\left(-P_w \frac{h}{h}\right) \quad \text{for } h > 0 \quad (4.10)$$

with

$$P_w = \int_0^{\infty} f(h)dh \quad ; \quad \bar{h} = \int_0^{\infty} h f(h)dh \quad (4.11)$$

where P_w = wet probability for the water depth $h > 0$; and \bar{h} = mean water depth for the wet duration. The dry probability of $h = 0$ is then $(1-P_w)$. The mean water depth for the entire duration is $P_w\bar{h}$. The overbar in Equations (4.8) and (4.9) indicates time-averaging for the wet duration only. The free surface elevation $(\eta - \bar{\eta})$ above MWL is equal to $(h - \bar{h})$. The standard deviation of η and h are the same and given by

$$\frac{\sigma_{\eta}}{\bar{h}} = \left(\frac{2}{P_w} - 2 + P_w \right)^{0.5} \quad (4.12)$$

The cross-shore velocity U is assumed to depend on the depth h in the swash zone and expressed as

$$U = \alpha\sqrt{gh} + U_s \quad (4.13)$$

where α = positive constant; and U_s = steady velocity spatially varying with x . The steady velocity U_s accounts for offshore return flow on the foreshore slope. Holland et al. (1991) measured the bore speed and flow depth on a barrier island using video techniques and obtained $\alpha = 2$ where the celerity and fluid velocity of the bore are assumed to be approximately the same. The value of $\alpha = 1.6$ was calibrated by Figlus et al. (2012) for their wave overtopping tests. Using Equations (4.10) and (4.13), the mean \bar{U} and standard deviation σ_U of the cross-shore velocity U can be expressed as

$$\bar{U} = \frac{\sqrt{\pi}}{2} \alpha (P_w g \bar{h})^{0.5} + P_w U_s \quad (4.14)$$

$$\sigma_U^2 = \alpha^2 g \bar{h} - 2(\bar{U} - U_s)(\bar{U} - P_w U_s) + P_w (\bar{U} - U_s)^2 \quad (4.15)$$

Equation (4.13) was substituted into Equations (4.8) and (4.9) which were averaged for the wet duration using Equation (4.10). The continuity equation (4.8) yielded

$$\frac{3\sqrt{\pi}\alpha}{4} \bar{h} \left(\frac{g\bar{h}}{P_w} \right)^{0.5} + U_s \bar{h} = q_o \quad (4.16)$$

The cross-shore momentum equation (4.9) was expressed as

$$\frac{d}{dx} \left(B \frac{g\bar{h}^2}{P_w} + \frac{q_o^2}{\bar{h}} \right) = -g S_b \bar{h} - \frac{f_b}{2} \alpha^2 g \bar{h} G_b(r_s) \quad (4.17)$$

with

$$B = \left(2 - \frac{9\pi}{16} \right) \alpha^2 + 1 ; \quad r_s = \frac{3\sqrt{\pi}}{4} \frac{U_s \bar{h}}{q_o - U_s \bar{h}} \quad (4.18)$$

The function $G_b(r_s)$ in Equation (4.17) was given by Kobayashi et al. (2010b).

Equations (4.16) and (4.17) are used to predict the cross-shore variation of \bar{h} and U_s for known q_o where σ_η , \bar{U} and σ_U are computed using Equations (4.12), (4.14) and (4.15), respectively. The momentum equation (4.17) was integrated using the following empirical formula for the wet probability P_w (Kobayashi et al. 2010b).

$$P_w = \left[(1 + A_o) \left(\frac{\bar{h}_1}{\bar{h}} \right)^n - A_o \left(\frac{\bar{h}_1}{\bar{h}} \right)^3 \right]^{-1} ; A_o = \frac{q_o^2}{Bg\bar{h}_1^3} \quad \text{for } x \leq x_c \quad (4.19)$$

where \bar{h}_1 = mean water depth at the location of $P_w = 1$; n = empirical parameter for P_w ; A_o = parameter related to the wave overtopping rate q_o normalized by the depth \bar{h}_1 where water is present always. The transition point x_1 from the wet ($P_w = 1$ always) zone to the wet and dry ($P_w < 1$) zone was taken at $x_1 = x_{SWL}$ where x_{SWL} is the cross-shore location of the still water shoreline of an emerged slope (see Figure 4.1). Equation (4.19) was assumed on the seaward slope and crest in the region of $x \leq x_c$ where x_c = most landward location of the crest (maximum z_b). Equation (4.19) allowed the analytical integration of Equation (4.17) to reduce numerical difficulties in the zone of very small water depth.

Integration of Equation (4.17) using P_w from Equation (4.19) with $\bar{h} = \bar{h}_1$ at $x = x_1$ gave $\bar{h}(x)$ for $x_1 \leq x \leq x_c$

$$B_n(1 + A_o)\bar{h}_1 \left[\left(\frac{\bar{h}_1}{\bar{h}} \right)^{n-1} - 1 \right] = z_b(x) - z_b(x_1) + \frac{\alpha^2}{2} \int_{x_1}^x f_b G_b dx \quad (4.20)$$

where $B_n = \frac{B(2-n)}{(n-1)}$; and $z_b(x)$ = bottom elevation at the cross-shore location x . The mean water depth \bar{h} at given x is obtained by iteratively solving Equation (4.20). The formula for n was expressed as $n = 1.01 + 0.98[\tanh(A_o)]^{0.3}$ using the 107 tests of wave overtopping and overflow on a dike by Kobayashi et al. (2010b).

The wave overtopping and overflow rate q_o was predicted by imposing $U_s = 0$ in Equation (4.16) at the crest location x_c

$$q_o = \frac{3\sqrt{\pi}\alpha}{4} \bar{h}_c \left(\frac{g\bar{h}_c}{P_c} \right)^{0.5} \quad \text{at } x = x_c \quad (4.21)$$

where \bar{h}_c and P_c are the computed mean depth \bar{h} and wet probability P_w at x_c . If the landward marching computation does not reach the crest location, $q_o = 0$.

For assumed q_o , the landward marching computation of \bar{h} , σ_η , \bar{U} and σ_U is initiated using the wet model from the seaward boundary $x = 0$ to the landward limit located at $x = x_r$ where the computed \bar{h} or σ_η becomes negative or \bar{h} becomes less than 0.1 cm for an emerged crest. The landward marching computation is continued using the wet and dry model from the location of $x = x_1$ where $\bar{h} = \bar{h}_1$ in Equation (4.20) to the landward end of the computation domain or until the mean depth \bar{h} becomes less than 0.001 cm. In the wet and dry zone, the rate q_o is computed using Equation (4.21). The value of $q_o = 0$ is initially assumed and the landward computation is repeated until the difference between the computed and assumed values of q_o is less than 1%. This convergency is normally obtained after several iterations. The computed values of \bar{h} , σ_η , \bar{U} and σ_U in the overlapping zone $x_1 < x < x_r$ are then averaged to smooth the transition from the wet zone to the wet and dry zone. In this experiment, no wave overtopping occurred and $q_o = 0$. The landward marching computation did not reach the crest location and the computed q_o was zero as well.

4.3 Sediment Transport Model

In the following, the sediment transport formulas proposed by Kobayashi et al. (2008) for the wet zone are summarized and the modification for the wet and dry zone is explained. The probability P_b of sediment movement under the Gaussian velocity U in the wet zone is estimated using the critical Shields parameter ψ_c (Madsen and Grant 1976) which is taken as $\psi_c = 0.05$. The instantaneous bottom shear stress τ'_b is assumed to be given by $\tau'_b = 0.5\rho f_b U^2$. The initial movement of sediment occurs when the absolute value of the instantaneous bottom shear stress exceeds the critical shear stress with the critical Shields parameter of 0.05. The value of P_b computed from the seaward boundary ($x = 0$) outside the surf zone increases landward and fluctuates in the surf and swash zones as it is affected by the presence of a bar or a terrace that increases the local velocity. The probability P_s of sediment suspension is estimated assuming that sediment suspension occurs when the turbulent velocity associated with the instantaneous energy dissipation rate due to bottom friction exceeds the sediment fall velocity w_f . If $P_s > P_b$, use is made of $P_s = P_b$ to ensure that sediment suspension occurs only when sediment movement occurs.

The time-averaged bed load transport rate q_b is expressed as

$$q_b = bP_b G_s \sigma_U^3 / [g(s - 1)] \quad (4.22)$$

where b = empirical bed load parameter; G_s = empirical function of the bottom slope S_b with its upper limit 0.63 of the sand slope; and s = sediment specific gravity. The bed load parameter b (normally $b = 0.002$) was calibrated using available water tunnel and

large-scale wave flume tests on horizontal bottoms for which $G_s = 1$. This simple bed load formula is consistent with the sheet flow model for onshore bar migration by Trowbridge and Young (1989) and the energetics-based bed load formula for steady flow by Bagnold (1966) provided that the steady flow formula is applied in the time-averaged manner. The onshore bed load transport predicted by Equation (4.22) is consistent with the field observations of onshore ripple migration by Becker et al. (2007) and Masselink et al. (2007).

The wave energy dissipation rates D_B and D_f in the wave energy equation (4.6) are assumed to cause sediment suspension against the sediment fall velocity w_f . The time-averaged cross-shore suspended sediment transport rate q_s is expressed as

$$q_s = a_x \bar{U} V_s \quad (4.23)$$

with

$$a_x = [a + (S_b / \tan\phi)^{0.5}] \geq a \quad (4.24)$$

$$V_s = P_s V_{Bf} (1 + S_b^2)^{0.5} \quad (4.25)$$

$$V_{Bf} = \frac{e_B D_B + e_f D_f}{\rho g (s - 1) w_f} \quad (4.26)$$

where a = empirical suspended load parameter under the action of waves and wave-induced current; ϕ = angle of internal friction of the sediment with $\tan\phi = 0.63$ for sand (Bailard 1981). The parameter a (normally $a = 0.2$) accounts for the onshore suspended sediment transport due to the positive correlation between the time-varying cross-shore velocity and suspended sediment concentration. The effect of the cross-shore bottom slope on a_x was included by Kobayashi et al. (2009) to increase berm and dune erosion.

For $S_b \leq 0$, use is made of $a_x = a$. The cross-shore suspended sediment transport rate q_s is negative (offshore) due to negative return (undertow) current \bar{U} (offshore). V_s = suspended sediment volume per unit horizontal area; V_{Bf} = potential suspended sediment volume on a horizontal bottom when $P_s = 1$; e_B and e_f = suspension efficiencies (previously calibrated as $e_B = 0.005$ and $e_f = 0.01$) for the energy dissipation rates D_B and D_f due to wave breaking and bottom friction in Equation (4.6).

For the wet and dry (swash) zone, the sediment transport model for the wet zone is modified for normally incident waves (Kobayshi et al. 2010b) where U in the wet and dry zone is expressed as Equation (4.13) and the probability density function $f(h)$ of the instantaneous water depth h is assumed to be exponential as given by Equation (4.10). The initial movement of sediment particle occurs when the instantaneous bottom shear stress exceeds the critical shear stress with the critical Shields parameter $\psi_c = 0.05$. The probability P_b of sediment movement is then the same as the probability of $|U| > U_{cb}$ where $U_{cb} = [2g(s-1)d_{50}\psi_c f_b^{-1}]^{0.5}$ where s and d_{50} are the specific gravity and medium diameter of the sediment. Based on Equations (4.11) and (4.13), P_b can be expressed as

$$P_b = P_w \quad \text{for } U_s > U_{cb} \quad (4.27)$$

$$P_b = P_w \exp \left[-\frac{P_w(U_{cb} - U_s)^2}{\alpha^2 g \bar{h}} \right] \quad \text{for } |U_s| \leq U_{cb} \quad (4.28)$$

$$P_b = P_w \left\{ 1 - \exp \left[-\frac{P_w(U_{cb} + U_s)^2}{\alpha^2 g \bar{h}} \right] + \exp \left[-\frac{P_w(U_{cb} - U_s)^2}{\alpha^2 g \bar{h}} \right] \right\}$$

$$\text{for } -U_s > U_{cb} \quad (4.29)$$

where the upper limit of P_b is the wet probability P_w because no sediment movement occurs during the dry duration. For the probability P_s , sediment suspension occurs when the instantaneous turbulent velocity estimated as $(f_b/2)^{1/3} |U|$ exceeds the sediment fall velocity w_f . The probability P_s of sediment suspension is then the same as the probability of $|U| > U_{cs}$ where $U_{cs} = w_f (2/f_b)^{1/3}$. The probability P_s is then given by Equations (4.27)-(4.29) with U_{cb} replaced by U_{cs} .

The bed load transport rate q_b in the wet and dry zone is estimated using Equation (4.22) where the empirical bed load parameter b is chosen in such a way that the values of q_b computed for the wet zone and the wet and dry zone are the same at the still water shoreline located at $x = x_{SWL}$. The suspended sediment transport rate q_s in the wet and dry zone is estimated using Equation (4.23). The suspended sediment volume V_{Bf} in the wet and dry zone is assumed constant and chosen to obtain the same suspended sediment volume V_s at $x = x_{SWL}$ as that of the wet zone. The suspended sediment volume V_s per unit horizontal area is assumed to be proportional to the probability P_s of sediment suspension which decreases landward.

The cross-shore sediment transport rates q_s and q_b computed for the wet zone and the wet and dry zone are averaged in the overlapping zone of $x_{SWL} < x < x_r$. For normally incident waves on impermeable beaches of alongshore uniformity, the beach profile change is computed using the continuity equation of bottom sediment

$$(1 - n_p) \frac{\partial z_b}{\partial t} + \frac{\partial}{\partial x} (q_s + q_b) = 0 \quad (4.30)$$

where n_p = porosity of the bottom sediment ($n_p = 0.4$ in this experiment); t = slow morphological time for the bottom elevation change z_b . Equation (4.30) is solved using an explicit Lax-Wendroff numerical scheme (e.g., Nairn and Southgate 1993) to obtain the bottom elevation at the next time level. This computation is started from the initial bottom profile and repeated until the end of the profile evolution test. The computation time is of the order of 10^{-3} of the test duration.

4.4 Time-averaged Model for Tracking Small Discrete Object

A numerical model is required to generalize the findings of the six tests in the wave flume which facilitated tracking small discrete objects. The cross-shore model CSHORE (Kobayashi 2016) was extended to predict the displacements of a finite number of small discrete objects on a sand beach. Sparse and small objects are assumed transparent with no effect on hydrodynamics and sand transport. The wave transformation and beach profile evolution were computed using the main components of CSHORE: a combined wave and current model (section 4.1) based on time-averaged continuity, cross-shore momentum, and wave energy equations; a sediment transport model (section 4.3) for suspended load and bed load coupled with the continuity equation of bottom sediment; and a probabilistic swash model (section 4.2) on an impermeable sand beach. The CSHORE input parameters were taken as representative values used by Kobayashi et al. (2008) for simulating equilibrium beach profiles and Kobayashi et al. (2009) for simulating berm erosion.

The trajectory of an individual object is normally predicted using a dynamic model based on the equation of motion for a solid object. For example, Kobayashi and Otta (1987) computed the movement of individual stone units on the armor layer of a coastal structure. The time-dependent wave motions on the structure was computed using the finite-amplitude shallow-water equations. The computation was limited to 7 regular waves. Therefore, a new time-averaged model is proposed to predict the displacement of a small discrete object averaged over a number of waves. This time-averaged Lagrangian model is compared with the measured trajectories of the G, L, and S DOs in Chapter 3. The experiment in this study was limited to the case of alongshore uniformity and normally incident waves.

The time-averaged cross-shore location X_i of i -th DO, with $i = 1, 2, \dots, I$ and I = number of DOs, is assumed to be given by

$$\frac{dX_i}{dt} = P_b C_b \sigma_U + P_s C_s \bar{U} \quad \text{at } x = X_i(t) \quad (4.31)$$

where t = time associated with the net (time-averaged) DO movement; P_b = probability of DO movement as bed load; C_b = positive bed load parameter; σ_U = standard deviation of depth-averaged cross-shore velocity; P_s = probability of DO suspension; C_s = positive suspended load parameter; and \bar{U} = depth-averaged cross-shore current. Equation (4.31) is solved iteratively using an implicit finite-difference method where P_b , σ_U , P_s , and \bar{U} are computed at the DO location $X_i(t)$ varying with time t .

Equation (4.31) expresses the cross-shore DO velocity as the sum of the DO velocities inferred from the sediment formulas of bed load and suspended load. For the

case of $P_b = 1$, $C_b\sigma_U$ is the onshore bed load velocity where the velocity standard deviation σ_U is positive. For the case of $P_s = 1$, $C_s\bar{U}$ is the offshore suspended load velocity where the return current \bar{U} is negative. The DO parameter C_s is assumed to be similar to the suspended load parameter a in Equation (4.24), and $C_s = 0.2$ is used in the following computations. The DO bed load parameter C_b is assumed as $C_b = 0.1C_s$ crudely. This assumption might yield zero DO velocity in Equation (4.31) for the case of $P_b = P_s$ and if the order of magnitude of $(-\bar{U})/\sigma_U$ is 0.1. The sensitivity of the computed DO trajectories for $(C_b/C_s) = 0.1-0.2$ is presented in the next section. In addition, the trajectories of hypothetical sand DOs in the equilibrium profile tests are computed to examine the degree of net sand movement on the equilibrium sand beach in this experiment.

The DO bed load probability P_b is estimated using the equation for the probability of sediment movement (section 4.3) where the sediment diameter and density are replaced by the DO diameter and density. The sediment movement is assumed to occur when the Shields parameter exceeds 0.05. For the DO movement on the sand surface, the stability number used for the stone movement (Kobayashi et al. 2010a) has been found to be more promising. The DO movement is assumed to occur when the critical stability number N_c of the DO movement initiation exceeds 0.7. On the other hand, the DO suspension probability P_s is estimated using the equation for the probability of sediment suspension where the sediment fall velocity is replaced by the DO fall velocity. Table 2.2 lists the diameter, density, and fall velocity of the gravel,

large and small plastics, and sand used to estimate the values of P_b and P_s for each DO. It is noted that Equation (4.31) assumes exposed DO on the sand surface. This assumption was appropriate for the large and small plastics. The effect of local scour around the gravel DO on the DO movement is not accounted for in Equation (4.31).

Chapter 5

Comparison with Data

The small-scale laboratory tests were conducted to measure the trajectories of 20 small discrete objects (gravel and microplastics) in the surf and swash zones on an equilibrium beach and a nourished foreshore beach with erosion and accretion in the swash zone. In this chapter, the cross-shore model CSHORE coupled with the time-averaged model for tracking small discrete objects is compared with the six tests consisting of 100 runs with each run lasting 400 s.

5.1 Cross-shore Wave Transformation

Figures 5.1-5.6 depict the comparison between the computed and measured cross-shore variations of the mean and standard deviation of the free surface elevation η and horizontal velocity U during EG1-EG20, EL1-EL20, ES1-ES10, NG1-NG20, NL1-NL20, and NS1-NS10, respectively. The measured incident wave height H_{mo} and period T_p are specified as input at the seaward boundary ($x = 0$) of the CSHORE computation. The computed and measured values for each of the six tests are plotted together to indicate the degree of overall agreement. The breaker ratio parameter γ involved in the energy dissipation rate D_B in Equation (4.7) is normally taken as 0.6 or 0.7. The increase of γ implies that waves breaking shifts slightly landward. The calibrated value of $\gamma =$

0.7 produced slightly better agreements for $\bar{\eta}$, σ_η and \bar{U} but underpredicted σ_U in the fourth panel of each figure. The comparisons of \bar{U} and σ_U are not rigorous because the horizontal velocity measured at an elevation above the local bed of one-third of the local depth was not the same as the computed depth-averaged velocity. The differences between the measured and computed values of $\bar{\eta}$, σ_η , \bar{U} , and σ_U were within about 20% for each of the six tests.

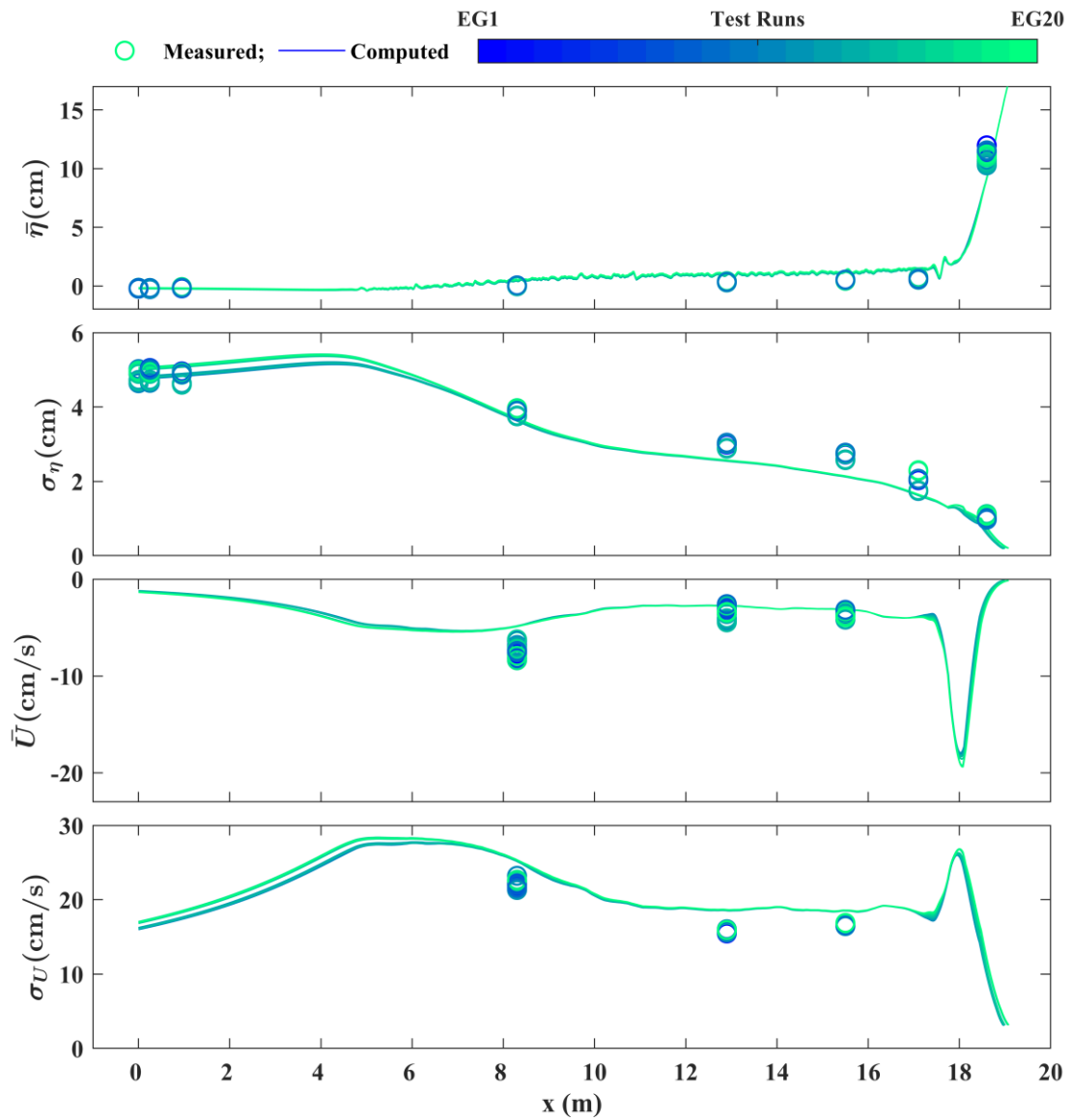


Figure 5.1 Measured and computed cross-shore variations of mean and standard deviation of free surface elevation η and horizontal velocity U for 20 runs during EG1-EG20.

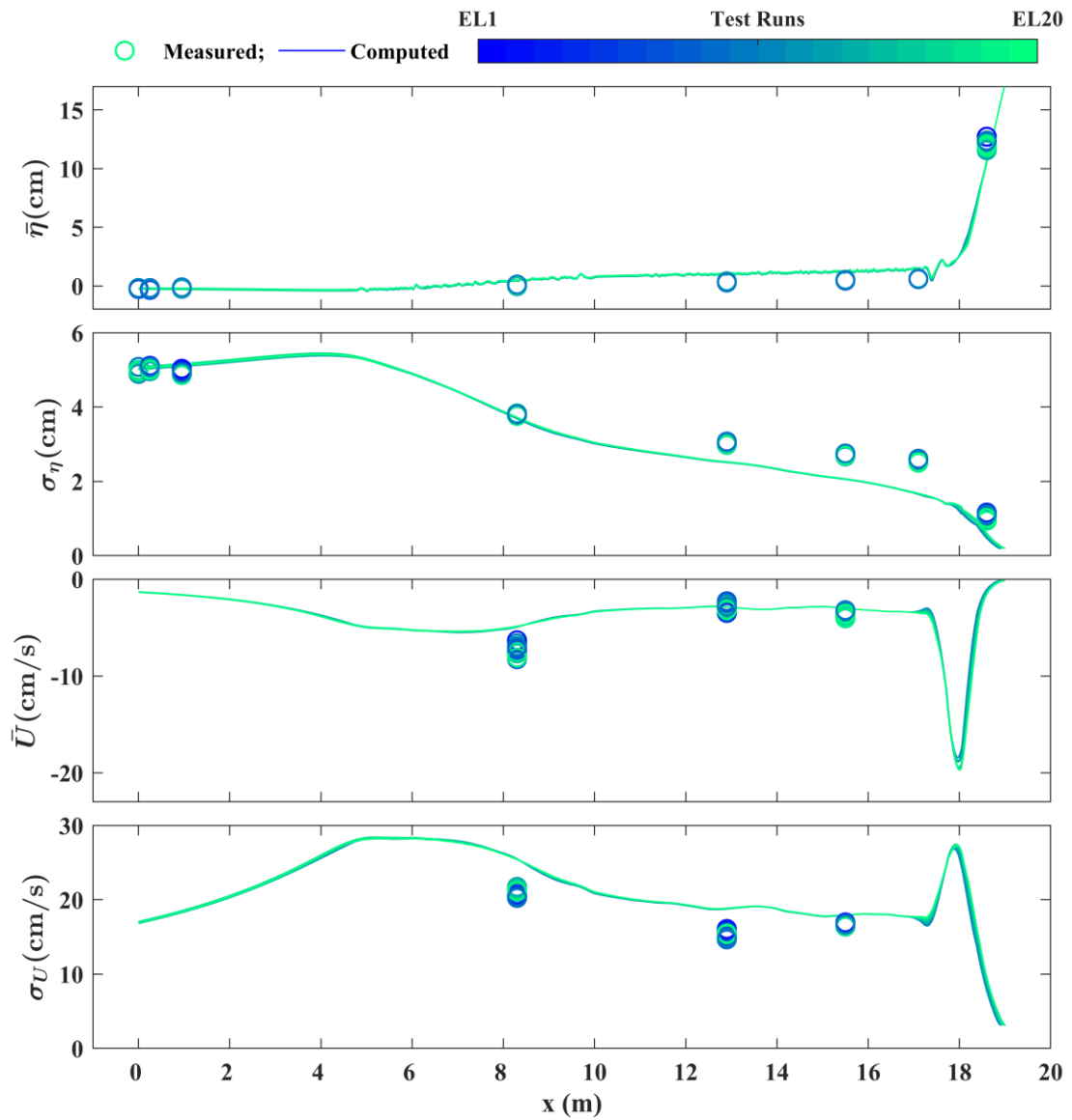


Figure 5.2 Measured and computed cross-shore variations of mean and standard deviation of free surface elevation η and horizontal velocity U for 20 runs during EL1-EL20.

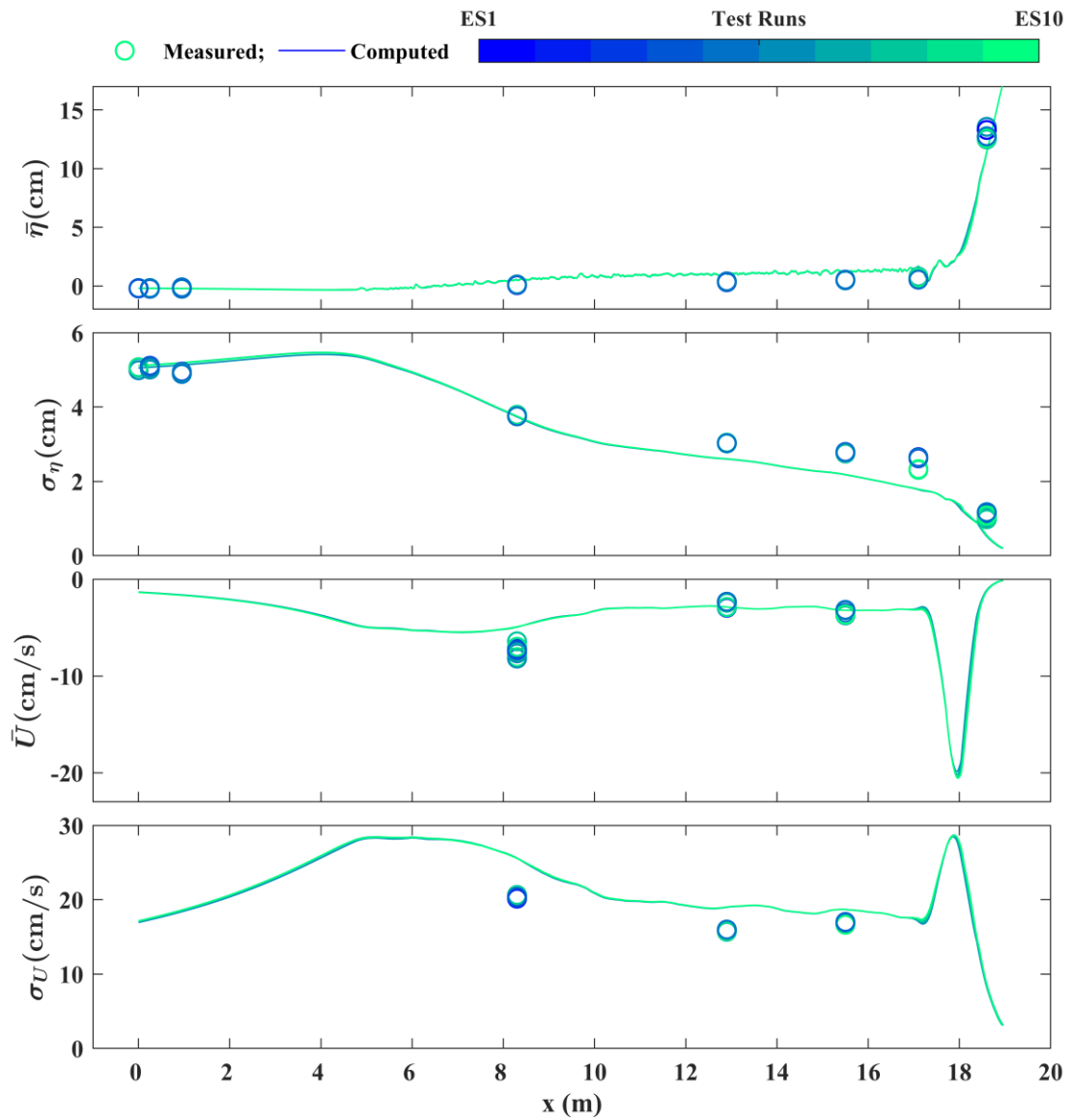


Figure 5.3 Measured and computed cross-shore variations of mean and standard deviation of free surface elevation η and horizontal velocity U for 10 runs during ES1-ES10.

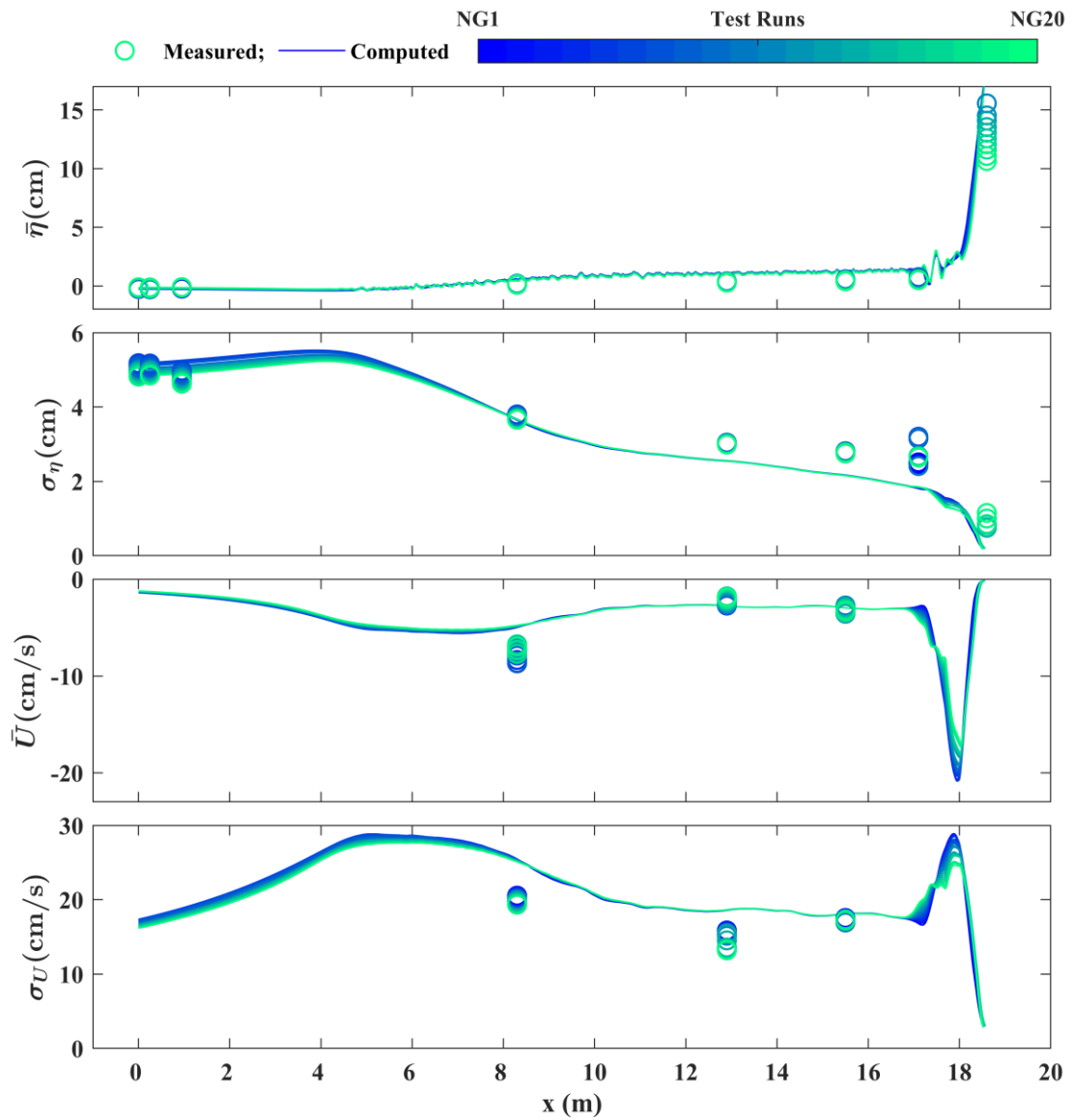


Figure 5.4 Measured and computed cross-shore variations of mean and standard deviation of free surface elevation η and horizontal velocity U for 20 runs during NG1-NG20.

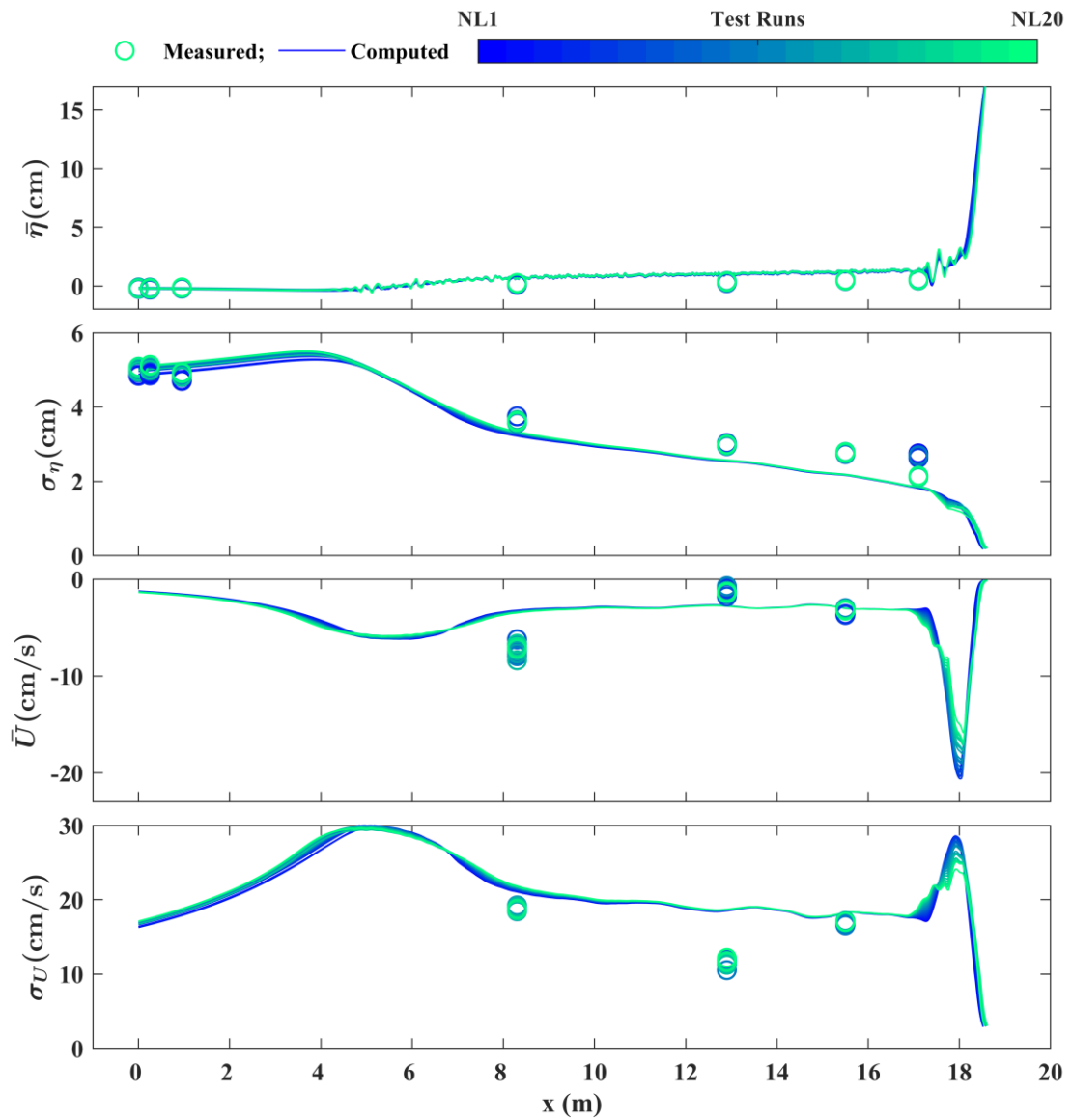


Figure 5.5 Measured and computed cross-shore variations of mean and standard deviation of free surface elevation η and horizontal velocity U for 20 runs during NL1-NL20 (WG8 was not functional in this test).

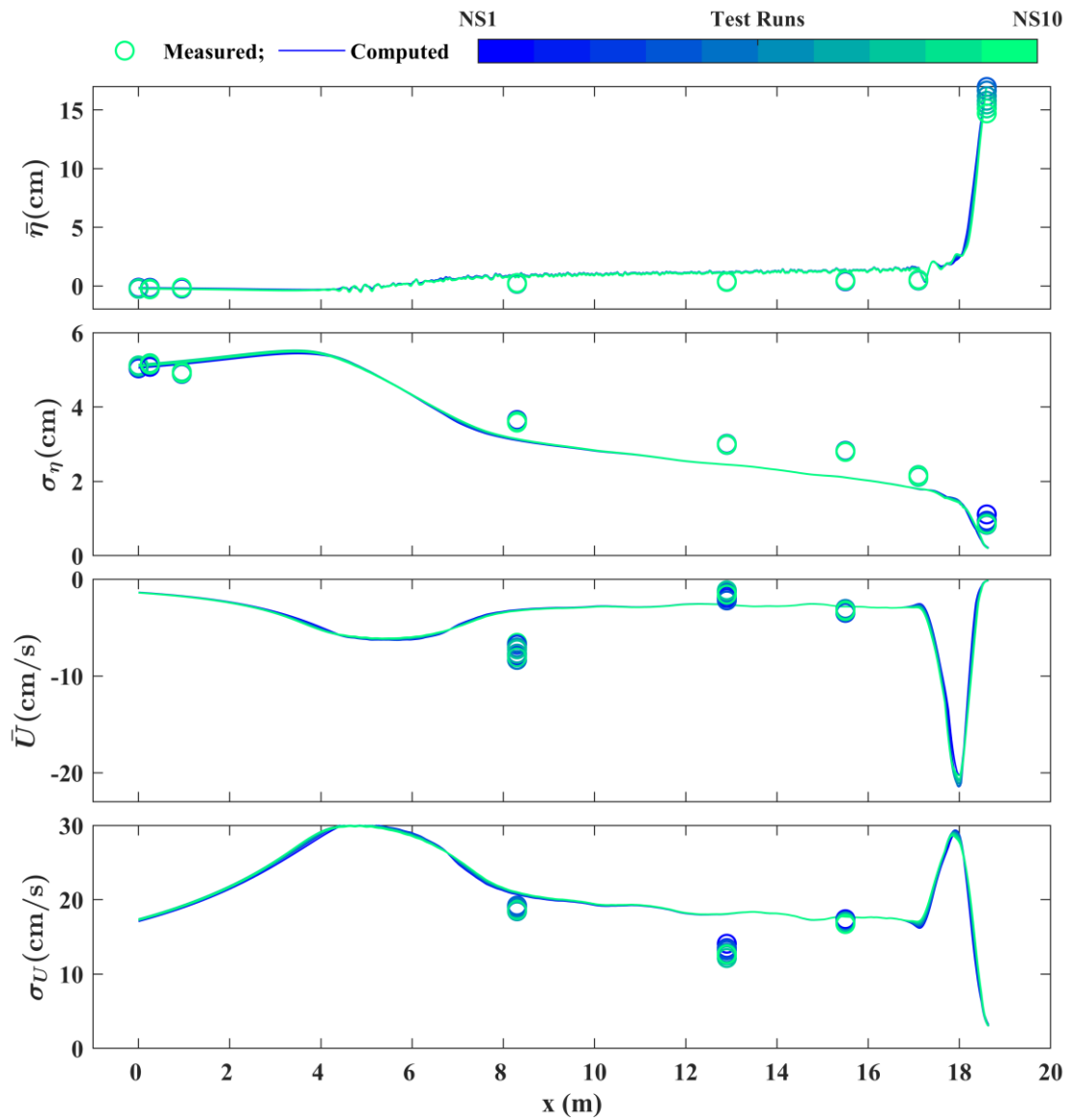


Figure 5.6 Measured and computed cross-shore variations of mean and standard deviation of free surface elevation η and horizontal velocity U for 10 runs during NS1-NS10.

5.2 Beach Profile Evolution

Figures 5.7-5.12 compare the measured and computed profiles for each of the six tests. The initial equilibrium profile of each test is specified as input to compute the profile evolution during EG1-EG10, EL1-EL10, and ES1-ES5 in Figures 5.7-5.9. CSHORE generally reproduced the equilibrium profile in a reasonable agreement with the measured profiles except for the lower swash zone of wave rundown. For the nourished profile test, the initial profile used as input for CSHORE included the nourished foreshore. The computed profiles of NG10, NL10, and NS10 in Figures 5.10-5.12 exhibited erosion above the SWL and deposition in the lower swash zone as observed in the corresponding measured profiles. However, the erosion at the seaward edge of the berm was not predicted probably because of the underprediction of wave uprush and downrush on the upper foreshore. CSHORE could not reproduce the upper foreshore erosion in the N test series. The swash model in CSHORE was not calibrated because it was satisfactory for the E test series. This difference between the E and N test series is used to assess the sensitivity of the profile prediction error on the prediction of the DO displacement using Equation (4.31) with $C_s = 0.2$ and $C_b = 0.02$.

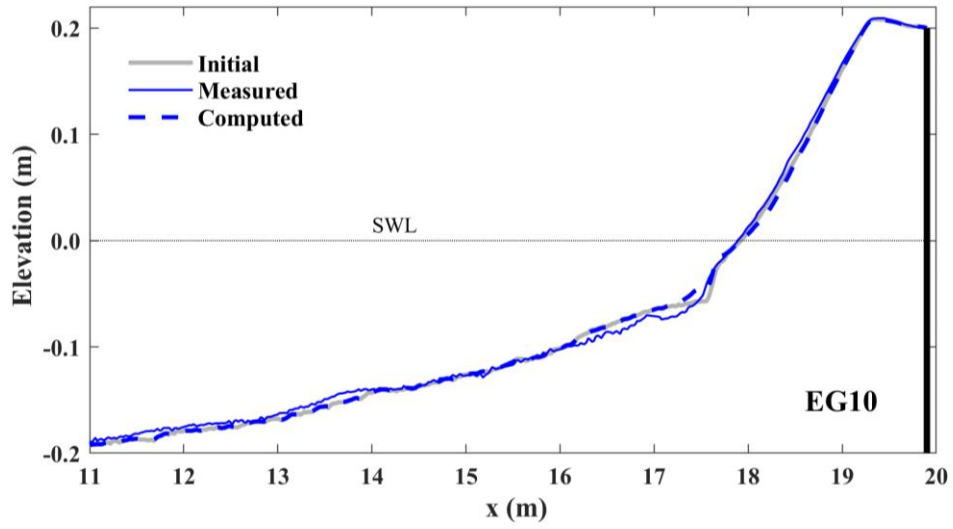


Figure 5.7 Measured and computed beach profiles for equilibrium profile test EG10

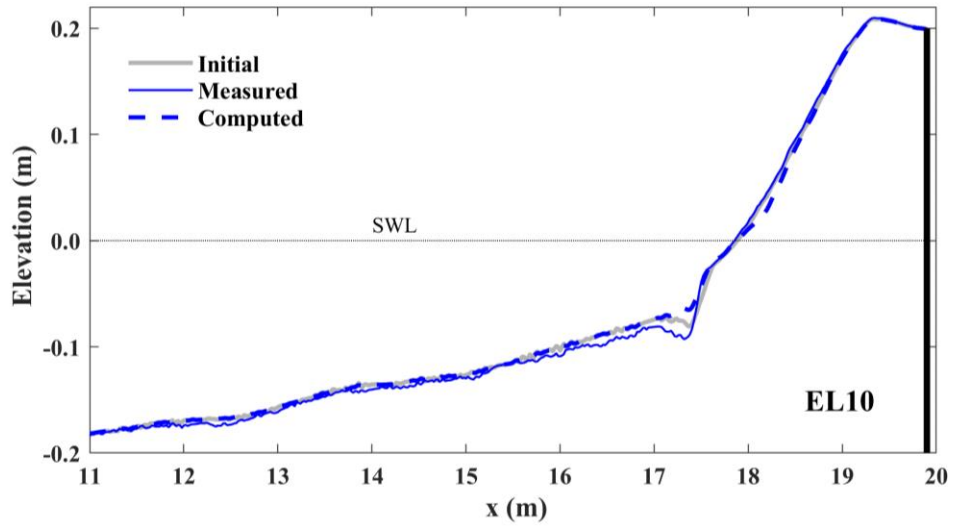


Figure 5.8 Measured and computed beach profiles for equilibrium profile test EL10

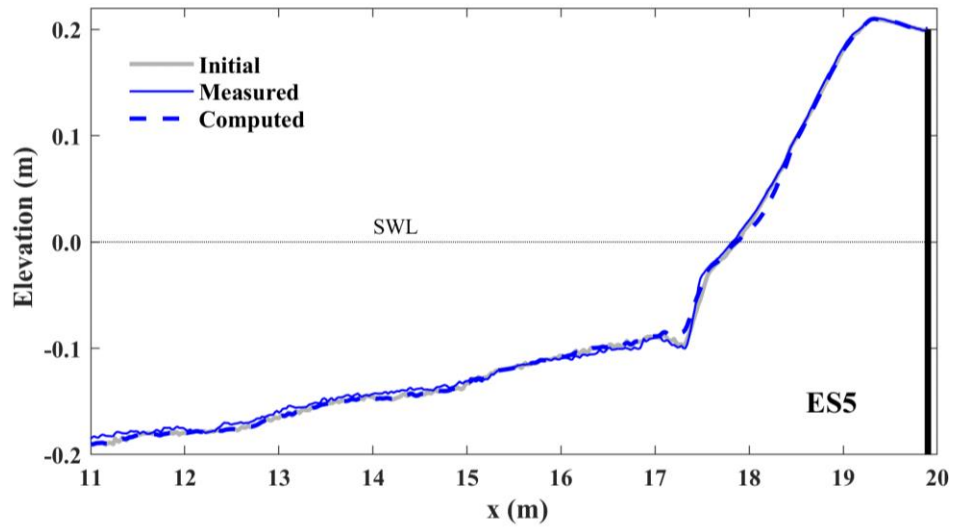


Figure 5.9 Measured and computed beach profiles for equilibrium profile test ES5

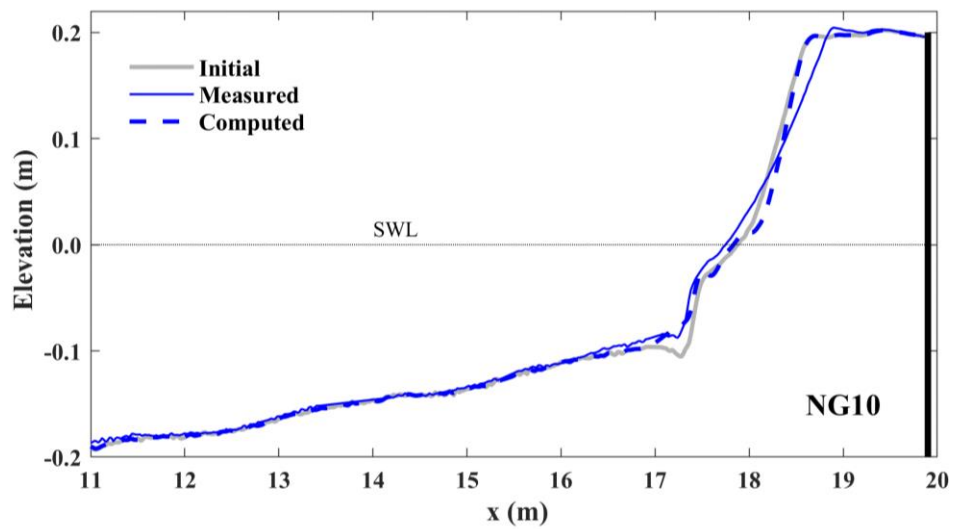


Figure 5.10 Measured and computed beach profiles for nourished foreshore profile test NG10

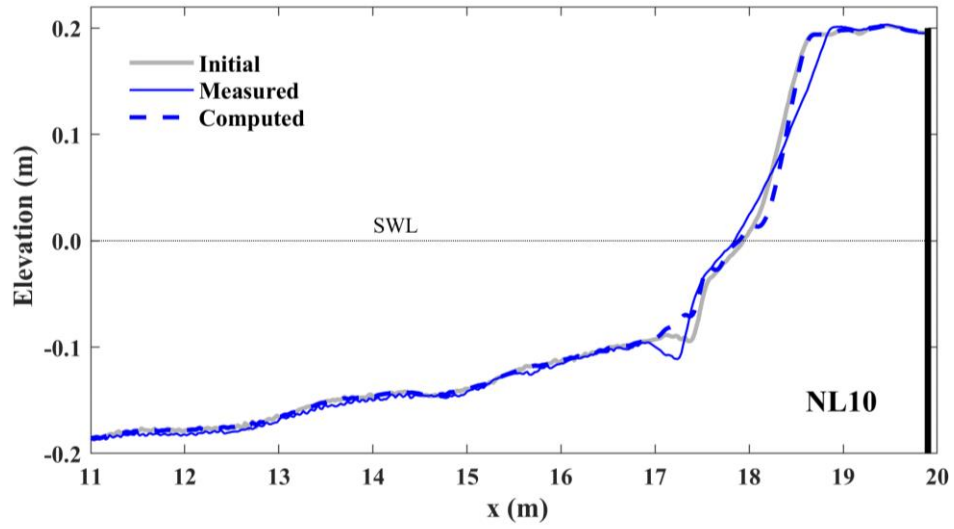


Figure 5.11 Measured and computed beach profiles for nourished foreshore profile test NL10

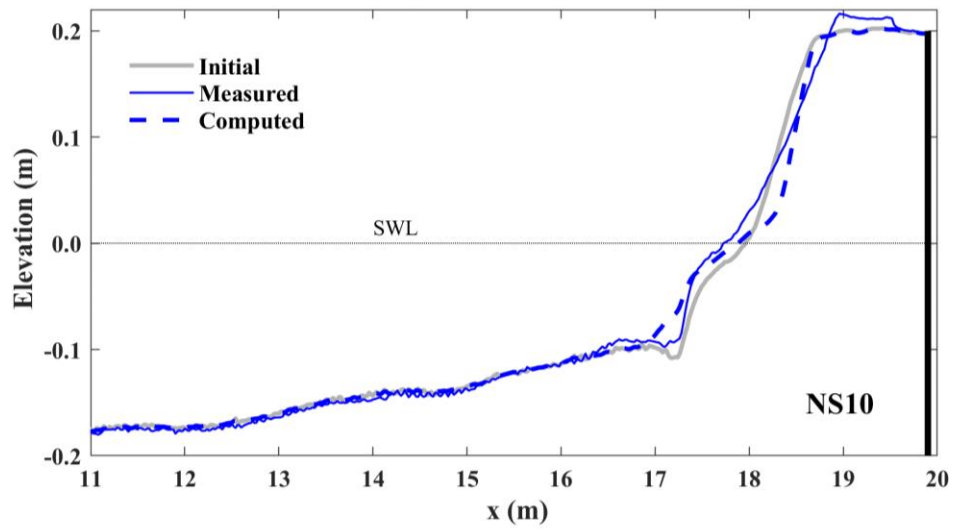


Figure 5.12 Measured and computed beach profiles for nourished foreshore profile test NS10

5.3 Temporal Variation of Cross-shore Location of Discrete Object

Due to the alongshore uniformity assumption, CSHORE predicts identical results for the computed trajectories of 10 DOs at $y = -0.3$ m and 10 DOs at $y = 0.3$ m. Figure 5.13 shows the computed temporal variations of the cross-shore locations of 10 DOs during EG0-EG10 (left), EL0-EL10 (middle), and ES0-ES5 (right) in the same format as in Figures 3.26, 3.27, and 3.28. The gravel (G) DO movement is predicted to occur in the swash zone as in Figure 3.26. However, the predicted DO movement direction is onshore as opposed to the measured offshore direction. The large (L) plastics DOs are computed to move onshore like those shown in Figure 3.27 for the EL test. The computed DOs at $x = 18.7$ and 19.0 are immobile unlike the measured DOs at the same locations which were transported up to the seaward edge of the berm. The small (S) plastics DOs are computed to move onshore in the outer and inner surf zones like those in Figure 3.28 for the ES test. However, the computed onshore DO movement stops in the lower swash zone and cannot reproduce the onshore DO movement in the upper swash zone. Table 3.35 compares the measured and computed numbers of DOs found in the outer surf, inner surf, swash, and berm zones at the end of each E test. The computed numbers indicated in Figure 5.13 are doubled and listed in Table 3.35. CSHORE predicts the gross patterns of the DO movement but cannot predict DO deposition on the berm.

The degree of the DO movement computed using Equation (4.31) depends on the DO probabilities of P_b and P_s where the return current \bar{U} and the oscillatory wave

velocity standard deviation σ_U were similar in the six tests in Figures 5.1-5.6. The cross-shore variations of P_b and P_s are computed for the specified DO whose characteristics are listed in Table 2.2. Figure 5.14 shows the computed cross-shore variations of the DO bed load probability P_b and the DO suspension probability P_s for EG10, EL10, and ES5 as well as for hypothetical ES5 (sand) where the small (S) plastics DOs are replaced by the sand particles in the wave flume during the computation of ES0-ES5 starting from the initial profile of ES0. The computed P_b and P_s during EG0-EG10, EL0-EL10, and ES0-ES5 varied little during the 10 or 5 runs and are represented by the values of P_b and P_s during the last run in Figure 5.14 for $x = 11-20$ m.

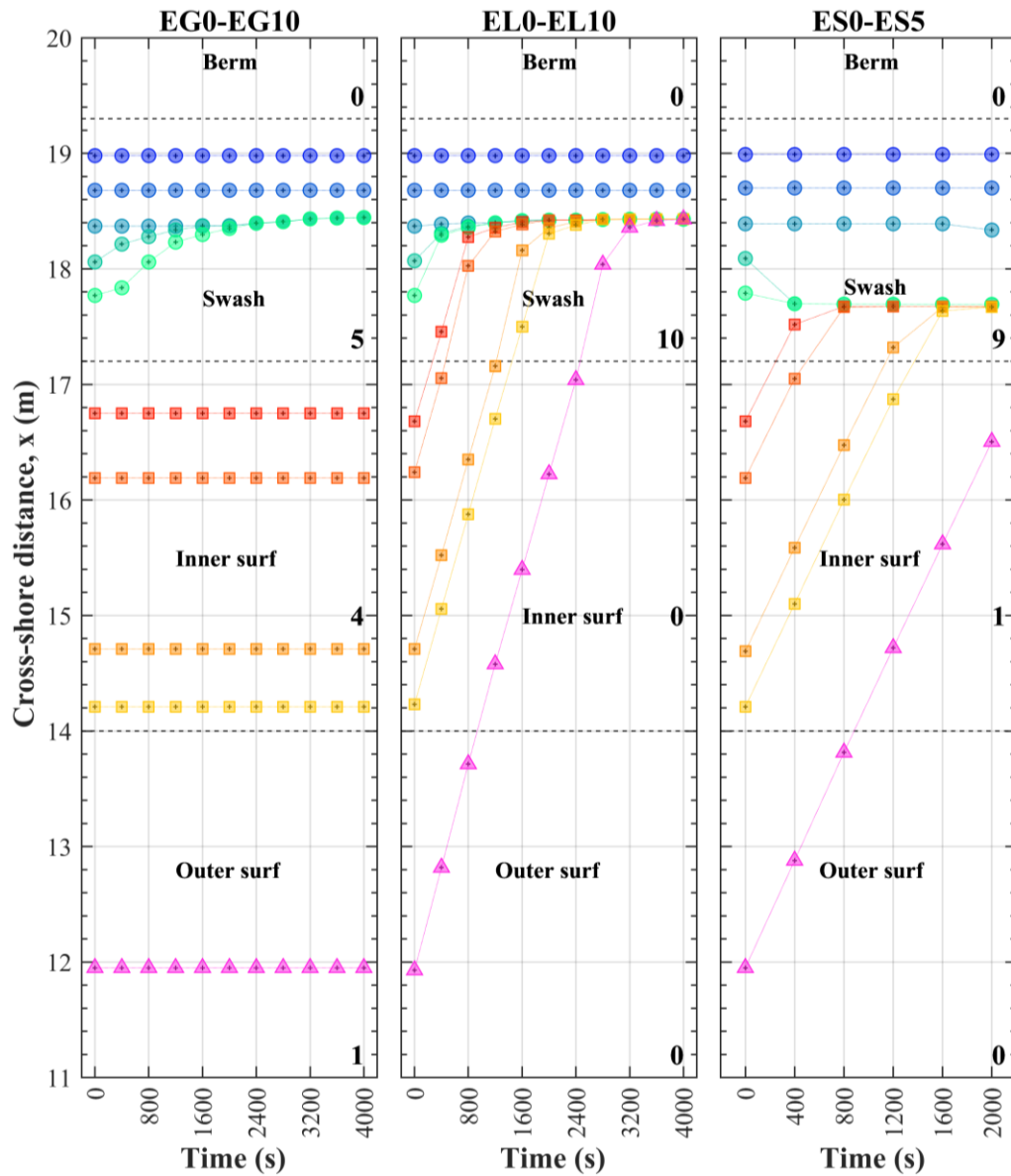


Figure 5.13 Computed temporal variations of cross-shore locations of 10 DOs during EG0-EG10 (gravel), EL0-EL10 (large plastics), and ES0-ES5 (small plastics).

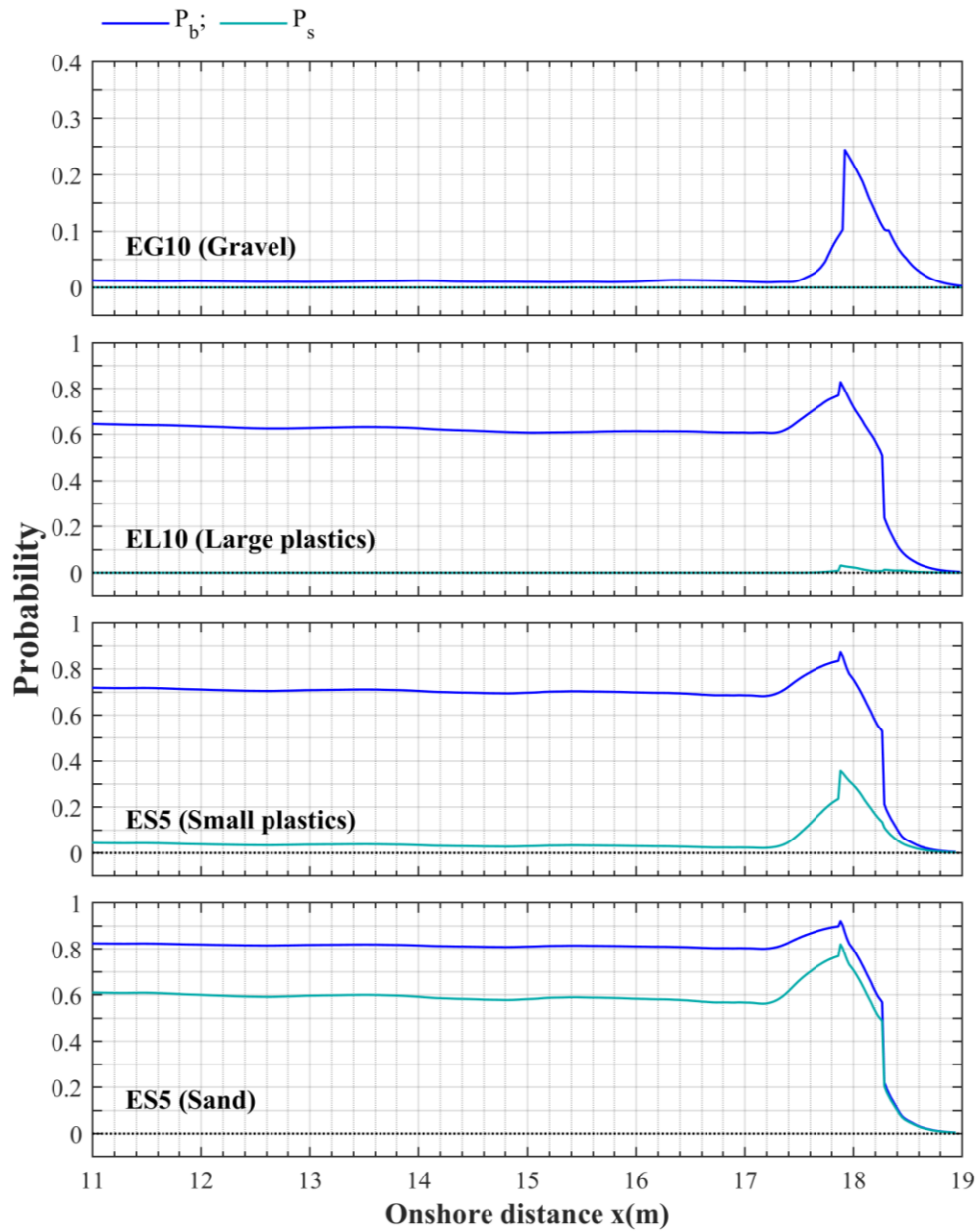


Figure 5.14 Computed cross-shore variations of DO bed load movement probability P_b and DO suspension probability P_s during EG10, EL10, and ES5 as well as for hypothetical ES5 (sand).

The gravel DO bed load probability P_b is negligible except in the swash zone. The gravel DO suspension probability is essentially zero and Equation (4.31) predicts onshore gravel DO movement. The bottom slope effect on bed load included in the bed load formula of Equation (4.22) might produce offshore gravel transport on a steep slope but is not included in Equation (4.31) for simplicity. For the large (L) plastics DOs, the bed load probability P_b is as large as 0.8 but the suspension probability P_s is negligibly small. The computed P_b approaches zero in the upper swash zone near $x = 19$ m, resulting in no L DO movement at $x = 18.7$ and 19.0 m in Figure 5.13. For the small (S) plastics DOs, the computed P_b is slightly larger, and the noticeable suspension probability P_s in the swash zone predicts the computed offshore movement of the DOs at $x = 17.8$ and 18.1 m during the first run of ES0-ES5. For the hypothetical sand DOs, the suspension probability P_s becomes almost as large as the bed load probability. This is assumed to obtain the crude relationship of $C_b = 0.1C_s$ in Equation (4.31).

To examine the sensitivity of the parameter C_b , the computed temporal variations of the cross-shore locations of 10 hypothetical sand DOs for the beach profile and wave conditions of ES0-ES5 in Figure 5.15 where the bed load parameter $C_b = 0.02$ and 0.04 are assessed. The computed sand DOs are immobile in the upper swash zone and move offshore in the lower swash zone for $C_b = 0.02$ and 0.04 . The sand DOs in the inner and outer surf zones move slowly offshore for $C_b = 0.02$ but move rapidly onshore for $C_b = 0.04$. Given that the initial profile for ES0 was near equilibrium and the profile change during ES0-ES5 was less than 1 cm, the negligible net movement of sand particles on the ES0 profile is assumed for the selection of $C_b = 0.02$ for this experiment.

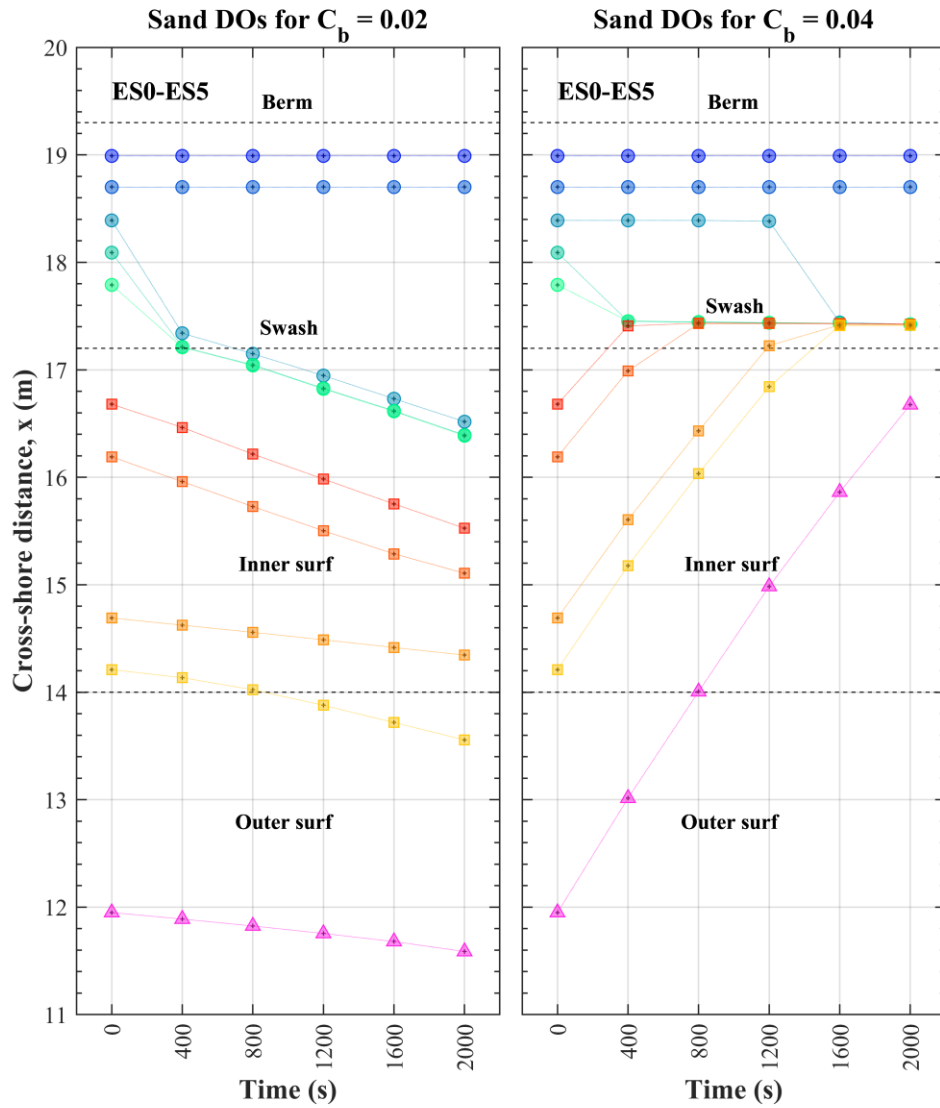


Figure 5.15 Computed temporal variations of cross-shore locations of 10 hypothetical sand DOs for the beach profile and wave conditions of test ES0-ES5 to show the sensitivity to the bed load parameter $C_b = 0.02$ and 0.04 .

For the nourished profile tests, CSHORE predicts the computed temporal variations of the cross-shore locations of 10 DOs on the nourished foreshore during NG0-NG20, NL0-NL20, and NS0-NS10 (Figure 5.16). The gravel DOs near the SWL ($x = 18$ m) are computed to move slightly onshore unlike the measured offshore movement in the lower swash zone for NG0-NG20 in Figure 3.29. The large plastics DOs in the inner and outer surf zones are computed to move onshore and stop near $x = 18.4$ m above the SWL. The computed DOs at $x = 18.4$ - 19.0 m do not move unlike the measured DO movement up to the berm for NL0-NL20 in Figure 3.29. The small plastics DOs in the inner and outer surf zones are computed to move onshore and stop near $x = 17.8$ m slightly below the SWL like the measured DOs below the SWL for NS0-NS10 in Figure 3.29. However, similar to the L DO movement, Equation (4.31) cannot predict the onshore S DO movement on the berm. Table 3.36 summarized the measured and computed numbers of DOs found in the outer surf, inner surf, swash, and berms zones for the N test series. The computed numbers for NG20 are the same as the initial numbers in each zone because the computed gravel DOs remain in their initial zones. The offshore movement of the gravel DOs from the berm to the swash zone is not reproduced. The onshore movement of the L and S plastics DOs up to the berm from the swash and surf zones is not predicted. It may be necessary to improve the probabilistic swash model in section 4.2.

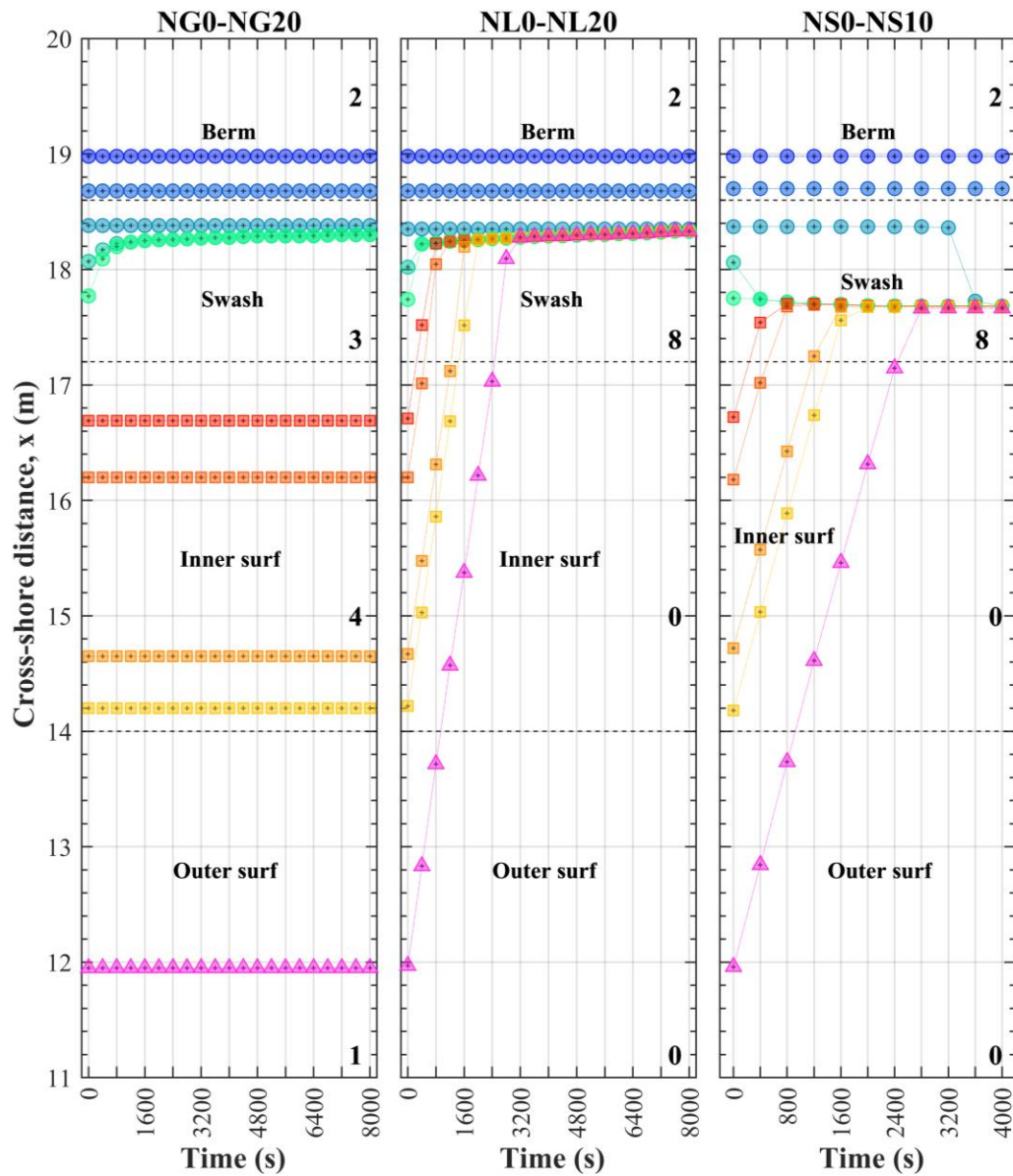


Figure 5.16 Computed temporal variations of cross-shore locations of 10 DOs during nourished foreshore tests NG0-NG20, NL0-NL20, and NS0-NS10.

Chapter 6

Conclusions

A laboratory wave flume experiment was conducted to measure the trajectories of 20 small objects (gravel and microplastics) in the surf and swash zones on a near-equilibrium sand beach and a nourished foreshore beach. The net cross-shore displacement, alongshore variability, and test repeatability of the trajectories were examined in six tests consisting of 100 runs with each run lasting 400 s. The alongshore variability and test repeatability became noticeable for mobile objects but the net cross-shore displacement of each object was measurable with some randomness. Gravel particles were mobile only in the swash zone and moved seaward under wave downrush. Large and small microplastics moved onshore from the surf zone and accumulated in the lower swash zone of wave rundown or in the upper swash or berm zone of wave runup. Erosion and accretion of the steep foreshore had little effect on the net onshore movement of mobile microplastics. The steep foreshore increased wave runup and the landward migration of microplastics. The experiment was limited to the small objects transported mainly as bed load. Sand particles on the near equilibrium beach were transported as both bed load and suspended load. The sand particles were regarded as very small mobile objects with little net cross-shore displacement on the equilibrium beach.

The cross-shore model CSHORE is extended to predict the trajectory of a small object that settles in water. The object is assumed to remain on the sand surface with no burial in sand. This assumption is acceptable for the microplastics used in this experiment. Local scour around the gravel particle is not taken into account for the prediction of gravel movement. The cross-shore velocity of a discrete object is presumed using the bed load and suspended load formulas in CSHORE and consists of its bed load and suspended load velocities. The bed load probability indicates the frequency of the onshore movement of the object on the sand surface, whereas the suspended load probability represents the frequency of the object suspension and exposure to the wave-induced offshore (undertow) current. In the computation, the bed load parameter was calibrated to yield the hypothetical sand movement with little net displacement on the equilibrium sand beach. The calibrated CSHORE predicted the limited onshore movement of the gravel DO contrary to the measured offshore movement of the gravel DO in the swash zone. CSHORE predicted the measured onshore movement of the large and small microplastics from the surf zone to the swash zone. However, the time-averaged swash model could not reproduce the onshore microplastic transport up to the landward limit of wave runup. This transport and deposition process in the swash zone will need to be investigated in the future. The present experiment was limited to the incident significant wave height of 0.2 m. Larger incident waves may increase microplastic suspension and more offshore transport. Furthermore, it will be necessary to examine the longshore movement of discrete objects under obliquely incident waves.

REFERENCES

- Abolfathi, S., Cook, S., Yeganeh-Bakhtiary, A., Borzooei, S., and J. Pearson. 2020. "Microplastics transport and mixing mechanisms in the nearshore region." In Proc. 37th Coastal Engineering Conf., 1-10.
- Bagnold, R.A. 1966. "An approach to the sediment transport problem from general physics." U.S. Geol. Surv., Prof. Paper 422-I.
- Bailard, J.A. 1981. "An energetics total load sediment transport model for a plane sloping beach." J. Geophys. Res., 10,938-10,954.
- Battjes, J. and M.J.F. Stive. 1985. "Calibration and verification of a dissipative model for random breaking waves." J. Geophys. Res., 90(C5), 9159-9167.
- Beck, T.M., Wang, P., Li, H., and W. Wu. 2020. "Sediment bypassing pathways between tidal inlets and adjacent beaches." J. Coastal Res., 36(5), 897-914.
- Becker, J.M., Firing, Y.L., Aucan, J., Holman, R., Merrifield, M., and G. Pawlak. 2007. "Video-based observations of nearshore sand ripples and ripple migration." J. Geophys. Res., 112, C01007.
- Cohn, N., Brodie, K.L., Johnson, B., and M.L. Palmsten. 2021. "Hotspot dune erosion on an intermediate beach." Coastal Eng., 170, 103998, 1-21.

- Demir, S.T., and M.H. Garcia. 2007. "Experimental studies on burial of finite-length cylinders under oscillatory flow." *J. Waterway, Port, Coastal, Ocean Eng.* 133(2): 117-124.
- Figlus, J., Kobayashi, N., and C. Gralher. 2012. "Onshore migration of emerged ridge and ponded runnel." *J. Waterway, Port, Coastal, Ocean Eng.* 138(5), 331-338.
- Figlus, J., Kobayashi, N., Gralher, C., and V. Iranzo. 2011. "Wave overtopping and overwash of dunes." *J. Waterway, Port, Coastal, Ocean Eng.*, 137(1), 26-33.
- Holland, K.T., Holman, R.A., and A.H., Jr. Sallenger. 1991. "Estimation of overwash bore velocities using video techniques." *Proc. Coastal Sediments '91*, ASCE, Reston, Va., 489-497.
- Kalligeris, N., Smit, P.B., Ludka, B.C., Guza, R.T., and T.W. Gallien. 2020. "Calibration and assessment of process-based numerical models for beach profile evolution in southern California." *Coastal Eng.*, 158, 103650, 1-14.
- Kobayashi, N. 2016. "Coastal sediment transport modeling for engineering applications." *J. Waterway, Port, Coastal, Ocean Eng.* 142(6): 03116001.
- Kobayashi, N., Buck, M., Payo, A., and B.D. Johnson. 2009. "Berm and dune erosion during a storm." *J. Waterway, Port, Coastal, Ocean Eng.* 135(1): 1-10.
- Kobayashi, N., DeSilva, G., and K. Watson. 1989. "Wave transformation and swash on gentle and steep slopes." *J. Geophys. Res.*, 94(C1), 951-966.
- Kobayashi, N., Farhadzadeh, A., and J. Melby. 2010a. "Wave overtopping and damage progression of stone armor layer." *J. Waterway, Port, Coastal, Ocean Eng.* 136(5): 257-265.

- Kobayashi, N., Farhadzadeh, A., Melby, J.A., Johnson, B.D., and M. Gravens. 2010b. "Wave overtopping of levees and overwash of dunes." *J. Coastal Res.*, 26(5). 888-900.
- Kobayashi, N., and B.D. Johnson. 2001. "Sand suspension, storage, advection, and settling in surf and swash zones." *J. Geophys. Res.*, 106(C5), 9363-9376.
- Kobayashi, N., and H. Jung. 2012. "Beach erosion and recovery." *J. Waterway, Port, Coastal, Ocean Eng.*, 138(6), 473-483.
- Kobayashi, N., Herrman, M., Johnson, B.D., and M. Orzech. 1998. "Probability distribution of surface elevation in surf and swash zones." *J. Waterway, Port, Coastal, Ocean Eng.*, 124(3), 99-107.
- Kobayashi, N., Meigs, L.E., Ota, T., and J.A. Melby. 2007. "Irregular breaking wave transmission over submerged porous breakwater." *J. Waterway, Port, Coastal, Ocean Eng.*, 133(2), 104-116.
- Kobayashi, N., and A. Otta. 1987. "Hydraulic stability analysis of armor units." *J. Waterway, Port, Coastal, Ocean Eng.* 113(2): 171-186.
- Kobayashi, N., Payo, A., and L. Schmied. 2008. "Cross-shore suspended sand and bed load transport on beaches." *J. Geophys. Res.*, 113(C7), C07001: 1-17.
- Kobayashi, N., and Y. Tega. 2002. "Sand suspension and transport on equilibrium beach." *J. Waterway, Port, Coastal, Ocean Eng.* 128(6), 238-248.
- Kobayashi, N., Zhu, T., and S. Mallavarapu. 2018. "Equilibrium beach profile with net cross-shore sand transport." *J. Waterway, Port, Coastal, Ocean Eng.* 144(6), 04018016, 1-10.

- Lesser, G.R., Roelvink, J.A., Van Kester, J.A.T.M., and G.S. Stelling. 2004. "Development and validation of a three-dimensional morphological model." *Coastal Eng.*, 51, 883-915.
- Madsen, O.S., and W.D. Grant. 1976. "Quantitative description of sediment transport by waves." *Proc. 15th Coastal Engineering Conf.*, ASCE, Reston, Va., 1093-1112.
- Masselink, G., Austin, M.J., O'Hare, T.J., and P.E. Russell. 2007. "Geometry and dynamics of wave ripples in the nearshore zone of a coarse sandy beach." *J. Geophys. Res.*, 112, C10022.
- Nairn, R.B., and H.N. Southgate. 1993. "Deterministic profile modeling of nearshore processes. Part 2. Sediment transport and beach profile development." *Coastal Eng.*, 19, 57-96.
- Raimundo, G.I., Sousa, M.C., and J.M. Dias. 2020. "Numerical modelling of plastic debris transport and accumulation throughout Portuguese coast." *J. Coastal Res.*, SI(95): 1252-1257.
- Roelvink, D., Reniers, A., Van Dongeren, A., Van Thiel de Vries, J. McCall, R., and J. Lescinski. 2009. "Modeling storm impacts on beaches, dunes and barrier islands." *Coastal Eng.*, 56(11-12), 1133-1152.
- Suzuki, T., Inami, Y., Yanagishima, S., Sakihama, S., and D.T. Cox. 2019. "Sediment particle movements observed using tracers under accretive wave conditions in the nearshore zone." *Coastal Eng. J.*, 61(4), 472-485.
- Trowbridge, J., and D. Young. 1989. "Sand transport by unbroken water waves under sheet flow conditions." *J. Geophys. Res.*, 94, 10, 971-10, 991.

Williams, A.T., and N. Rangel-Buitrago. 2019. "Marine litter: Solutions for a major environmental problem." *J. Coastal Res.*, 35(3). 648-663.